Fakultät Wissenschaftszentrum Weihenstephan für Ernährung, Landnutzung und Umwelt

Helmholtz Zentrum München, Institut für Entwicklungsgenetik

Mitochondrial Function in Cellular Models of Idiopathic Parkinson's Disease

Constantin Alexander Stautner

Vollständiger Abdruck der von der Fakultät Wissenschaftszentrum Weihenstephan für Ernährung, Landnutzung und Umwelt der Technischen Universität München zur Erlangung des akademischen Grades eines

Doktors der Naturwissenschaften

genehmigten Dissertation.

Vorsitzende:		**Prof. Dr. Aphrodite Kapurniotu**
Prüfer der Dissertation:	**1.**	**Prof. Dr. Wolfgang Wurst**
	2.	**Prof. Dr. Martin Klingenspor**

Die Dissertation wurde am 10. April 2018 bei der Technischen Universität München eingereicht und durch die Fakultät Wissenschaftszentrum Weihenstephan für Ernährung, Landnutzung und Umwelt am 17. September 2018 angenommen.

♦ Zusammenfassung

Der medizinische Fortschritt der letzten Jahrzehnte hat Großartiges geleistet. Dies hat gleichzeitig zur Folge, dass immer höheres Alter und der begleitende demographische Wandel, insbesondere in westlichen Kulturen, für eine immer größer werdende Anzahl degenerativer Erkrankungen verantwortlich sind. Die Parkinson'sche Erkrankung, die zweithäufigste neurodegenerative Erkrankung nach Alzheimer, ist von ebendiesem Anstieg stark betroffen. Trotz Jahrzehnten intensiver Forschung, konnte bei Parkinson bisher kein einzelner pathologischer Ursprung entdeckt werden. Daher wird Parkinson als eine Krankheit betrachtet, die durch eine Kombination multipler Defekte verursacht wird, welche grundlegend unterschiedlich sein können aber molekular miteinander verbunden sind, wie zum Beispiel krankhafte Alterungsprozesse, Proteinopathien oder bioenergetische Defizite. Das Krankheitsbild gewinnt weiter an Komplexität durch die Tatsache, dass all diese Prozesse genetisch verursacht werden können, ebenso aber durch Umwelteinflüsse. Dank umfangreicher Forschung auf dem Gebiet kann Parkinson heute symptomatisch behandelt werden, ist allerdings, obwohl seit über 200 Jahren bekannt, bis heute nicht heilbar.

Diese Arbeit ist ein Teilprojekt des bayrischen Forschungsverbunds „ForiPS" und analysiert eine Kohorte Patienten mit idiopathischer Parkinson'scher Erkrankung und passend abgestimmten Kontrollen. Dabei liegen Fokus und Ziel der Arbeit auf der Prüfung der bioenergetischen Funktion von induziert pluripotenten Stammzellen (iPSZ) und deren neuronale Differenzierungsprodukte von Parkinson Patienten. Die zugrundeliegende Hypothese ist, dass, gleich dem physiologischen System, eine bioenergetische Defizienz vorhanden ist, die kompensiert werden kann und deshalb ohne Stressoren, wie Toxine, Substratentzug oder Alterungsprozesse nicht detektiert werden kann.

Die Ergebnisse dieser Arbeit zeigen, dass bereits auf der Stufe der iPSZ und den neuronalen Vorläufer Zellen eine bioenergetische Defizienz zu finden ist. Patientenzellen zeigen eine verminderte mitochondriale Atmung mit Glukose als Substrat, welche auch ein Hauptsubstrat für das Hirn ist. Die detaillierte Analyse der mitochondrialen Funktion in Patienten iPSZ zeigt, dass der Phänotyp des geminderten Sauerstoffkonsums allerdings nicht mitochondrial verursacht ist, sondern eher ein metabolischer Phänotyp ist, da Substrat aus dem mitochondrialen Zyklus abgezogen zu werden scheint. Nach Differenzierung zu neuronalen Vorläuferzellen konnte zusätzlich einen mitochondrialen Phänotyp gezeigt werden. Beide Befunde können gut in die aktuelle Forschung integriert werden, da ein gestörter Glukose Metabolismus und mitochondriale Dysfunktion bereits in anderen Modellen der Parkinson'schen Erkrankung entdeckt wurden. Diese Studie zeigt im Vergleich zu bereits vorhandener Literatur eine detailliertere Analyse der mitochondrialen Funktion in einem erst kürzlich erforschten Modellsystem und kann somit zu einem besseren Verständnis der Erkrankung sowie des Modellsystems der iPSZ beitragen.

♦ Abstract

Medical advances resulting in extended ageing periods and changing demographic developments towards an older population, especially in western cultures, have resulted in a drastic increase in the number of degenerative diseases diagnosed in the last decades. Parkinson's disease, the second most prominent neurodegenerative disease, next to Alzheimer's disease, is one of those degenerative illnesses, which has been showing strongly rising incidence for decades now. It appears with high prevalence and despite decades of extensive research, the one pathological origin of the disease has not been discovered yet. Today, Parkinson's disease is thought to be a "multiple hit" disease, with a variety of possible, yet interplaying pathological origins which range from an "unhealthy" ageing process over proteinopathy to bioenergetic dysfunction, all of which, to add even more complexity, may be of genetic origin or stem from environmental circumstances. Thanks to the broad research conducted in this field, Parkinson's disease is now symptomatically treatable and progressively better manageable, yet still cannot be cured despite 200 years having passed since the first description of the disease by James Parkin.

This thesis is embedded into the research of the Bavarian "ForiPS" consortium and concerns itself with a cohort of idiopathic Parkinson's disease patients and age matched control individuals. The focus and aim of this work lie on the assessment of bioenergetic function of Parkinson's disease patients' induced pluripotent stem cells (iPSCs) and their derivatives, as well as the analysis of metabolic changes in Parkinson's disease patients' cells, accompanied by changes in the differentiation potential towards neuronal lineages. The underlying hypothesis is that just like in the physiological system, bioenergetic deficiencies are present in Parkinson's disease patients' cells but can be compensated, are not readily detectable and have to be unmasked by cellular stressors like toxins, nutrient deprivation or ageing. This thesis shows that bioenergetic deficiencies are already well detectable at induced pluripotent stem cell level as well as in neuronal precursor cells differentiated from those cells. Decreased mitochondrial respiration could be detected in Parkinson's disease patients' cells when given glucose as substrate, which also functions as major energy substrate for the brain. In depth analysis of mitochondrial function in Parkinson's disease patients' iPSCs, however, revealed that decreased respiration is not due to faulty mitochondria, but rather due to a whole cell metabolic phenotype, as substrate drawn from intact mitochondria likely seems responsible for the detected respiratory deficiencies. Upon differentiation to neuronal precursor cells, additionally a mitochondrial phenotype was detected. Both findings integrate well into current Parkinson's disease research, as both, deranged glucose metabolism and mitochondrial dysfunction have been reported in other models of Parkinson's disease. In comparison to other published research, this thesis offers an in-depth analysis of mitochondrial function in an only recently emerged model system, and thereby can contribute to the understanding of Parkinson's disease and induced pluripotent stem cells as disease model.

Index

1. Introduction

The principal long-standing medical success of our time is to enable people to become old. The World Population Ageing Report from the United Nations reports a substantial increase of older population with no change in sight. Between 2015 and 2030, the number of people in the world aged 60 years or older is predicted to grow by 56%, from 901 million to 1.4 billion, reaching up to 2.1 billion by 2050 (United Nations World Population Prospects, 2015).

This development is accompanied by the major medical obstacle that ageing is one of the greatest risk factors for many diseases. Hence, it is no surprise that the incidence for many diseases, especially degenerative diseases, is rising continuously. High age is definitely not a risk factor for all degenerative diseases, yet nowadays patients generally become diagnosed earlier and survive longer, further accounting for increasing numbers. Degenerative diseases present themselves affecting many different organs, ranging from bones (e.g. osteoporosis) to muscles (e.g. muscular dystrophy), the body's digestive system (e.g. inflammatory bowel disease) and metabolism (e.g. diabetes type II) and further to the nervous system (e.g. multiple sclerosis) and the brain (e.g. Alzheimer's and Parkinson's disease). Even though all those diseases cause loss of quality of life for affected patients, some can be treated relatively easy nowadays, for example by giving insulin to diabetes patients. Neurodegenerative diseases stick out in all regards, since they often associate with age, their pathology is rarely fully understood and current treatments are usually neither well performing nor readily available.

Parkinson's disease has emerged to be one of the most controversial examples of a neurodegenerative disease: it appears with high prevalence and yet is the root of the disease even today not fully understood and state of the art research has no cure impending. Thanks to decades of research, today there are multiple ways to treat Parkinson's effectively, promising life prolongation and relief from the most severe symptoms to the patients affected by a seemingly manageable disease. However, no one should forget that Parkinson's disease is a progressive disorder, treatments will be subject to resistance and in the end the disease will overcome any obstruction put in its way.

"With Parkinson's, it's like you're in the middle of the street and you're stuck there in cement shoes and you know a bus is coming at you, but you don't know when. You think you can hear it rumbling, but you have a lot of time to think. And so you just don't live that moment of the bus hitting you until it happens. There's all kinds of room in that space" [Michael J. Fox, 2011].

1.1. Parkinson's disease

The probably most famous description of Parkinson's disease (PD) was in 1817 by the British physician James Parkinson in his monograph *An Essay on the Shaking Palsy* (Parkinson, 2002). Already in his time, he described most of today's predominant clinical motor symptoms of PD. Yet, only about 70 years later, James Parkinson was actually accredited as eponym of Parkinson's disease when the French neurologist Jean-Martin Charcot refined several features of the disease description and suggested naming it Parkinson's disease (Goetz, 2011).

Today it is known that PD encompasses a multitude of symptoms and PD-associated symptoms appear in a large number of other (related) disorders. Disorders that display some or all of the PD symptoms are clinically termed Parkinsonism, while disorders in which Parkinsonism is a prominent part are referred to as parkinsonian disorders (Dickson, 2012). At the time of diagnosis, all PD patients usually already show some or all of the clinically characteristic symptoms: stooped posture, rigidity, rest tremor, bradykinesia and hypokinesia (reduced frequency and amplitude of movement). These symptoms are progressive although the rate of progression varies between each patient individually (Alkhuja, 2013). PD is accompanied and preceded by a multitude of other symptoms, starting with a so-called prodromal phase up to 20 years before motor symptoms occur and a diagnosis can be secured. These symptoms display a great diversity in appearance and severity depending on the individual patient. Amongst the most common ones are general cognitive and behavioral changes, autonomic nervous system disturbances, sleep disturbances, anxiety and depressive episodes (Jain, 2011). Even though symptoms and their severity vary strongly from patient to patient, studies have shown that almost 90% of PD patients suffer from non-motor symptoms during the progression of the disease (Löhle et al., 2009).

1.1.1. Epidemiology and etiology of PD

Being the second most common neurodegenerative disease after Alzheimer's disease (AD), studies attest PD a worldwide incidence from 5 – 35 cases per 100.000 individuals yearly, depending on geographical circumstances, population prevalence and population genetics. Before the age of 50, PD diagnoses are quite rare and often of genetic origin, while after the age of 60 the incidence of developing PD increases 5-10-fold (Poewe et al., 2017). A recent study conservatively estimated a global prevalence of 0.3%, increasing up to 3% when only people older than 80 were taken into account (Pringsheim et al., 2014). In terms of disease progression, it was shown that no increase in mortality rates can be observed in the first 10 years after disease onset, while afterwards PD groups show nearly doubled death rates in comparison to matched control groups (Pinter et al., 2015). In accordance with the previously mentioned UN world populations report, it is estimated that the number of PD patients between the years 2015 and 2030 will approximately

double (Dorsey et al., 2007). Noteworthy is also a gender-bias as PD is diagnosed twice as much in males compared to females in most populations (Baldereschi et al., 2000; Van Den Eeden et al., 2003). This might be related to protective effects of female sex hormones, a sex associated genetic mechanism or sex specific differences in exposure to environmental risk factors (Poewe et al., 2017).

Traditionally, PD was considered an idiopathic disease. Reports of 20% - 30% of PD patients with a first-degree relative also developing the disease were thought to be a consequence of a shared environment (Farrer, 2006; Gao and Hong, 2011). As a matter of fact, a lot of studies on geographical and racial circumstances showed a relation of those factors and the development of PD in several populations like the Ashkenazi Jews, Inuit, Alaska Native and Native American (Gordon et al., 2012). Today we know that PD can be separated into different classes, which can, but don't necessarily present themselves alike: toxin- or drug-induced Parkinsonism (sometimes transient), familial inherited PD (fPD) and idiopathic PD (iPD). Even though the majority of PD cases still are attributed to iPD, a solid estimation of about 10% of all PD cases can nowadays be attributed to fPD cases (Hawkes, 2008). As for whole populations with unusually high PD incidences, like the Ashkenazi Jews and others, it has been demonstrated that this is likely due to higher prevalence of incompletely penetrant genes associated with PD (Chillag-Talmor et al., 2011; Gordon et al., 2012). Additionally, it could be shown that not only fPD is caused by monogenic mutations, but also frequent polymorphic (risk) variants may contribute to or prime the development of PD (Lesage and Brice, 2012).

Generally, PD pathogenesis can be split into three major genetic groups according to the risk of developing PD and allele frequency: (a.) very rare, monogenic mutations, often in autosomal recessively inherited genes which are associated with extremely high risks (up to more than twenty-fold) of developing PD, such as mutations in the "*PARK*" genes *Parkin, PTEN-induced putative kinase-1 (Pink1), DJ-1, alpha-synuclein (SNCA), vacuolar protein sorting-associated protein 35 (Vsp35)* or *leucine-rich repeat kinase 2 (Lrrk2)*; (b.) more frequent mutations, often of autosomal dominant nature like in the *glucocerebrosidase (GBA)* gene or the *SNCA* gene, which appear fairly recurrent and present a moderate risk (two- to ten-fold) of developing PD and (c.) polymorphic variants in PD associated, autosomal dominantly inherited genes like *SNCA, Lrrk2* or *microtubule-associated protein tau (MAPT)* which can be detected at high frequencies but have comparatively low coincides in terms of risk of development (up to 1.5-fold) of PD (Lesage and Brice, 2012). Accordingly, depending on the gene(s) affected, the pathogenesis of fPD presents itself highly variable (Tab.1). Monogenic, recessively inherited forms, for example the L166P mutation in *DJ-1*, a loss-of-protein-function (LOF) mutation, are extremely rare, yet extremely aggressive with the youngest diagnosed patient in the late thirties (Bonifati et al., 2003; Zhang et al., 2005). In contrast, frequent mutations like the R1441C mutation in the dominantly inherited gene *Lrrk2* are often not associated with an early

onset aggressive PD phenotype, but rather present themselves like iPD in terms of disease progression (Martin et al., 2011; Rideout and Stefanis, 2014). A summary can be taken from Tab.1.

Locus Symbol	Gene	Gene Locus	Clinical Phenotype	Lewy-Body Pathology
Autosomal dominant Parkinson's disease				
PARK1/ PARK4	SNCA	4q22.1	Missense mutations (=PARK1) cause classic PD phenotypes. Duplications / triplications of this gene (=PARK4) cause early-onset PD with prominent dementia	Yes
PARK8	LRRK2	12q12	Classic PD phenotype. Variations in LRRK2 include risk-conferring variants and disease-causing mutations	Varies
PARK17	VPS35	12q11.2	Classic PD phenotype	Unknown
	MAPT	17q21.1	Dementia, sometimes Parkinsonism	Neurofibrillary tangles
Autosomal recessive Parkinson's disease (early onset)				
PARK2	Parkin	6q26	Often presents with lower limb dystonia	Rarely
PARK6	PINK1	1p36.12	Psychiatric features are common	Rarely
PARK7	DJ-1	1p36.23	Early-onset PD	Unknown
PARK19B	DNAJC6	1p31.3	Onset of Parkinsonism between the third and fifth decade of life	Unknown
Complex genetic forms (autosomal recessive inheritance)				
PARK9	ATP13A2	1p36.13	Early-onset Parkinsonism with a complex phenotype	Unknown
PARK14	PLA2G6	22q13.1	Complex clinical phenotype which does not include Parkinsonism in most cases	Yes
PARK15	FBXO7	22q12.3	Early-onset Parkinsonism with pyramidal signs and a variable complex phenotype	Unknown
PARK19A	DNAJC6	1p31.3	Juvenile-onset Parkinsonism that is occasionally associated with mental retardation and seizures	Unknown
PARK20	SYNJ1	21q22.11	Patients may have seizures, cognitive decline, abnormal eye movements and dystonia	Unknown
	GBA	1q21	Early-onset PD	Unusual

Table 1: Classification of hereditary Parkinson's disease. *Taken and modified from Martin et al., 2011 and Poewe et al., 2017.*

However, it's not only the genetic background resulting in different phenotypes of PD. A "traditional" pathology of iPD is Lewy-related neuropathology. As shown in Tab.1 this feature is also represented in most, but not all forms of fPD. The term Lewy body (LB) describes the abnormal deposition of mainly

alpha-synuclein in the cytoplasm of neurons in various brain regions (Braak et al., 2003) which then forms insoluble protein aggregates. By today, protein aggregates have even been detected in synapses which, since they are inclusions within neuronal cell processes, are called Lewy neurites (Dickson, 2012). The combination of all these Lewy body and Lewy neurite pathologies is termed Lewy-related pathology (Dickson et al., 2009). Lewy-related pathology usually originates in cholinergic and monoaminergic brainstem neurons and in the olfactory system, but is also found in limbic and neocortical brain regions with progression of the disease (Poewe et al., 2017). Today, we know that not only alpha-synuclein inclusions are responsible for Lewy-related pathology. It has been shown that most degenerative parkinsonian disorders fall into one of two molecular classes – either alpha-synucleinopathies or tauopathies which are based on the pathologic accumulation of the microtubule associated protein tau (Dickson, 2012).

The discovery that PD can be of genetic origin offered great opportunities for research. It allowed the generation of animal models and the identification of multiple pathways involved in the pathogenesis of PD. Pathological analyses of patients revealed a lot about the neuropathology of PD, while production and analyses of various models of fPD using mice or human pluripotent stem cells (hPSCs) as well as toxin-induced Parkinsonism models revealed the involvement of several cellular organelles, maintenance systems and pathways involved in neuronal death in course of PD.

1.1.2. Neurobiology of PD

The two characteristic features of PD are the loss of specific populations of vulnerable neurons as well as a widespread Lewy-related pathology. Even though both don't occur exclusively in PD, these two neuropathologies are specific for a definite diagnosis of iPD when presenting together (Dickson et al., 2009; Poewe et al., 2017). Common to all variants of PD is the selective loss of dopaminergic neurons in the substantia nigra pars compacta (SNpc) that project to the putamen (dopaminergic nigrostriatal pathway) (Dickson, 2012). However, there are multiple variants of PD which show that more regions than just the dopaminergic nigrostriatal pathway are affected, e.g. the progressive supranuclear palsy (PSP), in which also tau inclusions are found within glial cells (astrocytes and oligodendrocytes) and which is considered a "Parkinsonism plus" disorder (Dickson, 2012; Dickson et al., 2007).

In early stages of the disease, neuronal loss begins probably in the brain stem and the midbrain, but spreads out during disease progression. Generally, the most severe loss of neurons is observed in the SNpc, the amygdala, the basal nucleus of Meynert, the hypothalamus, the locus ceruleus and the medullary tegmentum (including dorsal motor nucleus of vagus) (Dickson, 2012). For a long time, it has been assumed that motor symptoms only occur when about 70 - 80% of the dopaminergic neurons in the SNpc are lost, newer studies,

however, correct this figure to loss of about 30% of neuronal cell bodies and 50 - 60% of axonal terminal (Kordower et al., 2013).

In the classic model of the pathophysiology of the basal ganglia (Fig. 1), a dysregulation of two main pathways in PD is postulated: the monosynaptic gamma-aminobutyric acid (GABA) direct circuit from the putamen to the globus pallidus pars interna (GPi) and the trisynaptic circuit (putamen – globus pallidus pars externa (GPe) – subthalamic nucleus (STN) – Gpi / substantia nigra pars reticulate (SNpr). In healthy individuals, cortical motor areas project directly into the putamen with glutamatergic axons, regulating the inhibitory GPe projections which in turn regulate the excitatory STN activation. Additionally, cortical motor areas can also directly activate the STN by excitatory projections via the "hyperdirect" pathway. Usually, the dopamine released from the SNpc facilitates the neurons from the putamen in the direct pathway and inhibits those in the indirect pathway, which directly facilitates or suppresses movement correspondingly and is controlled in a very fine-tuned manner. In PD, however, the dopamine deficit causes increased activity of the indirect circuit resulting in STN hyperactivity, as the STN still is stimulated by the motor cortex via the hyperdirect pathway and, in parallel, hypoactivity in the direct circuit. Together, these actions result in an increased inhibitory GPi/SNpr output towards the ventrolateral (VL) nucleus of the thalamus which in turn yields a reduced activation of cortical and brainstem motor regions (Rodriguez-Oroz et al., 2009). However, this basic model is recognized limited nowadays, since it cannot provide explanations for all clinical observations. A more current model which takes into account that basal ganglia networks are anatomically and physiologically subdivided into motor, oculomotor, associative and limbic territories that are involved in learning, planning, working memory, emotions and timing mechanisms is reviewed in Obeso et al., 2008 and Rodriguez-Oroz et al., 2009.

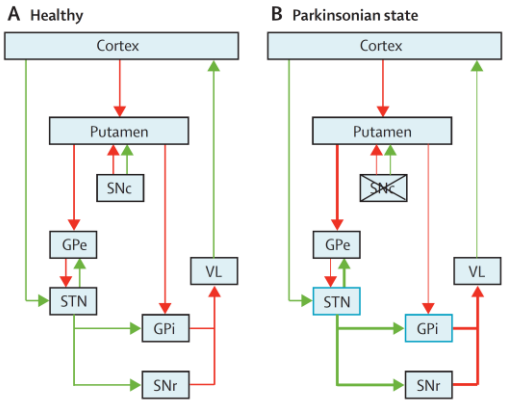

Fig. 1: The initial and basic model of PD pathophysiology based on cortico-basal ganglia-cortical loops vs. a newer model of basal ganglia networks (taken from Rodriguez-Oroz et al., 2009)*. It demonstrates the dysregulation of the monosynaptic GABAergic direct circuit and the trisynaptic (putamen-GPe-STN-GPi/SNpc) circuit in PD patients in comparison to healthy controls. Green arrows indicate excitatory activity, red arrows inhibitory activity. As shown, lack of dopamine from the SNpc ultimately causes lack of excitatory activity from the VL into the motor cortex areas. (Abbreviations: SNc – substantia nigra pars compacta; SNr – substantia nigra pars reticulate; GPe – globus pallidus pars externa; GPi – globus pallidus pars interna; STN – subthalamic nucleus; VL – ventrolateral nucleus)*

1.1.3. Vulnerability of dopaminergic neurons

It has become clear over the last decades that not every dopaminergic neuron equals another. Today, dopaminergic neurons are classified in nine different groups termed A8-A16 for historical reasons (reviewed in Vogt Weisenhorn et al., 2016). Only three groups of dopaminergic neurons however, A8 – A10, are found in the ventral mesencephalon: the A8 group is located in the retrorubral field, the A9 group in the SNpc and partially in the SNpr and the A10 group in the ventral tegmental area (VTA) (Vogt Weisenhorn et al., 2016). As neuronal loss of the A9 group of mesodiencephalic dopaminergic neurons (mDANs) is rarely observed in other diseases, the question arose why this particular group of neurons seems to exhibit a selective vulnerability in the specific context of PD.

Unfortunately, this question presents itself tremendously difficult if one is looking for just one answer. A lot of laboratories succeeded in yielding feasible answers by analyzing (animal) models of fPD, bringing up current theories of the molecular pathogenesis of PD i.e. defective protein folding and turnover, mitochondrial dysfunction and, as consequence, oxidative stress and neuroinflammation. Other laboratories showed that PD could be specifically modelled using toxins like 1-Methyl-4-phenyl-1,2,3,6-tetrahydropyridin (MPTP), a prodrug of the neurotoxin 1-Methyl-4-phenyl-pyridin (MPP^+), which is selectively taken up via the dopamine transporter (DAT) into dopaminergic neurons, where it specifically inhibits complex I (nicotinamide adenine dinucleotide (NADH) dehydrogenase) of the mitochondrial respiratory chain (Langston et al., 1984). However, it has to be noted that MPP^+ only models some of the clinical motor symptoms of PD, bradykinesia and tremor, but is unable to elicit non-motor symptoms or Lewy-related pathology (Langston et al., 1984). Later it was shown that not only MPP^+, but also other toxins like rotenone or paraquat produce similar effects, most of them affecting mitochondrial respiration, yet not displaying the pronounced specificity for dopaminergic neurons (Betarbet et al., 2000; Brooks et al., 1999).

Another line of research followed endogenous gene expression and its dysregulation in PD patients. Studies showed that PD development and dopaminergic survival can be clearly linked to dosage differences of the homeodomain transcription factors Engrailed-1 and -2 (En-1/-2) (Simon et al., 2005; Sonnier et al., 2007). Furthermore it was demonstrated that En-1/-2 play vital roles not only in the development, but also in the maintenance and metabolism of these dopaminergic neurons. Noteworthy here is also that mainly the A9 group of mDANs seem to have a stringent dependency on pituitary homeobox 3 (Pitx3) signaling, a homeobox protein vitally involved in mDAN maturation and maintenance, which also has been shown to crosstalk with En-1/-2 (Rekaik et al., 2015a; Zhang et al., 2015). This will be discussed in more detail in the sections 1.1.4.4 and 3.4 of this thesis.

Another important role in the specific vulnerability of group A9 mDANs seems to be occupied by their physiological function. Using dopamine as a neurotransmitter brings along several risks: dopamine itself is

an unstable molecule that can undergo auto-oxidation to form quinones and free radicals (Muñoz et al., 2012), contributing to and possibly tipping the general cellular oxidative stress level over the edge. The obtained quinones can cyclize to form aminochromes, a highly reactive group of molecules which can lead to the generation of superoxides, and, in consequence, the depletion of cellular NADH (Hastings, 2009). Dopamine becomes predominantly metabolized by the monoamine-oxidase A (MAO-A), which is mostly localized in catecholaminergic neurons (Dias et al., 2013; Riederer et al., 1987), to 3,4-dihydroxyphenyl-acetaldehyde (DOPAL) and further by the aldehyde dehydrogenase 2 (Ahd-2) to 3,4-dihydroxyphenylacetic acid (DOPAC). However, it has been shown that when neuronal degeneration increases in PD, monoamine-oxidase B (MAO-B), located in glial cells, becomes the predominant enzyme metabolizing the dopamine which is released from mDANs and subsequently is taken up by astrocytes. The products of the MAO-B metabolization of dopamine in astrocytes are DOPAL, an ammonium-molecule and hydrogen peroxide (reviewed in Dias et al., 2013). The hydrogen peroxide is highly likely to react with iron to form hydroxyl radicals, again likely contributing to the oxidative stress levels in mDANs. DOPAL itself is described to be a neurotoxin and its accumulation has been postulated to be causative of PD (Marchitti et al., 2007). Reactivity of DOPAL can be reduced through oxidation to DOPAC, a step which is catalyzed by Ahd-2. It seems noteworthy at this point, that it has been shown that a subset-specific activation in the group A9 mDAN of the *Adh2* gene depends on Pitx3 and, if dysregulated, might further contribute to a derailed dopamine metabolism (Jacobs et al., 2007; Smidt, 2009). Last but not least, metabolism and proper storage of dopamine are very energy demanding, making dopaminergic neurons high energy consumers resulting in high mitochondrial respiratory activity – again likely contributing to oxidative stress levels (Anandhan et al., 2017). To compensate for this highly oxidative environment, high levels of reduction equivalents, i.e. nicotinamide adenine dinucleotide phosphate (NADPH) are produced in those neurons – with the consequence that those too might contribute to oxidative stress by mediating reactive oxygen species (ROS) generation through NADPH-oxidases (NOXs) (Anandhan et al., 2017). In summary, it becomes clear that the specific vulnerability of A9 mDANs in PD is not an easy question to address. Since not a single cause can be made clearly responsible for mDAN degeneration, PD is considered a multiple hit disease, as an interplay of many factors seems to be necessary to develop PD, especially when one thinks about the extraordinary compensatory capabilities of the human body – after all, the clinical motor symptoms of PD only appear when more than 30% of mDANs and more than 50% of axonal terminals are lost.

1.1.4. Risk-factors and molecular pathways in the pathogenesis of PD

It has been mentioned before that the multitude of dysregulations and –functions found in both iPD and fPD, makes it highly difficult to pinpoint the origin of the pathogenesis of PD. However, as the majority of

hypotheses beyond neuroinflammation circle around two major cellular pathways, mitochondrial function and protein clearance, only those will be introduced here.

1.1.4.1. The proteinopathy PD

It has been talked about previously that Lewy Bodies are a hallmark of PD and occur in most forms of PD. Accumulation of a specific protein with abnormal conformation that is prone to induce aggregation, often a hallmark of neurodegenerative diseases, is termed proteinopathy. In PD, the protein with the major contribution to Lewy Body composition is alpha-Synuclein (α-Syn). α-Syn is a rather small protein with only 140 amino acids, containing a highly hydrophobic N-terminal lipid binding and a negatively charged, acidic C-terminal domain. α-Syn does not adapt a consistent secondary structure in solution, but rather a natively unfolded structure - hence it is believed to belong to a family of proteins which are intrinsically unstructured (Dikiy and Eliezer, 2012; Ottolini et al., 2017). Despite conformational differences, both, the *in vivo* and *in vitro* form of α-Syn can form fibrillary aggregates (Ottolini et al., 2017). While the physiological function of this protein is not fully understood, it became clear that it plays a major role in PD since it is not only associated with the emerging proteinopathy but also with e.g. synaptic plasticity, vesicle transport and mitochondrial function and integrity, where it has been shown to exert a highly beneficial role (Ganguly et al., 2017; Menges et al., 2017).

It is not entirely clear why α-Syn accumulates in iPD patients brains, whether this is due to an over-functioning of transcriptional or post-transcriptional pathways or a dysfunction in protein clearance pathways, or maybe both (Ganguly et al., 2017). Multiplications of the whole gene (*SNCA)* have been recognized causal in familial forms of PD (Chartier-Harlin et al., 2004). Also, it still has not been elucidated whether accumulation of α-Syn in LBs has a causative role in the development of PD or rather a neuroprotective one. Currently it is assumed that the neurotoxic molecules among the different α-Syn species are the soluble oligomeric forms rather than the fibrillary end deposits (Ottolini et al., 2017; Winner et al., 2011). In any case, misfolded proteins generally can be considered cytotoxic. Hence, cells possess two essential clearance mechanisms: the ubiquitin-proteasome-system (UPS) and the autophagy-lysosomal pathway (ALP). α-Syn usually is degraded by both pathways, with an emphasis on the UPS pathway under normal physiological conditions (Webb et al., 2003). It has been shown that the ALP pathway can compensate for the UPS pathway and vice versa (Shen et al., 2013), yet, how protein degradation is affected in detail has not been completely understood. To make this even more complicated, it has been demonstrated that the different protein clearance pathways seem to exhibit a kind of specificity towards which type of α-Syn species they remove: studies have shown that the ALP pathway mainly accounts for the control of the regular α-Syn turnover and the removal of oligomeric intermediates rather than the mature inclusion bodies

(reviewed in Ottolini et al., 2017). Other studies hypothesized that, in addition, oxidative modifications play an important role by oxidatively modifying proteins which then may miss-fold and make up highly stable protein aggregates. In accordance, it has been demonstrated that the adenosine triphosphate (ATP) - driven UPS pathway degradation machinery is not only sensitive to oxidative stress, but also to age-related energy depletion (Tan et al., 2009). In conclusion, despite extensive studying of the α-Syn protein, its accumulations and toxic species and the corresponding cellular responses, no clear function can yet be attributed to PD's most prominent protein, nor are its pathological consequences fully understood.

1.1.4.2. Ageing

Ageing has emerged as a far too complex process in order to be elucidated with just one explanation. Today, there are several theories of ageing, which can be classified into two primary categories: (1) the programmed theories and (2) the damage and error theories. The programmed theories encompass programmed ageing (programmed longevity), the endocrine theory of ageing and the immunological theory of ageing. They all imply that the ageing process follows a biological timetable which is regulated depending on changes in gene expression responsible for cellular maintenance, repair and defense responses. Programmed longevity describes the decline of genetic stability during ageing and the resulting dynamics in the process, while the endocrine theory proposes a hormonal control of the pace of aging. The immunological theory proposes that the immune system is programmed to decline over time, pathing the way for infections and tumors. The damage and error theories are subdivided in the "wear and tear", "rates of living", somatic deoxyribonucleic acid (DNA) damage, "cross-linking" and free radicals theories. The common denominator that can be depicted here is that cellular stressors, may they be endogenous and natural or endo- or exogenous pathological, wear down the body in various molecular and finally systemic ways, which are responsible for the ageing process and ultimately death (reviewed in Jin, 2010). The combination of these theories, even though none of them have been proven exclusively correct, makes the phenomenon of ageing so interesting when viewed in the light of PD, since there is a remarkable overlap in the molecular backgrounds of especially the damage and error theories in ageing and PD. Being the major risk factor for the development of PD, ageing, unfortunately, is likely also the most complex factor in the pathogenesis of PD. The issue presents itself in a multitude of clinical diagnoses associated with neurodegenerative disease, which do not correlate with the applicable pathological features, and with increased age, there are only very few brains which lack those pathological features (Wyss-Coray, 2016). Several population-based post-mortem studies of aged healthy individuals' brains revealed that Lewy-related pathologies, amyloid plaques, neurofibrillary tangles, synaptic dystrophy, neuronal loss and loss of brain volume are normal to most brains (Elobeid et al., 2016), while originally being associated with neurodegenerative disease. There is a high variability in-

between individuals in regard to those features and their regional specificity in the brain. It remains to be revealed whether these are features of, or contributors to ageing and whether they are precursors to neurodegeneration or, at least some, byproducts of compensatory mechanisms (Wyss-Coray, 2016)

Another interesting aspect of ageing is that it cannot be viewed as an opposite of longevity. Longevity has been associated with several markers (e.g. the *Tomm40-APOE-APOC1* locus (Newman and Murabito, 2013; Shadyab and LaCroix, 2015)), yet none of this markers has been linked to ageing. Rather, the major marker for healthy ageing (i.e. ageing without developing a disease) has been the absence of risk factors of neurodegenerative or cardiovascular disease (Erikson et al., 2016). A variety of studies has identified five different, yet eventually interdependent, ageing associated cell- and pathway specific mechanisms which may accelerate ageing: loss of protein homeostasis, DNA damage, lysosomal dysfunction, epigenetic changes and immune dysregulation (reviewed in Wyss-Coray, 2016). It has been postulated that, depending on which pathway is affected in particular, specific neurodegenerative diseases may emerge as consequence of accelerated ageing in specific regions affected.

PD seems to be affected by the process of ageing mediated by two pathways in particular. The presence of age-related protein abnormalities and inclusion bodies points towards a progressively flawed protein degradation apparatus. This is supported by a multitude of observations and studies, and hypothesized to often being accompanied by increased cellular (oxidative) stress, resulting in oxidized macromolecules which cannot be degraded by lysosomes anymore (Brunk and Terman, 2002). The other pathway has been postulated to be mitochondrial dysfunction, since a lot of evidence from fPD and iPD models points towards mitochondria and their dysfunction seems to aggravate also in ageing as stated by the mitochondrial theory of ageing (see section 1.1.4.3.1) (Gasser et al., 2011).

1.1.4.3. Mitochondrial dysfunction in ageing and PD

This section will highlight the centrality of mitochondria in the process of ageing and PD. General mitochondrial biology and function are introduced in section 1.2.2 below.

1.1.4.3.1. The mitochondrial free radical theory of ageing

The mitochondrial free radical theory of ageing states that the production of ROS during mitochondrial metabolism results in an overall increased oxidative stress within cells. This includes, but isn't specific for, oxidation of mostly mitochondrial but also nuclear DNA, causing mutations and defective proteins especially in the cellular respiratory system. Impaired cellular respiratory systems are thought to further increase ROS production, hence creating a vicious circle of oxidative stress which ultimately will lead to cell death (Birch-Machin and Bowman, 2016). ROS are free oxygen radicals, a naturally occurring

byproduct of aerobic respiration, thereby putting mitochondria at the center of ROS production as the majority of cells produces the majority of chemical energy equivalents in mitochondria (see chapter 1.2.2). ROS are at the center of oxidative stress in cells, making their contribution through a variety of mechanisms. They have the capability to oxidize nearly all organic molecules, ranging from proteins over lipids to nucleic acids. Oxidation of lipids may lead to disruption in membranes and premature cell death (Birch-Machin and Bowman, 2016), while oxidation of proteins might result in an increasing amount of defective proteins in the cells, which potentially might bring cellular protein clearance mechanisms to its limits and result in proteinaceous inclusions within or outside of cells. Particularly dangerous, however, is oxidative damage of nucleic acids, introducing mutations or resulting in predisposition for double strand breaks. Mitochondria contain multiple copies of their own, small circular genome, which is approximately 16.5kb in size and encodes for 13 subunits of respiratory complexes as well as 22 transfer ribonucleic acids (tRNAs) and 2 ribosomal RNAs (rRNAs) (Tan et al., 2015). Since mitochondria store their DNA within the mitochondrial matrix, close to the sites of oxygen metabolism, mitochondrial DNA (mtDNA) is specifically vulnerable towards oxidation (Birch-Machin and Bowman, 2016). Damage to the sugar-phosphate backbone seems to be the predominant lesion site (Shokolenko et al., 2009), while the frequency of oxidation induced point mutations is a subject of controversy (Alexeyev et al., 2013). By today, it is well established that mitochondria do contain DNA repair mechanisms, although there is still controversy to which extent. Base excision repair (BER) seems to be the predominant mechanism, and while homologous recombination (HR) and non-homologous end joining (NHEJ) as mechanisms of DNA strand break repair have been observed in mitochondria of lower eukaryotes and plants, they seem to be rather infrequent events in mammalian cells (Alexeyev et al., 2013). Some studies also show that increased ROS levels are not necessarily accompanied with a reduced lifespan or even claim that ROS could promote longevity in some species (Van Raamsdonk and Hekimi, 2009, 2012). The questions arising, are not only whether mitochondria acquire a progressive dysfunction during healthy ageing and are actively contributing to the ageing process but also whether this dysfunction is responsible for the development of neurodegenerative diseases like PD. The aspect of mitochondrial function in ageing becomes even more interesting if one takes cellular senescence into consideration, a state of irreversible growth arrest. Many studies have shown that, for example, impaired mitochondrial dynamics or increased ROS levels may not only contribute to premature cell death, but are also involved in driving cells into a senescent state. Cellular senescence has been clearly linked to and shown to contribute to ageing processes (reviewed in Ziegler et al., 2015). However, so far, research has only been able to offer associative explanations of the context of mitochondria, ageing and neurodegenerative diseases.

1.1.4.3.2. Association of mitochondria and idiopathic PD

The majority of evidence providing a link between mitochondria and PD is derived from fPD patients and models since a multitude of genetic animal models have been created in the past decades. The discovery that the neurotoxin MPTP could induce parkinsonian syndromes in humans and animals after being oxidized to MPP^+ (Nicklas et al., 1985) gave the first link of mitochondria to environmental factors and toxins. It could be demonstrated that MPP^+ is selectively taken up by dopaminergic neurons using the dopamine transporter (DAT) and subsequently accumulates and inhibits complex I of the respiratory chain in mitochondria, efficiently depleting these neurons of any kind of NADH-dependent respiration. Over the years, a variety of toxins have been identified which are able to cause parkinsonian symptoms by inhibiting mitochondrial function (reviewed in Exner et al., 2012). To take it a step further and away from animal models, a lot of researchers dared to tackle the phenomenon of molecular mechanisms of iPD in human models over the years. Supporting the MPP^+ data, it was reported from post-mortem analyses that complex I activity was found to be decreased up to about 30% in iPD patients' substantia nigra and frontal cortex (reviewed in Exner et al., 2012; Schapira et al., 1989). Furthermore, in accordance with the proposed mitochondrial free radical theory of ageing, Keeney et al., 2006 reported an increased amount of oxidatively damaged nuclear and mitochondrial DNA and suggested a miss-assembly of complex I subunits due to oxidative damage. Increased, age-dependent mutational load in the mtDNA of dopaminergic neurons, with consequences for the expression of mitochondrial proteins involved in the respiratory chain, has also been shown in other studies (reviewed in Exner et al., 2012). Several groups found in human cases, and subsequently demonstrated in animal models that mutations in or deletion of the mitochondrial transcription factor (TFAM) or the DNA polymerase subunit gamma (POLG), which are both essential for transcription and maintenance of mitochondrial DNA, cause parkinsonian phenotypes (Ekstrand et al., 2007; reviewed in Exner et al., 2012 and Orsucci et al., 2011). Ambrosi et al., 2014 demonstrated that upon exposure to the complex I inhibitor rotenone iPD patients' fibroblasts showed a significantly enhanced rate of necrotic cell death indicating higher sensitivity of iPD patients' cells to complex I insults. Furthermore, using extracellular flux analysis (Seahorse Bioscience), they were able to demonstrate that PD patients' cells displayed decreased maximal and rotenone sensitive respiration while no changes in basal respiration, glycolytic activity or ATP levels could be detected. Approaching from the transcriptional side, Zheng et al., 2010 could show that, on the basis of transcriptional profiling of the SN from PD patients, an early dysregulation of the electron transport chain was detected. Tackling the issue from yet another side, Santos et al., 2015 showed that cybrids containing mtDNA from PD patients' platelets display alterations in complex I activity, calcium buffering and mitochondrial membrane potential, accompanied by decreased ATP production and an increase in ROS levels. Moreover, dynamics were changed as the mitochondria

presented themselves in a more fragmented manner with an increased perinuclear distribution of the mitochondrial network, accompanied or caused by changes in the expression of the mitochondrial fission / fusion proteins dynamin-related protein 1 (Drp1) and optic atrophy 1 (Opa1) (for further details on mitochondrial dynamics see section 1.2.2). In summary, it can be put on record that mitochondrial function seems to have a close relation to the development of idiopathic PD as a broad spectrum of mitochondrial biology, ranging from complex activity over the electron transport and mitochondrial dynamics, has been found to be affected in PD.

1.1.4.3.3. The link of familial PD and mitochondria

As previously mentioned, PD pathology is associated with a multitude of genes which may be dysregulated due to mutations causing decrease- / or loss-of-function or even gain-of-function in their corresponding protein. A variety of those has been associated with PD by genome wide association studies (GWAS). Others have been found in families which show abnormal (early-onset / severe diseases progression) PD pathologies with high frequencies. Those genes have been validated to be at the pathological basis of PD development, yet it is even in these cases unclear how the disease actually develops. However, all of those genes have been associated with mitochondrial function, metabolism or dynamics. In the following, the most important genes will be introduced shortly within the mitochondrial context.

The most prominent, mitochondria associated pathway dysregulated in PD is the Pink-1/Parkin pathway. With over a hundred mutations reported in PD, *Parkin* makes top scorer in autosomal recessive PD cases. *Parkin* is an E3 ubiquitin ligase mediating covalent attachment of ubiquitin moieties to its substrates (Shimura et al., 2000). It has been shown to convey poly- and mono-ubiquitination, thereby being able to mediate proteasomal degradation and / or signaling, depending on the manner of ubiquitination. *Parkin* has been associated with a high protective capacity by shielding against a variety of stressors like mitochondrial stress, endoplasmic reticulum (ER) stress or proteotoxic stress. Generally, *Parkin* expression has been found to be upregulated upon increased cellular stress levels (reviewed in Exner et al., 2012). A variety of studies showed that these protective effects may be communicated by modulation of several pathways like the C-Jun-N-terminal kinase (JNK) pathway, the nuclear factor kappa-light-chain-enhancer of activated B-cells (NF-κB) pathway or the p53 pathway. A direct link to mitochondrial function has been established by discovering that Parkin directly induces proteasomal degradation of Parkin-interacting substrate (PARIS), which is an interactor of the peroxisome-proliferator-activated receptor gamma-co-activator 1-alpha (PGC-1α), a stimulator of mitochondrial biogenesis. Depletion of Parkin results in accumulation of PARIS and therefore inhibition of PGC-1α, effectively obstructing mitochondrial biogenesis (Castillo-Quan, 2011; Shin et al., 2011). *Pink1* encodes a serine/threonine kinase which is located in various mitochondrial regions, the

inner and outer mitochondrial membrane as well as the intermembrane space. In cell culture models, various studies associated Pink1 dysregulation with a reduction of mitochondrial respiration, accompanied with decreased mitochondrial ATP synthesis and higher susceptibility towards oxidative stress (Gautier et al., 2008; Gispert et al., 2009; Li et al., 2009a). Other studies showed that loss of Pink1 in neurons is accompanied by changes in mitochondrial morphology, likely due to deficiencies in mitochondrial dynamics, as well as reduced membrane potential, increased ROS production, Calcium (Ca^{2+}) overload, complex I deficiency and increased sensitivity to apoptosis (reviewed in Moon and Paek, 2015). A recent study showed that Pink1 is able to free protein kinase A (PKA) from its molecular anchor, allowing it to phosphorylate Drp1 at its serine 637 (Ser^{637}), thereby modulating mitochondrial fission (Pryde et al., 2016). In accordance with this, loss of Pink1 in mammalian cells is associated with increased fragmentation of mitochondria (Scarffe et al., 2014). Next to their single, separated actions on mitochondria, it has to be mentioned that Pink1 and Parkin act in a common pathway, with the major task of mitochondrial quality control and induction of mitophagy. Mitophagy is an essential process in the cell to reduce the load of defective mitochondrial components like mutated mtDNA or proteins with undesired oxidative modifications. Pink1 and F-box only protein 7 (FBOX7) work upstream from Parkin. Upon depolarization of mitochondria, Pink1 is not imported into mitochondria anymore and accumulates on the outer mitochondrial membrane. At the same time, cytosolic FBOX7 localizes at the mitochondrial outer membrane in a Pink1-dependent manner. Now, Pink1 and FBOX7 recruit Parkin which subsequently is activated through phosphorylation by Pink1. Next, Parkin ubiquitinates proteins on the outer mitochondrial membrane and induces the autophagy process (Scarffe et al., 2014; reviewed in Scott et al., 2017). In summary, dysregulation of Pink1 and / or Parkin does not only directly affect mitochondrial function and dynamics but also impairs clearance of impaired mitochondrial contents, mediating great effects on mitochondrial integrity in a cell.

Less is known about the direct interactions of other PD associated genes with mitochondria, although there are clear indications that they also affect mitochondrial function. To pick a few examples, DJ-1 has been shown to act as redox sensor, quickly translocating from the cytosol into the nucleus and the mitochondria upon induction of cellular stress. A variety of models exhibited that loss of DJ-1 affects mtDNA levels, respiratory control ratio and ATP production in a negative way and that DJ-1 deficient cells have increased sensitivity to mitochondrial insults (reviewed in Moon and Paek, 2015). Lrrk2, an autosomal dominantly inherited PARK gene, can localize on the outer mitochondrial membrane. Consequences and implications of this are still unclear, as loss-of or gain-of Lrrk2 function is rather implicated in neuronal and neurite outgrowth. Studies showed that overexpression of Lrrk2, no matter if wildtype or with gain-of- or loss-of-function mutation, can lead to increased mitochondrial fragmentation and Drp1 recruitment. So far, no underlying mechanism has been found (reviewed in Johri and Beal, 2012; Martin et al., 2014; Moon and

Paek, 2015). In summary, it becomes clear that mitochondria not only play a pivotal in idiopathic PD, but also seem to accommodate a central position in genetically inheritable PD, since most of the PD associated genes have been shown to influence mitochondrial processes.

1.1.4.4. Engrailed and its implications in PD

En-1 /-2 belong to the family of homeobox transcription factors and have been suggested to play a role in the development of PD for nearly 20 years. They contain a highly conserved helix-turn-helix homeodomain protein fold for DNA binding, which is in-fact conserved to such an extent that in the murine system En-1 can be replaced by its paralogue En-2 or even by drosophila engrailed homolog and still will preserve its function (Alavian et al., 2014; Hanks et al., 1995, 1998). The Engrailed proteins came into focus when it was discovered that they play a role in the isthmic organizer (IO), which is responsible for the correct and specific signaling during mid- and hindbrain development (Kouwenhoven et al., 2016). These two brain regions contain two, for the development of PD essential types of neurons, mDANs as well as serotonergic (5-HT) neurons. mDANs are characterized by the expression of a variety of specific markers, amongst which Pitx3, nuclear receptor related protein 1 (Nurr1), En-1/-2, LIM homeobox transcription factor-1 (Lmx1-A and -B), orthodenticle homeobox 2 (Otx2) and tyrosine hydroxylase (TH) present the probably most important ones. Here, the IO takes a vital role in determining correct function and size of these neuronal systems (Kouwenhoven et al., 2016). During the induction and patterning phase of mDAN development, En-1/-2 and the other transcription factors in the Nurr1-Pitx3-Lmx1a-Engrailed network (Arenas et al., 2015; Prakash, 2006) have the function to regulate and maintain fibroblast growth factor 8 (Fgf8), Sonic hedgehog (Shh), Transforming growth factor beta (Tgf-beta) and Wnt1 expression in this region in a concerted manner, which has been shown to be critical for correct mDAN development and patterning (reviewed in Alavian et al., 2014; Rekaik et al., 2015a). Later, it became clear that En-1/-2 do not only play a role in the development of mDANs but also are essential for the survival and maintenance of those neurons from late-embryonic stages onwards throughout the whole life of those neurons (Rekaik et al., 2015a). This makes the *En-1/ -2* genes even more interesting in the context of PD, as PD classically is regarded an ageing, not a developmental disease. Already in 2005, it was shown that Engrailed is not only important for the transcription of several genes, but also regulates the translation of capped messenger ribonucleic acids (mRNAs) (Brunet et al., 2005). Around the same time, it became clear that En-1/-2, like other homeobox family proteins, are able to bind the eukaryotic translation initiation factor 4E (eIF4E) (Topisirovic and Borden, 2005), therefore not only regulating transcription of a multitude of genes, but also actively regulating translation of some targets.

Since complete knockout of *En-1* and *En-2* leads to neonatal lethality (depending on the background of the mouse strain) (Rekaik et al., 2015a), several studies were conducted in *En-1*$^{+/-}$ or *En-1*$^{+/-}$ / *En-2*$^{-/-}$ mouse models. These mice develop normally, yet, after about 6 weeks after birth start losing mDANs in the SNpc until about 40% are lost until the age of 48 weeks, when their number stabilizes (Nordströma et al., 2015; Sonnier et al., 2007). Sonnier et al., 2007 were able to show that En-1/-2, if supplied as recombinant, exogenous protein to cells, causes a complete arrest of cell death. Subsequently, Alavian et al., 2009 demonstrated that Engrailed dependent survival of mDANs is mediated by repression of the pro-apoptotic activity of the neurotrophin receptor p75^{NTR} while activating in parallel the pro-survival pathway extracellular-signal-regulated kinases / mitogen activated protein kinase (Erk-1/2 MAPK). In 2011, Alvarez-Fischer et al., were able to show that Engrailed protects mDANs when exposed to rotenone, MPP^+ or 6-hydroxydopamine (6-OHDA) against induced complex I stress. This was again recapitulated when Engrailed expression antagonized cell death of mDANs when exposed to toxic α-Syn species. Furthermore, injection of En-1 protein into the striatum significantly increased dopamine content in the striatum of mice, elevating the percentage of surviving mDANs and increasing dopamine content (Alvarez-Fischer et al., 2011). Upon En-1 injection, Alvarez-Fischer et al. identified 26 regulated proteins, of which 16 located to mitochondria. Amongst those, Engrailed enhanced the production of two complex I subunits, mitochondrial NADH-ubiquinone oxidoreductase 75kDa subunit (Ndufs-1) and mitochondrial NADH dehydrogenase [ubiquinone] iron-sulfur protein 3 (Ndufs-3), thereby likely rescuing complex I function in response to toxic insults. In addition, an increase of complex I activity in En-1 treated synapto-neurosomes could be measured, which de-facto lead to an enhancement of mitochondrial metabolism (Alvarez-Fischer et al., 2011). Along this line, a more recent study showed that En-1/-2 have a strong dosage-dependent role in cellular protection against oxidative stress (Rekaik et al., 2015b). Rekaik et al. showed that loss of even one out of four alleles (2 alleles for each *En* homolog) was enough to accelerate stress-dependent cell death, against which fully functioning *En* expression protects as key regulator of DNA damage and chromatin changes, which are observed upon exposure to oxidative stress in mDANs. In summary, Engrailed is placed by many studies not only as key developmental protein but also as vital factor for mDANs maintenance and metabolism by exerting its function as transcriptional, translational and epigenetic modifier, activating short- and long-term survival pathways. As En specifically acts on mDANs, it is a highly interesting therapeutic target in the specific treatment of PD.

1.2. Cellular energy metabolism

No life can exist without energy. In eukaryotic systems, energy is largely obtained from the metabolism of chemical nutrients and stored either directly in form of the ubiquitous, intracellular chemical energy carrier ATP or chemical gradients (e.g. the mitochondrial proton gradient) with the aid of several cofactors. The energy needed for cell growth, division, protein and nucleotide synthesis or other metabolic pathways is then regained by hydrolyzing the terminal high-energy phosphoanhydride bond of ATP, yielding adenosine diphosphate (ADP) and energy which is then used to drive energetically unfavorable processes. ATP is primarily produced by two cellular processes: (a) glycolysis, which describes the process of glucose metabolization to pyruvate and is independent of the presence of oxygen and (b) oxidative phosphorylation (OXPHOS), which describes the oxygen dependent steps of aerobic oxidation of chemical nutrients and occurs only in mitochondria. OXPHOS requires the presence of acetyl-coenzyme-A (acetyl-CoA) which can be synthesized either from pyruvate – and therefore requires previous processing of glucose through glycolysis – or from fatty acid oxidation, a process called beta-oxidation, also taking place in mitochondria. It has been shown that ketone bodies are more efficient in fueling ATP synthesis than glucose, and yet, overall, the body's primary and most readily available energy substrate seems to be glucose, especially in the brain (Clarke and Sokoloff, 1999). This is the consequence of several circumstances, yet the critical one seems to be the yield of ATP synthesis tied to the response of the uncoupling of mitochondria in the corresponding cell types. The electron donor used, when metabolizing carbohydrates, is NAD^+/NADH, while ketone oxidation uses flavin adenine dinucleotide (FAD/FADH/$FADH_2$). It has been shown that OXPHOS' yield is higher when NADH is used as electron donor and since the NADH/$FADH_2$ ratio is increased for glycolysis compared to beta-oxidation, the ratio of ATP-synthesis in relation to oxygen consumption is better upon the oxidation of glucose (Leverve et al., 2007). Next, a decrease in proton motive force by uncoupling favors $FADH_2$ oxidation, thus fatty acid oxidation. It has been published that ketosis itself already induces a moderate uncoupled state and decreases oxidative efficiency compared to glucose oxidation (Prince et al., 2013) as the resulting oxygen to ATP ratio is larger in beta-oxidation. As discussed briefly before, increased oxygen consumption may lead to increased oxidative stress levels especially in highly respiratory active cells like in neuronal cell types – however, under certain conditions like fasting, even the brain is able to metabolize ketones as energy substrate yet at expense of its glucose metabolism (LaManna et al., 2009). Therefore it can be concluded that beta-oxidation provides a high rate of ATP synthesis, but comes with a high rate of oxygen consumption (Leverve et al., 2007) and brings along several other metabolic modifications. Under normal conditions and in most cell types, glycolysis will usually be the preferred pathway to precede OXPHOS and naturally the most efficient way of producing ATP in the absence of oxygen. It has to be noted that OXPHOS can also be preceded by the metabolization of several

amino acids, however under physiological conditions these are the energetically most unfavorable processes.

1.2.1. Glycolysis and its role in energy and biomass production

Glycolysis is the process by which one molecule of intracellular glucose is converted in two molecules of pyruvate. The overall chemical equation of this first stage of glucose metabolism is

$$[C_6H_{12}O_6 + 2\ NAD^+ + 2\ ADP^{3-} + 2\ P_i^{2-} \rightarrow 2\ C_3H_4O_3 + 2\ NADH + 2\ ATP^{4-}].$$

Generally, glycolysis can be divided into three process stages: (1) glucose becomes trapped and destabilized in the cell, (2) two three-carbon molecules are generated by cleavage of one six carbon molecule and (3) ATP and NADH are generated. The conversion of glucose to pyruvate encompasses a total of ten steps: first, energy needs to be invested in the form of two ATP to transform glucose to glucose-6-phosphate in order to trap the glucose in the cell and start the glycolytic process. Subsequently another ATP is invested to convert fructose-6-phosphate to fructose-1, 6-bisphosphate to energetically destabilize the six carbon molecule. After the breakdown of fructose-1, 6-bisphosphate into two molecules of glyceraldehyde-3-phosphate, the energy-yielding part of glycolysis is reached, producing two molecules of NADH and ATP per molecule of glyceraldehyde-3-phosphate. The net outcome consists of two molecules of ATP and NADH per one molecule of glucose as two ATP had to be invested at first. The key regulatory steps in this cascade are the activities of the hexokinase (step 1), the phosphofructokinase-1 (step 3) and the pyruvate kinase (step 10). The activity of hexokinase is allosterically controlled by its product, glucose-6-phosphate. The principal rate limiting enzyme is phosphofructokinase-1 which is activated by high levels of adenosine monophosphate (AMP) and fructose-2, 6-bisphoshate, which usually are increased if the cell is running low on ATP levels; vice versa, high levels of ATP and citrate inhibit phosphofructokinase-1 activity. Last, the pyruvate kinase's activity is controlled by ATP levels to slow down glycolysis if necessary. All three enzymes catalyze reactions with large free enthalpy which are virtually irreversible at biological conditions, making them perfect targets for regulation. However, even though glycolysis is an energy yielding pathway, restricting the reaction from glucose to pyruvate only results in a shift in the redox balance since glycolysis only produces NADH yet is not capable of regenerating NAD^+. Therefore, pyruvate becomes metabolized in further steps. While some organisms like e.g. yeast are capable of producing ethanol from pyruvate, the fate of pyruvate in higher organisms is usually restricted to either the production of lactate under anaerobic conditions thereby regenerating one molecule of NAD^+ per one molecule of lactate produced, or to

converting pyruvate into acetyl-CoA and feeding it into the tri-carbonic cycle (TCA) by investing another NAD^+ and CoA:

$$\text{Pyruvate} + NAD^+ + \text{CoA} \rightarrow \text{acetyl-CoA} + CO_2 + \text{NADH}$$

Even though this step consumes another NAD^+, redox balance is maintained as NAD^+ is regenerated when NADH transfers its electrons to the electron transport chain (ETC) via the NADH:ubiquinone oxidoreductase (complex I of the mitochondrial ETC) (chapter reviewed in more detail in Berg et al., 2012; Lodish et al., 2013).

Glycolysis also has a latter of other functions apart from energy production. It is a much faster process compared to OXPHOS. Some cell types, especially cells in niches with low oxygen availability, prefer glycolysis over OXPHOS even though net ATP yield is by far less and substrate demand therefore increases dramatically. Another advantage of elevated levels of glycolysis lies in its intermediary products, of which a lot are educts for many metabolic processes in the generation of biomass which allows a more rapid growth rate to those cells. For example, glucose-6-phosphate can be diverged and metabolized in the pentose phosphate pathway (PPP). This is a major source of $NADP^+$/NADPH or ribose-5-phosphate (R5P) in most cell types and provides a variety of other sugars in higher organisms. NADPH is in contrast to NADH not used as electron donor for ATP production but rather in a variety of redox-reactions (e.g. the regeneration of glutathione) or anabolic pathways like lipid biosynthesis and fatty acid metabolism. R5P is a major source for the synthesis of nucleotides and nucleic acids. A variety of other sugars serve other purposes or become metabolized to glycolysis intermediates and refed into the glycolytic cascade. 3-Phosphoglycerate is a precursor in the amino acid production, more specifically for serine, cysteine and glycine. Pyruvate itself serves not only as precursor for lactate or acetyl-CoA but is also metabolized to e.g. alanine. Further downstream, acetyl-CoA intersects with lipid biosynthesis and / or oxidation. Even more downstream, intermediates of the TCA, explicitly alpha-ketoglutarate and oxaloacetate serve as educts for glutamine and proline, aspartate and asparagine synthesis and other products, respectively. In summary, intermediary products of glucose metabolism are diverged into a variety of other processes like lipid biosynthesis and amino acid production as well as reduction equivalent production and regeneration and many more, allowing the cell to build up a working redox system as well as to gain the necessary biomass for growth and division (reviewed in Berg et al., 2012; Lehninger et al., 2008; Lodish et al., 2013).

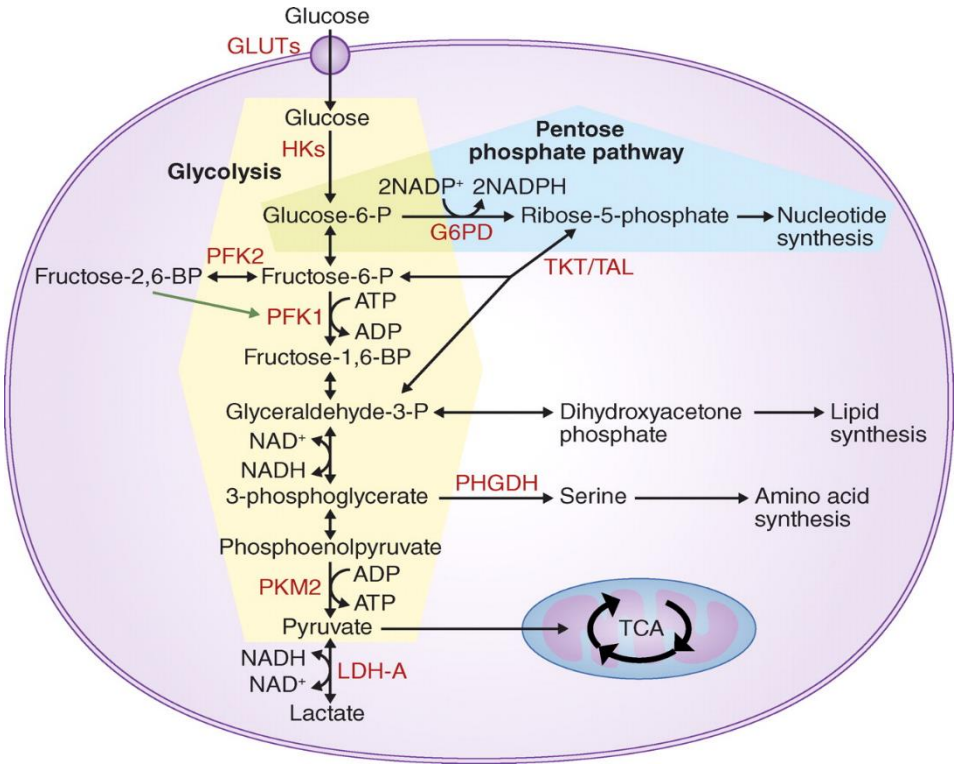

Fig. 2: The glycolytic pathway and its affiliations in cellular metabolism. *Displayed are the metabolism of glucose and its major fates upon entry into the glycolytic pathway. Abbreviations: GLUTs = glucose transporters; HK = hexokinase; PFK1/2 = phosphofructokinase; G6PD = glucose-6-phosphate dehydrogenase; TKT = transketolase; TAL = tyrosine ammonia lyase; PHGDH = phosphoglycerate dehydrogenase; PKM2 = pyruvate kinase isozyme M2; LDH-A = lactate dehydrogenase A. Figure taken from (Hamanaka and Chandel, 2012).*

1.2.2. Mitochondria: function and metabolism

Mitochondria are specialized, membrane enclosed organelles whose blatant function is to convert energy through a process called chemiosmotic coupling, next to a huge variety of other functions which have developed during evolution. Depending on the cell type in question, mitochondria can take up to 20% of the cytoplasmic volume. They are dynamic and plastic organelles, often associated with the microtubular system which determines their orientation and distribution. This allows the allocation of mitochondria to points of high energy demand which might naturally be the cytoplasm or specialized cellular superstructures like e.g. neuronal synapses. Mitochondria contain their own genome which encodes for some proteins of their complex electron transport chain, yet are also heavily dependent on nuclearly encoded proteins which have to be imported into the organelle for proper functioning. Being the main source of energy supply in aerobic conditions, acquisition of mitochondria was vital for complex organisms to evolve. Without mitochondria or oxygen, cells would have to derive all their ATP through (aerobic) glycolysis which, as already discussed, is a very quick but comparably inefficient process in terms of ATP production. In mitochondria, oxidation of glucose is completed when the pyruvate produced during glycolysis becomes

imported and ultimately oxidized to H_2O and CO_2 using oxygen. This process generates approximately sixteen times more ATP made from glucose compared to glycolysis alone.

Today we know that mitochondria originated from endocytosed prokaryotic cells which were functionalized during evolution. Like their ancient bacterial predecessors, mitochondria are made up from two separate membranes: (1) the outer membrane which surrounds the whole organelle and is, like in bacteria, freely permeable to ions and small molecules as it contains a lot of porins (membrane proteins that create aqueous pores); (2) the inner mitochondrial membrane which surrounds the mitochondrial matrix and is impermeable for hydrophilic molecules. This membrane contains highly folded structures which reach far into the mitochondrial matrix, called cristae and containing the highest amount of protein known in mammalian membranes - almost 75% protein and 25% lipid content by weight. Cristae are the site of the complexes of the respiratory system while the enzymes of the TCA are located in the mitochondrial matrix. Selected, essential molecules, ions and even electrons (from cytoplasmic NADH) are transported across the cristae and inner membrane using specialized mitochondrial transporter systems. The degree of folding, therefore the amount of cristae, is cell type dependent as its main purpose is the increase of area available for OXPHOS – highly specialized cells which rely heavily on oxidative respiration like e.g. neurons or cardiomyocytes have large mitochondria full of cristae, while less specialized cells like stem cells have premature, round mitochondria with a drastically reduced amount of cristae in comparison. The protrusion of cristae into the matrix is called cristae space and the connections where the cristae membrane intersect the surrounding inner membrane and their membranes join are termed crista junctions. Due to the aqueous pores in the outer membrane, the pH in the intermembrane space, a 20-30nm gap between the inner boundary membrane and the outer membrane, is equal to the one in the cytoplasm (physiological pH of about 7.4). The proton gradient across the inner mitochondrial membrane is needed for ATP production is generated by the proton pumps of the respiratory chain (mitochondrial complex I, III and IV) by pumping out protons from the matrix. This not only generates a pH difference across the inner mitochondrial membrane, high pH in the matrix and physiological pH in the intermembrane space, but as consequence a voltage gradient, the so called membrane potential with the negative side in the matrix and the positive side in the cristae space (reviewed in Berg et al., 2012; Lehninger et al., 2008).

The proton pumps and the F_0F_1-ATPase (mitochondrial complex V) are located in the cristae membrane. The proton pumps are usually organized in bigger super-complexes, probably to aid the electron transfer by quinones or cytochromes which diffuse across the cristae membrane and the cristae space. The remaining "mitochondrial complex" of the respiratory chain is the succinate dehydrogenase (mitochondrial complex II), an enzyme of the TCA and therefore located within the mitochondrial matrix. The NADH

dehydrogenase complex (complex I) and complex II are the responsible complexes for the coupling of the TCA to the ETC. In general terms, the ETC can be described as a series of super-complexes containing a series of iron-sulphur or heme-cytochrome / iron-copper centers, with increasing affinity for electrons along the chain. Upon shuttling of electrons through these complexes, electrons with a high energy state are gradually conveyed to electrons with a lower energy state until ultimately being used to reduce the molecule present with the highest electron affinity - an oxygen molecule ($^1/_2\, O_2$) to water (H_2O). The gradual release of energy from each electron is used by the proton pumps to transfer protons from the mitochondrial matrix into the cristae space, thereby generating a proton gradient. Complex I accepts electrons from NADH generated in the TCA or shuttled into the ETC from cytoplasmic NADH generated during glycolysis. When NADH is oxidized to NAD^+ by complex I, it gives two electrons ($2e^-$) to complex I. These electrons are wired through complex I using iron-sulphur clusters and transferred to one ubiquinone. The wiring of $2e^-$ causes a net translocation of four protons (H^+) from the mitochondrial matrix into the cristae space. Ubiquinone can freely diffuse through the hydrophobic membranes and shuttles the electrons to the coenzyme-Q:cytochrome-c-oxidoreductase (complex III), which, however, can only accept one electron at a time. As result, a complex redox loop mechanism (Q-cycle) is established allowing the recycling of the second electron by ubiquinol. In total, this process releases two protons per electron, since upon reduction, ubiquinone takes up two protons from the mitochondrial matrix and the resulting ubiquinol releases these protons into the cristae space upon oxidation at complex III. Complex III wires the electrons through an iron-sulphur cluster to the next carrier, cytochrome c. Cytochrome c can also only take up one electron at a time as it only contains one iron cluster and is reduced to ferrocytochrome c. Last but not least, the cytochrome c oxidase (complex IV) accepts the electron from ferrocytochrome c and transfers it through its iron-copper center to $^1/_2\, O_2$, reducing oxygen to water. This process again yields a net shuttling of four protons across the membrane into the cristae space. Next to complex I, an additional source for electrons is complex II which transfers electrons released during the oxidation of succinate to fumarate, using an $FAD^+/FADH_2$ group, to an ubiquinone and subsequently to complex III. Complex II itself does not shuttle protons across the membrane and is therefore not considered a proton pump. The generated proton gradient is then used by the F_0F_1-ATPase to create ATP from ADP. The F_0F_1-ATPase is considered an ancient molecular machine, originating from the initial endocytosed bacteria. The protons flow through the ATPase back into the matrix thereby causing a rotation of the ATPase. This rotation causes conformational shifts, of which one conformation has a high affinity binding site for ADP and inorganic phosphate (P_i). Upon further rotation, these two substrates are mechanically forced together to form ATP, creating chemical energy from mechanical force. In general terms, every molecule of NADH and its electrons flowing through the ETC result in the formation of approximately 2.5 molecules of ATP, while every $FADH_2$ produces about 1.5 molecules of ATP. For one molecule of glucose this adds up to a total of roughly 30-32 ATP produced

if oxidized completely to H_2O and CO_2. Complete oxidation of one molecule of glucose, that is two molecules of pyruvate imported into mitochondria, requires the TCA. The TCA comprises eight reactions which result in the full oxidation of acetyl-CoA, producing three NADH, one $FADH_2$ and one guanine triphosphate (GTP) (or ATP) per molecule of acetyl-CoA (reviewed in Berg et al., 2012; Lehninger et al., 2008).

Again, the intermediates of the TCA serve more purposes than just ATP production, they are also needed in a variety of biosynthetic pathways. To name only a few examples, citrate serves as precursor for fatty acid and sterol synthesis, alpha-ketoglutarate for glutamate, glutamine, arginine and proline as well as purine synthesis. Succinyl-CoA is used in the synthesis of porphyrins and heme and oxaloacetate functions in the biosynthesis of aspartate, asparagine and pyrimidines as well as several of other molecules like serine or glycine. However, once more there is a higher purpose to mitochondria than "just" metabolizing carbohydrates, fats and amino acids in catabolic reactions and exerting critical anabolic roles to provide the carbon frame for the biosynthesis of many biomolecules. Mitochondria are essential for the biosynthesis of heme groups – iron sulfur clusters are not only necessary for proper function of the mitochondrial electron transfer but also play major roles in oxygen transport and stability of the nuclear genome. Mitochondria are even indispensable for the biosynthesis of membranes: first, cardiolipin, a phospholipid that only occurs in and is essential for the inner mitochondrial membrane, is synthesized there. Second, mitochondria are also a major source of phospholipids, needed for the biogenesis of other cellular membranes. Furthermore, there are several other metabolic pathways that mitochondria play major roles in, like the one-carbon metabolism, the central nitrogen metabolism (metabolizing glutamate by transamination reactions) and the urea cycle, of which half of the reactions take place in mitochondria (reviewed in Brand et al., 2013). Next to metabolic functions, mitochondria also are critical organelles for buffering the redox potential in the cytosol, are important calcium buffers which has many implications but is particularly important in neuronal signaling or muscle cell contraction. Last but not least, mitochondria play a major role in (the initiation of) apoptosis, which often is connected to their other functions like ATP production or calcium buffering (reviewed in Berg et al., 2012; Lehninger et al., 2008).

It's been mentioned earlier that mitochondria are dynamic organelles, which will now be introduced in more detail. Mitochondrial dynamics largely depend on a few members of the dynamin protein family, which mediate mitochondrial fission and fusion. Fusion is mainly facilitated by three proteins in mammals, two homologs called mitofusin-1 (Mfn1) and mitofusin-2 (Mfn2) as well as Opa1, which mediate outer and inner mitochondrial membrane fusion, respectively (Chen et al., 2003). All three proteins contain common motives in form of a GTPase domain, a middle domain, a variable domain and a GTPase effector domain

(GED). Accordingly, fusion (and also fission) has been shown to require GTP, while only inner membrane fusion additionally requires an intact membrane potential. Fusion is proposed to function by a soluble NSF attachment protein receptor (SNARE)-like mechanism, i.e. two opposing proteins on each membrane dimerize and force the membranes together (reviewed in van der Bliek et al., 2013). Fusion of outer and inner membrane is usually coordinated. In some cases however, inner membrane fusion has been observed to be not coordinated, due to loss of membrane potential or mutations in *Opa1*. Underlying biological implications or relevance are not clear (van der Bliek et al., 2013; Olichon et al., 2003). In contrast, fission is largely regulated by only one protein (and few adaptor proteins), Drp1, which also contains a GTPase, middle, variable and GED domain similar to the fusion proteins. In short, Drp1 is thought to assemble into multimers, with the GTPase domain facing away from the membranes and forming spirals, turning upon GTP hydrolysis and in this manner driving inner and outer mitochondrial membrane apart (reviewed van der Bliek et al., 2013). While mitochondrial fusion is mainly regulated by proteolysis of the fusion proteins, mitochondrial fission is mainly regulated by phosphorylation and ubiquitination of Drp1 at three different sites, Serine at position 616 (Ser^{616}), at position 637 (Ser^{637}) and at position 693 (Ser^{693}). Depending on which kinase phosphorylates Drp1 at which site, protein function is activated or inhibited by increased or decreased binding affinity to other fission proteins. For example, S616 can be phosphorylated by protein kinase C (PKC) δ, cyclin dependent kinase 1 (CDK1/CyclinB) or Ca^{2+}/calmodulin-dependent protein kinase 1 (CAMK-Ia), resulting in a Drp1 activating phosphorylation (reviewed in van der Bliek et al., 2013; Knott et al., 2008). Phosphorylation of S637 by PKA on the other hand has been shown to be an inactivating phosphorylation (Cereghetti et al., 2008; Chang and Blackstone, 2010).

Mitochondrial fission and fusion are crucial to the central function of mitochondria in the cell, ranging from cell division over quality control to response to metabolic stress. For example, as mitochondria are not generated “de-novo” in a cell, an appropriate amount of mitochondria needs to be provided by fission/fusion events for a daughter cell upon cell division. In quality control, fission / fusion events are used to remove defective compartments, proteins or mtDNA molecules from mitochondria which then undergo autophagy and are degraded. Without fission, fusion and mitophagy, homogeneity could not be ensured and accumulation of defective proteins and mutated mtDNA molecules would be severe. Fission and fusion are also needed to respond to opposing effects of metabolic stress: when nutrients are scarce, fusion is increased (or fission decreased) to form large mitochondrial networks in order to avoid excessive autophagosomal degradation of mitochondria, while in times of high stress, e.g. when ROS are produced excessively, mitochondrial fission has been found increased (van der Bliek et al., 2013; Safiulina and Kaasik, 2013; Westermann, 2010; Youle and van der Bliek, 2012). Moreover, energy requirements in the cell need to be adapted to the fate of a cell. As a consequence, it is often observed that mitochondria in certain cell types like neurons undergo more fission than others. Increased fission accounts for an increased number of

mitochondria in a cell which allows precise fine-tuning of energy metabolism in distinct compartments of the cell, for example in synapses (Safiulina and Kaasik, 2013). On the other hand, increased fusion has been observed in strongly proliferative cells as it's been related to increased energy production, protection against apoptotic stress and increased cell proliferation as well as regulation of several other cellular pathways (Hoitzing et al., 2015).

As a concluding remark, it has become clear that mitochondria are central in mammalian metabolism. Not only are they the major source of energy for most cells, they are also place of many crucial cellular biochemical pathways and take vital parts in the control of cellular integrity and cellular signaling by a vast variety of mechanisms.

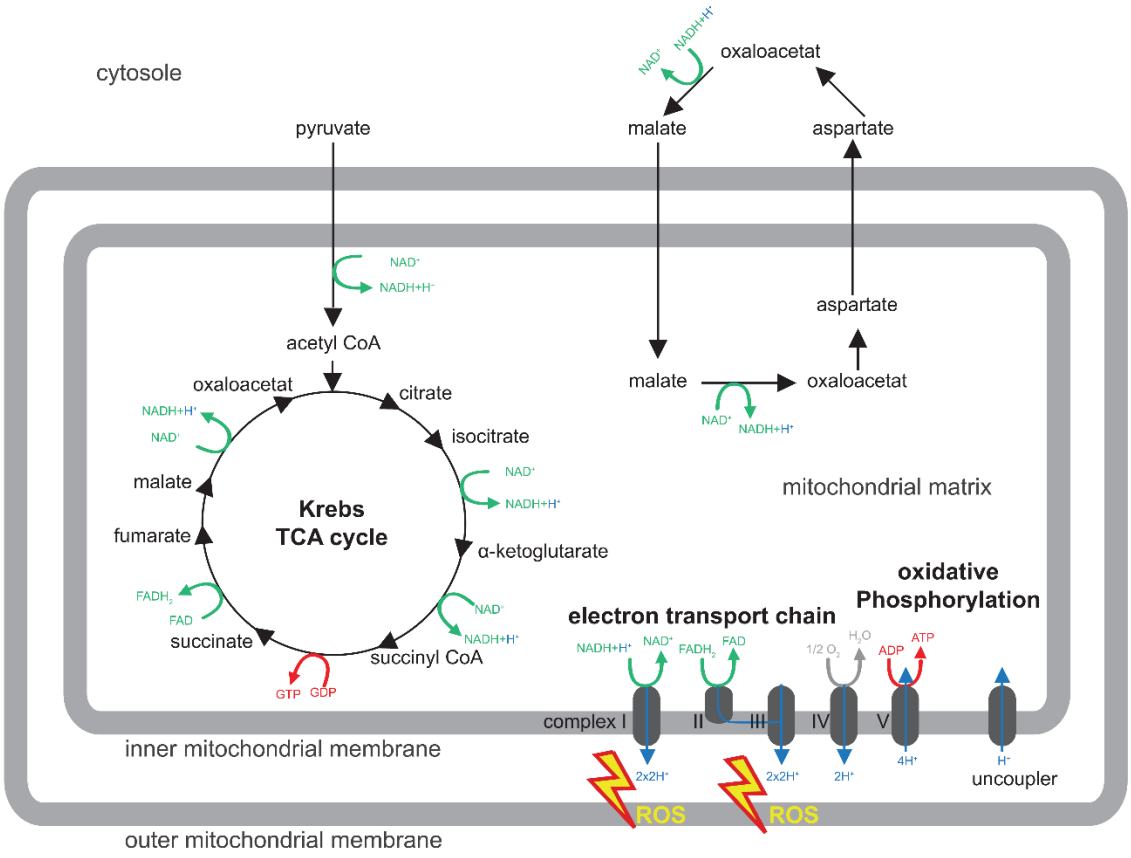

Fig. 3: Schematic illustration of mitochondrial metabolism. *Displayed are the TCA in its single steps, as well as the electron transport chain, its sites of ROS production (complex I and III) and sites of oxidative phosphorylation (complex V). Additionally, the mitochondrial malate-aspartate shuttle is displayed as example of a mitochondrial shuttle system. Fatty acid metabolism is not taken into account here. Figure taken from (Beckervordersandforth, 2017).*

1.3. Induced pluripotent stem cells

In 2007, the lab of Shinya Yamanaka succeeded in reprogramming adult, human fibroblasts into pluripotent cells, so called "induced pluripotent stem cells" (iPSCs) by retroviral delivery of four factors: octamer binding transcription factor 4 (Oct3/4), (sex determining region Y)-box 2 (Sox2), c-Myc and kruppel-like factor 4 (Klf4) (Takahashi et al., 2007), later termed *OSKM* factors. This opened the door for the whole research community to explore a spectrum of stem cell based research which was difficult to access before as the process of reprogramming basically eliminates the ethical factor attached to human embryonic stem cells. Envisioned possibilities ranged from *in vitro* derived cells and even organs for targeted drug screenings over organoids for modelling diseases affecting tissues which are difficult to obtain from human sources to autologous cell replacement therapy, i.e. taking easily accessible cells from a patient, reprogram them into iPSCs and afterwards differentiate them to a desired cell type like neurons and transplant them back into the diseased tissue. Ten years later, iPSC research has made great advantages with steadily improving reprogramming and differentiation protocols. Some of these ideas, like tissue specific drug and toxin screenings, were realized or are within grasp today even though improvement is still necessary. Nowadays, iPSC based disease models are a well-established constitution with an increasing amount of research in *in vitro* models, which can to some extent replace *in-vivo* models.

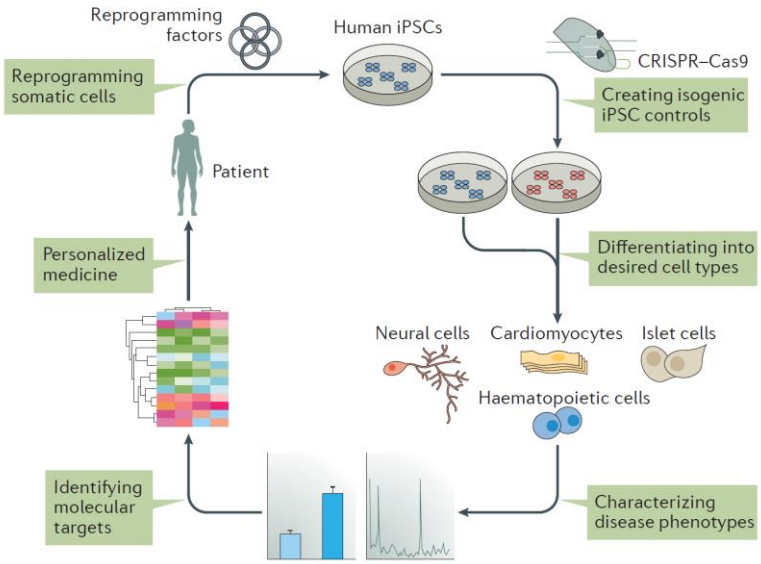

Fig. 4: iPSC based disease modeling and personalized medicine. *Easy accessible cells like fibroblasts are taken from patients and reprogrammed into human iPSCs. As next step, if applicable, iPSC may be genetically modified and then differentiated into the cell type of interest in order to further characterize the disease and personalize treatment. Figure taken from (Shi et al., 2017).*

Induced pluripotent stem cells are characterized by a variety of factors. By morphological analysis, they show properties of human embryonic stem cells (hESCs). As measurement of pluripotency cells have to at

least stain positive for Oct3/4, Sox2, stage-specific embryonic antigen-1 / -3 or -4 (SSEA-1 / -3 / -4), Tra-1-60 and Nanog. Furthermore, iPSCs have the capability to form teratoma, a tumor with cell types from all germ layers, when injected into immune-deficient mice. Instead of teratoma assays, tetraploid complementation assays (4n complementation) have been suggested as new gold standard, since this not only demonstrates capability of producing all germ layers but also capability of producing extra-embryonic tissue (Carey et al., 2011).

During the process of reprogramming, the target cells undergo several phases: initiation, maturation and stabilization. In the initiation phase which usually encompasses the first 3-4 days of the reprogramming process, cells downregulate markers for their specific cell type and undergo a major wave of transcriptional changes involving mRNAs, micro RNAs (miRNAs) and long-non-coding RNA (lncRNAs) and starting with OSKM expression. These changes modulate cellular proliferation, metabolism, cytoskeleton organization and developmental processes. Examples of the upregulated genes range from epithelial genes (e.g. *cadherin-1 (Cdh1))* over early pluripotency genes (e.g. *alkaline phosphatase (Alp1) and F-box protein 15 (Fbx15*)) to genes regulating DNA replication and cell cycle progression (e.g. *DNA polymerase iota (Poli) and Cyclin-D1 (Ccnd1)).* In the maturation phase, cells undergo an initial period of stability, which towards the end is followed by a second wave of transcriptional and proteomic changes, mostly affecting hypoxia-responsive genes and stem cell genes (*Oct3/4, Sal-like protein 4 (Sall4), Nanog, estrogen-related receptor beta (Essrb)*). The maturation phase comes to an end when *Sox2,* among other pluripotency genes, is upregulated. However, it seems that at this stage not the classical OSKM factors seem to be the important pluripotency genes, but rather pluripotency genes like *Lin28* and *Essrb*. The last phase, the stabilization phase, is characterized by the iPSCs becoming independent from the "exogenous" expression of the OSKM factors. Now, telomeres are actively elongated, DNA changes occur including reactivation of the second X chromosome in female cells and genes responsible for epigenetic changes are upregulated (section reviewed in detail in González and Huangfu, 2016).

Over time, a variety of reprogramming factors and methods have been found, all with specific (dis-) advantages. The Yamanaka lab used retroviral delivery of four reprogramming factors and could report an efficiency of approximately 0.01% (Takahashi et al., 2007). Since retroviral delivery only targets dividing cells, soon lentiviral delivery was performed, which approximately doubled reprogramming efficiency. However, this did not solve the issue of transgene and viral backbone integration into the genome, making these approaches unsuitable for cell replacement approaches (reviewed Rao and Malik, 2012). Even though systems combined with a *Cre/loxP*-system, with *cre*-sites flanking the 3' and 5' untranslated regions (UTR) of the viral genomes, resulted in a stable generation of iPSCs, a residual *loxP* site remains in the genome (Soldner et al., 2009). Today, there is a latter of integration-free delivery methods for reprogramming: adenoviral delivery shows no transgene integration, however, a reprogramming efficiency of approximately

0.0002% makes it not really make it feasible. Much more promising is delivery by Sendai virus. Sendai viruses contain only a RNA genome and are thereby able to produce large amounts of protein without integrating their genomic material into the host genome. Indeed, reprogramming efficiencies of over 1% were achieved with human fibroblasts and the Sendai viruses were faded out of the hosts' cytosol with passaging (Fusaki et al., 2009; Rao and Malik, 2012). A variety of non-viral delivery methods has been developed, ranging from direct protein delivery over synthetic or modified messenger RNA (smRNA / mmRNA) and miRNA transfection to DNA delivery in form of transposons (piggiyBac, sleeping beauty (SB)), minicircle vectors and episomal plasmid delivery (reviewed in Rao and Malik, 2012; Sebe and Ivics, 2016). Of those, the most promising approach in terms of efficiency, price and handling is the delivery of an episomal plasmid, reaching efficiencies of up to 0.02% (Rao and Malik, 2012). As delivery of genetic material never comes without the risk of undesired foot-printing in the target cells, methods of chemically inducing pluripotency have been started to be developed. Until today, a variety of groups has published the generation of iPSCs by chemical means without aid of genetic material (Hou et al., 2013; Park et al., 2015). However, also those approaches do not resolve the issue of low efficiency either (reviewed in Biswas and Jiang, 2016). In summary, so far, the most promising, footprint-free reprogramming methods are factor delivery by Sendai virus and episomal plasmid transfection, as both methods show good reprogramming efficiencies in a variety of cell types without leaving a DNA footprint in the host cell. Cells in this thesis were reprogrammed by TP1 (Supplementary Tab.1) of the Bavarian ForiPS consortium using the Yamanaka protocol, retroviral delivery of the OSKM factors.

Next to the delivery of reprogramming factors, it turned out that a variety of other factors are important for generating iPSCs for human disease-based models of good quality. It has been reported that the majority of OSKM reprogrammed iPSCs have reduced differentiation potential in comparison hESCs and that they may show (epi-)genetic aberrations distinct from ESCs (Buganim et al., 2014). Several studies demonstrated that during the reprogramming process, the quality of iPSCs can be affected by factors like stoichiometry, culture conditions and supplements to derive iPSCs. Factors like absence of serum but presence of vitamin C or high levels of Oct3/4 and Klf4 in comparison to Sox2 and Myc have been shown to play vital roles during the derivation of iPSCs (Carey et al., 2011; Esteban and Pei, 2012). In a concluding remark it can be noted that the field of iPSC research had to and still has to overcome many challenges before iPSCs actually may be used in mainstream therapeutic applications, ranging from the multiplicity of factors influencing the derivation of iPSCs to the multiplicity of factors needed for differentiation of the same. However, despite all challenges, after ten years, iPSCs have proven themselves a highly useful resource for research, ranging from *in vitro* disease modeling to a better understanding of developmental processes.

1.3.1. Metabolism of iPSCs

It has been mentioned shortly that during the reprogramming process cells undergo a variety of changes ranging from transcriptional and epigenetic changes to metabolic ones. In order to reprogram cells, they have to undergo a so-called metabolic switch. As already explained above, most of the terminally differentiated cells in the body produce the majority of their ATP using OXPHOS, whereas PSCs and also cancer cells rely on glycolysis as main ATP supply. It has been shown a long time ago that cancer cells, or all rapidly dividing cells for that matter, switch their metabolism to a glycolytic one for multiple reasons: (a) in solid tumors, oxygen supply often becomes scarce the larger the tumor becomes, (b) a high rate of glycolysis is needed to create the precursors for biomass production which are needed for fast growth (due to which reason tumor cells prefer an incomplete mitochondrial metabolism, rather exporting citrate and alpha-ketoglutarate from the mitochondria) and (c) tightened maintenance of an appropriate redox balance (Cairns et al., 2011; Cheong et al., 2012). Physiologically speaking, PSCs experience similar environments, since the oxygen content in blastocysts ranges somewhat around 1% and cells have to maintain relatively quick growth rates and therefore may have adapted to a metabolism with increased glycolytic rates (Mohyeldin et al., 2010). In consequence, it is not surprising that reprogramming under low oxygen availability significantly enhances the process (Yoshida et al., 2009), likewise does induction of glycolysis or inhibition of OXPHOS (Zhu et al., 2010). For the coordination of this metabolic switch, hypoxia-inducible factors (HIFs) have been shown to play a vital role, as they represent the predominant oxygen sensing and controlling mechanism in the cell. In context of reprogramming, HIF2α has been shown to bind the promotor region of *Oct3/4* and knockdown of HIF1α or HIF2α resulted in decreased reprogramming efficiency (Covello et al., 2006; Mathieu et al., 2014). In the last section, it was mentioned that c-Myc, and for that matter also other oncogenes, enhances reprogramming efficiency – here it has to be noted that HIF and c-Myc have been shown to act in concerted manner to reprogram cellular metabolism and induce a metabolic switch (Gordan et al., 2007).

The metabolic switch is not only exerted through an increase in glycolysis. As reprogramming goes along with an increased growth rates, also the PPP metabolism is increased as it delivers important intermediates for biomass production as well as high levels of NADPH needed for cellular redox reactions. Furthermore, mitochondria undergo drastic changes: while in terminally differentiated cells like neurons or fibroblasts, mitochondria are responsible for the majority of ATP production, and therefore often assume large and / or interconnected structures with a high amount of cristae, located all over the cell or at locations of high energy demand, mitochondria in PSCs are comparatively small with roundish morphology and aligned around the nucleus. This change in morphology has been termed “re-maturation” since they develop back into premature, ESC-like mitochondria with less cristae and decreased mitochondrial metabolism (Folmes

et al., 2011; Prigione et al., 2010). Furthermore, mitochondrial DNA copy number, oxidative stress, expression of antioxidant genes and ATP production have been reported to decrease upon reprogramming, while expression of mitochondrial biogenesis genes and lactate production have been reported to be increased (Prigione et al., 2010). Another more recent study, however, shows that mtDNA copies in fact increase upon reprogramming, not decrease (Kang et al., 2016), which will be discussed in detail later on.

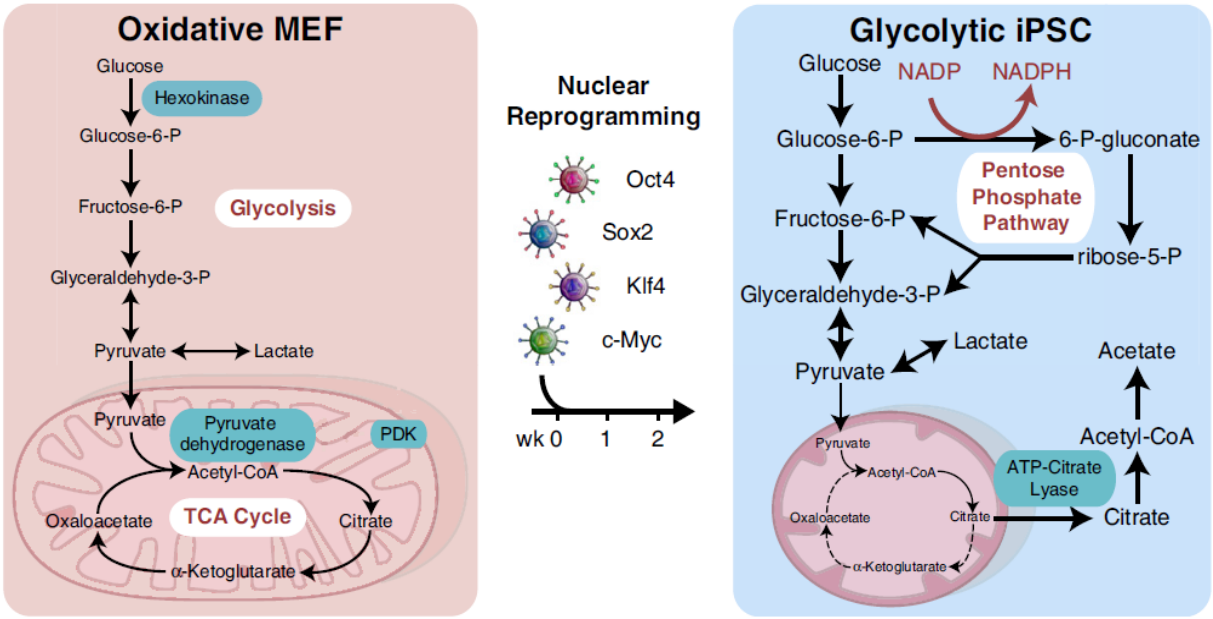

Fig. 5: Metabolic switch upon reprogramming. *Terminally differentiated cells have fully mature mitochondria with high cristae content as they usually rely on OXPHOS to produce the majority of their ATP. Upon reprogramming, they adapt ESC-like mitochondria, which are premature and aligned around the nucleus. Premature mitochondria show round morphology with drastically reduced amount of cristae, as PSCs rely to great extent on glycolytic energy production. Figure taken from (Folmes et al., 2011). Abbreviations: Oct4 – octamer binding transcription factor 4; Sox2 – (sex determining region Y)-box 2; Klf4 – kruppel-like factor 4; TCA cycle – tricarbonic acid cycle.*

Upon differentiation of iPSCs into precursor or terminally differentiated cells, it has been shown that mitochondria mature again and cells assume the metabolism suitable for the specific cell type (Choi et al., 2015; Folmes et al., 2012).

1.4. Aim of this thesis

This thesis is embedded into the PD research of the Bavarian ForiPS consortium. As previously explained, iPD is thought to be a multiple hit disease, for whose development more than one pathological factor has to be present at one time. Today we know that some of these factors are of genetic origin, while also ageing, environmental contributions like toxins, which lead to the association of mitochondria to PD, and other factors play a major role in PD development. A huge variety of studies conducted could strengthen the association of mitochondrial pathology in PD in both, hereditary and idiopathic cases of PD.

Reprogramming of patient specific cells into induced pluripotent stem cells opened up a whole new field of models for research as it is possible now to analyze both, early and late pathological developments in, already diagnosed patients' specific cells. To this purpose, the work of this thesis focused on three different major points: (1) assessment of mitochondrial function in iPSCs and their derivates, (2) analysis of bioenergetic and metabolomics differences in iPD patients' in relation to matched controls' cells and (3) changes in the differentiation potential of patients iPSCs. These issues are of high importance, as they may deliver new starting points and strategies for novel drug research or early diagnosis of PD.

The hypothesis investigated behind this thesis is that mitochondrial dysfunction in the cells of iPD patients is already present at iPSC stage but will not be readily detectable but rather has to be unmasked by cellular stressors, such as toxins, nutrient deprivation or ageing. To this purpose, this thesis describes a thorough metabolic and molecular analysis of iPD patient's iPSCs and neural precursor cells compared to matched controls.

2. Results

2.1. Model systems and the ForiPS consortium

This thesis was embedded in the research of the ForiPS consortium (Erlangen, Bayern). A complete list of the ForiPS consortium participants is given in supplementary Tab. 1. A group of patients and corresponding controls was collected by the core project of the ForiPS consortium (J. Winkler, Z. Kohl and B.Winner, UKFZ and IZKF Erlangen respectively) and the patients thoroughly examined. These individuals donated skin samples which were subsequently reprogrammed into human induced pluripotent stem cells by the core project. In total, at least three clones per patient were reprogrammed and pluripotency as well as karyotype of each individual clone was assessed by the core project (supplementary Fig. 1). Following, the core project distributed patient and control iPSCs to the other projects within the consortium. To ensure that all samples represent cases and molecular features of idiopathic PD only, all cells were screened in the side projects 2 and 3 (A. Reis, FAU, UKFZ Erlangen and M. Riemenschneider University of Regensburg) for known genetic and epigenetic markers of fPD. Samples which displayed fPD markers were excluded from this thesis.

In total, this project received 24 iPSC lines from 7 iPD patients and 5 age-matched control individuals (2 clones per individual) from the core project, which were all used in this thesis (Tab. 2). Those cells were analyzed in the iPSC stadium as well differentiated into a neuronal precursor stadium and further terminally into neurons, of which both were again analyzed.

Patient	Age (at Biopsy) [years]	Gender	Time since Diagnosis (at Biopsy) [years]
UKERiJ2C-R1-012 UKERiJ2C-R1-015	73	Male	3
UKERi1JF-R1-011 UKERi1JF-R1-018	42	Male	Control
UKERiM89-R1-005 UKERiM89-R1-006	64	Male	3
UKERiC99-R1-007 UKERiC99-R1-008	68	Male	7
UKERiR66-R1-007	54	Male	3

UKERiR66-R1-014			
UKERiG3G-R1-032 UKERiG3G-R1-039	69	Female	Control
UKERi1E4-R1-012 UKERi1E4-R1-016	53	Male	Control
UKERiAY6-R1-003 UKERiAY6-R1-004	37	Male	4
UKERiPX7-R1-001 UKERiPX7-R1-002	49	Male	1
UKERi88H-R1-001 UKERi88H-R1-002	63	Female	6
UKERiO3H-R1-003 UKERiO3H-R1-005	71	Male	Control
UKERi82A-R1-001 UKERi82A-R1-002	66	Female	Control

Table 2: Collection of patients and control individuals including corresponding clones within the ForiPS consortium, UKFZ Erlangen. *Individuals were acquired and biopsied by the core project (J. Winkler, Z. Kohl, UKFZ Erlangen). Reprogramming from fibroblasts to induced pluripotent stem cells was done by the core project and subproject 1 (B. Winner, IZKF Erlangen). All lines are encompassed in low-passage analyses, lines marked in blue were encompassed in high-passage analysis (see section 2.2.1, section 2.2.3 and section 2.3).*

2.2. Respiratory analysis

Respiratory analysis of all samples in this thesis was done using a Seahorse XF96 analyzer. The Seahorse XF technology allows real-time parallel assessment of the oxygen consumption rate (OCR) and the extracellular acidification rate (ECAR). The OCR can be used to assess mitochondrial function and ATP production as oxygen consumption is coupled to OXPHOS and therefore is an indirect function of mitochondrial metabolism (Divakaruni et al., 2014). By adding several components in a defined series of injections, an integral picture of mitochondrial and cellular respiration can be obtained, which is subdivided into measurements of basal respiration, oxygen consumption attributed to ATP production and to the proton

leak, maximal respiration and spare respiratory capacity. In a first step, the basal cellular oxygen consumption is measured, which is, after subtraction of the non-mitochondrial oxygen consumption, composed of oxygen consumption for ATP synthesis plus the oxygen consumption which is associated with proton leak pathways (Divakaruni et al., 2014). The proportion of each factor contributing to the basal respiration can be measured by the addition of oligomycin, which is a potent and specific F_0F_1-ATPase inhibitor. By binding subunit-c of F_0-portion of the F_0F_1-ATPase, oligomycin has been proposed to block proton translocation through the F_0F_1-ATPase, thereby effectively making the protein non-functional while leaving the mitochondrial proton gradient intact (Symersky et al., 2012). The resulting oxygen consumption devoted to ATP production is influenced by three major factors, cellular ATP consumption, ATP synthesis and substrate supply and oxidation. Naturally, ATP production is adapted to cellular ATP consumption for maintenance of the normal cellular metabolism, making this a major contributor. However, variances in oxygen consumption devoted to ATP production can also be the result of an impaired F_0F_1-ATPase, substrate deprivation or oxidation deficiency, resulting in a decrease in the proton gradient driving the F_0F_1-ATPase (Divakaruni et al., 2014). Proton-leak linked respiration consists of oxygen consumption due to protons being shuttled back through the membrane, thereby uncoupling the proton gradient to a small extent and not contributing to ATP production, but rather stimulating the respiratory chain to maintain its proton gradient (Divakaruni et al., 2014). After the assessment of basal respiration and its proportions of oxygen consumption for ATP production and due to the proton leak, the maximal respiratory capacity is measured by the addition of carbonyl cyanide 4-(trifluoromethoxy)phenylhydrazone (FCCP). FCCP, a so-called protonophore, shuttles protons from the intermembrane space into the matrix of mitochondria, thereby breaking down the proton gradient. FCCP is a protonated weak lipophilic acid (A^-H^+) which can diffuse as A^-H^+ from the intermembrane space through the membrane into the matrix, where it dissipates from its proton reducing ΔpH and diffuses back into the intermembrane space as anion (A^-). The anion is also soluble in lipid phase since the charge distributes across its aromatic ring (Benz and McLaughlin, 1983). The resulting breakdown of the protein gradient stimulates maximal mitochondrial respiration, since the cells will try to re-establish the proton gradient necessary for ATP synthesis. The measurement of maximal respiratory capacity also reveals the spare respiratory capacity, i.e. the un-used respiratory capacity, by subtracting basal from maximal respiration. The spare respiratory capacity can be, usually depending on the cell type, a very important asset of mitochondrial respiration. While cells which predominantly grow and divide, like e.g. tumor cells, will highly likely not have a large spare respiratory capacity as they will have a constant high energy demand, cells like e.g. neurons will have high respiratory capacity to be capable of coping with the energetic challenges of firing and building up the necessary action potential (Divakaruni et al., 2014). After obtaining the maximal respiratory capacity, mitochondrial respiration is blocked by addition of the complex I and III inhibitors, rotenone and antimycin-A respectively. This is necessary to

assess the non-mitochondrial oxygen consumption, which in the end is subtracted from all other measured values to normalize for mitochondrial oxygen consumption.

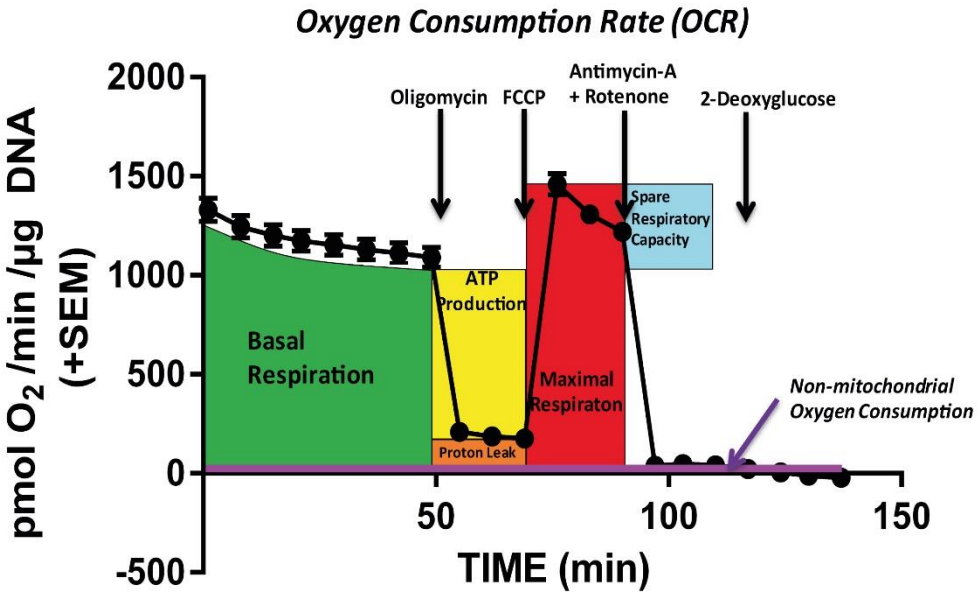

Fig. 6: Exemplary presentation of the oxygen consumption rate (OCR) obtained in a standard Seahorse XF96 run. *First, basal respiration is obtained, which then is subdivided into oxygen-consumption devoted to ATP production and due to the proton leak, by the addition of oligomycin, a selective F_0F_1-ATPase inhibitor. Next, the mitochondrial proton gradient is uncoupled using FCCP, a protonophore which allows the measurement of the maximal respiration, while cells try to re-establish the mitochondrial proton gradient. Finally, complex I and complex III are inhibited using rotenone and antimycin-A to obtain the non-mitochondrial oxygen consumption in order to normalize the OCR to mitochondria.*

Respiratory analyses are carried out in a special medium, supplied from the manufacturer, which is not buffered against pH changes (Agilent Seahorse XF Assay Medium). This allows the parallel measurement of OCR and ECAR. While OCR measures oxygen consumption, ECAR is thought to be a rough function of glycolytic metabolism. Without regard for reactions involved in biosynthesis and anabolism, the oxidation of glucose produces protons (H^+), anions (pyruvate and lactate) as well as CO_2 (during OXPHOS), all of which have the capability of acidifying the medium. Without taking exact numbers in consideration, it is important to note that cellular ATP met by glycolytic production acidifies the environment substantially stronger (1 H^+/ATP) in comparison to glucose being fully oxidized by OXPHOS (Divakaruni et al., 2014). Yet one needs to remember that the ECAR only offers a rough overview about glycolytic rates and is therefore much more complex to interpret (for details see Divakaruni et al., 2014), since a variety of other processes and reactions simultaneously occurring in the cell also contribute to acidification of the cellular environment.

Like when measuring the OCR, first the basal ECAR, i.e. the basal rate of glycolysis is assessed. Following oligomycin addition, mitochondrial contribution towards ATP synthesis is inhibited, leading to increased

rates of glycolysis in order to level cellular ATP demand and synthesis. This is considered the maximal glycolytic capacity. Measuring maximal glycolytic capacity directly also gives an estimation of the glycolytic reserve, i.e. the maximal possible increase of the rate of glycolysis above basal levels (maximal – basal glycolytic activity). Addition of FCCP spikes the ECAR again, since it leads to an increase in OXPHOS and therefore increased CO_2 production in the TCA. Finally, glycolytic activity is inhibited by addition of large excess of 2-deoxyglucose (2-DG), which allosterically inhibits glycolysis at the step of hexokinase, where it accumulates in the form of 2-deoxyglucose-6-phosphate. This delivers the non-glycolytic ECAR, which is subtracted from all other values for normalization purposes.

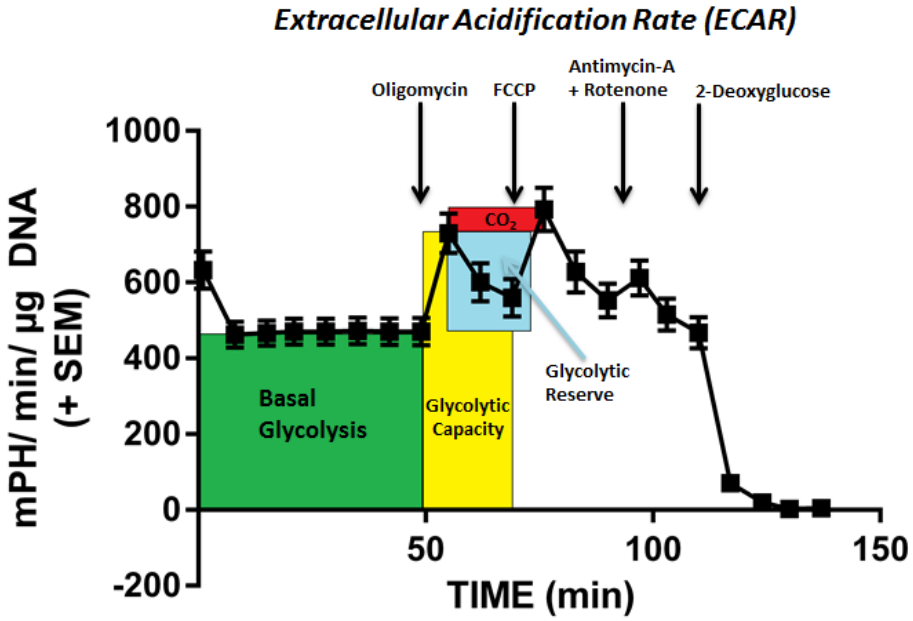

Fig. 7: Exemplary presentation of the extracellular acidification rate (ECAR) obtained in a standard Seahorse XF96 run. *First, basal ECAR, i.e. basal rates of glycolysis are measured. By addition of oligomycin, maximal glycolytic capacity and glycolytic reserve can be assessed. Addition of FCCP yields acidification of the medium by increased release of CO2 from the mitochondria. The whole measurement is finally inhibited by the addition of 2-deoxyglucose, which delivers the non-glycolytic ECAR for normalization purposes.*

2.2.1. Respiratory characterization of low- and high passage iPSCs form iPD patients

Low passage iPSCs (passage 15 to 30, with passage 1 being the first passage as iPSCs after reprogramming), as obtained from the core unit from the ForiPS platform, from iPD patients and corresponding controls (in total 24 lines, 7 PD patients and 5 controls with 2 clones per individual) were analyzed using the Seahorse XF96 analyzer. Cells were analyzed in Seahorse XF assay medium supplemented with either 25mM glucose (Fig. 8) or 5mM pyruvate (Fig. 10), like described in methods section 4.2.3.1.2. 25mM glucose were chosen as excess substrate wanted to be given as the cells and their mitochondria are exposed to high stress levels which might consume substantial amounts of substrate. Similar, a concentration of 5mM was chosen for pyruvate, as an intracellular concentration of above 5mM pyruvate might result in free diffusion rather than controlled transport of pyruvate into mitochondria.

It has been mentioned earlier that idiopathic PD is an age-associated disease, which usually only develops in individuals of higher age. Furthermore, it has been published that iPSCs per se could be unsuitable models of ageing diseases, since upon reprogramming a process of rejuvenation seems to occur. Models for artificial ageing of cells have been established rather recently, usually by overexpressing progerin or the exogenous addition of the protein progerin into the medium of cells (reviewed in Miller and Studer, 2014; Miller et al., 2013). However, as ageing modelled by progerin very likely does not represent a clean PD model anymore, but rather is also accompanied by changes observed in the corresponding disease Hutchinson-Gilford progeria syndrome, it was not used in this thesis. Instead, it was attempted to recapitulate an ageing phenotype in iPSC models by simply passaging the cells for an extensive period as published by Petrini et al., 2017. They indicated that ageing of iPSCs using extensive passaging is possible and a good model compared to senescence in somatic cells (Petrini et al., 2017). Cells were passaged up to 35 to 50 times, which corresponds to an increase of 20 passages for every line with 1 passage per week. These cells and their derivates are from here on termed high-passage iPSCs or NPCs. As, at the time the passaging was started, not all clones from all lines were accessible within the ForiPS consortium, high-passaged iPSCs encompass 7 PD patients and 5 controls summing up to a total of 16 lines (iPD: 2 patients with 2 clones analyzed, 5 patients with 1 clone analyzed; control: 1 individual with 2 clones analyzed, 4 individuals with 1 clone analyzed, see color code in Tab.2).

At first, a comparative analysis of both, low-passage and high-passage iPSCs from iPD and corresponding controls exposed to a specific substrate, was done to assess possible health state phenotypes, i.e. a general comparison of diseased to healthy samples. Subsequently, a more detailed analysis of the health states exposed to the substrates was done. General analysis across health state and passages was evaluated using

two-way Anova analysis, detailed analysis of health state exposed to particular substrates was done using Tukey's Post-hoc test.

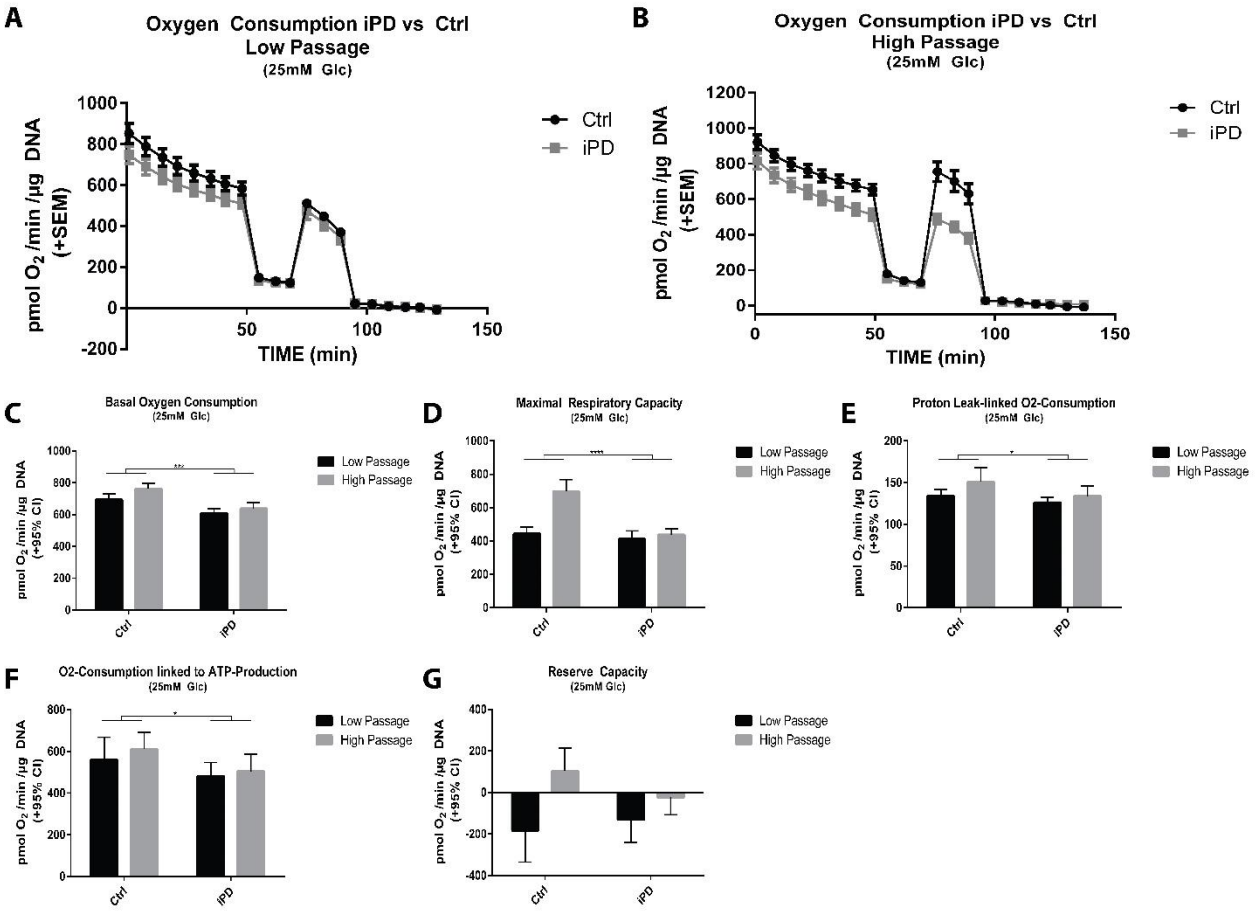

Fig. 8: Oxygen consumption analysis of iPD patients' iPSCs compared to corresponding controls with glucose as energy substrate. *Respiratory analysis of 7 iPD patients' iPSCs and 5 corresponding controls individuals' iPSCs with 2 clones per individual for low-passage iPSCs, corresponding to 24 lines in total analyzed, and 16 lines analyzed in total for high-passage iPSCs. As described in section 4.2.3.1.2 cells were analyzed with 25mM glucose as energy substrate, OCR and ECAR were assessed in parallel and normalized to DNA content. (A) Shows the progression of the measurement in low passage iPSCs, (B) in high passage iPSCs respectively (starting with basal respiration). After the addition of oligomycin, ATP-dependent oxygen consumption and proton leak are assessed, followed by maximal respiration upon addition of FCCP. Last, mitochondrial oxygen consumption is inhibited by adding rotenone and antimycin-A to obtain the non-mitochondrial oxygen consumption, which has been subtracted from all other values as initial normalization to mitochondrial oxygen consumption. (C) displays the mean differences in basal respiration, (D) the mean differences in maximal respiratory capacity, (E) the mean proton-leak linked oxygen consumption, (F) the mean oxygen consumption devoted to ATP production, (G) the mean calculated reserve capacities. Every line was analyzed with at least n =3, statistical analysis was done with Graphpad Prism 6, using two-way Anova with Tukey's Post-hoc test, $p < 0.05$ was considered significant (* $p < 0.05$; ** $p < 0.01$; *** $p < 0.001$).*

Comparison of oxygen dependent respiration in iPD patients' cells with just 25mM glucose as substrate to corresponding controls in high- and low-passage iPSCs revealed several iPD specific, as well as several passage depending effects. Mean basal oxygen consumption was significantly reduced in iPD patients' cells (*low passage: control 702.98 ± 94.32 and iPD 604.34 ± 78.19; high passage: control 761.41 ± 67.93 and iPD 637.93 ± 89.65; $p < 0.0001$;* Fig. 8C). Furthermore, a significant passage effect could be detected in

the mean basal respiration between low- and high-passage cells of iPD and control individuals' cells (*p = 0.0053*), while no significant interaction between passage and health state could be found (*p = 0.3007*). In addition, a significant reduction in the mean proton-leak linked oxygen-consumption was found in iPD patients' cells (*low passage: control 137.31 ± 6.98 and iPD 126.47 ± 11.70; high passage: control 150.99 ± 18.07 and iPD 133.89 ± 21.94; p = 0.0201;* Fig. 8E), and again a significant passage (*p = 0.0209*) but not interaction effect *(p = 0.3810*) was observed. Next to basal oxygen consumption and proton-leak linked oxygen consumption, iPD patients' cells also showed a general significant reduction in the mean oxygen consumption linked to mitochondrial ATP production (*low passage: control 565.67 ± 88.06 and iPD 477.89 ± 68.68; high passage: control 610.42 ± 59.50 and iPD 504.05 ± 81.43; p = 0.0106;* Fig. 8F) with no passage (*p = 0.2707*) or interaction (*p = 0.6828*) effect. Maximal respiration displayed a general health state dependence, with significantly reduced maximal respiratory capacity in iPD patients' cells (*low passage: 503 .68 ± 45.55 and iPD 469.60 ± 107.80; high passage: control 756.12 ± 11.49 and iPD 489.58 ± 69.56*; *p < 0.0001;* Fig. 8D) as well as a strong passage effect (*p < 0.0001)*. However, these values need to be taken with precaution as a strong interaction between health state and passage could be detected (*p < 0.0001*), for which reason no general health state nor passage effect can be claimed here – Post-hoc testing revealed a significant decrease of maximal respiration in high-passage but not in low-passage iPSCs from iPD patients' cells (presented in section 2.2.3). For mitochondrial reserve capacity with glucose as substrate, no health state dependent changes were detected (*low passage: control -183.09 ± 109.21 and iPD -131.04 ± 111.00; high passage: control 102.92 ± 80.15 and iPD -22.37 ± 85.70; p = 0.4186;* Fig. 8G). However a passage dependent significant increase of reserve capacity from low- to high-passage iPSCs (*p = 0.0002*) was observed, while no significant interaction was calculated (*p = 0.0593*).

To get a more comprehensive picture of cellular metabolism, ECAR was assessed, in parallel to OCR, as framework for glycolytic activity of the cells when only supplied with 25mM glucose as energy substrate (Fig. 9).

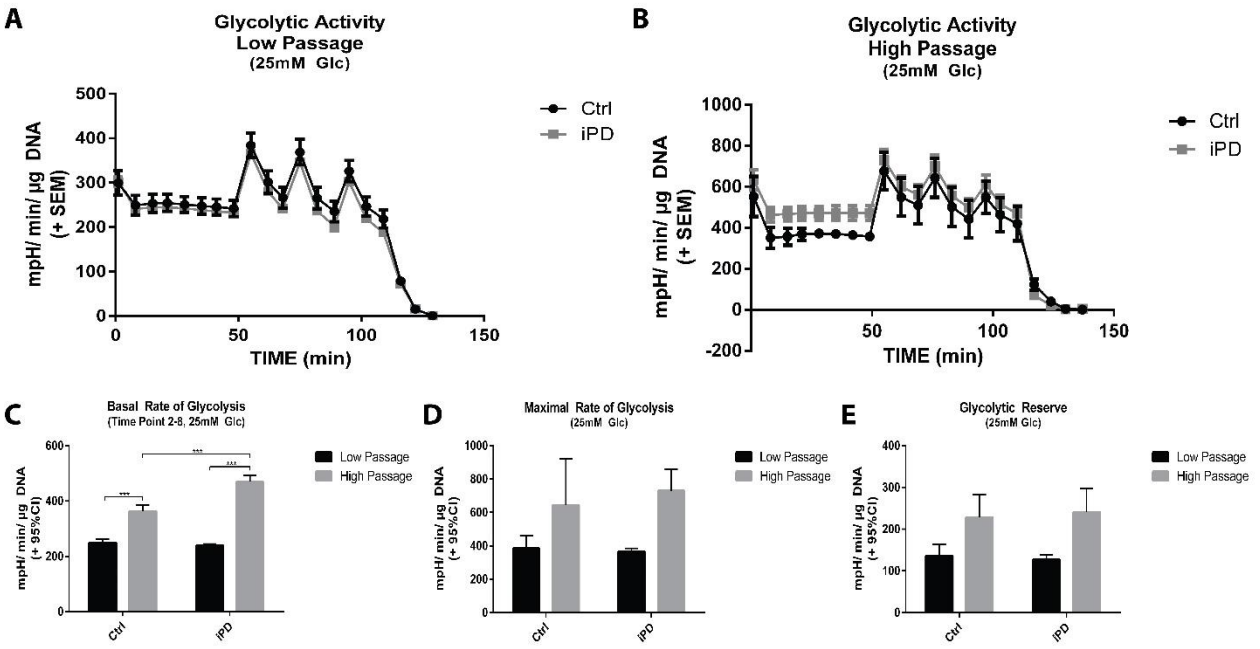

Fig. 9: Extracellular acidification rate (ECAR) analysis of iPD patients' iPSCs compared to corresponding controls with glucose as energy substrate. *Respiratory analysis of 7 iPD patients' iPSCs and 5 corresponding controls individuals' iPSCs with 2 clones per individual for low-passage iPSCs, corresponding to 24 lines in total analyzed, and 16 lines analyzed in total for high-passage iPSCs. As described in section 4.2.3.1.2, cells were analyzed with 25mM glucose as energy substrate, OCR and ECAR were assessed in parallel and normalized to DNA content. (A) shows the progression of the measurement in low passage iPSCs, (B) in high passage iPSCs respectively, starting with basal glycolytic activity. After the addition of oligomycin, maximal glycolytic activity is assessed. Glycolytic reserve is deduced from maximal and basal glycolytic capacity. Last, glycolytic activity is inhibited by the addition of 2-deoxyglucose to obtain the non-glycolytic acidification rate, which has been subtracted from all other values as initial normalization to glycolytic activity. (C) Displays the mean differences in basal glycolytic activity, (D) the mean differences in maximal glycolytic capacity, (E) the mean glycolytic reserve. Every line was analyzed with at least n =3, statistical analysis was done with Graphpad Prism 6, using two-way Anova with Tukey's Post-hoc test, $p < 0.05$ was considered significant (* $p < 0.05$; ** $p < 0.01$; *** $p < 0.001$).*

When compared to OCR, a vice versa effect in the mean basal glycolytic activity, being now increased in iPD patients' cells (*low passage: control 284.84 ± 38.39 and iPD 329.66 ± 15.48; high passage: control 377.81 ± 62.85 and iPD 489.58 ± 88.90; $p < 0.0001$;* Fig. 9C) could be observed. However, again a strong interaction ($p < 0.0001$) between health state and passage ($p < 0.0001$) was detected, for which reason Post-hoc testing was applied. This revealed a significant increase in glycolytic activity between low- and high-passage iPSCs ($p < 0.0001$) and a significant increase of glycolytic activity in high-passage iPD patients' cells compared to corresponding controls ($p < 0.0001$), which, however, cannot be found in low-passage iPD patients' cells ($p = 0.8859$) (presented in section 2.2.2). Maximal rate of glycolysis did not show a health state dependent change (*low passage: control 384.04 ± 54.54 and iPD 366.59 ± 19.06; high passage: control 675.95 ± 182.44 and iPD 729.87 ± 128.73; $p = 0.5287$*; Fig. 9D), but only a strong passage dependent increase from low- to high-passage iPSCs ($p < 0.0001$) with no interaction ($p = 0.3452$). Similarly, no health state dependent change in glycolytic reserve (*low passage: control 135.20 ± 20.71 and*

iPD 126.93 ± 11.32; high passage: control 227.38 ± 39.90 and iPD 240.28 ± 57.74; p = 0.8939; Fig. 9E) could be assessed, yet a passage dependent increase (*p < 0.0001*) with no interaction (*p = 0.5443*).

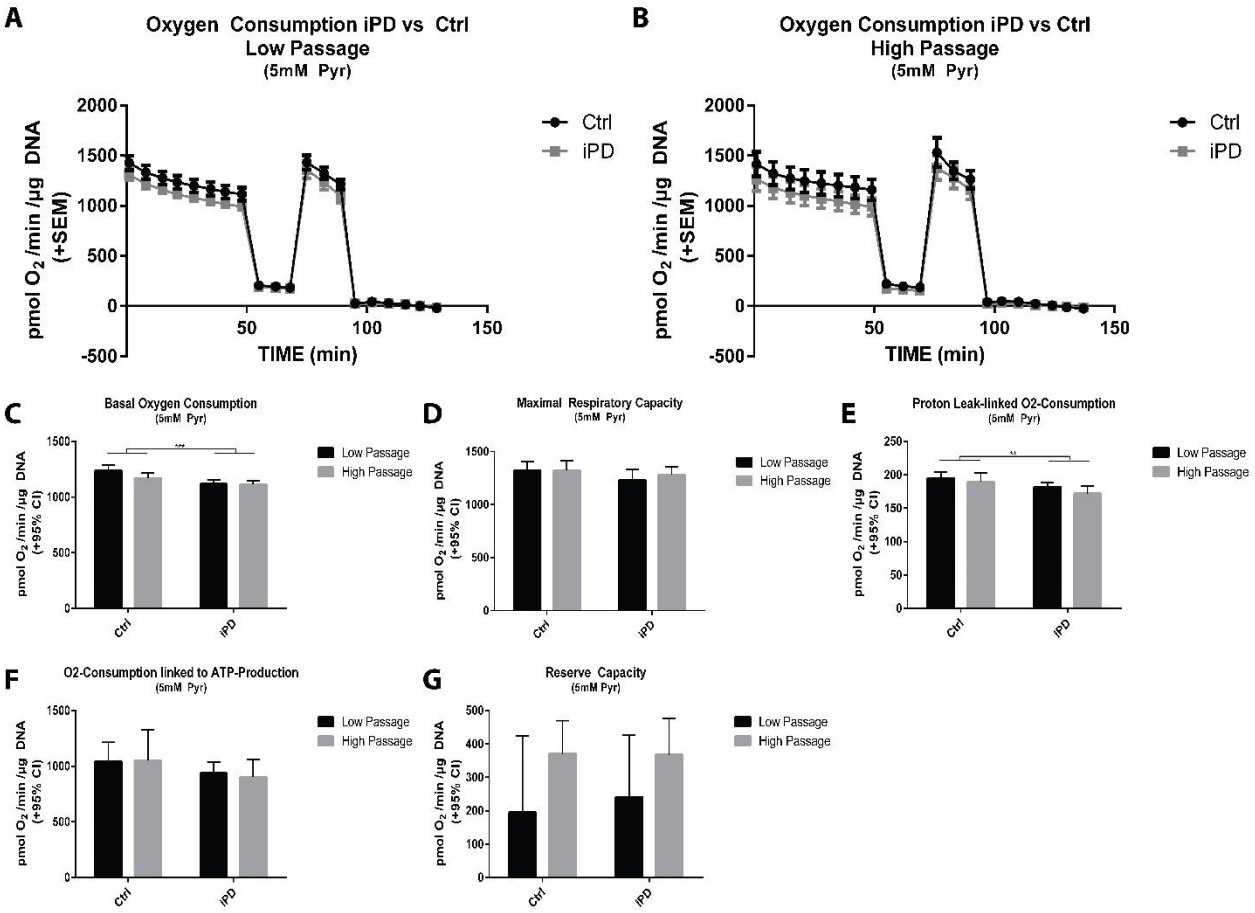

Fig. 10: Oxygen consumption analysis of iPD patients' iPSCs compared to corresponding controls with pyruvate as energy substrate. *Respiratory analysis of 7 iPD patients' iPSCs and 5 corresponding controls individuals' iPSCs with 2 clones per individual for low-passage iPSCs, corresponding to 24 lines in total analyzed, and 16 lines analyzed in total for high-passage iPSCs. As described in section 4.2.3.1.2, cells were analyzed with 5mM pyruvate as energy substrate, OCR was assessed and normalized to DNA content. (A) Shows the progression of the measurement in low passage iPSCs, (B) in high passage iPSCs respectively (starting with basal respiration). After the addition of oligomycin, ATP-dependent oxygen consumption and proton leak are assessed, followed by maximal respiration upon addition of FCCP. Last, mitochondrial oxygen consumption is inhibited by adding rotenone and antimycin-A to obtain the non-mitochondrial oxygen consumption, which has been subtracted from all other values as initial normalization to mitochondrial oxygen consumption. (C) displays the mean differences in basal respiration, (D) the mean differences in maximal respiratory capacity, (E) the mean proton-leak linked oxygen consumption, (F) the mean oxygen consumption devoted to ATP production, (G) the mean calculated reserve capacities. Every line was analyzed with at least n =3, statistical analysis was done with Graphpad Prism 6, using two-way Anova with Tukey's Post-hoc test, p < 0.05 was considered significant (* p < 0.05; ** p < 0.01; *** p < 0.001).*

To further asses mitochondrial contribution to the respiratory phenotype found with 25mM glucose as substrate in more detail, cells were analyzed with only 5mM pyruvate as substrate (Fig. 10). As shown, respiration with glucose (Fig. 8) and respiration with pyruvate (Fig. 10) display some striking differences: first, generally speaking, oxygen consumption greatly increases, which clearly shows that mitochondria are not running at theoretical maximal capacity when supplied with glucose, probably due to substrate

limitation, as cells have to break down glucose via glycolysis first. The general increase in oxygen consumption is most likely due to two major effects: first, cells have to solely rely on mitochondrial ATP supply to cover their demand, and second, the ATP demand of the cells is presumably increased with only pyruvate as substrate, as anabolic processes (like gluconeogenesis) will become more prominent, since otherwise essential intermediates for cellular metabolism, which are for example created through glycolysis, would be missing. Second, it becomes obvious that even with pyruvate as substrate, basal oxygen consumption can still be increased upon uncoupling mitochondria, hinting towards that ATP supply and demand may be met more efficiently when cells are supplied with pyruvate in comparison to glucose. ECAR values were not assessed for pyruvate as substrate, as it cannot be accounted for which processes contribute to extracellular acidification in this case.

Coupling efficiency in cells is the degree of coupling of oxygen usage to ATP production. In Fig. 8E, a decreased proton-leak linked oxygen consumption is shown in iPD patients' cells with glucose as energy substrate. This decreased proton leak is reflected at cellular level in a trend towards decreased coupling efficiency in iPD patients' iPS cells with glucose as substrate (*low passage: control 0.8140 ± 0.0445 and iPD 0.7908 ± 0.050; high passage: control 0.7996 ± 0.025 and iPD 0.7831 ± 0.047; p = 0.0506;* Fig. 11).

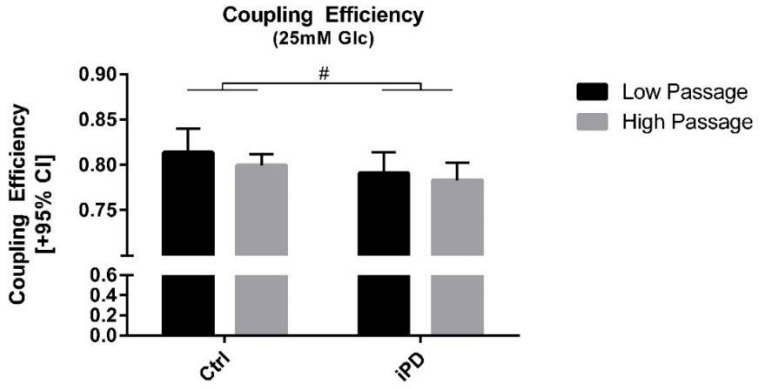

Fig. 11: Coupling efficiency (CE) of low- and high-passage iPSCs of iPD patients' cells and corresponding controls. *Coupling efficiency shows a trend towards decreased coupling in iPD patients' cells across passages. Coupling efficiency was calculated from the obtained respiratory data with the formula* $CE = [1 - (\frac{Proton-Leak\ linked\ Oxygen\ Consumption}{Basal\ Oxygen\ Consumption})]$. *All samples were analyzed with at least n = 3, statistical analysis was done with Graphpad prism 6 using two-way Anova and Tukey's Post-hoc test, p < 0.05 is considered significant (# p < 0.1; * p < 0.05; ** p < 0.01; *** p < 0.001).*

No interaction or passage effects were observed ($p = 0.7385$ and $p = 0.2719$ respectively). This hints towards the proton-leak possibly playing a substantial role in iPD patients' cells observed phenotypes with glucose as substrate. Furthermore, it becomes obvious, albeit not surprising, that coupling efficiency significantly increases when comparing glucose and pyruvate (supplementary Fig 5A.) No significant effects were found when comparing low- and high-passage cells' coupling efficiency with pyruvate as substrate (supplementary Fig. 5B)

2.2.2. Respiratory characterization of low passage iPSCs from iPD patients

As stated in the previous section, not only health state was compared using two-way Anova analysis, but also comparison of iPD and corresponding control cells was done for each passage and substrate individually using Post-hoc testing.

Fig. 12 and 13 display the respiratory characterization of iPD patients' iPSCs with low passages (15 to 30). iPD patients' cells and corresponding controls generally display a continuously decreasing oxygen dependent respiration when supplied with 25mM glucose as sole energy substrate (Fig. 12A). Measurements of basal OCR could be stabilized if measured in normal growth medium (mTesR1) (data not shown), excluding a technical error, which however only allows assessment of basal OCR due to medium compositions. It is obvious when comparing basal and maximal respiration that both, iPD and control cells, already respire at maximal oxidative capacity, since maximal respiration does not surpass basal respiration and maximal respiration is simply a function of substrate availability and oxidative capability. This suggests that oxidation of glucose alone is not sufficient to meet the energy demand of the cells. When comparing OCR and ECAR under glucose, it furthermore becomes obvious that cells do not increase their basal rate of glycolysis which by definition may ultimately limit the substrate for mitochondrial ATP generation, further accounting for the decrease in ATP demand. Why cells do not increase their glycolytic metabolism cannot be addressed at this point.

Significant differences between iPD patients' cells and corresponding control iPSCs respiration could only be detected in the mean basal oxygen consumption, with iPD cells displaying decreased respiration in comparison to the controls (*low passage: control 702.98 ± 94.32 and iPD 604.34 ± 78.19; p = 0.0033;* Fig. 12B). No significant differences in oxygen consumption could be detected in the mean maximal oxygen consumption (*control 503.68 ± 45.55 and iPD 469.60 ± 107.80; p = 0.7911;* Fig. 12C), the mean O_2-consumption attributed to ATP-production (*control 565.67 ± 88.06 and iPD 477.89 ± 68.68; p = 0.3491;* Fig. 12D) and the mean proton leak (*control 137.31 ± 6.98 and iPD 126.47 ± 11.70; p = 0.7148;* Fig. 12E) as well as in the mean spare respiratory capacity *(control -183.09 ± 109.21 and iPD -131.04 ± 111.00; p = 0.8396;* Fig. 12F). Also, no differences in Post-hoc testing could be found in the mean basal glycolytic activity (*control 284.84 ± 38.39 and iPD 329.66 ± 15.48; p = 0.8859;* Fig. 13B), the mean glycolytic capacity (*control 384.04 ± 54.54 and iPD 366.59 ± 19.06; p = 0.9956*; Fig. 13C) and the mean glycolytic reserve (*control 135.20 ± 20.71 and iPD 126.93 ± 11.32; p = 0.9860*; Fig. 13D) when comparing iPD and control iPSCs.

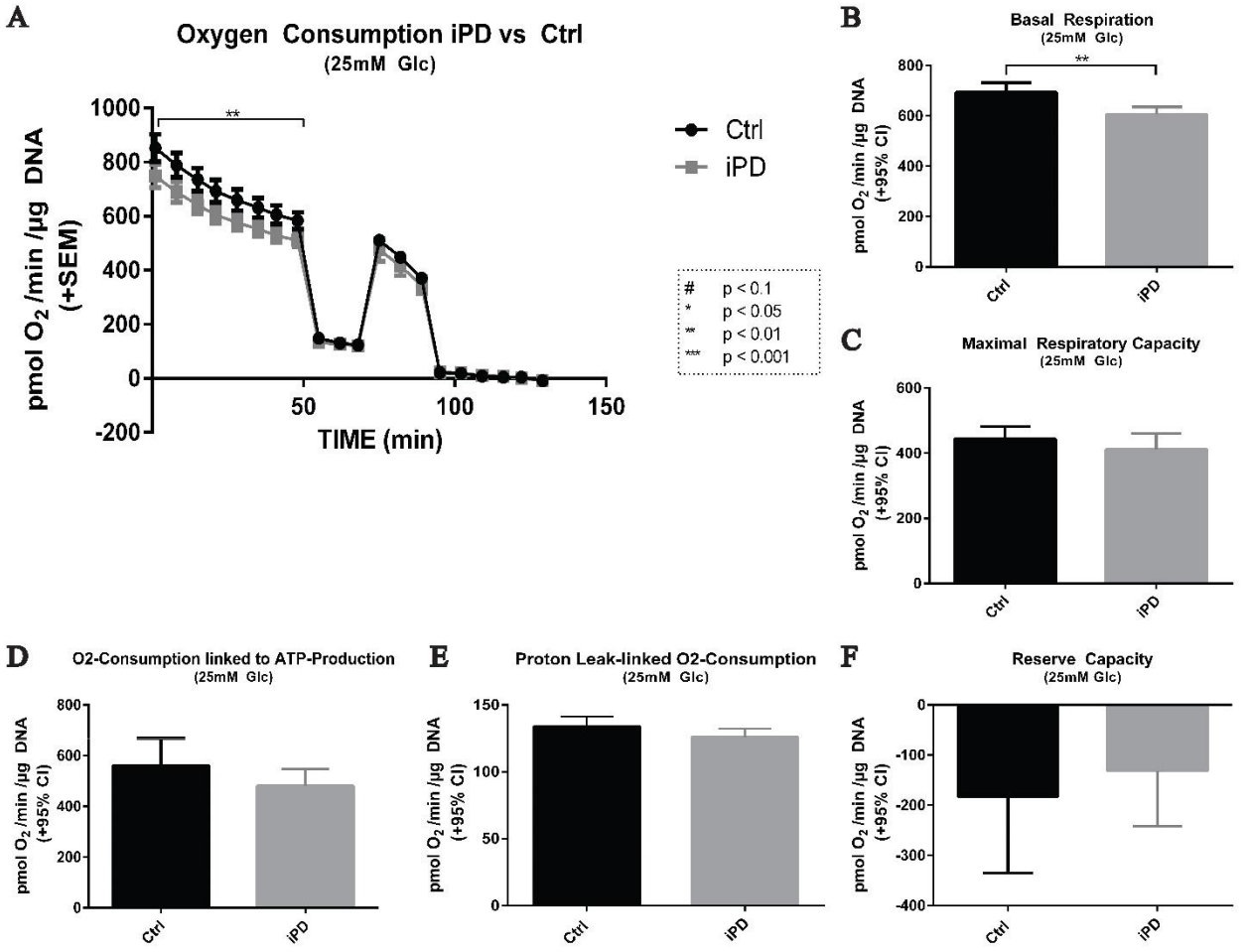

Fig. 12: Oxygen consumption analysis of iPD patients' low-passage iPSCs compared to corresponding controls with glucose as energy substrate. *Respiratory analysis of 7 iPD patients' iPSCs and 5 corresponding controls individuals' iPSCs with 2 clones per individual (corresponding to 24 lines in total analyzed). (A) Shows the progression of the measurement, starting with basal respiration. After the addition of oligomycin, ATP-dependent oxygen consumption and oxygen consumption devoted to proton leak are assessed, followed by maximal respiration upon addition of FCCP. Last, mitochondrial oxygen consumption is inhibited by the addition of rotenone and antimycin-A to obtain the non-mitochondrial oxygen consumption, which has been subtracted from all other values as initial normalization to mitochondrial oxygen consumption. (B) Displays the mean difference in basal respiration, (C) the mean difference in maximal respiratory capacity, (D) the mean oxygen consumption devoted to ATP production, (E) the mean proton-leak linked oxygen consumption and (F) the mean calculated reserve capacities. Every line was analyzed with n =3, statistical analysis (testing for outliers, normality of distribution and significance) was done using Graphpad Prism 6, either with Student's t-test for normally distributed values or Man-Whitney-test for non-parametrical distribution, $p < 0.05$ was considered significant.*

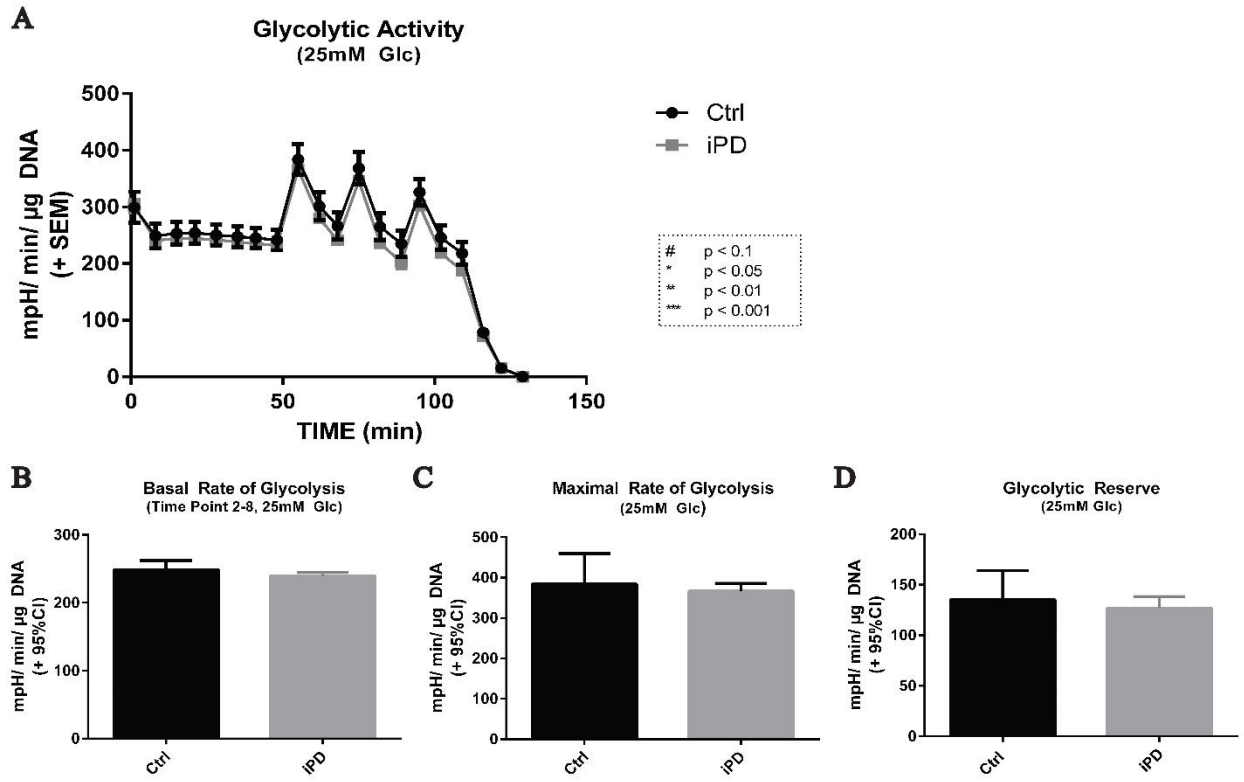

Fig. 13: ECAR analysis of iPD patients' low-passage iPSCs compared to corresponding controls with glucose as energy substrate. *Paralleled to OCR measurements is the assessment of the ECAR as framework for glycolytic activity. Analysis encompasses 7 iPD patients and 5 matched controls with a total of 2 clones per individual (a total of 24 lines). To assess specifically glycolytic activity, 25mM glucose were supplied as energy substrate. (A) Shows the progression of the ECAR during measurement, (B) displays the mean basal rate of glycolysis, (C) the mean maximal glycolytic capacity and (D) the glycolytic reserve. Every line was analyzed with n =3, statistical analysis was done with Graphpad Prism 6 using two-way Anova analysis and Tukey's Post-hoc test,, p < 0.05 was considered significant.*

As displayed in Fig. 15, comparing respiration under glucose and under pyruvate reveals some striking effects: first, basal oxygen consumption greatly increases, which clearly shows that mitochondria under basal conditions with just glucose as sole energy substrate are not charged to full capacity, but rather seem to be limited by substrate supply. Second, it becomes obvious that even with pyruvate as substrate, basal oxygen consuming respiration can be still increased upon uncoupling and hinting towards that ATP supply and demand may be met much more efficiently when cells are supplied with pyruvate in comparison to glucose. This is a rather surprising effect, since induced pluripotent stem cells are thought to be predominantly glycolytic (see section 1.3.1). That the predominance of glycolytic ATP production in these iPSCs might not be entirely true is also reflected when considering the mean OCR/ ECAR ratio with glucose as substrate, even though no significant changes in the OCR/ECAR ratio in low-passage iPSCs (*control 2.31 ± 0.39 and iPD 2.00 ± 0.34; p = 0.6010;* Fig. 14) could be detected using Post-hoc testing.

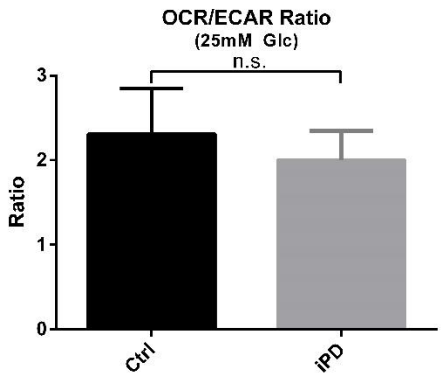

Fig. 14: OCR to ECAR ratio of iPD patients' low-passage iPSCs compared to healthy controls' iPSCs. *OCR to ECAR ratio was calculated by dividing the oxygen consumption attributed to ATP production (oligomycin dependent respiration) through the basal glycolytic respiration and reflects the cells' tendencies of ATP production. A ratio larger than one represents predominantly mitochondrial ATP production, while a ratio below one would represent largely glycolytic ATP production. Every line was analyzed with n =3, statistical analysis (testing for outliers, normality of distribution and significance) was done using Graphpad Prism 6, either with Student's t-test for normally distributed values or Man-Whitney-test for non-parametrical distribution, $p < 0.05$ was considered significant.*

The mitochondrial contribution to the phenotype observed in the OCR measurements with glucose was analyzed, by exposing cells to pyruvate as sole energy substrate in parallel (Fig. 15). When comparing iPD iPSCs to healthy control iPSCs, the same pattern, a significant decrease in mean basal respiration (*control 1236.59 ± 135.54; iPD 1116.68 ± 106.42; p = 0.0009;* Fig. 15B) but no differences in mean maximal respiration (*control 1431.45 ± 143.35; iPD 1357.37 ± 206.14; p = 0.1713;* Fig. 15C), mean oxygen consumption attributed to ATP production (*control 1042.00 ± 124.40; iPD 935.19 ± 98.76; p = 0.1616;* Fig. 15D) or mean reserve capacity (*control 194.86 ± 164.60; iPD 240.68 ± 185.19; p = 0.6948;* Fig. 15F) are observed. Again, a significant difference in the mean proton leak dependent oxygen consumption (*control 194.54 ± 14.03; iPD 181.49 ± 13.14; p = 0.0195;* Fig. 15E) was observed. The reduction in basal respiration hints towards a series of possibilities, like variances in ATP utilization or production as well as possible defects in substrate supply and oxidation. Substrate supply and oxidation can, however, be excluded here since the cells were offered a primarily mitochondrial substrate and no differences in maximal respiratory capacity could be detected, which is a plain function of substrate supply and mitochondrial functionality. Therefore it is rather likely that under basal conditions some processes in iPD' iPSCs consume less ATP than in corresponding controls' iPSCs, which results in decreased basal oxygen consumption and can be seen but is not reflected significantly when looking at oligomycin dependent respiration.

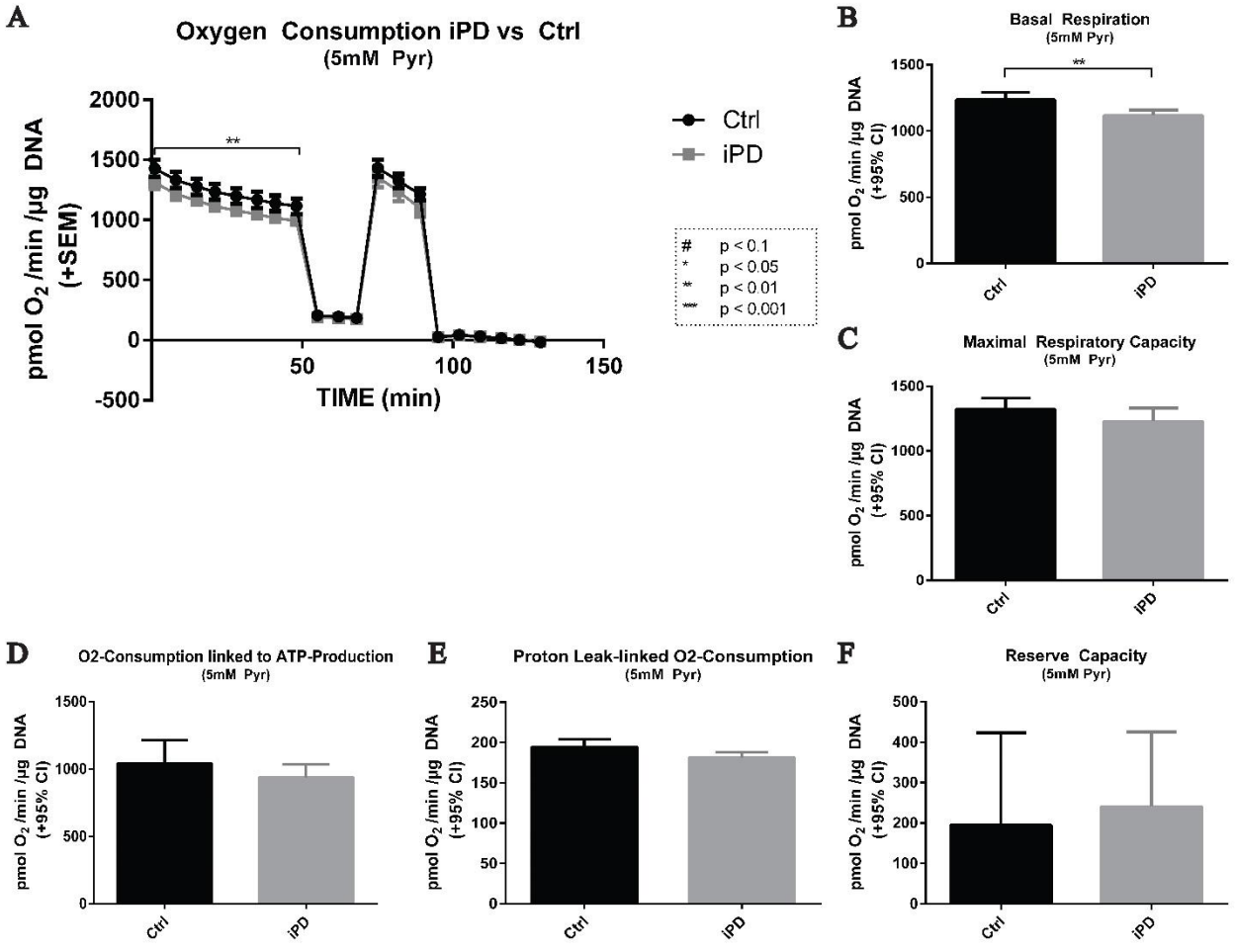

Fig. 15: Oxygen consumption analysis of iPD patients' low-passage iPSCs compared to corresponding controls with pyruvate as energy substrate. *Respiratory analysis of 7 iPD patients' iPSCs and 5 corresponding controls individuals' iPSCs, with 2 clones per individual (corresponding to 24 lines in total analyzed). As previously described, cells were analyzed with 5mM pyruvate as energy substrate, OCR was assessed and normalized to DNA content. (A) Shows the progression of the measurement, (B) displays the mean difference in basal respiration, (C) the mean difference in maximal respiratory capacity, (D) the mean oxygen consumption devoted to ATP production, (E) the mean proton-leak linked oxygen consumption and (F) the mean calculated reserve capacities. Every line was analyzed with n =3, statistical analysis was done with Graphpad Prism 6 using two-way Anova and Tukey's Post-hoc test, p < 0.05 was considered significant.*

2.2.3. Respiratory characterization of high passage iPSCs from iPD patients

Before respiratory analysis of high-passage iPSCs was done, iPSCs were stained for the most important pluripotency factors (Oct3/4, Nanog and Sox2) to verify that cells still were pluripotent. Examples of pluripotency staining of 2 iPD and 2 control lines are shown in supplementary Fig. 2.

Subsequently, respiratory analysis was performed for the high-passage iPSCs using the same protocol and substrates as for low-passage iPSCs.

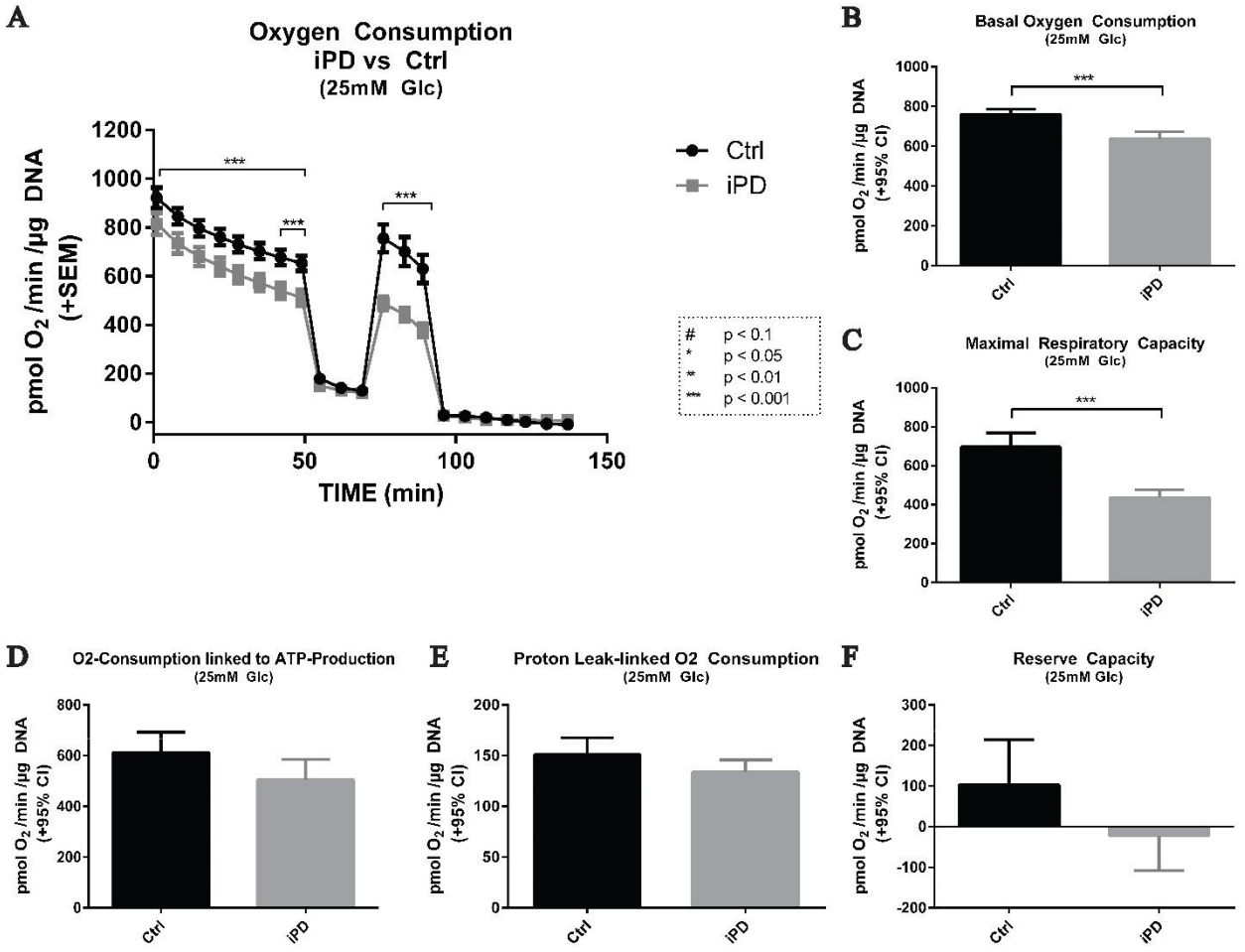

Fig. 16: Oxygen consumption analysis of iPD' high-passage iPSCs compared to corresponding controls with glucose as energy substrate. *Respiratory analysis of 7 iPD patients' iPSCs and 5 corresponding controls individuals' iPSCs with 1-2 clones per individual (corresponding to 16 lines in total analyzed). Cells were analyzed with 25mM glucose as energy substrate, OCR and ECAR were assessed in parallel and normalized to DNA content. (A) Shows the progression of the measurement, starting with basal respiration, (B) displays the mean difference in basal respiration, (C) the mean difference in maximal respiratory capacity, (D) the mean oxygen consumption devoted to ATP production, (E) the mean proton-leak linked oxygen consumption and (F) the mean calculated reserve capacities. Every line was analyzed with at least n =3, statistical analysis was done with Graphpad Prism 6, using two-way Anova and Tukey's Post-hoc test, p < 0.05 was considered significant.*

Like for low-passage iPSCs, with only glucose as energy substrate a dropping basal oxygen consumption can be observed. In a similar manner, mean maximal oxygen consumption of iPD patients' samples does not exceed or level their measured mean basal oxygen consumption. In contrast, control individuals' cells not only display a higher basal oxygen consumption than their PD counterparts, but also a mean maximal respiration which at least levels their mean basal oxygen consumption. In summary, Post-hoc testing revealed a significant decrease of mean basal oxygen consumption *(control 761.41 ± 67.93 and iPD 637.94 ± 89.65; p < 0.0001;* Fig 16B) and mean maximal oxygen consumption (*control 756.12 ± 113.49 and iPD 489.58 ± 69.56; p < 0.0001;* Fig. 16C), while no significant changes in the mean oxygen-consumption attributed to ATP production (*control 610.42 ± 59.50 and iPD 504.05 ± 81.43; p = 0.1346;* Fig. 16D), the

mean mitochondrial reserve capacity (*control 102.92 ± 80.15; iPD -22.37 ± 85.70; p = 0.2219*; Fig. 16F) and in the mean oxygen-consumption attributed to the proton-leak (*control 150.99 ± 18.07 and iPD 133.89 ± 21.94; p = 0.1065;* Fig. 16E) could be observed. Unlike in the low-passage iPSCs, the combination of reduced basal oxidative respiration and reduced maximal oxidative respiration of iPD patients' cells, supplied with just glucose, hints towards either deficiency in substrate supply and / or oxidation, or changes in mitochondrial mass or mitochondrial complex expression resulting in a decrease of mitochondrial efficiency or functionality. To get a more cumulative picture of the metabolic activity of high-passage iPSCs, also testing of the ECAR with just glucose as substrate was performed with Post-hoc testing (Fig.17).

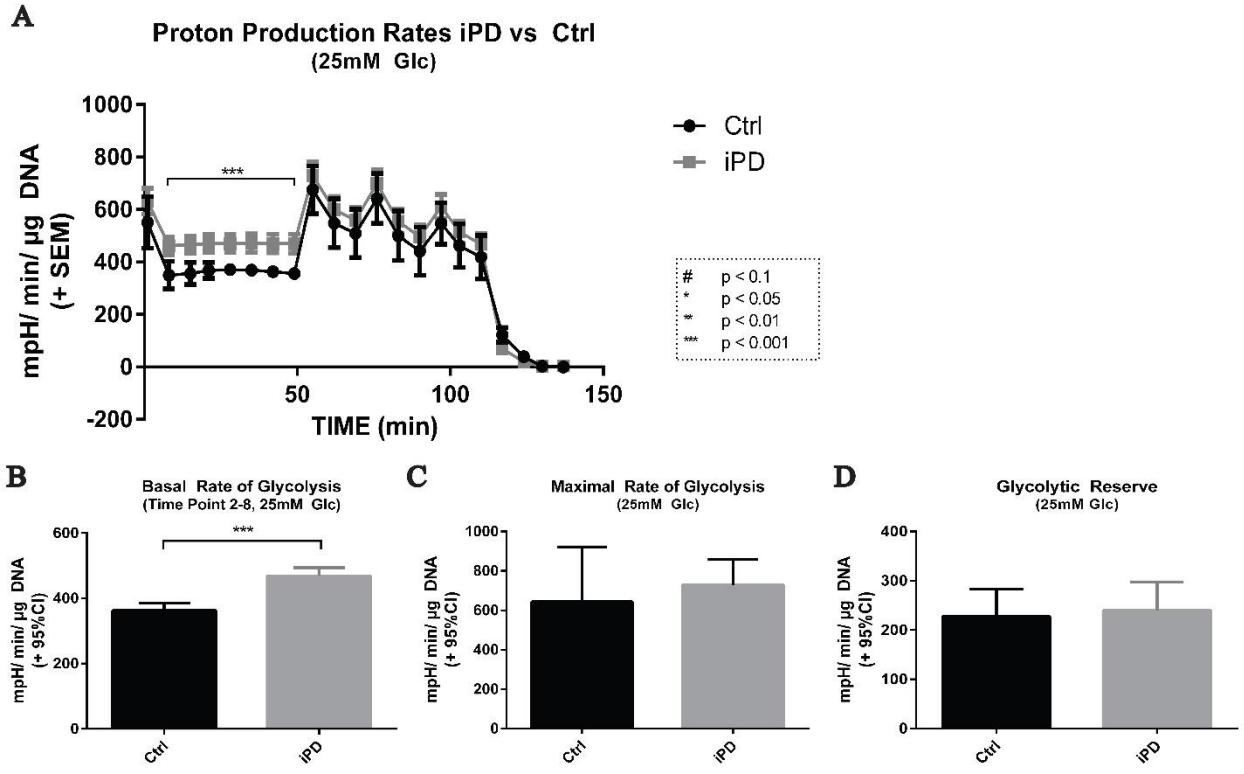

Fig. 17: ECAR analysis of iPD patients' high-passage iPSCs compared to corresponding controls with glucose as energy substrate. *Respiratory analysis of 7 iPD patients' iPSCs and 5 corresponding controls individuals' high-passage iPSCs, with 1-2 clones per individual (corresponding to 16 lines analyzed in total). To assess specifically glycolytic activity, 25mM glucose were supplied as energy substrate. (A) Shows the progression of the ECAR during measurement, (B) displays the mean basal rate of glycolysis and (C) the mean maximal glycolytic capacity. Every line was analyzed with at least n =3, statistical analysis was done with Graphpad Prism 6, using two-way Anova and Tukey's Post-hoc test,, p < 0.05 was considered significant.*

Analysis of glycolytic activity of high-passage iPSCs (Fig. 17) again shows a comparable overall pattern like low-passage iPSCs (Fig. 13). As depicted in Fig. 17B, an iPD-specific significant increase in the mean basal rate of glycolysis can be seen *(control 377.81 ± 62.85 and iPD 489.58 ± 88.90; p < 0.0001*). No significant variances in the mean maximal rate of glycolysis *(control 675.95 ± 182.44 and iPD 729.87 ± 128.73; p = 0.6717;* Fig. 17C) and the mean glycolytic reserve capacity (*control 227.38 ± 39.90 and iPD 240.28 ± 57.74; p = 0.9503;* Fig. 17D) can be observed. The increase in mean basal respiration might be a

compensation mechanism for the mitochondrial metabolism in these cells (Fig. 16A and -B), hinting towards an overall deficiency in oxidative ATP production in those cells compared to their corresponding controls. Furthermore, the OCR to ECAR ratio of these cells shifts slightly, yet without reaching significance (*control 1.49 ± 0.60 and iPD 1.10 ± 0.48; p = 0.3203;* Fig. 18).

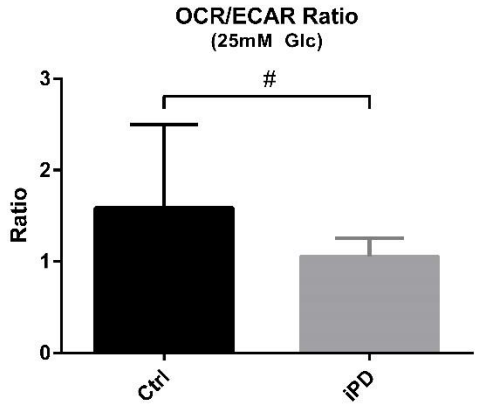

Fig. 18: OCR to ECAR ratio of iPD patients' high-passage iPSCs compared to healthy controls' iPSCs. *OCR to ECAR ratio was calculated by dividing the oxygen consumption attributed to ATP production (oligomycin dependent respiration) through the basal glycolytic respiration and reflects the cell's tendencies of ATP production. A ratio larger than 1 represents predominantly mitochondrial ATP production, while a ratio below 1 would represent largely glycolytic ATP production. Every line was analyzed with at least n =3, statistical analysis was done with Graphpad Prism 6, using two-way Anova and Tukey's Post-hoc test, p < 0.05 was considered significant.*

In the light of the results obtained from the measurements with just glucose as energy substrate, a vital point was to enlighten the mitochondrial contribution to these phenotypes. Therefore, respiratory analysis was made with pyruvate as energy substrate (Fig. 19). Again, it can be seen that mitochondria are not at maximum capacity when supplied with glucose, as OCRs increase drastically when cells are supplied with pyruvate (control about 1.54-fold and iPD about 1.74-fold). And once more it can be observed that cells seem to sustain better when supplied with pyruvate, as again oxygen consumption is not dropping to such an extent as before. In similar fashion to what has been observed before, FCCP-dependent oxygen consumption is larger than basal oxygen consumption, resulting in a rather large respiratory capacity in comparison to measurements with glucose as substrate. Like for all measurements with pyruvate, it has to be taken into consideration that now predominantly oxidative ATP production can be done within the cell and therefore basal respiration probably increases naturally, as now predominantly OXPHOS can and has to be done and a variety of anabolic processes have to be fueled to provide necessary intermediary metabolites for cellular metabolism. However, when comparing iPD patients' cells to controls' cells, it becomes clear that supply of pyruvate is able to rescue all phenotypes observed when glucose was supplied as energy substrate. Now, no changes in mean basal oxygen consumption (*control 1169.25 ± 123.27 and iPD 1111.72 ± 114.96; p = 0.2605;* Fig. 19B), mean maximal oxygen consumption (*control 1452.43 ±125.46 and iPD 1377.24 ± 151.27; p = 0.9202;* Fig. 19C), mean oxygen consumption attributed to ATP

production (*control 979.92 ± 107.17 and iPD 939.91 ± 98.81; p = 0.4317;* Fig. 19D) and mean reserve capacity (*control 370.07 ± 71.89 and iPD 367.62 ± 108.65; p > 0.9999;* Fig. 19F) between iPD patients' and controls' cells could be detected. Only mean oxygen consumption attributed to the proton-leak (*control 189.32 ± 16.46; iPD 171.80 ± 21.67; p = 0.0680;* Fig. 19E) becomes a trend. This suggests that in these cells a non-mitochondrial cause of phenotype is present, however still cannot entirely exclude a mitochondrial phenotype, as significant changes were observed with pyruvate as substrate in low-passage iPD' iPSCs. Therefore, a more thorough analysis of mitochondrial function is required which cannot be provided by only respiratory measurements, in order to identify the cause of phenotypes observed in the respiratory measurements (section 2.3.1).

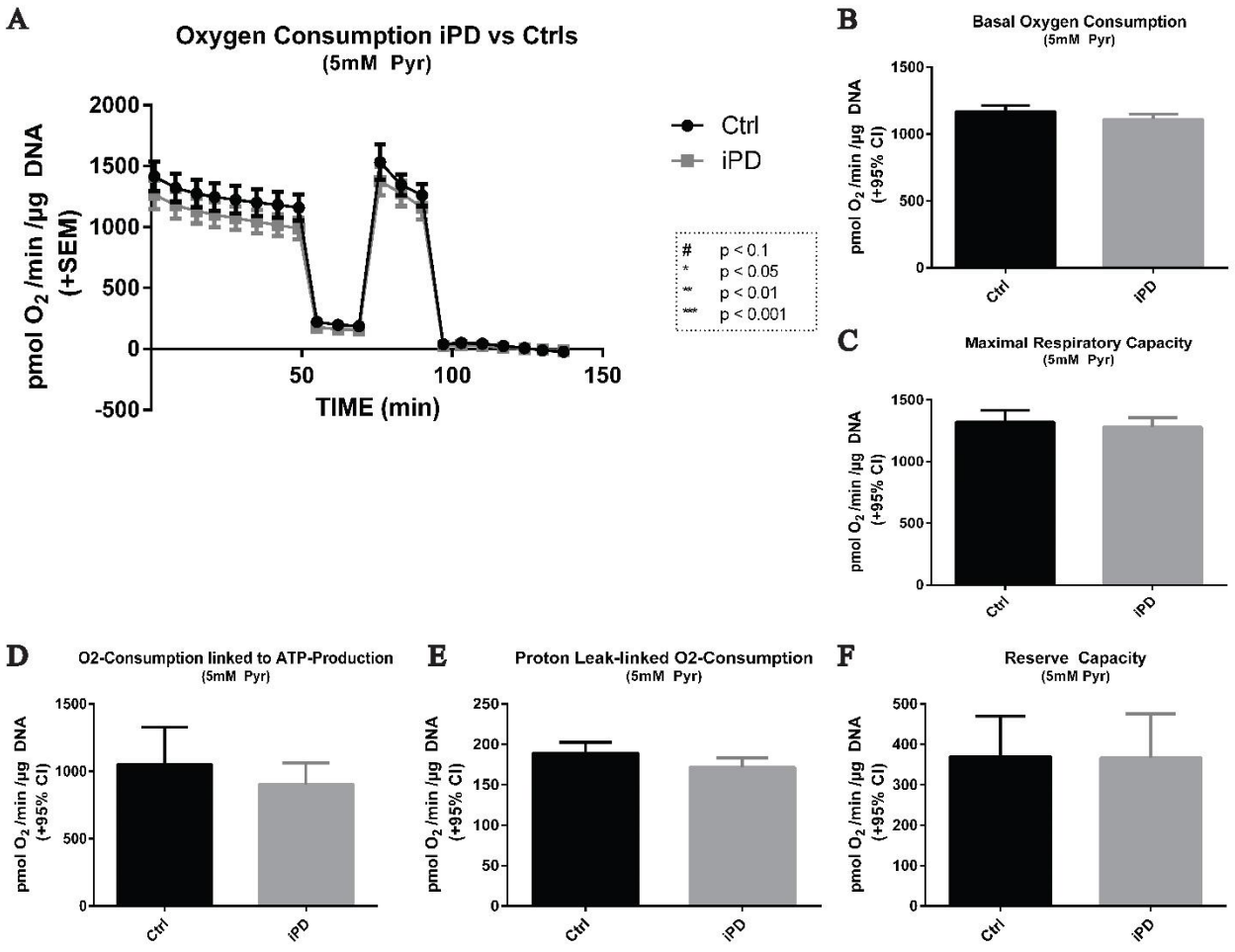

Fig. 19: Oxygen consumption analysis of iPD' high-passage iPSCs compared to corresponding controls with pyruvate as energy substrate. *Respiratory analysis of 7 iPD patients' iPSCs and 5 corresponding controls individuals' high-passage iPSCs, with 1-2 clones per individual (corresponding to 16 lines analyzed in total). Cells were analyzed with 5mM pyruvate as energy substrate, OCR was assessed and normalized to DNA content. (A) Shows the progression of the measurement, (B) displays the mean difference in basal respiration, (C) the mean difference in maximal respiratory capacity, (D) the mean oxygen consumption devoted to ATP production, (E) the mean proton-leak linked oxygen consumption and (F) the mean calculated reserve capacities. Every line was analyzed with at least n =3, statistical analysis was done with Graphpad Prism 6, using two-way Anova and Tukey's Post-hoc test, p < 0.05 was considered significant.*

2.2.4. Respiratory characterization of NPCs derived from low passage iPSCs

Low passage iPSCs (passage 15 to 30) were differentiated into neuronal precursor cells (NPCs) using a modified protocol from (Reinhardt et al., 2013) as described in section 4.2.2.3. After 10 days of differentiation and three subsequent passages, neuronal precursor identity was confirmed with positive staining for the neuronal precursor markers paired box protein Pax-6 (Pax-6), Sox-1 and -2 and Nestin (supplementary Fig. 3). NPCs differentiated from low passage iPSCs will be termed low-passage NPCs from here on forth. Subsequent to differentiation, cells were subjected to respiratory analysis after passage 5 and before passage 10 using the same protocol used for iPSCs. Like for the corresponding iPSCs, OCR and ECAR were assessed for two different substrates, glucose and pyruvate, to get a comparative analysis of both, whole cell respiration and predominantly mitochondrial respiration (Fig. 20 – 23).

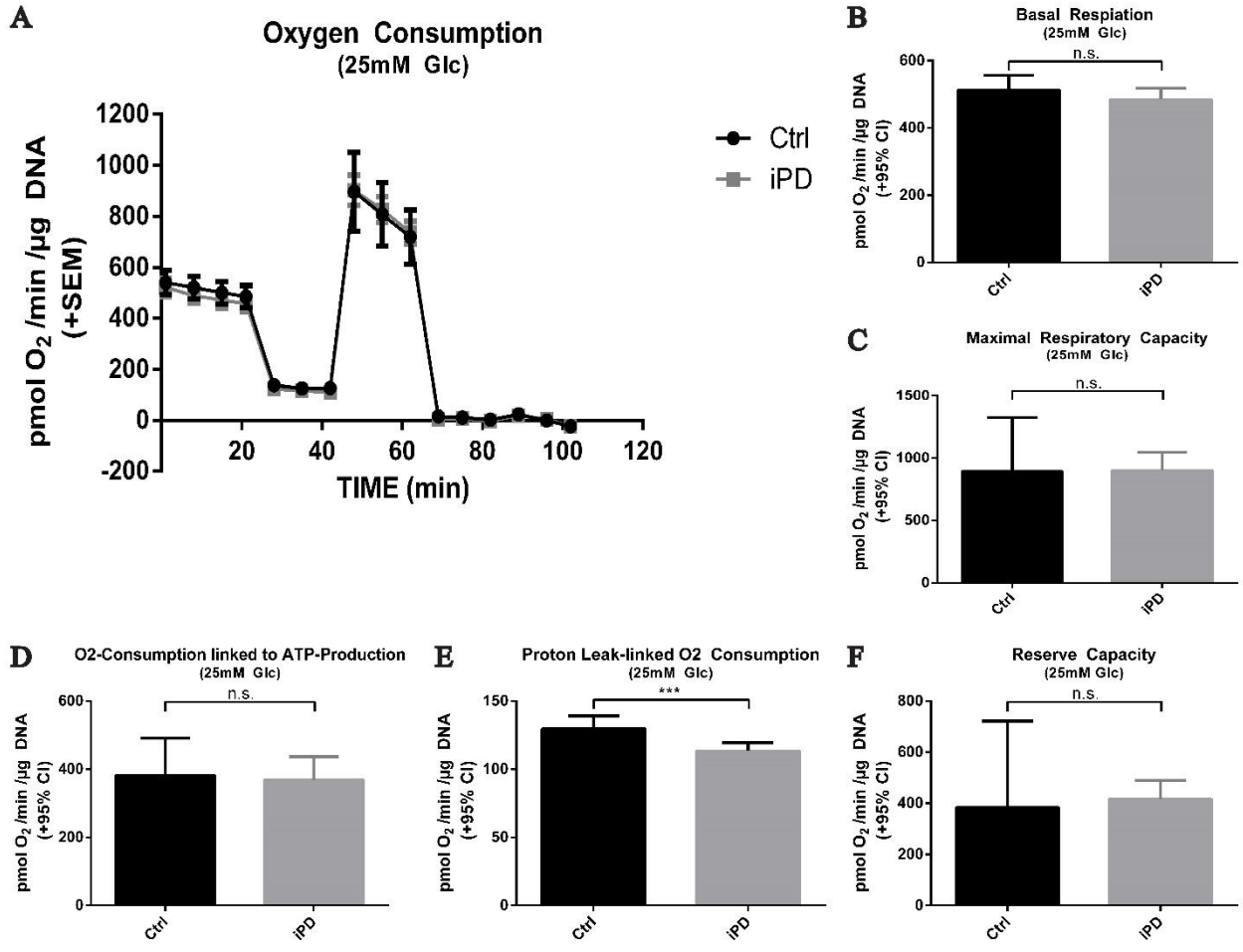

Fig. 20: Oxygen consumption analysis of iPD patients' NPCs differentiated from low passage iPSCs (passage 15-30) in comparison to corresponding controls' NPCs with glucose as sole energy substrate. *Respiratory analysis of 7 iPD patients' NPCs and 5 corresponding controls individuals' NPCs, with 2 clones per individual (corresponding to 24 lines in total analyzed). Cells were analyzed with 25mM glucose as energy substrate, OCR was assessed and normalized to DNA content. (A) Shows the*

progression of the measurement, (B) displays the mean difference in basal respiration, (C) the mean difference in maximal respiratory capacity, (D) the mean oxygen consumption devoted to ATP production, (E) the mean proton-leak linked oxygen consumption and (F) the mean calculated reserve capacities. Every line was analyzed with n =3, statistical analysis (testing for outliers, normality of distribution and significance) was done using Graphpad Prism 6, either with Student's t-test for normally distributed values or Man-Whitney-test for non-parametrical distribution, $p < 0.05$ was considered significant.

At first glance on Fig. 20, it becomes obvious that NPCs are better able to meet their energy demand in comparison to their corresponding iPSCs when supplied with 25mM glucose as energy substrate. Basal oxygen consumption is more stable and, in addition, lower in comparison to the corresponding iPSCs. Furthermore, there is an approximately 1.8-fold increase between maximal respiration in comparison to basal respiration in low-passage NPCs, indicating that the mitochondria in those cells generally have spare capacity and do not work at maximum substrate availability to meet ATP demands. When looking at the variations between iPD patients' cells and corresponding controls, no significant differences with exception for mean proton-leak dependent oxygen consumption (*control 129.65 ± 13.13; iPD 115.94 ± 14.99; p = 0.0006;* Fig. 20E) can be found. Mean basal oxygen consumption (*control 511.59 ± 90.30; iPD 484.58 ± 80.89; p = 0.4106;* Fig. 20B) and mean maximal oxygen consumption *(control 895.88 ± 308.44; iPD 901.47 ± 145.99; p = 0.9703;* Fig. 20C), as well as mean oxygen consumption attributed to ATP production (*control 381.94 ± 78.89; iPD 368.65 ± 67.91; p = 0.7814;* Fig. 20D) and the mean respiratory capacity (*control 384.29 ± 242.47; iPD 416.88 ± 72.98; p = 0.7660;* Fig. 20F) are not changed in a disease dependent manner. The picture of the cellular metabolism is further completed when looking at ECAR measurements of low-passage NPCs (Fig. 21). In comparison to their iPSC counterparts, ECAR has further increased indicating that low-passage NPCs have an even higher glycolytic activity. This also may be reflected in the comparison of basal and maximal oxygen consumption, as a higher glycolytic rate by default leads to the production of an increased amount of possible substrate for mitochondria, reflected in a higher, substrate dependent, spare respiratory capacity of NPCs. Again, when comparing for variations between iPD patients' and corresponding controls' cells, no significant differences could be observed neither in the mean basal rate of glycolysis (*control 496.24 ± 83.65; iPD 453.19 ± 44.11; p = 0.1096*; Fig. 21B) nor the mean maximal rate of glycolysis *(control 594.12 ± 76.78; iPD 544.30 ± 41.92; p = 0.2174*; Fig. 21C) nor in the mean glycolytic reserve (*control 97.87 ± 13.02; iPD 91.11 ± 14.06; p = 0.4573*; Fig. 21D).

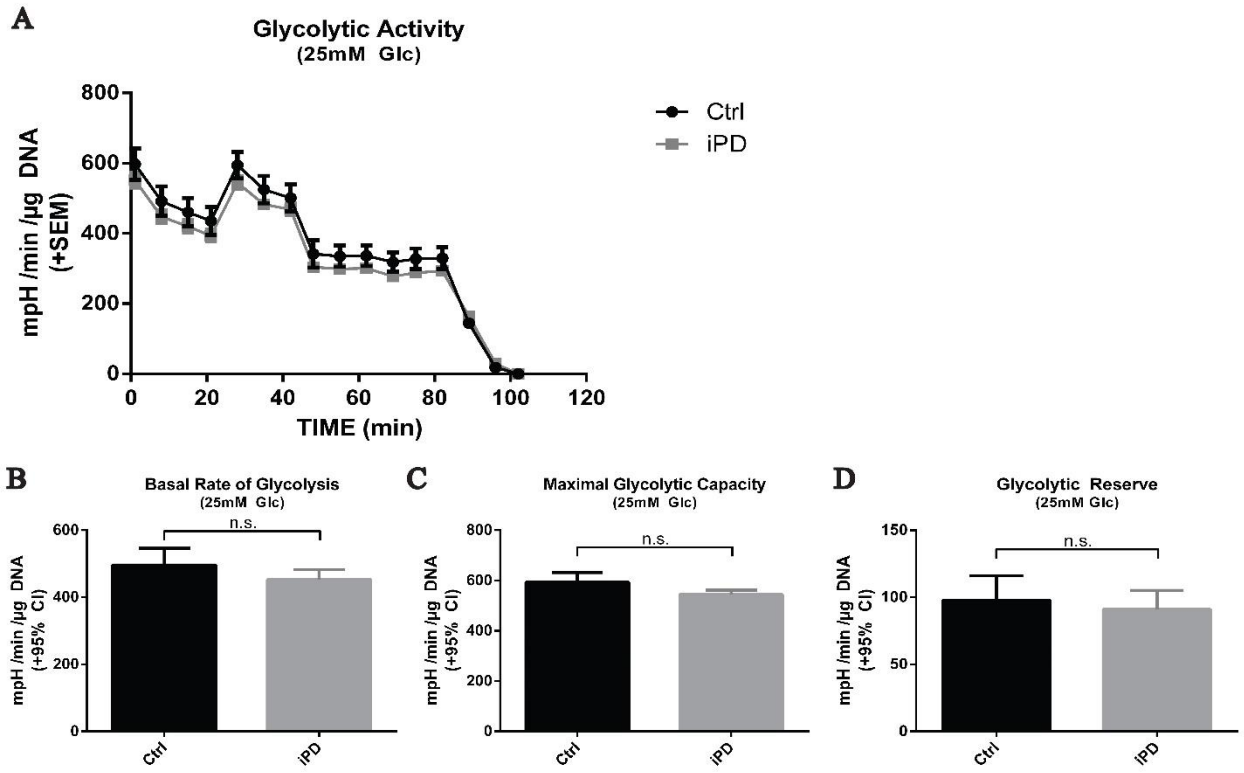

Fig. 21: ECAR analysis of iPD patients' NPCs compared to corresponding controls with glucose as energy substrate. *Parallel to OCR measurements is the assessment of the ECAR as framework for glycolytic activity. Analysis encompasses 7 iPD patients and 5 matched controls with a total of 2 clones per individual (a total of 24 lines). To assess specifically glycolytic activity, 25mM glucose were supplied as energy substrate. (A) Shows the progression of the ECAR during measurement, (B) displays the mean basal rate of glycolysis and (C) the mean maximal glycolytic capacity. Every line was analyzed with n =3, statistical analysis (testing for outliers, normality of distribution and significance) was done using Graphpad Prism 6, either with Student's t-test for normally distributed values or Man-Whitney-test for non-parametrical distribution, $p < 0.05$ was considered significant.*

When looking at the mean OCR/ECAR ratio, it becomes further obvious that there seems to be a better balance between glycolysis and mitochondrial respiration in comparison to their iPSC counterparts (Fig. 22).

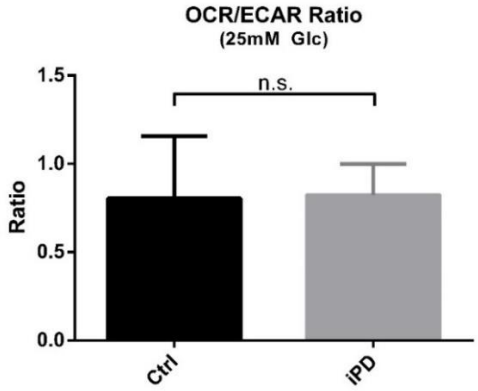

Fig. 22: OCR to ECAR ratio of iPD patients' NPCs compared to healthy controls' NPCs. *OCR to ECAR ratio was calculated by dividing the oxygen consumption attributed to ATP production (oligomycin dependent respiration) by the basal glycolytic respiration and reflects the cells' tendencies of preferred ATP production. A ratio larger than 1 represents predominantly*

mitochondrial ATP production, while a ratio below 1 indicates largely glycolytic ATP production. Every line was analyzed with n=3, statistical analysis (testing for outliers, normality of distribution and significance) was done using Graphpad Prism 6, either with Student's t-test for normally distributed values or Man-Whitney-test for non-parametrical distribution, $p < 0.05$ was considered significant.

The mean ratio of OCR/ECAR in NPCs, when only supplied with glucose *(control 0.80 ± 0.25; iPD 0.82 ± 0.17; p = 0.8950*; Fig. 22), shifts towards smaller than, but close to 1, indicating that cells have a close to equal ratio of glycolysis to OXPHOS. This still means that far less ATP is produced in glycolysis (1 ATP per H^+ in glycolysis vs. approx. 4.5 ATP per molecule of O_2 in OXPHOS), but according to the observations made here, the rate of glycolysis is more than sufficient to produce an excess of substrate for mitochondrial respiration.

Like the corresponding iPSCs, NPCs were supplied with only pyruvate to elucidate sole mitochondrial contribution to cellular respiration (Fig. 23). Like already for the corresponding iPSCs, it becomes obvious that the cells' mitochondria under glycolytic conditions are not at limits. When supplying cells with pyruvate, basal respiration increases approximately to the amount of the previously observed maximal respiration under glycolytic conditions. As for iPSCs, this increase might be explained by supplying (1) excess substrate while in parallel (2) effectively abolishing glycolysis, which will force the cells to increase anabolic, ATP consuming processes to properly maintain cellular metabolism. Furthermore, upon uncoupling mitochondria, an additional about 1.5-fold increase in oxygen consumption can be observed, which might account for the true, practical maximal capacity of the mitochondria in NPCs. However, when comparing iPD to control individuals' cells, again no differences in mean basal oxygen consumption (*control 886.51 ± 122.51; iPD 874.96 ± 100.35; p = 0.7434;* Fig. 23B) and mean maximal oxygen consumption (*control 1342.92 ± 364.04; iPD 1406.87 ± 173.68; p = 0,7194*; Fig. 23C), as well as no differences in mean oxygen consumption attributed to ATP production (*control 704.30 ± 118.51; iPD 709.08 ± 85.22; p = 0.7194*; Fig. 23D) and mean spare capacity (*control 456.41 ± 250.30; iPD 531.91 ± 79.08; p = 0.5105;* Fig. 23F) could be observed. Like for conditions with glucose as substrate, a significant change in the mean proton-leak linked oxygen consumption (*control 182.21 ± 4.19; iPD 165.89 ± 16.21; p = 0.0121*; Fig. 23E) was observed.

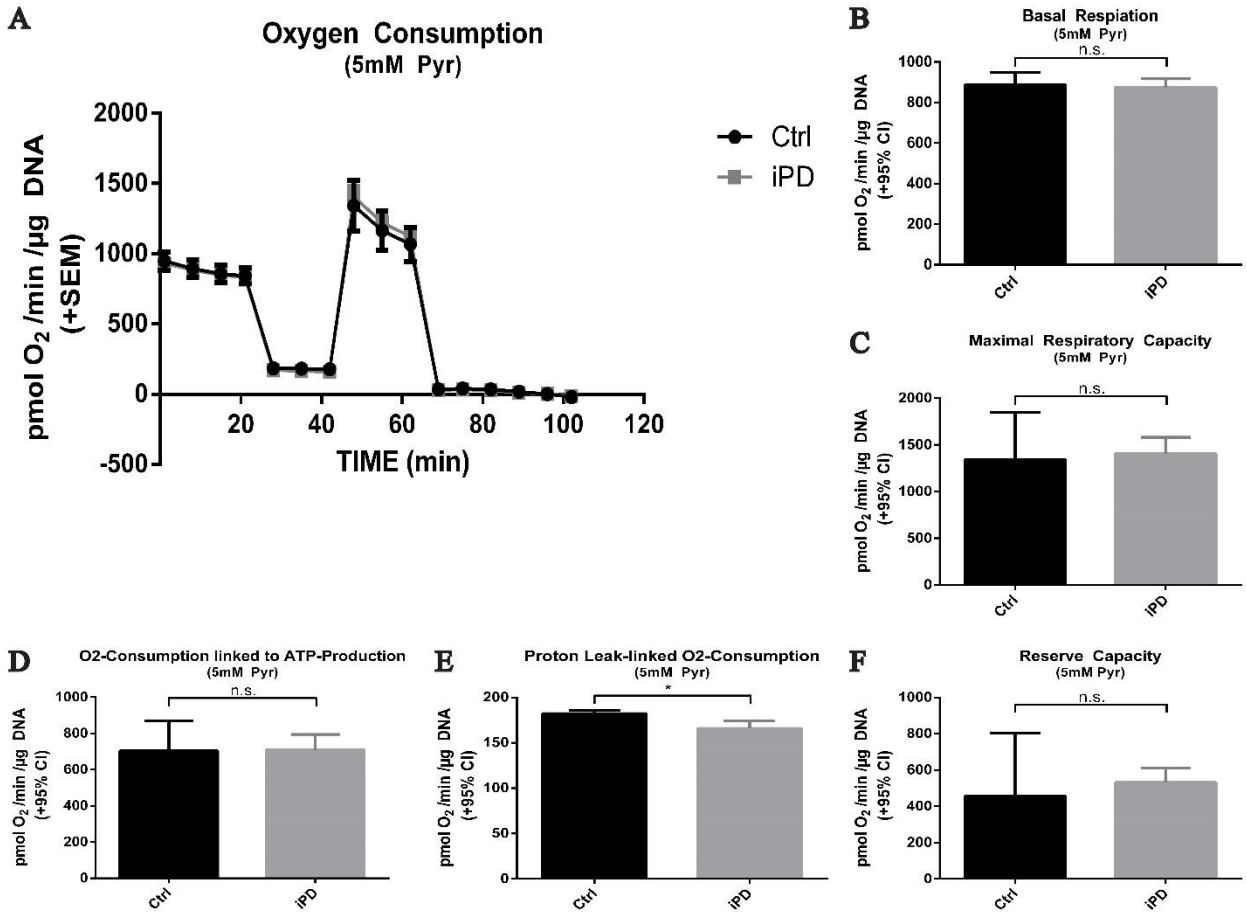

Fig. 23: Oxygen consumption analysis of iPD NPCs compared to corresponding controls with pyruvate as energy substrate. *Respiratory analysis of 7 iPD patients' iPSCs and 5 corresponding controls individuals' NPCs, with 2 clones per individual (corresponding to 24 lines in total analyzed). Cells were analyzed with 5mM pyruvate as energy substrate, OCR was assessed and normalized to DNA content. (A) Shows the progression of the measurement, (B) displays the mean difference in basal respiration, (C) the mean difference in maximal respiratory capacity, (D) the mean oxygen consumption devoted to ATP production, (E) the mean proton-leak linked oxygen consumption and (F) the mean calculated reserve capacities. Every line was analyzed with n =3, statistical analysis (testing for outliers, normality of distribution and significance) was done using Graphpad Prism 6, either with Student's t-test for normally distributed values or Man-Whitney-test for non-parametrical distribution, $p < 0.05$ was considered significant.*

2.2.5. Respiratory characterization of NPCs derived from high-passage iPSCs

Respiratory analysis and molecular characterization of NPCs from high-passage iPSCs was done in collaboration with Sebastian Schmidt, whose Master's thesis ("*Engrailed in Parkinson's disease and its link to mitochondrial complex I deficiency", Sebastian Schmidt, February 2017*) was incorporated into this PhD project and was supervised and planned by the author of this thesis. Data obtained from Sebastian Schmidt in course of his Master's thesis will be cited as (Schmidt, 2017).

High passage iPSCs (passage 35 to 50) were differentiated into NPCs using a modified protocol from (Reinhardt et al., 2013) as described in section 4.2.2.3. After 10 days of differentiation and three subsequent passages like for low-passage NPCs, neuronal precursor identity was confirmed with positive staining for the neuronal precursor markers Pax-6, Sox-1 and -2 and Nestin (Schmidt, 2017). NPCs differentiated from high passage iPSCs will be termed high-passage NPCs from here on. Differentiation of cells and respiratory analysis was done by the author of this thesis, maintenance culture by S. Schmidt.

Subsequent to differentiation, cells were subjected to respiratory analysis after passage 5 and before passage 10 using the same protocol used for their corresponding iPSCs and low-passage NPCs. Like before, OCR and ECAR were assessed for two different substrates, glucose and pyruvate, to get a comparative analysis of both, whole cell respiration and predominantly mitochondrial respiration (Fig. 24 – 27).

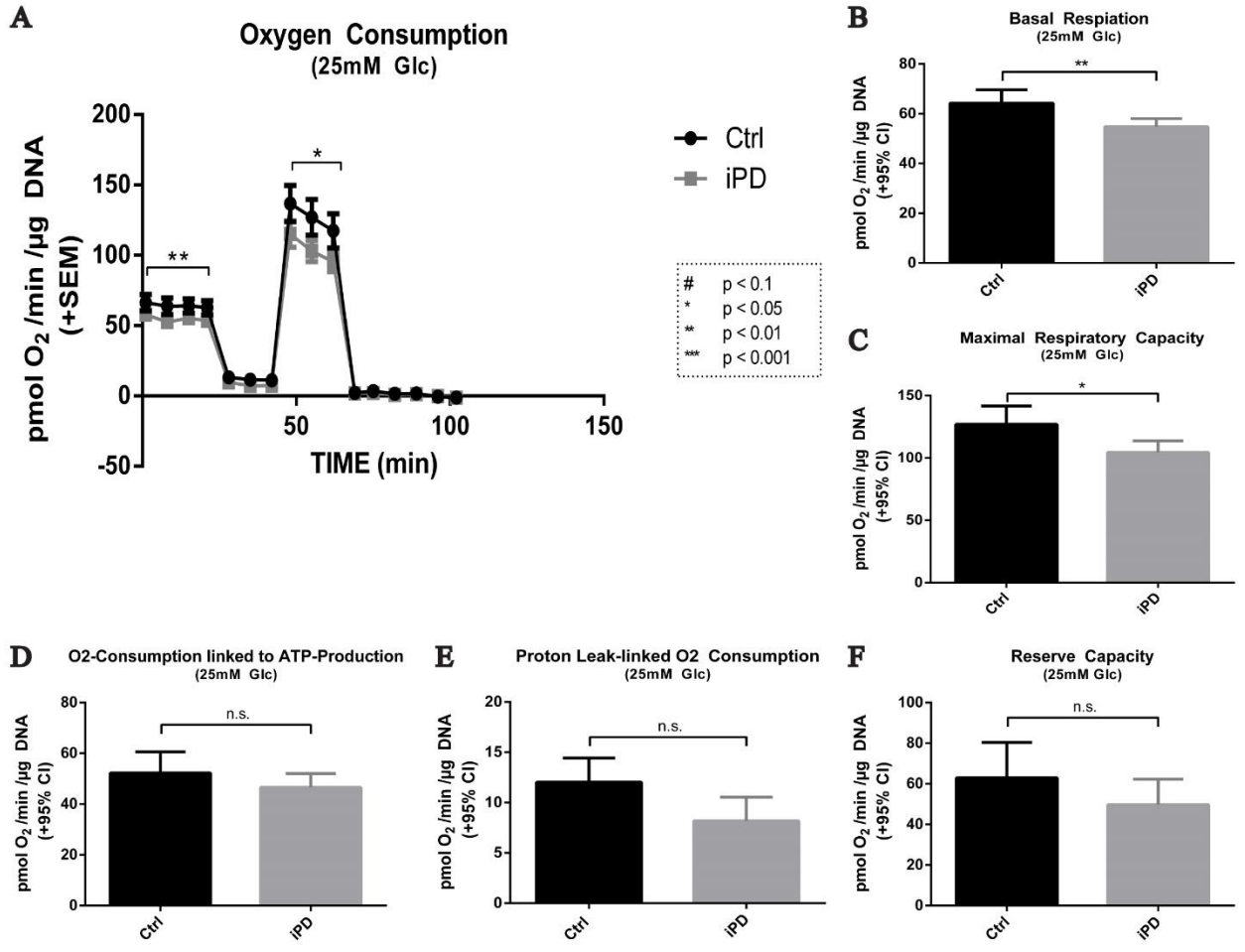

Fig. 24: Oxygen consumption analysis of iPD high-passage NPCs compared to corresponding controls with glucose as energy substrate. *Respiratory analysis of 7 iPD patients' iPSCs and 5 corresponding controls individuals' high-passage iPSCs, with 1-2 clones per individual (corresponding to 16 lines analyzed in total). Cells were analyzed with 25mM glucose as energy substrate, OCR was assessed and normalized to DNA content. (A) Shows the progression of the measurement, (B) displays the mean difference in basal respiration, (C) the mean difference in maximal respiratory capacity, (D) the mean oxygen consumption devoted to ATP production, (E) the mean proton-leak linked oxygen consumption and (F) the mean calculated reserve capacities. Every line was analyzed with n =3, statistical analysis (testing for outliers, normality of distribution and significance) was done using Graphpad*

Prism 6, either with Student's t-test for normally distributed values or Man-Whitney-test for non-parametrical distribution, $p < 0.05$ was considered significant.

It has to be noted here that low-passage NPCs respiratory assays cannot be compared to the other respiratory assays in absolute values, since a different way of DNA normalization was necessary here as cells detached from the plate after the Seahorse measurements. However, when looking at the pattern of the measurement, it becomes clear in Fig. 24A that high-passage NPCs display a very similar oxygen consumption pattern like their precursors, high-passage iPSCs. In general it can be observed, that low- and high-passage NPCs display similar respiratory patterns to each other, just as low- and high-passage iPSCs do. High-passage NPCs again show stable (not dropping) basal respiration, a maximal oxygen consumption which is much higher than their basal respiration, therefore yielding a rather high amount of spare respiratory capacity of mitochondria. These results indicate that a metabolic switch has been made from the iPSC state to NPC state, which, for example, may be exerted by maturation of mitochondria. Furthermore, the metabolic difference becomes obvious when looking at the OCR/ECAR ratios – while iPSCs display ratios around 2, NPCs show ratios of 1 (Fig. 14, 18, 22 and 26), indicating that there is less mitochondrial contribution despite greater mitochondrial capacity in relation.

Again, significantly reduced mean basal oxygen consumption (*control 64.24 ± 10.67; iPD 54.75 ± 10.09; $p = 0.0018$*; Fig. 24B) of iPD patients' cells can be observed in high-passage NPCs with just glucose as substrate, as previously already observed for high-passage iPSCs and low-passage iPSCs, yet not in low-passage NPCs. In addition, a significant decrease of mean maximal oxygen consumption (*control 127.08 ± 32.62; iPD 104.43 ± 29.39; $p = 0.0193$*; Fig. 24C) was observed for iPD patients' cells with glucose as substrate, while no significant differences could be observed for mean oxygen consumption attributed ATP production (*control 52.23 ± 7.91; iPD 46.57 ± 7.09; $p = 0.2198$;* Fig. 24D), the mean proton leak (*control 12.02 ± 5.39; iPD 8.17 ±5.00; $p = 0.1088$*; Fig. 24E) or the mean spare respiratory capacity (*control 62.84 ±16.99; iPD 49.68 ± 22.18; $p = 0.1943$*; Fig. 24F). Just like for high-passage iPSCs, this might hint towards either deficiency in substrate supply and / or oxidation, or changes in mitochondrial mass or mitochondrial complex expression resulting in a decrease of mitochondrial efficiency or functionality. To obtain a full image of cellular respiratory state, ECAR values were measured (Fig. 25)

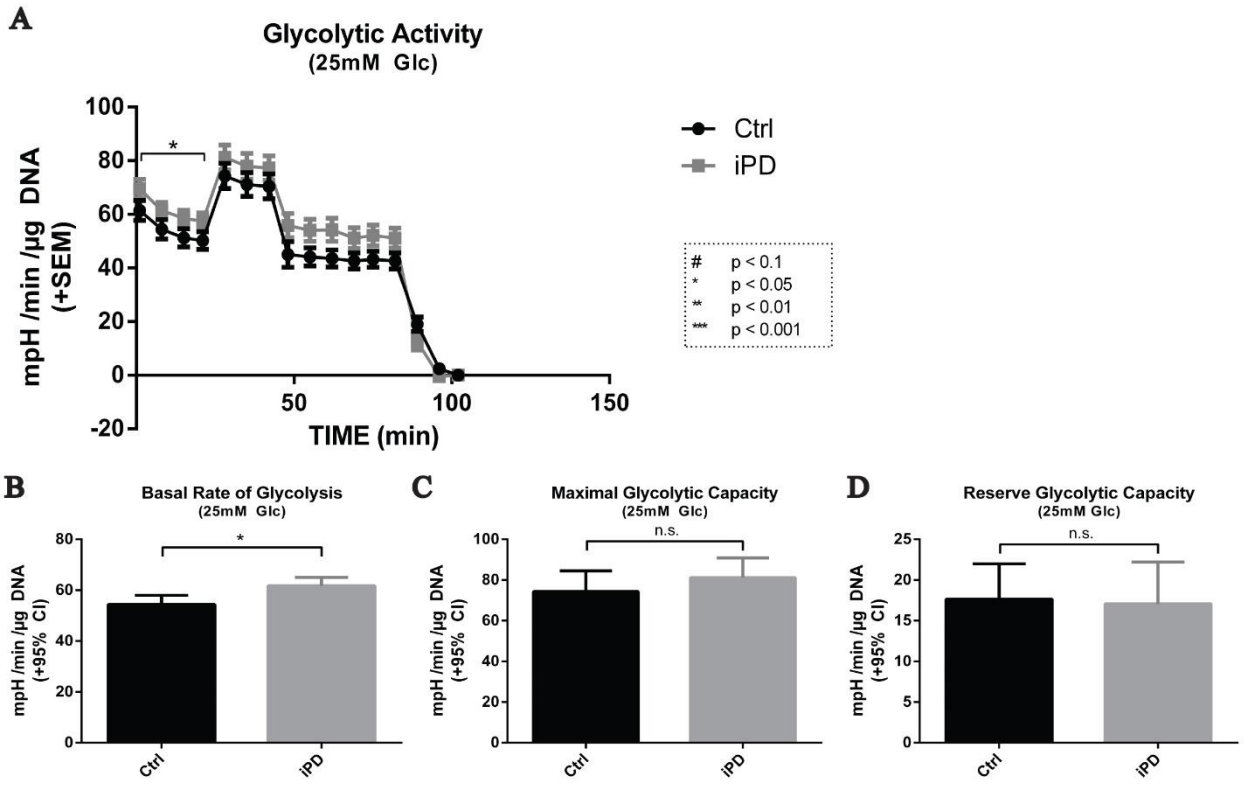

Fig. 25: ECAR analysis of iPD patients' high-passage NPCs compared to corresponding controls with glucose as energy substrate. *Respiratory analysis of 7 iPD patients' iPSCs and 5 corresponding controls individuals' high-passage iPSCs, with 1-2 clones per individual (corresponding to 16 lines analyzed in total). To assess specifically glycolytic activity, 25mM glucose were supplied as energy substrate. (A) Shows the progression of the ECAR during measurement, (B) displays the mean basal rate of glycolysis and (C) the mean maximal glycolytic capacity. Every line was analyzed with n =3, statistical analysis (testing for outliers, normality of distribution and significance) was done using Graphpad Prism 6, either with Student's t-test for normally distributed values or Man-Whitney-test for non-parametrical distribution, $p < 0.05$ was considered significant.*

Like before, the ECAR of high-passage NPCs was assessed in parallel to get a rough estimation of glycolytic activity. While, unfortunately, absolute values cannot be compared with high-passage iPSCs as explained before, the same pattern like in high-passage iPSCs can again be observed. High-passage NPCs show a significant increase in the mean basal glycolytic respiration in PD patients' cells (*control 54.33 ± 4.85; iPD 61.75 ± 8.65; p = 0.0223*; Fig. 25B), while no differences were observed in the mean maximal glycolytic capacity *(control 71.99 ± 3.48; iPD 78.82 ± 9.68; p = 0.3172;* Fig. 25C) and the mean reserve glycolytic capacity (*control 17.66 ± 3.09; iPD 71.07 ± 3.71; p = 0.8622*; Fig. 25D). Just like in high-passage iPSCs, this might hint towards a compensatory mechanism to overcome more likely substrate than ATP production deficiency already observed in the OCR measurements of high-passage NPCs. Like before, the OCR/ECAR ratio for high-passage NPCs was assessed (Fig. 26). Similar to what has been observed in low-passage NPCs, a clear reduction of OCR/ECAR ratio (control 0.78 ± 0.15; iPD 0.62 ± 0.12; p = 0.0834) can be seen in high-passage NPCs in comparison to high-passage iPSCs. This clearly indicates that NPCs seem to have a higher tendency of ATP production by glycolysis than their corresponding iPSCs.

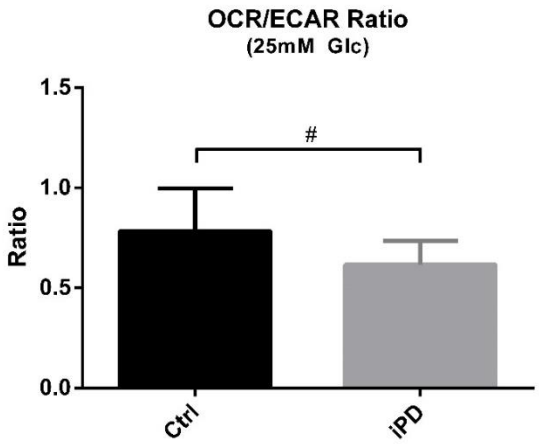

Fig. 26: OCR to ECAR ratio of iPD patients' high-passage NPCs compared to healthy controls' NPCs. *OCR to ECAR ratio was calculated by dividing the oxygen consumption attributed to ATP production (oligomycin dependent respiration) through the basal glycolytic respiration and reflects the cell's tendencies of ATP production. A ratio larger than 1 represents predominantly mitochondrial ATP production, while a ratio below 1 would represent largely glycolytic ATP production. Every line was analyzed with n =3, statistical analysis (testing for outliers, normality of distribution and significance) was done using Graphpad Prism 6, either with Student's t-test for normally distributed values or Man-Whitney-test for non-parametrical distribution, $p < 0.05$ was considered significant.*

Last but not least, cells were exposed to only pyruvate as energy substrate to evaluate mitochondrial contribution (Fig. 27). Again it becomes obvious that mitochondria are not at their maximal capacity when the cells are supplied with just glucose, as the absolute values between glucose and pyruvate differ towards increased respiratory capacity with pyruvate. Oxygen consumption with only pyruvate as substrate, measured in high-passage NPCs, shows for the first time a different pattern than all other measurements. No significant differences between iPD patients' cells and corresponding controls could be detected in the mean basal oxygen consumption (*control 111.21 ± 14.15; iPD 102.58 ± 14.15; p = 0.0549*; Fig. 27B), the mean oxygen consumption attributed to ATP production (*control 91.76 ± 11.50; iPD 85.12 ± 12.58; p = 0.2766*; Fig. 27D) or the mean proton leak (*control 19.45 ± 2.27; iPD 17.46 ± 3.56; p = 0.3132*; Fig. 27E), however, for the first time, a significant decrease in the maximal oxygen consumption (*control 169.08 ± 49.11; iPD 125.51 ± 39.92; p < 0.0001;* Fig. 27C) and reserve capacity (*control 57.88 ± 29.56; iPD 22.92 ± 28.79; p = 0.0112;* Fig. 27F) in iPD patients' cells was observed with pyruvate as substrate.

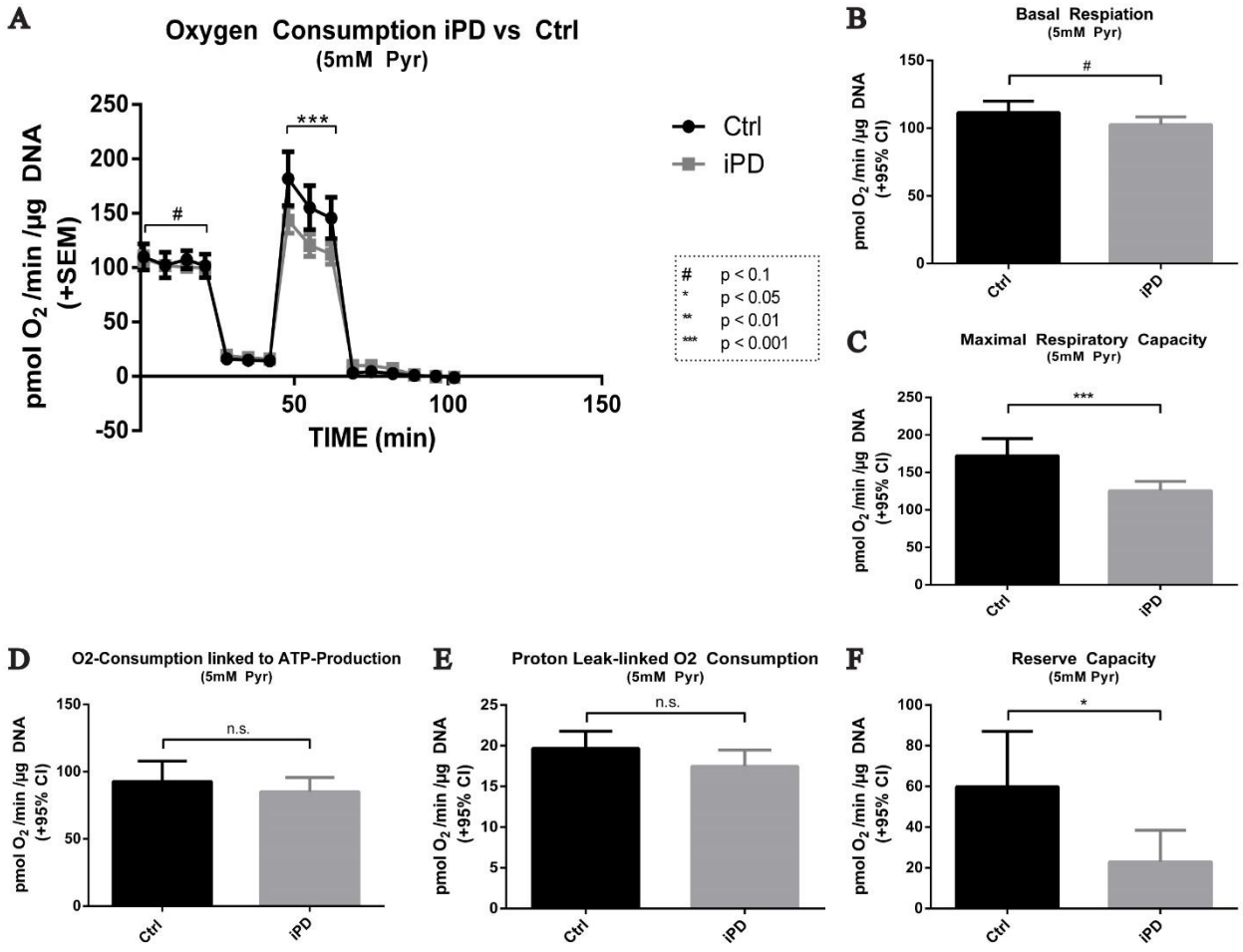

Fig. 27: Oxygen consumption analysis of iPD high-passage NPCs compared to corresponding controls with pyruvate as energy substrate. *Respiratory analysis of 7 iPD patients' iPSCs and 5 corresponding controls individuals' high-passage iPSCs, with 1-2 clones per individual (corresponding to 16 lines analyzed in total). Cells were analyzed with 5mM pyruvate as energy substrate, OCR was assessed and normalized to DNA content. (A) Shows the progression of the measurement, (B) displays the mean difference in basal respiration, (C) the mean difference in maximal respiratory capacity, (D) the mean oxygen consumption devoted to ATP production, (E) the mean proton-leak linked oxygen consumption and (F) the mean calculated reserve capacities. Every line was analyzed with n =3, statistical analysis (testing for outliers, normality of distribution and significance) was done using Graphpad Prism 6, either with Student's t-test for normally distributed values or Man-Whitney-test for non-parametrical distribution, $p < 0.05$ was considered significant.*

It has been mentioned before that maximal oxygen consumption is a plain function of substrate supply and mitochondrial efficiency (substrate oxidation, electron transport, complex efficiency). Indeed, when assessing complex I activity in these cells, a significant reduction of activity (*reduction of 34%, p=0.0019;* Fig. 28) could be observed (Schmidt, 2017), which explains the reduction in maximal respiration with pyruvate as substrate.

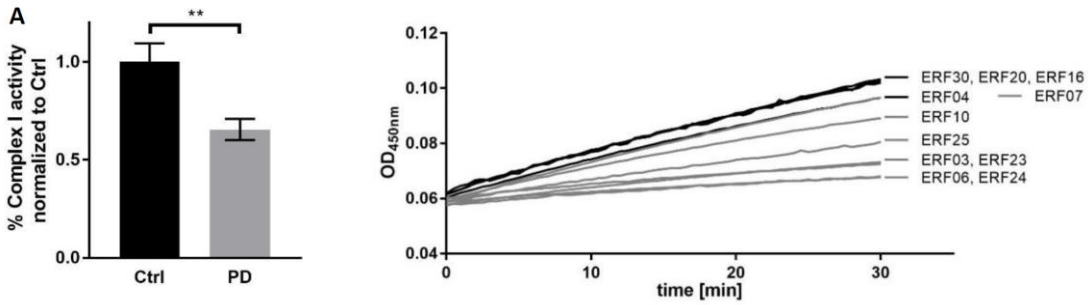

Fig. 28: Complex I activity measured in high-passage NPCs from iPD patients and corresponding controls. *Complex I activity was assessed with the complex I enzyme activity microplate assay kit (Abcam). Shown is the mean ± SEM of all iPD and control lines, measured with n=3, normalized to mean control. On the right, raw data of one measurement are displayed. Data and graph from (Schmidt, 2017).*

2.2.6. Metabolic profile of analyzed cells in comparison

In the light of the results obtained, it seemed worthy to take a closer look at the metabolic profile, i.e. the preferences in ATP production in iPSCs and NPCs of patients and corresponding controls. With just glucose as substrate, a trend towards decreased OCR/ECAR ratio, therefore increased ATP production by glycolysis, was observed in high passage iPSCs (Fig. 18) and NPCs (Fig. 26) from iPD patients compared to corresponding controls. This however does not compare high- and low-passage iPSCs or NPCs, for which reason a more detailed statistical analysis of the same data was done (Fig. 29 and 30). First, it becomes obvious that even though significant differences can be observed depending on passage and health state, high passage control and iPD cells as well as low-passage control and iPD cells have comparable metabolic profiles, independent from cell type (iPSCs or NPCs). As shown in Fig. 29, both, a significant decrease of OCR/ECAR ratio in iPD patients' cells ($p = 0.0411$), as well as a significant decrease in low- to high-passage cells ($p < 0.0001$) could be observed (*low passage: control 2.33 ± 0.80 and iPD 2.02 ± 0.95; high passage: control 1.49 ± 0.60 and iPD 1.10 ± 0.48;* Fig. 29), while no significant interaction of those two parameters was detected ($p = 0.8141$). This clearly demonstrates that (1) iPD cells either have a higher glycolytic metabolism or a decreased oxidative ATP production than the corresponding controls and (2) that iPSCs generally possess a more glycolytic metabolism over the course of time, as the ECAR values measured increase while the OCR values roughly do not change, accounting for an approximately 60% decrease in OCR/ECAR ratios.

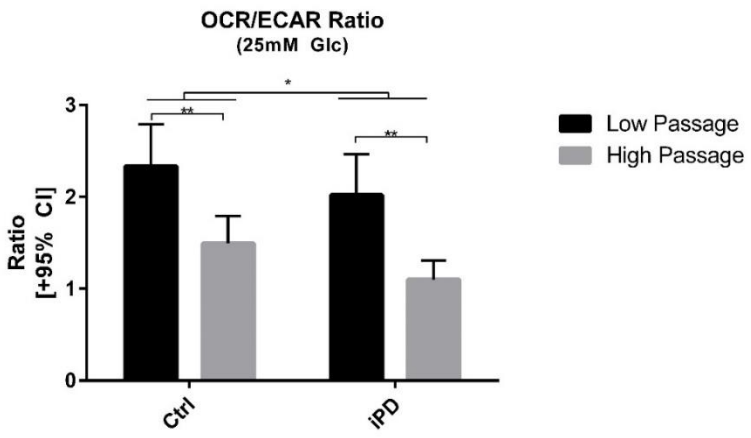

Fig. 29: OCR/ECAR ratios of low- and high-passage iPSCs of iPD patients' and corresponding controls' cells. *OCR/ECAR ratios were calculated using the respiratory data obtained in Seahorse XF96 measurements with the formula* $\frac{OCR}{ECAR} = (\frac{Oxygen\ Consumption\ attrubuted\ to\ ATP\ Production}{Basal\ Glycoylsis})$*. A ratio larger than 1 suggests that cells predominantly use mitochondrial ATP production, while a ratio smaller than 1 hints towards a predominantly glycolytic metabolism. Every line was analyzed with at least n =3, statistical analysis was done in Graphpad Prism 6, using two-way Anova analysis, p < 0.05 was considered significant.*

In contrast to what has been observed in iPSCs, OCR/ECAR ratios of NPCs did not reveal any significant differences, neither disease- nor cell-type specific. However, when looking at absolute values (*low passage NPCs: control 0.80 ± 0.29 and iPD 0.86 ± 0.30; high passage NPCs: control 1.04 ± 0.49 and iPD 0.78 ± 0.21; p = 0.2097;* Fig. 30) it becomes clear that the ratio between iPSCs and corresponding NPCs decreases 1.4 to 2.9 fold (*low passage iPSC/NPC: control 2.9; iPD 2.3; high passage iPSC/NPC: control 1.4; iPD 1.4*). This indicates that the strength of the metabolic switch upon differentiation does not depend on the health state (health or diseased) or on the passage of the iPSCs, since both times NPCs with comparable metabolic profile were obtained. Results will be discussed in more detail in section 3.5.

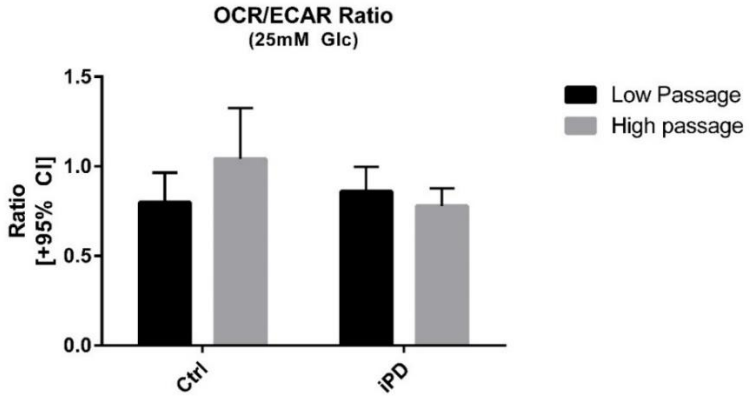

Fig. 30: OCR/ECAR ratios of high- and low-passage NPCs of iPD patients' cells and corresponding controls. *Shown is the comparison of high- and low-passage iPSCs of iPD patients' and corresponding control individuals' iPSCs. Every line was analyzed with at least n =3, statistical analysis was done in Graphpad Prism 6, using two-way Anova analysis, p < 0.05 was considered significant.*

2.3. Molecular characterization of high-passage iPSCs from iPD patients

Respiratory analyses of iPSCs and NPCs yielded a variety of phenotypes which might be related to mitochondrial function and efficiency. For this reason, a close look to certain features which possibly could explain the phenotypes observed had to be taken. Since this could not be done for all cell types, lines and substrates, all the following analyses were done on high-passage iPSCs, as here the strongest PD phenotype was observed and a complete rescue of phenotypes could be achieved by exposing the cells to pyruvate.

2.3.1. Viability of cells

As the respiratory analysis of iPSCs displayed phenotypes which could be explained by differing viability rates of iPD cells, viability of cells was assessed using the CellTiter-Glo™ Luminescent Cell Viability Assay. CellTiter-Glo™ Luminescent Cell Viability Assay can be used to determine the number of viable cells in culture based on quantization of ATP present, taking ATP as an indicator of metabolically active cells. In addition, this assay can be taken as first indication for strongly differing growth rates between iPD and control cells, as cell growth requires large amounts of ATP which should be reflected when quantifying present ATP levels. As seen in Fig. 31, no significant difference in ATP amount and therefore cell viability could be detected in high passage iPSCs from iPD patients when compared to corresponding controls.

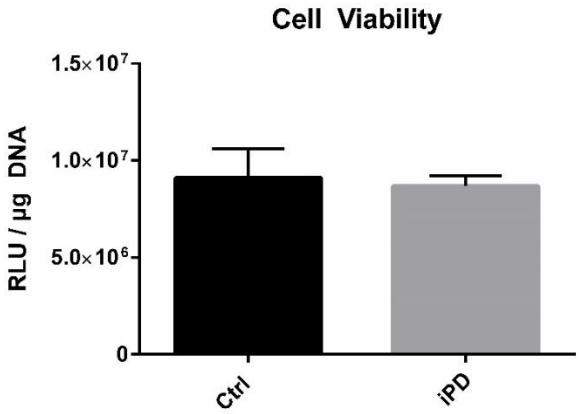

Fig. 31: Cell viability based on ATP content (CellTiter-Glo™ Luminescent Cell Viability Assay). *All lines were analyzed with n = 3 and an integration time of 0.1 seconds per well. Obtained relative luminescence units (RLU) were normalized to DNA content. Statistical evaluation was done with Graphpad prism 6 using student's t-test, a p-value < 0.05 is considered significant.*

2.3.2. Abundance of mitochondria and mitochondrial complexes

Section 1.2.2 gives a comprehensive introduction into mitochondrial function. Abundance of mitochondrial complexes and thereby changes in the expression level of any of the three proton pumps of the ETC as well as complex II and the F_0F_1-ATPase may account for respiratory changes, especially when pyruvate is given

as sole substrate. Even though no variances in OCR were detected in high-passage iPSCs when solely supplied with pyruvate, a reduction of complex I efficiency was found in high-passage NPCs and the respiration of iPD patients' low-passage iPSCs with pyruvate as substrate was also decreased. Furthermore, maximal respiration with glucose as substrate was decreased in iPD patients' high-passage iPSCs, which is a plain function of substrate supply and oxidation. For this reason, expression patterns of all five mitochondrial complexes were assessed by immunoblot analysis (Fig. 32A-C). However, despite the multitude of phenotypes observed in respiratory analyses, no significant changes in the abundance of mitochondrial complexes were observed. In addition, even though protein levels of the mitochondrial complexes do not give information about the amount and fission/fusion state of mitochondria, they give information about mitochondrial mass. Since no changes were observed in the protein levels of any mitochondrial complexes, but especially not in complex V, it can be assumed that iPD patients' cells and corresponding control cells have a roughly equal mitochondrial mass. To further undermine this statement, qRT-PCR analysis for expression of the mitochondrially encoded 12S RNA (*MT-RNR1)* was done, in order to assess the relative amount of mitochondrial DNA copies and their expression (Fig. 33). Again, no significant differences between iPD cells and corresponding control cells could be observed. In summary, this indicates that there are no differences in mitochondrial mass, mtDNA copy-number and expression as well as protein levels of the mitochondrial complex I – V.

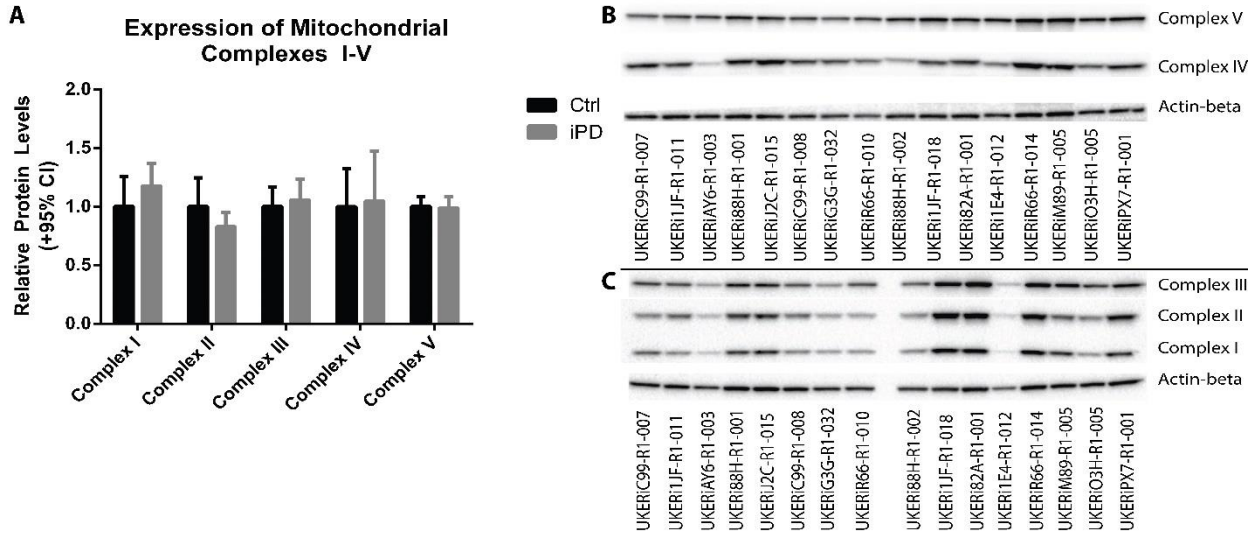

Fig. 32: Relative protein levels of mitochondrial complex I-V in iPD patients' high-passage iPSCs compared to corresponding control iPSCs. *Western Blot analysis of mitochondrial complex I-V revealed no differences in relative protein levels in iPD patients' cells to corresponding control cells. (A) Shows an overview of complex I-V protein levels iPD patients' high passage iPSCs normalized to corresponding control cells protein levels. (B) Is a representative picture for immunoblotting of complex IV and complex V normalized to beta-Actin protein levels, (C) a representative picture of complex I-III and beta-Actin protein levels. Statistical analysis was done with Graphpad Prism 6 using student's t-test, all samples were analyzed with n = 3, p < 0.05 is considered significant.*

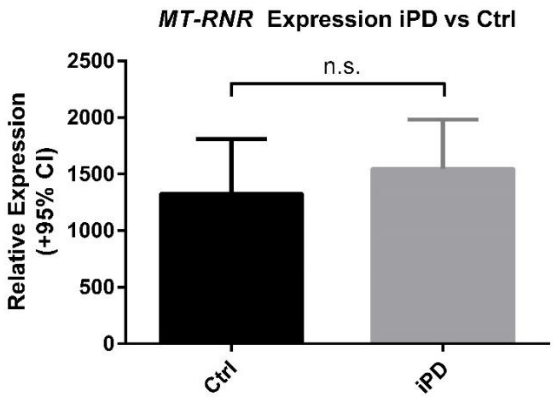

Fig. 33: qRT-PCR analysis of the mitochondrially encoded 12S RNA (MT-RNR1). *Expression analysis of MT-RNR1 was done to assess differences in expression of mtDNA and mtDNA copy numbers. Statistical analysis was done with Graphpad prism 6 using student's t-test, every sample was analyzed with n = 3, $p < 0.05$ is considered significant.*

2.3.3. Electron flow and coupling efficiency

Similar to complex expression, efficiency of electron flow and coupling efficiency may significantly affect the mitochondrial function previously assessed in respiratory experiments. Therefore, both, electron flow and coupling efficiency of mitochondria were assessed. Mitochondrial electron flow across the complexes and coupling efficiency can either be assessed in isolated mitochondria or in permeabilized cells using the Seahorse XF96 platform. In this thesis, the approach of permeabilizing cells with Digitonin was used. Digitonin is a steroidal saponin, which greatly facilitates permeabilization of cholesterol rich cellular membranes, i.e. the cellular membrane and the outer mitochondrial membrane. The inner mitochondrial membrane is devoid of cholesterol which has the advantage that low concentrations of Digitonin do not permeabilize the inner membrane, thereby not destroying the proton gradient and mitochondrial functionality (Anderson and Sims, 2000; Vercesi et al., 1991). In consequence, "isolated" measurements of intact mitochondria can be done. Measurements were performed in mitochondrial assay buffer (MAS-buffer) using a Seahorse XF96 analyzer, thereby analyzing oxygen consumption as a function of electron transport or coupling efficiency.

To measure electron flow, assay buffer was supplied with ADP, FCCP, Digitonin, fatty acid free BSA, malate and pyruvate. Digitonin is applied to permeabilize cellular membranes, fatty acid free BSA to stabilize mitochondria and "snatch away" fatty acids which might be used as alternative mitochondrial substrate. FCCP was added to uncouple mitochondria in order to assess maximal possible rates of oxygen consumption upon electron flow through the proton pumps of the ETC. ADP was added as test experiments revealed that higher levels of respiration could be achieved if the F_0F_1-ATPase was given a substrate, albeit theoretically not compelling. To ensure that respiration is only driven by complex I at first (using the

pyruvate applied, which subsequently becomes metabolized in the TCA to NADH to drive complex I driven respiration), malonate was applied as a competitive inhibitor of the succinate dehydrogenase (complex II). This allows to obtain complex I driven oxygen consumption. Subsequently, rotenone was added to inhibit complex I driven respiration and in a second step succinate was applied to obtain complex II and III driven respiration. Again, respiration was subsequently inhibited by the addition of Antimycin-A. Finally, complex IV driven oxygen consumption was measured by the addition of an excess amount of the electron donor Tetramethylphenylendiamin (TMPD).

To assess mitochondrial coupling efficiency, assay buffer was supplied with fatty acid free BSA, Digitonin, rotenone and succinate. Rotenone inhibits complex I driven respiration and succinate serves as substrate for complex II. Therefore, the basal measurement represents basal oxygen consumption which may run on ADP as substrate for the F_0F_1-ATPase and has not been removed by permeabilization. Subsequently, ADP is injected to bring OXPHOS and ETC at running capacity, since now substrate is present. Following, the F_0F_1-ATPase was inhibited by the addition of oligomycin, leaving the proton gradient intact and mitochondria uncoupled to gain insight into maximal possible rates of oxygen consumption. Finally, Antimycin-A was added to inhibit the ETC and get a readout for non-mitochondrial oxygen consumption for normalization. Both, oxygen-consumption for electron transfer and coupling efficiency were normalized to DNA content.

It becomes apparent in Fig. 34 that there are no significant differences, neither in electron transport efficiency nor in coupling efficiency in the mitochondria from iPD patients' iPSCs in comparison to corresponding control cells. Looking at electron transport across the complexes it becomes obvious that respiration driven by complex I is most efficient, as generally would be expected. When looking at coupling efficiency, it becomes clear that maximal respiration is reached upon the supply of ADP when comparing with the FCCP stimulated respiration, indicating that there is no issue in coupling OXPHOS and ECT. Furthermore, the combined presentation of coupling efficiency and electron transfer (Fig. 34E) reveals that complex II driven respiration does not differ between both experiments, providing for the stability of the obtained data.

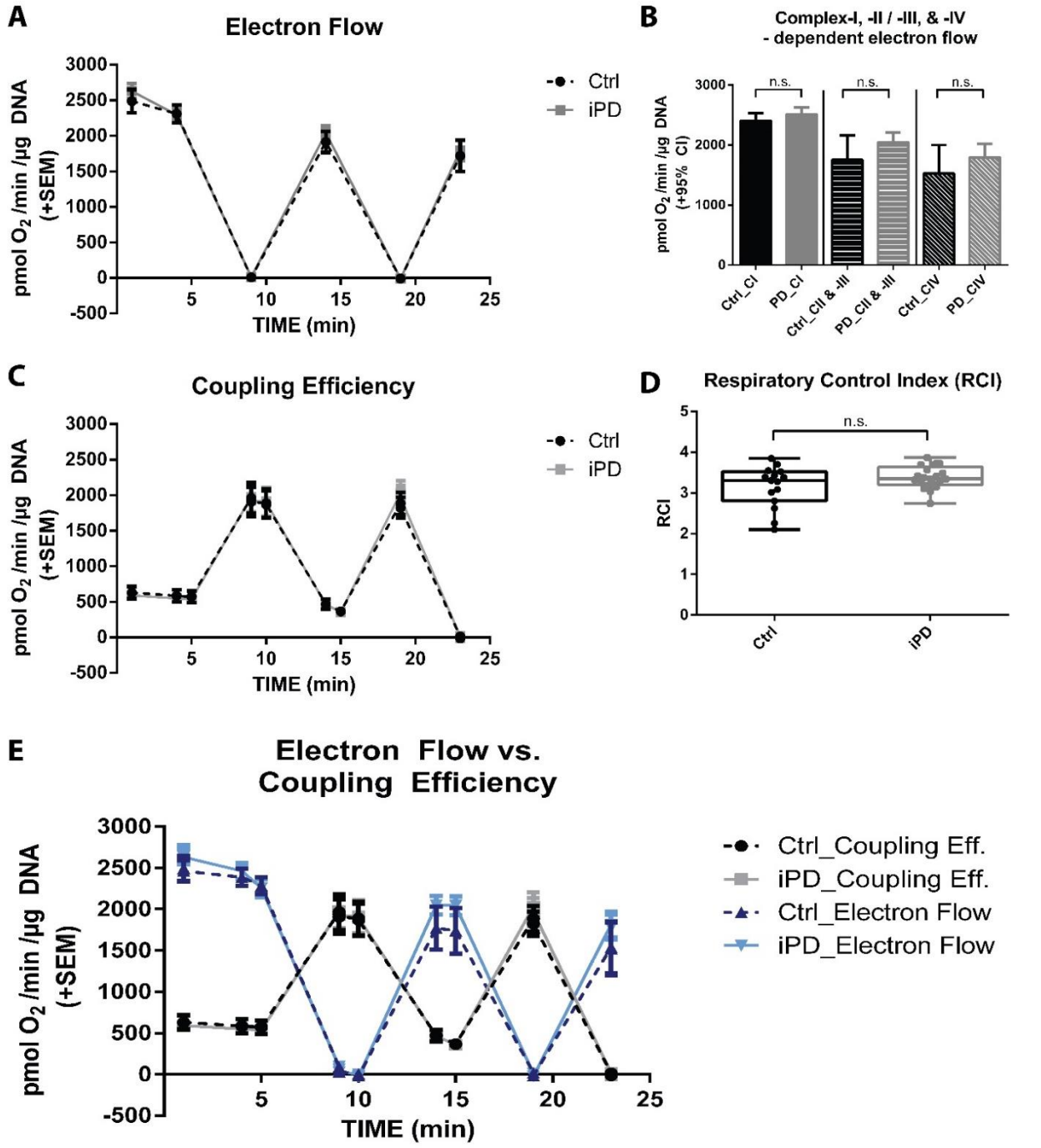

Fig. 34: Assessment of mitochondrial electron transport and coupling efficiency in permeabilized cells as a function of oxygen consumption using the Seahorse XF96 analyzer. *Mitochondrial electron transfer and coupling efficiency were assessed as described section 4.2.3.2 in high-passage iPSCs in iPD patients' and corresponding control individuals' cells. Injection-pattern for electron flow measurements were as follows: Port A: 25µM rotenone; Port B: 100mM succinate (pH7 – 7.2); Port C: 40µM Antimycin-A; Port D: 1mM TMPD + 100mM ascorbic acid (pH6). Injection-pattern for coupling efficiency measurements were Port A: 40mM ADP; Port B: 25µg/mL oligomycin; Port C: 5µM FCCP; Port D: 4µM Antimycin-A. (A) displays the progression of the electron flow measurement over time and injections, (B) the calculated complex dependent electron flow, (C) the progression of the coupling efficiency measurement over time, (D) the resulting calculated respiratory control index and (E) the combined measurements of electron flow and coupling efficiency. All samples were measured with an n = 3, statistical analysis was done with Graphpad prism 6 using student's t-test, p-value < 0.05 is considered significant.*

2.3.4. Mitochondrial dynamics

Mitochondrial fission and fusion are essential processes for mitochondrial quality control and functioning. However, they also play a role in "short-term" mitochondrial metabolism, adapting mitochondrial morphology to the appropriate state depending on substrate supply and mitochondrial demands. The cell usually maintains tight control over mitochondrial networks to deal with different types of stress. For example low levels of stress (e.g. during starvation) are countered with increased fusion and / or decreased fission, while high levels of stress are countered with decreased fusion and / or increased fission (reviewed in van der Bliek et al., 2013). As described in section 1.2.2, the process of mitochondrial fission is mainly regulated by regulation of Drp1 and its phosphorylation state. In contrast, the mitofusins mitofusin-1 (Mfn1), mitofusin-2 (Mfn2) and optic atrophy 1 (Opa1) are predominantly controlled by proteasome cleavage. Here, the expression levels of the mitofusins were assessed under the assumption that changes in cleavage of the proteins will result in changes in the expression of the mitofusins (Fig. 35), while regulation of fission was assessed by immunoblotting of Drp1 and its phosphorylation sites (Serin^{616} and Serin^{637}) (Fig. 36). In order to reproduce the environment present during respiratory measurements, cells were switched into Seahorse XF Assay medium supplied with either 25mM glucose or 5mM pyruvate and incubated at 37°C / 0% CO_2 for three hours (accounting for equilibration phase and run duration time of one Seahorse experiment) and subsequently lysed to obtain the protein or RNA for analysis.

As shown in Fig. 35 there are no changes in the expression pattern of the mitofusins between iPD patients' high passage iPSCs and corresponding controls. No significant changes could be observed in neither two-way Anova analysis nor Tukey's Post-hoc testing for the expression of *Mfn1* ($p = 0.1325$; Fig. 35A), the expression of *Mfn2* ($p = 0.2570$; Fig. 35B) or the expression of *Opa1* ($p = 0.2176$; Fig. 35C). A substrate effect could only be observed for *Mfn2* expression ($p = 0.0021$; Fig 35B), with decreased expression of *Mfn2* when exposed to pyruvate. No significant changes were detected when testing for interactions. This implies that the mitochondrial fusion machinery is likely not affected in these cells.

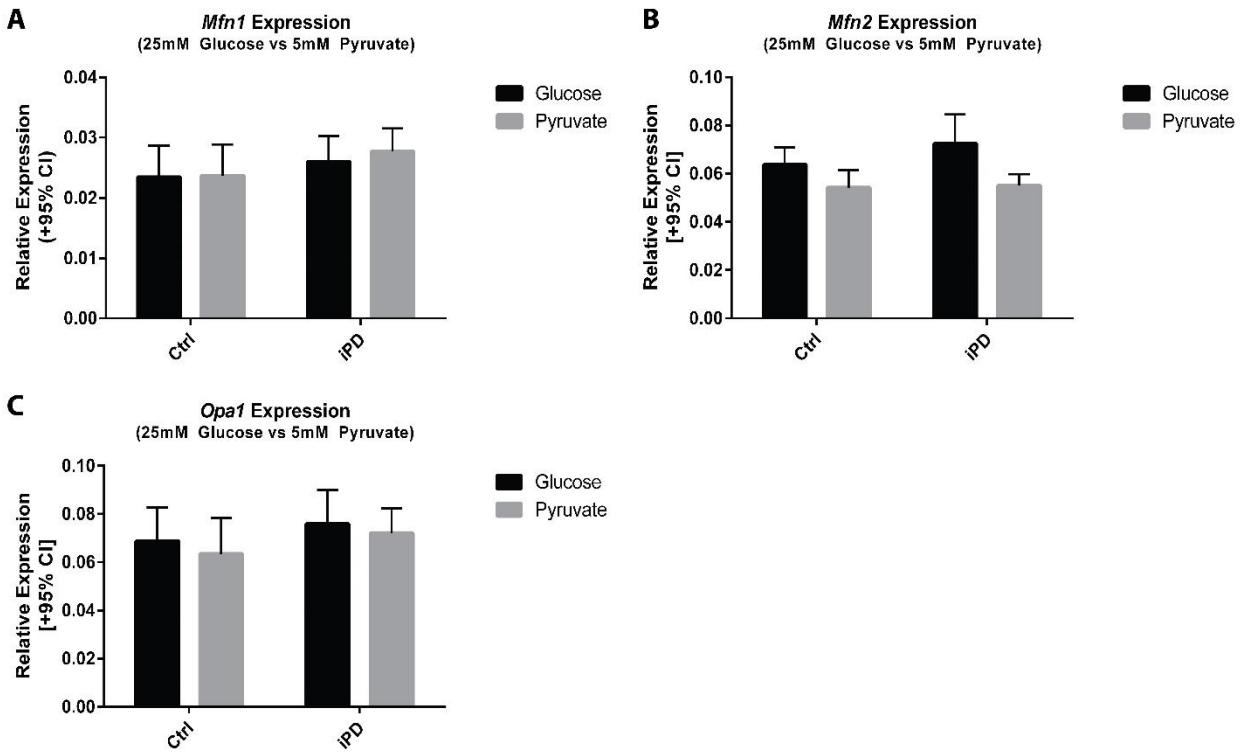

Fig. 35: Expression of the mitofusins Mfn1, Mfn2 and Opa1 using qRT-PCR in high passage iPSCs from iPD patients' and corresponding controls. *Expression of the mitofusins was analyzed as respective analysis of changes in the fusion machinery in iPD patients' cells compared to corresponding controls, depending on the different substrates used in the Seahorse XF96 analysis (25mM glucose or 5mM pyruvate). (A) Displays the expression levels of Mfn1 in iPD and control cells with glucose or pyruvate as substrate, (B) shows the expression levels of Mfn2 and (C) the expression levels of Opa1 under equal conditions. All samples were analyzed with an n = 3, statistical analysis was done with Graphpad prism 6 using two-way ANOVA and Tukey's Post-hoc test, p < 0.05 is considered significant.*

However, the fission and fusion processes regulating mitochondrial dynamics are often, but not necessarily concerted, e.g. decreased fission could be mediated by an increase in the activity of the fusion machinery or decrease in the activity of the fission machinery without previous changes in the fusion machinery. Fig. 36 shows that this might be the case in the high-passage iPD patients' cells when compared to corresponding controls. Fig. 36A depicts that Drp1, normalized against Actin-beta, is generally expressed at decreased levels in iPD patients' cells. Furthermore, two phosphorylation sites of Drp1, Serin^{616} (Fig. 36B) and Serin^{637} (Fig. 36C) were analyzed. Phosphorylation of Serin^{616} by Cyclin-dependent kinase 1 (Cdk1/cyclin B) has been published to be fission-promoting, while phosphorylation at site Serin^{637} by protein kinase A (PKA) is thought to change conformation of the Drp1-protein in such way that it is decreasing fission activity (reviewed in Knott et al., 2008). Detection of phospho-Serin^{637}-Drp1 showed only very weak levels of Serin^{637}-phopshorylation (Fig. 36D) and no changes in phospho-Serin^{637}-Drp1 could be detected neither when normalized to Actin-beta (*p = 0.3828;* supplementary Fig. 6B) nor when normalized to total Drp1 levels (*p = 0.2142;* Fig. 36C). In contrast, good detection of a phospho-Serin^{616}-Drp1 was possible and a significant decrease of phospho-Serin^{616}-Drp1 levels could be detected in iPD patients' cells compared to

corresponding controls, both when normalized to Actin-beta (*p = 0.0008;* supplementary Fig. 6A) and to total Drp1 levels (*p = 0.00159;* Fig. 36B), while no substrate dependence or interaction could be detected. This clearly indicates that there seems to be a general decrease in the expression and activation of the fission machinery in iPD patients' high-passage iPSCs compared to corresponding controls, which may explain some of the phenotypes observed.

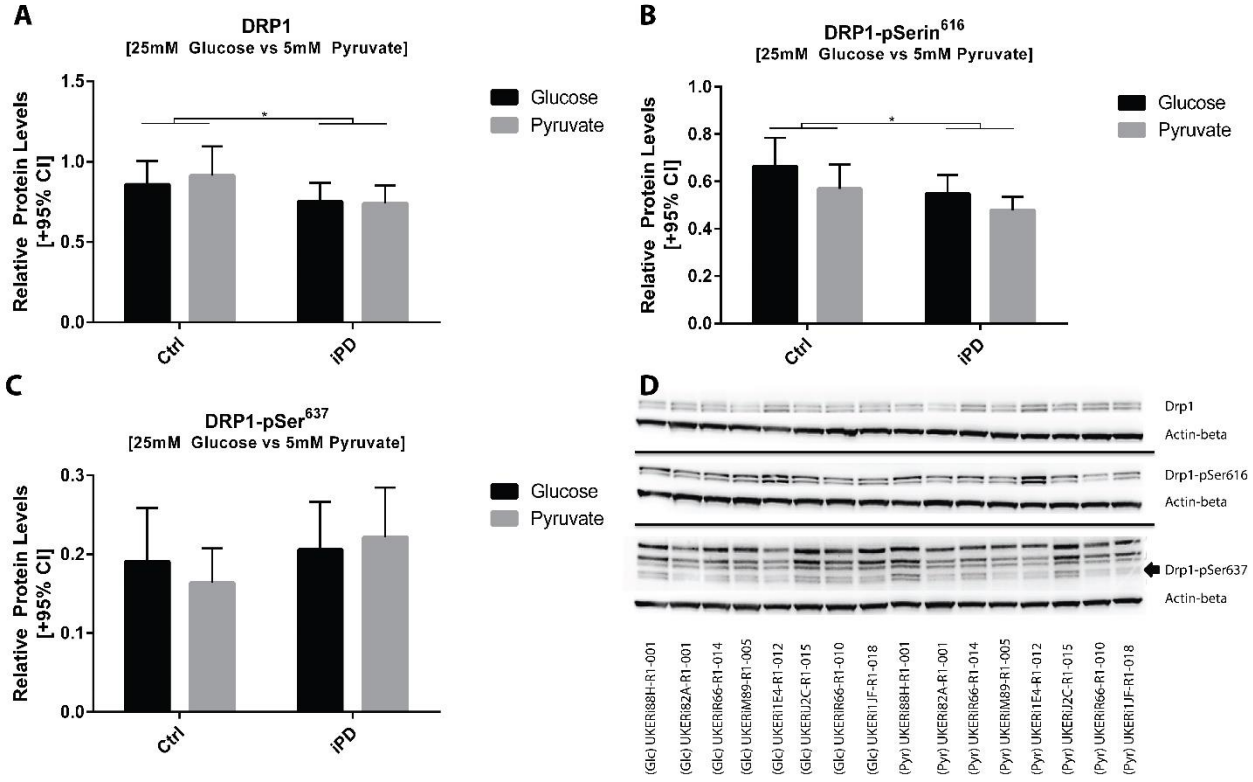

Fig. 36: Analysis of protein level and phosphorylation state of mitochondrial fission machinery by looking at Drp1 and its phosphorylation sites. *Drp1 expression and expression of phospho-Serin^{616}-Drp1 and phospho-Serin^{637}-Drp1 was assessed by immunoblotting. (A) Displays total expression of Drp1 normalized to Actin-beta levels, (B) shows the expression of phospho-Serin^{616}-Drp1 normalized to total Drp1 expression, (C) shows the expression of phospho-Serin^{637}-Drp1 normalized to total Drp1 expression and (D) an example of the immunoblotting with glucose and pyruvate as substrate. All samples were analyzed with n = 3, statistical analysis was done with Graphpad prism 6 using two-way Anova and Tukey's Post-hoc test, a value of p < 0.05 is considered significant. No significant p-values of interaction or substrate dependency were observed.*

2.3.5. Substrate availability

Next to cell viability, mitochondrial abundance, complex expression, efficiency and dynamics, limited substrate availability might account for the phenotypes observed during oxygen consumption measurements of both, low- and high-passage iPSCs from iPD patients' cells compared to control individuals' cells. To address this issue, glucose uptake was measured as a decreased ability to take up glucose will limit all downstream processes. Lactate levels were assessed as measurement of glycolytic activity as well as a hint of substrate usage. Total NAD^+/NADH ratios were determined as a shift towards either NAD^+ or NADH

will affect mitochondrial complex 1 driven respiration and might give a fair indication of which pathways might be dysregulated.

First, glucose uptake was assessed using a glucose uptake kit (Abcam). Cells were fed with 2-deoxyglucose (2-DG) instead of glucose, which is not discriminated against by glucose import proteins, yet accumulates after being metabolized to 2-deoxyglucose-6-phosphate as the glucose-6-phosphate isomerase is not able to take it as substrate. After a certain time period, cells were lysed and 2-deoxyglucose-6-phosphate levels analyzed (Fig. 37). Furthermore, expression of the glucose transporters (GLUT1-4, gene locus *SLC2A1-4)* was analyzed using qRT-PCR. No significant changes could be detected in either glucose import (*p = 0.6251*) or the expression of the glucose transporters (*SLC2A1 p = 0.3846; SLC2A3 p = 0.4507; SLC2A4 p = 0.2007;* Fig. 37). It has to be noted at this point that *SLC2A2* was virtually not detectable in neither iPD patients' iPSCs nor corresponding controls, albeit published to be found in human stem cells (Segev et al., 2012).

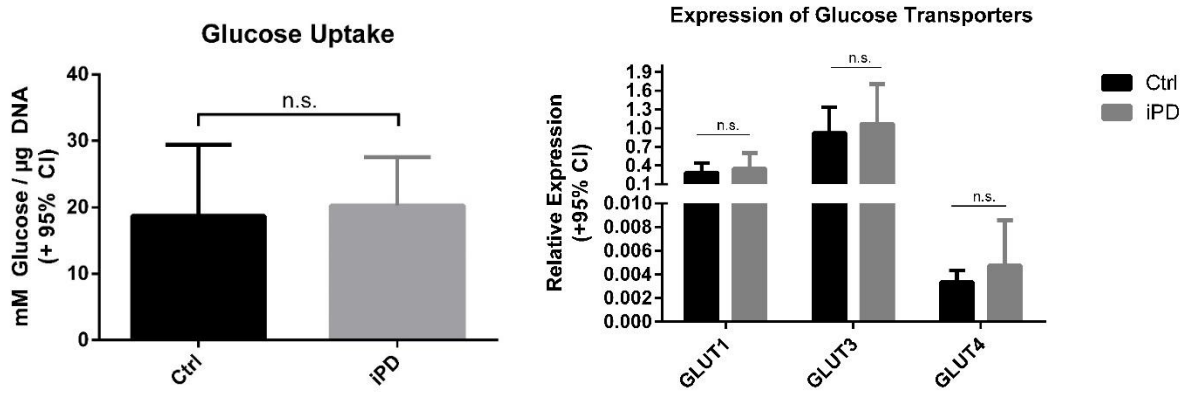

Fig. 37: Glucose uptake and expression levels of glucose transporters. *Glucose uptake was assessed using a commercially available kit, detecting the uptake and accumulation of 2-deoxyglucose, expression of glucose transporters was determined using qRT-PCR. GLUT-1, -3 and -4 were well detectable, expression of GLUT-2 could not be detected. All samples were analyzed with n=3, statistical analysis was done with Graphpad prism using either student's t-test or Mann-Whitney test, depending on normal distribution present, p < 0.05 is considered significant.*

Next, L-lactate levels were assessed. Usually, cells produce L-lactate from excess levels of pyruvate, which is not metabolized to CoA or fed into amino acid metabolism. Lactate production can also be a mechanism of regulation to control mitochondrial metabolism by limiting the pyruvate available for mitochondrial metabolism. L-Lactate levels were measured using a commercially available kit (Abcam) (Fig. 38). As for protein isolation and RNA preparation, conditions under which respiratory measurements were done were mimicked for L-Lactate level detection. Even though no significant differences could be observed on general terms between iPD patients' cells and control individuals' cells for both substrates, 25mM glucose and 5mM pyruvate (*p = 0.2699;* Fig. 38), interestingly enough a strong substrate dependent effect, with significantly reduced L-Lactate production was observed (*p = 0.0045*; Fig. 38) with pyruvate as substrate when compared to glucose as a substrate. This will be further discussed in section 3.1.

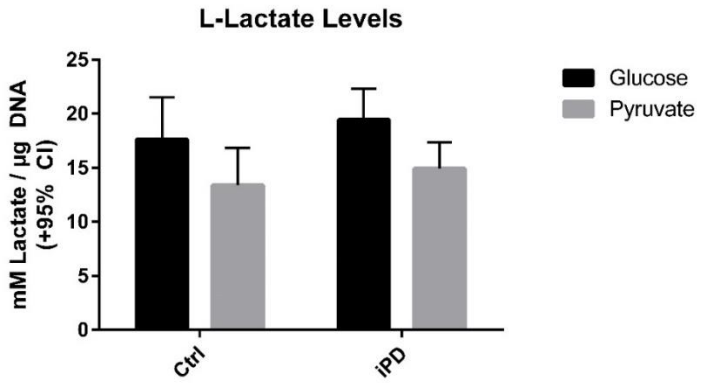

Fig. 38: Measurement of L-Lactate levels at Seahorse XF respiratory measurements conditions. *Shown are L-Lactate levels at conditions mimicking the conditions during Seahorse XF runs. No significant differences were observed between iPD patients' cells under neither glucose nor pyruvate compared to control individuals' cells. However, a significant substrate dependent effect in L-Lactate production was observed, with significantly reduced L-Lactate produced when pyruvate was supplied as substrate. All samples were measured with n = 3, statistical analysis was done with Graphpad prism 6 using two-way Anova and Tukey's Post-hoc test, p < 0.05 is considered significant.*

Finally, total NAD^+/NADH ratio was assessed in iPD patients' and control individuals' cells, as reduced levels of NADH, being a direct substrate of complex I, could explain the observed phenotypes. Additionally, as the majority of cellular NAD/NADH metabolism occurs during glycolysis and in the TCA, variations could hint towards several processes to take a closer look at. However, as shown in Fig. 39, no variances in NAD^+-levels or $NADH/H^+$-levels could be detected.

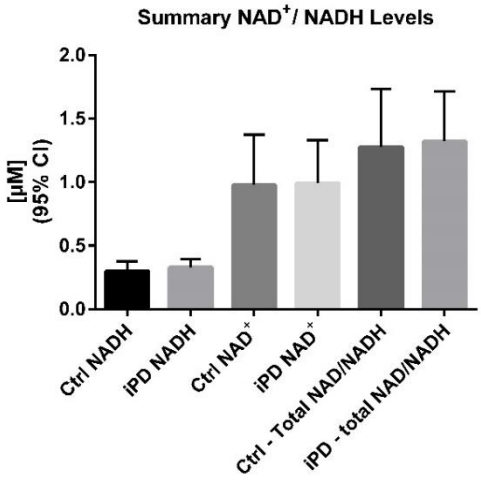

Fig. 39: NAD^+/NADH levels measured in high-passage iPSCs in iPD patients' compared to control individuals' samples. *For cellular NAD^+/NADH measurement, a commercially available kit (Abcam) was used, all samples were measured with n = 3. Statistical analysis was done with Graphpad prism using student's t-test after testing for out-layers and normality of data distribution, p < 0.05 is considered significant.*

2.4. Mitochondrial dynamics in NPCs derived from high-passage iPSCs

The presented molecular characterization of NPCs derived from high-passage iPSCs was done by Sebastian Schmidt in his Master's thesis, which was incorporated into this thesis and supervised by the author of this thesis. All data in this section are taken from (Schmidt, 2017) and are presented here to obtain a more comprehensive image.

In contrast to the results obtained in high-passage iPSCs, NPCs differentiated from those cells behaved differently. While similar respiratory phenotypes could be observed for some conditions, no significant changes in respect of health state could be observed when looking at mitochondrial fission and fusion (Fig. 40).

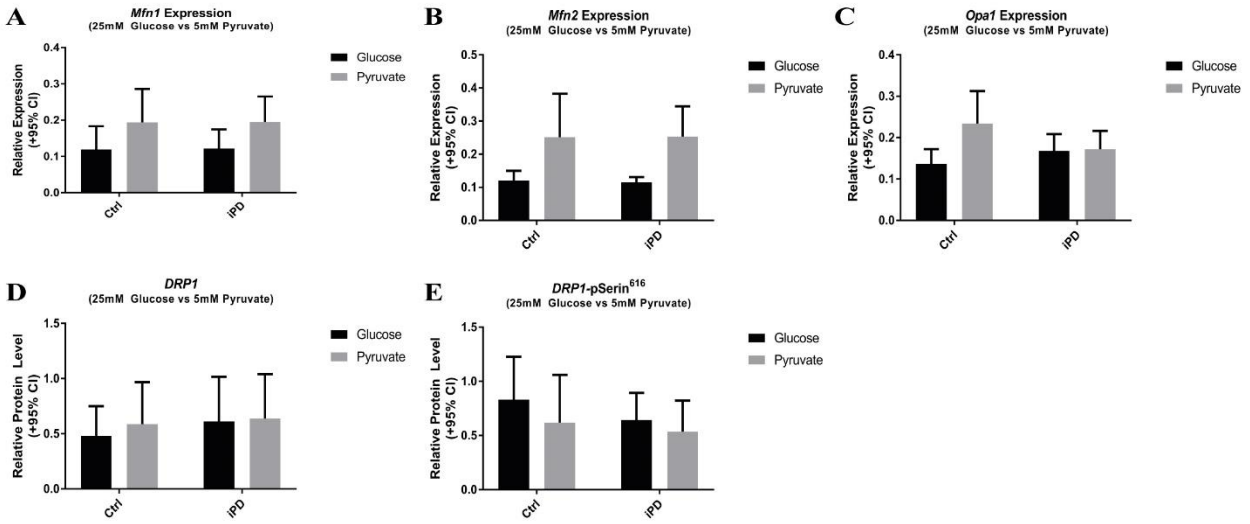

Fig. 40: Analysis of the expression of mitochondrial fusion proteins as well as the protein level and phosphorylation state of mitochondrial fission machinery by looking at Drp1 and its phosphorylation sites. *Expression of the mitofusins was analyzed as respective analysis of changes in the fusion machinery in iPD patients' cells compared to corresponding controls, depending on the different substrates used in the Seahorse XF96 analysis (25mM glucose or 5mM pyruvate). (A) Displays the expression levels of Mfn1 in iPD and control cells with glucose or pyruvate as substrate, (B) shows the expression levels of Mfn2 and (C) the expression levels of Opa1 under equal conditions. Drp1 expression and expression of phospho-Serin^{616}-Drp1 was assessed using immunoblotting. (D) Displays total expression of Drp1 normalized to beta-Actin levels, (E) shows the expression of phospho-Serin^{616} -Drp1 normalized to total Drp1 expression. All samples were analyzed with n = 3, statistical analysis was done with Graphpad prism 6 using two-way Anova and Tukey's Post-hoc test, a value of $p < 0.05$ is considered significant. No significant p-values of interaction or substrate dependency were observed. Data taken from (Schmidt, 2017).*

While no significant changes were observed in the fission machinery when looking at total Drp1 (*health state p = 0.5663; substrate p = 0.6685 and interaction p = 0.8031;* Fig. 40D) and phospho-Serin^{616}-Drp1 (*health state p = 0.3073; substrate p = 0.2316; interaction p = 0.6814;* Fig. 40E), this time, changes in the expression of the mitofusins could be observed. Expression of *Mfn1* (*p = 0.0289;* Fig. 40A), *Mfn2* (*p = 0.0004;* Fig. 40B) and *Opa1* (*p = 0.0360;* Fig. 40C) was significantly changed depending when comparing expression under glucose and pyruvate, being significantly increased under pyruvate (or significantly decreased under glucose).

2.5. Engrailed

Engrailed is an essential protein during the development of dopaminergic neurons and has been associated with PD for quite some time now. Therefore, expression of *Engrailed* (*En1 and En2*) and other related factors (*Pitx3, Nurr1* and *Lmx1a*) was analyzed in low- and high-passage iPSCs of iPD patients and all corresponding differentiation products, to investigate if *En1* and *-2* might influence the expression and development of other dopaminergic factors as well as the bioenergetic state of those cells and the differentiation capacity of iPD patients' cells compared to control cells. Low- and high-passage iPSCs and low-passage NPCs were analyzed by the author of this thesis, high-passage NPCs and their terminally differentiated products in form of dopaminergic neurons (mDANs) again by Sebastian Schmidt in course of his Master's thesis, yet incorporated into this thesis for a more comprehensive overview.

First, *En1* and *En2* expression were analyzed in low- and high-passage iPSCs of iPD patients' and control individuals' cells. As shown in Fig. 41A and B, both, *En1* and *En2* expression was significantly reduced in iPD patients' iPSCs.

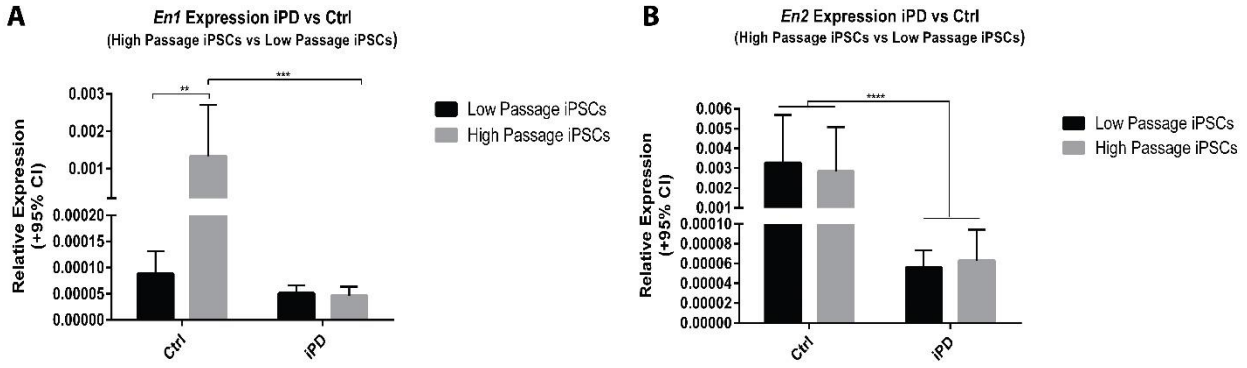

Fig. 41: Expression of Engrailed in low- and high-passage iPSCs. *(A) Displays the expression levels of En1 in low- and high-passage iPSCs, (B) the expression levels of En2 in low- and high-passage iPSCs. All samples were analyzed with at least n = 3, statistical analysis was done with Graphpad prism using two-way Anova and Tukey's Post-hoc test, $p < 0.05$ is considered significant.*

En1 expression was found to be significantly decreased in iPD patients' cells compared to corresponding controls ($p = 0.0034$; Fig 41A). In addition, a strong passage-dependent decrease ($p = 0.0058$) and interaction effect ($p = 0.0055$) could be detected. Tukey's Post-hoc test revealed a significant reduction of *En1* expression in high-passage iPSCs when comparing iPD patients' cells to corresponding controls' cells ($p = 0.0007$), while no significant decrease in low-passage iPSCs in iPD patients' cells could be detected ($p = 0.9993$). Furthermore, a passage-dependent significant increase in *En1* expression could be detected between control individuals' cells ($p = 0.0037$), which was not detected between iPD patients' cells ($p > 0.9999$).

En2 showed a significantly reduced expression in low- and high-passage iPSCs ($p < 0.0001$; Fig. 41B), while no passage-dependent effect or interaction could be detected ($p = 0.7301$ and $p = 0.7218$ respectively).

Tukey's Post-hoc test also revealed a significant decrease in *En2* expression in both, low- and high-passage iPSCs when comparing iPD samples to control samples ($p = 0.0009$ and $p = 0.0194$ respectively). As it has been published that both engrailed isoforms can exert each other's function, a general significant downregulation of *En* in iPD patients' iPSCs can be assumed when compared to corresponding controls.

When analyzing the expression of other factors important for the development of dopaminergic neurons (*Pitx3, Nurr1* and *Lmx1a*) in low- and high-passage iPSCs, no differences could be assessed. It needs to be considered though that the expression data of *Pitx3* and *Nurr1* could only be preliminary assessed with n = 1-2 as detection of expression in iPSCs proofed itself inconsistent and difficult, while *Lmx1a* expression could not be detected at all in iPSCs (data not shown).

A different picture however, is obtained when comparing *En1* and *En2* expression in NPCs derived from low- and high passage iPSCs (Fig. 42).

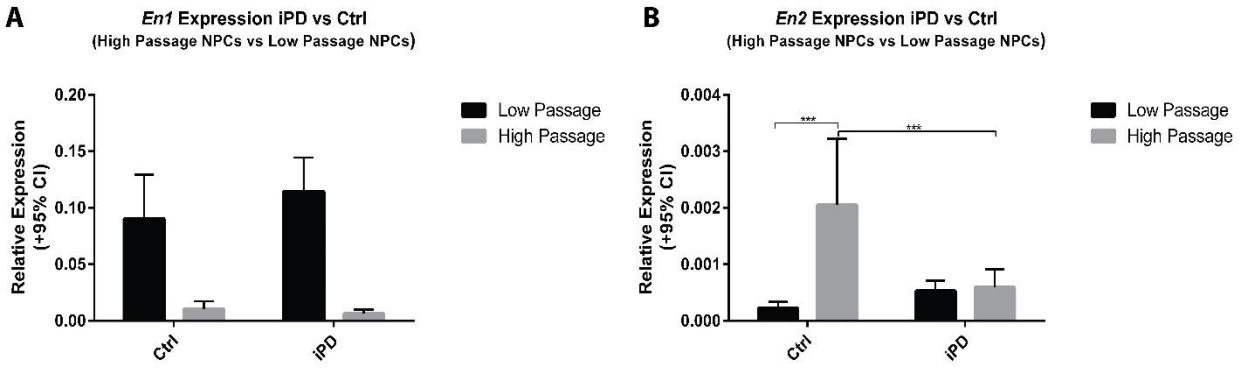

Fig. 42: Expression of En1 and En2 in NPCs differentiated from iPD patients' and control individuals' low- and high-passage iPSCs. *(A) Displays the expression pattern of En1 in low- and high-passage NPCs, (B) shows the expression pattern of En2 in the same cells. All samples were analyzed with n = 3, statistical analysis was done with Graphpad prism 6 using two-way Anova and Tukey's Post-hoc test, p < 0.05 is considered significant. Data for high-passage NPCs obtained from (Schmidt, 2017).*

En1 expression pattern in low- and high-passage NPCs changes drastically during differentiation. In NPCs, no changes in expression can be observed between iPD patients' and controls' cells anymore ($p = 0.4764$; Fig. 42A), but only a passage-dependent effect is detected, with strongly increased *En1* expression in NPCs differentiated from low-passage iPSCs when compared to NPCs differentiated from high-passage NPCs ($p < 0.0001$; *Post-hoc test: control low-high p =0.0023; iPD low-high p < 0.0001*). In contrast, expression pattern of *En2* has only changed during the differentiation of low-passage NPCs. While a general health state phenotype could be assessed ($p = 0.0220$; Fig. 42B), also a strong passage-dependent effect ($p = 0.0002$) and interaction effect ($p = 0.0007$) were observed. When applying Post-hoc tests, no significant changes in *En2* expression ($p = 0.8138$) could be found in low-passage NPCs, while a significant decrease of *En2* expression was detected in high-passage NPCs ($p = 0.0006$; Fig. 42B). Furthermore, a significant increase in *En2* expression was found in high-passage control NPCs when comparing to low-passage control NPCs, which could not be detected correspondingly in iPD patients' samples.

When looking at *Lmx1a*, *Pitx3* and *Nurr1* expression, also some changes could be detected now (Fig. 43A-C).

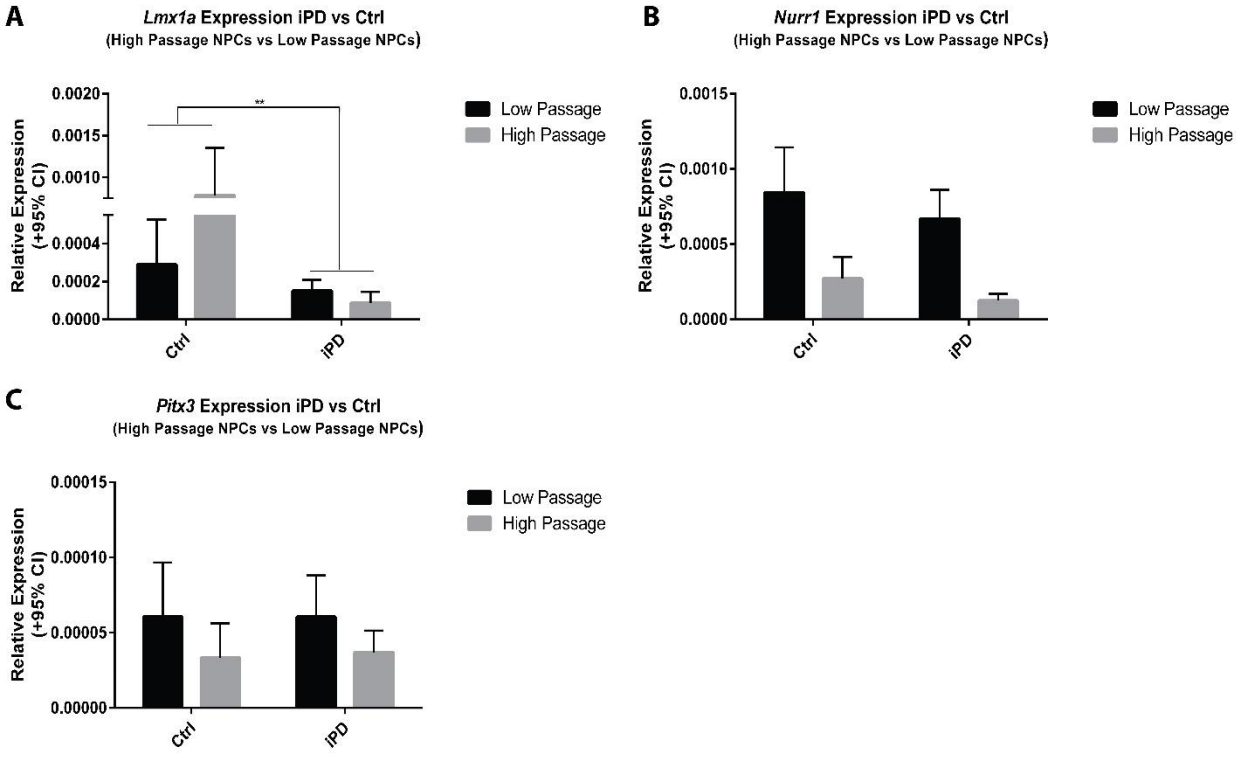

Fig. 43: Expression analysis of Lmx1a, Nurr1 and Pitx3 in NPCs derived from low- and high-passage iPSCs. *(A) Shows the expression of Lmx1a, (B) displays expression of Nurr1 and (C) Pitx3 expression. All samples were analyzed with n = 3, statistical analysis was done with Graphpad prism 6 using two-way Anova and Tukey's Post-hoc test, p < 0.05 is considered significant. Data for high-passage NPCs obtained from (Schmidt, 2017).*

Pitx3 only showed a passage-dependent decrease in expression between low- and high-passage NPCs ($p = 0.0405$; Fig. 43C), yet no significant differences when comparing iPD patients' and controls' cells ($p = 0.8881$) and no interaction between health state and passage ($p = 0.8778$). *Nurr1* also showed a significant passage dependent decrease in expression ($p < 0.0001$; Fig. 43B), yet also a trend for decreased expression in iPD patients' cells when compared to controls' cells ($p = 0.0776$) and no interaction between health state and passage ($p = 0.8717$). For *Lmx1a* however, a significant reduction in iPD patients' NPCs could be detected across passages ($p = 0.0041$; Fig. 43A), while no passage-dependent effect ($p = 0.1309$) or significant interaction between health state and passage could be detected ($p = 0.0516$). However, since the interaction between health state and passage is very close to statistical significance, Post-hoc testing was considered and revealed a significant decrease of *Lmx1a* expression in high-passage NPCs between iPD patients' and controls' cells ($p = 0.0024$), which however, cannot be recapitulated in low-passage NPCs ($p = 0.9101$), even though the overall result indicates a significant decrease in iPD patients' samples.

In the Master's thesis embedded into this thesis, S. Schmidt also differentiated high-passage NPCs to midbrain dopaminergic neurons and analyzed them correspondingly. Exemplary images of the dopaminergic differentiation are given in supplementary Fig. 4. When looking at the expression of *Engrailed* and the other developmental genes analyzed, again a significant reduction in *En-2* (*p = 0.0033;* Fig. 44B) and *Lmx1a* (*p = 0.0245;* Fig. 44C) expression could be detected, while no significant changes in the expression of *Pitx3* (*p = 0.6723;* Fig. 44E), *Nurr1* (*p = 0.4119;* Fig. 44D) and *En-1* (*p = 0.3619;* Fig. 44A) were observed.

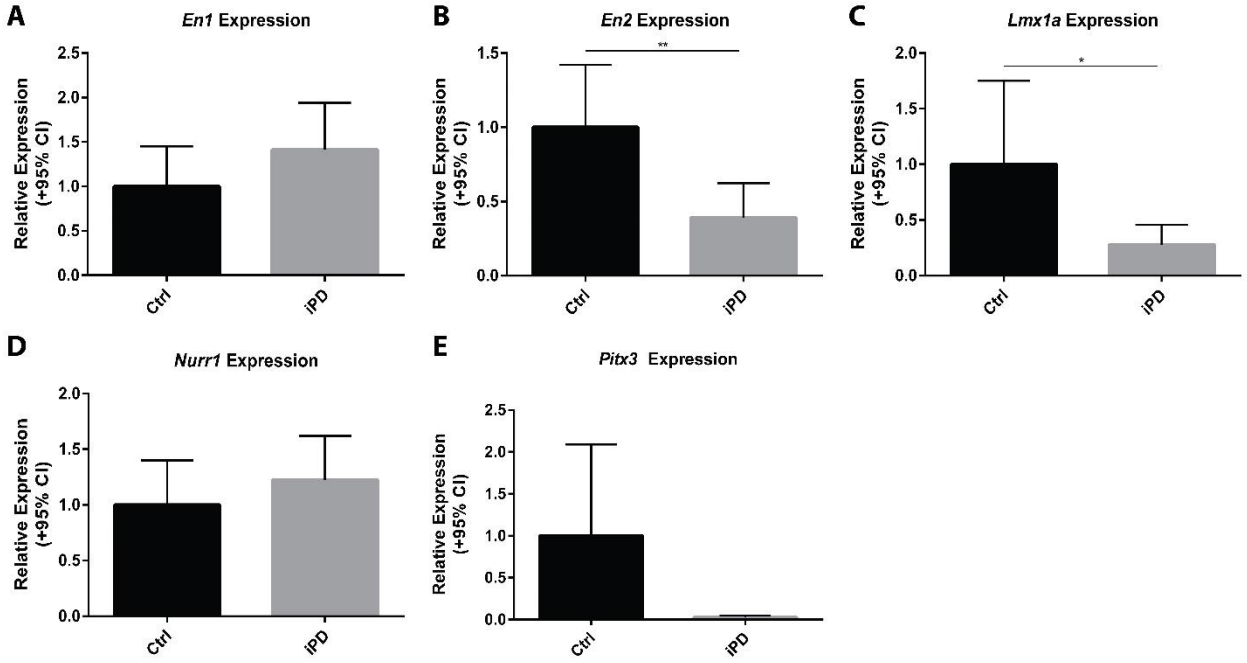

Fig. 44: Expression levels of En-1, En-2, Lmx1a, Nurr1 and Pitx3 in dopaminergic neurons differentiated from high-passage NPCs. *Expression of all five developmental genes in dopaminergic neurons differentiated from high-passage NPCs was determined using qRT-PCR. Cultures contained about 40% dopaminergic neurons (Fig. 45), which did not differ between iPD and corresponding controls. All samples were analyzed with n = 3 (differentiations), statistical analysis was done with Graphpad prism 6, using either student's t-test or Mann-Whitney test depending on normal distribution, p < 0.05 is considered significant. Data taken from (Schmidt, 2017).*

Expression levels of all five developmental genes were analyzed in mixed neuronal cultures with approximately 40% dopaminergic neurons. Differentiation efficiency and thereby number of TH^+-neurons did not differ for iPD patients' cells compared to corresponding controls (Fig. 45), albeit the varying expression patterns of the developmental genes, all of which are essential for the development of dopaminergic neurons.

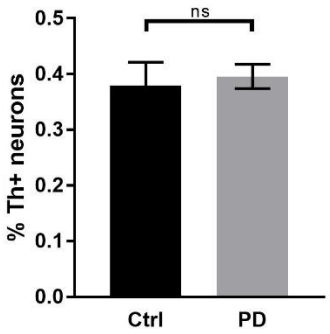

Fig. 45: Determination of differentiation efficiency of iPD patients' and control individuals' high-passage NPCs into TH$^+$-neurons (dopaminergic neurons). *Differentiation yields were stained for TH and total percentage of TH$^+$-neurons in culture was determined. No significant differences in differentiation efficiency could be observed for iPD patients' and control individuals' cells, about 40% of TH$^+$-neurons were found in both groups. Samples were analyzed with n = 3, statistical analysis was done with Graphpad prism 6 using student's t-test, p < 0.05 is considered significant. Data obtained from (Schmidt, 2017).*

While no respiratory data from terminally differentiated neurons from high-passage iPSCs is available, respiratory deficiency in neurons from iPD patients' cells is quite likely, as a significant decrease in the protein levels of complex II and complex IV could be detected by immunoblotting (Fig. 46).

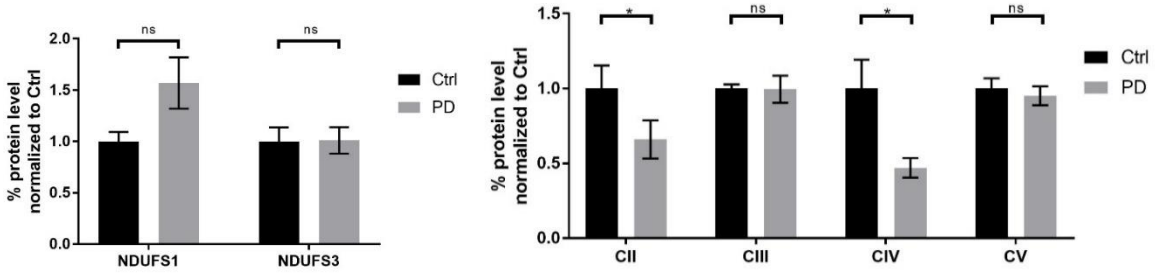

Fig. 46: Protein levels of mitochondrial complexes of the ETC and OXPHOS in neurons differentiated from iPD patients' and corresponding control individuals' high-passage iPSCs. *Protein levels were assessed by immunoblotting and normalized to Actin-beta and later to protein levels in control samples. Shown are the protein levels of complex I (NDUFS1 and NDUFS3) as well as protein levels of complexes II – V. All samples were analyzed with n = 3, statistical analysis was done with Graphpad prism 6 using student's t-test, p < 0.05 is considered significant. Data from (Schmidt, 2017).*

2.6. Tabular summary of respiratory data and *Engrailed* expression

To get a better overview of respiratory data and its possible correlation to *engrailed* expression, all data is summarized in Tab. 3.

iPD vs Ctrl	*En1*	*En2*	OCR Basal (Glc)	OCR Basal (Pyr)	ECAR Basal	OCR Max. (Glc)	OCR Max. (Pyr)	ECAR Max.	OCR PL (Glc)	OCR PL (Pyr)	OCR ATP (Glc)	OCR ATP (Pyr)
Two-way Anova analysis												
iPS, Health State	**X**	↓	↓	↓	**X**	**X**	=	=	↓	↓	↓	=
iPS, Passage	**X**	=	↑	=	**X**	**X**	=	↑	↑	=	=	=
NPCs, Health State	=	**X**										
NPCs, Passage	↓	**X**										
Tukey's Post-hoc test (iPSCs, iPD vs. Ctrl) or student's t-test if applicable (NPCs, iPD vs. Ctrl)												
iPSCs (LP)	=	↓	↓	↓	=	=	=	=	=	=	=	=
iPSCs (HP)	↓	↓	↓	=	↑	↓	=	=	=	=	=	=
NPCs (LP)	=	=	=	=	=	=	=	=	↓	↓	=	=
NPCs (HP)	=	↓	↓	=	↓	↓	↓	=	=	=	=	=
Neurons (HP)	=	↓										

Table 3: Tabular summary of respiratory phenotypes compared to Engrailed expression in the same cells. *Plotted is always iPD patients' samples against controls' samples with the corresponding change, if significant. Health state refers to two-way Anova analysis of corresponding cells (iPD vs. Ctrl), while "Passage" refers to passage-dependent (low- vs. high-passage) observed changes. Abbreviations: oxygen consumption rate (OCR), extracellular cellular acidification rate (ECAR), maximal respiratory capacity (Max.), Proton-leak (PL), oxygen consumption devoted to ATP-production (ATP), glucose (Glc), pyruvate (Pyr), low-passage (LP) and high passage (HP); (↓) stands for a significant decrease, (↑) for a significant increase and (=) for no significant changes observed (X) for statistical interaction detected. NPCs were not analyzed using two-way Anova, as normalization was done in differently in low- and high-passage NPCs and absolute values are therefore not comparable.*

It becomes evident that whenever a significant change in *En2* expression is observed, also phenotypes in the general energy metabolism are observed. Exception is the proton-leak linked oxygen consumption in low-passage NPCs, which however cannot be recapitulated when looking at the coupling efficiency in those cells which is not changed.

3. Discussion

3.1. Interpretation of the respiratory analysis iPSCs and NPCs with respect to health state

As explained previously, the Seahorse XF platform delivers the corner pillars of respiration and cellular metabolism. First, basal respiration is assessed, which is composed of the oxygen consuming processes driving ATP synthesis and the processes which consume oxygen by creating a proton leak across mitochondrial membranes. After subtracting proton-leak linked oxygen consumption from basal respiration, one is left with the ATP-linked respiration.

When analyzing the health state (iPD versus control cells) specific respiratory pattern, basal cellular oxygen consumption has been determined to be decreased in iPD patients' iPSC models compared to corresponding controls used in this thesis. As seen in Fig. 8C, basal oxygen consumption is decreased in iPD patients' iPSCs when given glucose as substrate. Upon taking a closer look, both, oxygen consumption linked to ATP production (Fig. 8F) as well as proton leak-linked oxygen consumption (Fig. 8E) are significantly reduced in iPD patients' iPSCs when compared to corresponding controls' iPSCs, likely accounting for the general decline in basal respiration.

The decline in oxygen consumption attributed to mitochondrial ATP production is mostly controlled by three large processes: first, cellular, basal ATP utilization is determined by the amount of ATP necessary for proper cellular function and thereby sets the demand the cell has to meet in ATP production. Second, changes in ATP synthesis may be seen if the ATP synthesis machinery (e.g. the F_0F_1-ATPase or other essential enzymes) is impaired and third, substrate supply and / or oxidation may be affected, limiting the substrate and / or the electrons necessary to drive the mitochondrial electron transport chain and thereby oxygen consumption (Divakaruni et al., 2014). As the high passage iPSCs best reflect and account for the changes seen when comparing iPD patients' and control individuals' cells, a more detailed analysis of mitochondrial and cellular functions was done with these cells only. To address the issues of basal ATP production and demand, cell viability, depending on ATP content, was assessed (Fig. 31). Since no changes were detected here, this is a clear indication that observed differences under basal conditions are not due to varying growth rate, i.e. ATP demand. Furthermore, detected differences with glucose as supplied substrate may be caused by impaired glucose uptake from the medium or varying abundance of glucose transporters between iPD patients' and controls' cells. As can be seen in Fig. 37, no significant differences in cellular glucose uptake nor expression of glucose transporters (mRNA) could be detected. This allows the assumption that glucose concentrations within the cells do not vary to such an extent that they might be rate-limiting for mitochondrial respiration in iPD patients' iPSCs. Furthermore, upon metabolism of glucose, no

significant differences in the ratio of $NADH/H^+$ (Fig. 39), the direct substrate of mitochondrial complex I, and NAD^+ were detected. Although this is only a rough framework of the cells' NAD^+/NADH concentrations, it can be assumed that the differences in the measured basal oxygen consumption and oxygen consumption for ATP production do not arise from a shift in NAD^+/NADH ratio, for which other dysregulated, NAD^+-regenerating or $NADH/H^+$ consuming processes within the cells might be accountable for. To get a more comprehensive picture, oxygen consumption upon uncoupling of mitochondria needs to be taken into account (maximal respiration, Fig. 8D). As a strong statistical interaction between passage and health state could be detected, again high passage iPSCs will serve the purpose of discussion here, as Post-Hoc analysis revealed a strong, significant decline in maximal respiration in iPD patients' iPSCs as well as a significant decrease in basal respiration. Changes in uncoupler stimulated oxygen consumption are controlled by two factors: first, there might be changes in abundance or efficiency of mitochondria or / and their complexes of the respiratory chain. Second, changes in substrate supply and oxidation may limit the electrons available to the respiratory chain, thereby accounting for subsequent changes in cellular oxygen consumption. Substrate supply and oxidation encompass all processes involved in general transport and delivery of substrates, i.e. directed and specific transport of substrates across membranes, as well as oxidation and production of intermediary substrates by glycolysis, TCA enzymes or other pathways (Divakaruni et al., 2014). When analyzing oxygen consumption attributed to ATP production with glucose as substrate in the context of maximal oxygen consumption with glucose as substrate, it becomes clear, that neither respiratory chain deficits nor abundance of mitochondria and respiratory complexes can be excluded, however it puts a stronger emphasis towards substrate supply and oxidation since both are significantly reduced in iPD patients' iPSCs (Fig. 8).

To better understand the contribution of respiratory chain deficits and abundance of mitochondria, parallel measurements with only pyruvate as substrate were done (Fig. 10). When switching substrate from glucose to pyruvate, several things become immediately obvious: first, absolute values of oxygen consumption increase dramatically, they nearly double. Most likely, this might be a cell type specific phenomenon, as iPSCs are thought to be predominantly glycolytic cells (Folmes et al., 2012; Mohyeldin et al., 2010; Prigione et al., 2010) and glycolytic provision of pyruvate might be rate controlling in these cells in order to maintain a pluripotent state (Divakaruni et al., 2014; Folmes et al., 2012). Furthermore, as glycolysis is effectively circumvented by supplying pyruvate to the cells directly, ATP demand in those cells will most likely increase drastically, as a much greater extent of anabolic processes (e.g. gluconeogenesis) is required to maintain normal cellular metabolism and provide for all the intermediate products for biosynthesis. With increasing demand for ATP, synthesis of ATP will rise and oxygen consumption increase. However, it also tells us that despite having premature, rounded mitochondria with a relatively low amount of cristae (Prigione and Adjaye, 2010; Prigione et al., 2015), iPS cells are in theory capable of a much higher oxidative

metabolism than they seem to maintain. Second, it becomes obvious that respiration with pyruvate as supplied substrate is much more stable when comparing slopes of the basal respiration with glucose and pyruvate as substrate (Fig. 8A-B and Fig. 10A-B respectively). This indicates that cells seem to succeed in meeting their ATP demand more efficiently in comparison to when just supplied with glucose. Third, it becomes clear that, even though basal respiration increases drastically with pyruvate as substrate, the mitochondria in iPSCs still do not work at their maximal capacity, as an increase in respiration is still obtained after uncoupling the mitochondria. Again, when comparing glucose and pyruvate as substrates it is evident that maximal respiration with glucose is much lower compared to pyruvate, most likely due to decreased substrate supply with glucose as substrate as cells have to metabolize glucose first via glycolysis. This again clearly indicates that the iPSCs are not running on full metabolic capacity, despite being highly proliferating cells.

As for respiration with glucose as substrate, significantly reduced basal oxygen consumption and proton leak-linked oxygen consumption were assessed with pyruvate as sole substrate, yet no significant differences in oxygen consumption for ATP production or maximal respiratory capacity were found. In the light of the interpretation of respiratory results with glucose as substrate, it now becomes clearer that mitochondrial dysfunction itself might not be affecting the respiratory phenotype observed. Even though there is a significant decrease in basal oxygen consumption with pyruvate as substrate, this likely can be attributed to the significant decrease in proton leak-linked oxygen consumption, which will be discussed in the next section. Post-hoc analysis of basal mitochondrial respiration with pyruvate as substrate revealed a significant decrease in basal respiration in low-passage iPD patients' iPSCs (Fig. 15B) but not in high-passage iPD patients' iPSCs when compared to corresponding controls (Fig. 19B), while analysis independent of the passage reveals a health state specific decrease in basal respiration (Fig. 10C). This however, could, other than an actual phenotype in ATP demand and supply, also be an artefact of the measurement conditions: as pyruvate is supplied directly and in high concentrations (5mM sodium pyruvate), the concentrations of the anion pyruvate will increase intracellularly as well. This might lead to a reduction in the pH gradient and therefore a reduction of the membrane potential, delivering an artificially modified proton leak-linked respiration and therefore basal respiration (Divakaruni et al., 2014). Why however this would affect particularly iPD patients' cells in this setup cannot be accounted for here. It can only be speculated that iPD patients' mitochondria might display an increased sensitivity to membrane potential changes, ultimately affecting performance of mitochondria (see e.g. Winklhofer and Haass, 2010). When comparing phenotypes with glucose and pyruvate as substrate, no changes in oxygen consumption linked to ATP production and maximal oxygen consumption with pyruvate as substrate indicate that there are no changes in the abundance of mitochondrial or respiratory chain complexes in iPD patients' cells or in the efficiency of those complexes. Instead, impaired substrate supply and oxidation are moved more into

the focus, as the phenotype obtained with glucose as substrate is nearly fully rescued when switching to pyruvate as substrate, indicating that there might be an impairment in the glucose metabolism in the iPD patients' iPSCs.

In the light of those results, a more focused analysis of the mitochondria was done to finally elucidate mitochondrial participation in these phenotypes. First, abundance of mitochondria and mitochondrial complexes was analyzed (Fig. 32 and Fig. 33). This thesis is based on a multitude of iPSC lines (see Table 2) stemming from patients, who show no clinically phenotypical scheme which would allow to classify and group them accordingly when considering disease progression and severity according to the unified Parkinson's disease rating scale (UPDRS) and response to treatment (Levodopa concentrations, data not shown here for reasons of data protection, available from the core project of the ForiPS consortium). Therefore, representative lines for analysis of smaller cohorts were not selected. Under these circumstances, confocal microscopy, although acknowledged as the best option for a mitochondrial count, could not be performed. It was attempted to stain mitochondria and count "semi-automatically" using an Opera Phenix High-Content Screening System in collaboration with S. Desbordes and the SCADEV platform, however, necessary resolution to count mitochondria could not be achieved with the available system (supplementary Fig. 7). For this reason, mitochondrial quantification was performed indirectly. First, qRT-PCR of the mitochondrial 12S RNA, mitochondrially encoded by the *MT-RNR1* gene was done (Fig. 33). Since no differences in expression could be detected, this indicates that (a) the mtDNA copy number in iPD patients' and controls' iPSCs are comparable and / or (b) expression of mtDNA in general is not changed between iPD patients' and controls' cells. This approach can be considered as indirect assessment of mitochondrial abundance, since, even though every mitochondrion can contain multiple mtDNA copies, usually there is an in average even distribution of mtDNA in all mitochondria of one cell. In consequence, average number and expression of mtDNA on cellular level are comparable between iPD patients' and controls' iPSCs. This becomes fortified when looking into expression of the mitochondrial complexes (Fig. 32). Abundance of all mitochondrial complexes was analyzed using immunoblotting and revealed no differences between iPD patients' and control individuals' iPSCs. First, this confirms mtDNA expression data, as amounts of mitochondrial complexes, especially complex I, III and IV, which are thought to be organized in super-complexes, but also the F_0F_1-ATPase, are thought to be proportional to mitochondrial mass. Taken together, mitochondrial mass does not seem to be affected, while unfortunately this cannot account for the state of mitochondrial networks, i.e. whether mitochondrial networks are in a more fissed, single mitochondria or in a more fused, large network state. This will be discussed separately later. Second, it becomes clear that observed respiratory phenotypes are not due to differential abundance of mitochondrial complexes, e.g. a lack of complex I or V in iPD patients' cells.

As mitochondrial mass and complex abundance are not responsible for the observed phenotypes, a more detailed look was taken at the efficiency of the mitochondria. To this purpose, cells were permeabilized and the mitochondria analyzed using the Seahorse XF platform. Permeabilization of cells allows the measurement of mitochondria as isolated system, independent from cellular metabolism or internal cellular storages of e.g. glycogen, triglycerides and other endogenous substrate pools (Divakaruni et al., 2014). By directly offering selected substrates to mitochondria, a more reliable assessment of mitochondrial efficiency can be done. By offering the specific substrate as electron donor for each proton pump of the electron transport chain and sequential inhibition of the same, efficiency of complex I, II/III and IV could be assessed (Fig. 34A-B). First, pyruvate (i.e. $NADH/H^+$ after the oxidative decarboxylation by the pyruvate dehydrogenase within mitochondria) was offered as substrate for complex I, while complex II was allosterically inhibited and oxygen consumption as function of complex I assessed. Subsequently, complex I was inhibited and the same procedure was done for complex II/III (with succinate as substrate) and complex IV (TMPD as electron donor). As seen in Fig. 34A and B, no differences could be detected in the oxygen consumption as function of the single complexes between iPD patients' and controls' iPSCs, indicating that there are no differences in the functionality and efficiency of mitochondrial complexes I, II, III and IV. In addition, mitochondrial coupling efficiency was assessed (Fig. 34C-D). Mitochondrial coupling efficiency examines the degree of coupling between the ETC and OXPHOS. To this purpose, complex I was inhibited and the mitochondria were supplied with succinate as substrate for complex II. This causes complex II activity and feeding of electrons into the ETC when succinate is converted to fumarate by the succinate dehydrogenase. However, as cells are permeabilized, no ADP as substrate for the F_0F_1-ATPase is present, accounting for low oxygen consumption. When ADP is added, oxygen is consumed for ATP synthesis as function of electrons supplied by the TCA into electron transport chain. Subsequently, inhibiting the F_0F_1-ATPase and uncoupling mitochondria gives information about the degree of the tightness of coupling of OXPHOS and ETC. As depicted in Fig. 34D, no differences were observed between iPD patients' and corresponding controls' iPSCs. Taken together, the results from the indirect measurement of the electron flow across the respiratory chain complexes, the measurement of the mitochondrial coupling efficiency as well as the mitochondrial complex expression analyses indicate that the mitochondria in iPD patients' iPSCs are not impaired compared not corresponding control cells' mitochondria, neither in complex abundance or efficiency, nor in activity of the TCA enzymes or the coupling of OXPHOS to the ETC. This in return confirms the hypothesis based on the respiratory data and supported by the phenotypical rescue when supplying the cells with pyruvate: it seems highly likely that observed respiratory deficiencies in iPD patients' iPSCs are caused by substrate oxidation and supply to mitochondria, not by actual mitochondrial deficiencies in iPD patients' iPSCs'.

To complement the metabolic picture which the measurements of the oxygen consumptions paint, also the ECAR as framework for glycolytic measurement has to be considered. ECAR measurements are largely based on the release of protons during the oxidation of glucose, where glycolysis will take the major share. Utilization of glucose in glycolysis releases an average of $1H^+$ per molecule of ATP produced and in addition produces two pyruvate anions (pKa 2.5), while metabolization of pyruvate in OXPHOS only releases an average of $0.18H^+$ and 0.18 molecules CO_2 per ATP produced (6 molecules of CO_2 per one molecule of glucose utilized, which averages to 33.5 molecules of ATP per 1 molecule of glucose oxidized) (Divakaruni et al., 2014). Albeit contributing to cellular acidification and thereby to acidification of the extracellular medium, the proportion of OXPHOS in acidification is much lower. Besides, still one has to take into account that ECAR represents only a framework for glycolytic activity, as a multitude of other cellular processes also have the capability to acidify the cellular environment. When considering ECAR values obtained from iPD patients' and corresponding controls' iPSCs (Fig. 9), a strong passage effect (discussed later) and health state effect, with an increase in basal ECAR in iPD patients' cells could be observed. However, a statistical interaction effect was also detected. Considering Post-hoc testing, this increase in glycolytic activity was only observed to be significant in high passage iPD patients' iPSCs, while no changes were detected in low-passage iPSCs. As discussed earlier, high-passage iPSCs generally showed stronger phenotypes, representing the overall observed health state phenotypes better than the low-passage iPSCs.
Since basal oxygen consumption and oxygen consumption attributed to ATP production are reduced in iPD patients' iPSCs, it makes perfect sense at first sight that basal glycolytic activity in the same cells increases as no differences in viability of those cells was detected (Fig. 31) and synthesis and utilization of ATP underlie a demand and supply function. As less ATP is produced in the course of mitochondrial respiration, more ATP has to be produced using (aerobic) glycolysis in order to maintain cellular ATP levels and functions. Additionally, the increase in glycolytic activity was only observed under basal conditions, no changes in the maximal rate of glycolysis and glycolytic reserve were detected in iPD patients' iPSCs compared to corresponding controls (Fig. 9; Fig. 13; Fig. 17). It has to be noted though that the maximal rate of glycolysis, obtained after the addition of oligomycin, may not account for the actual maximal rate of glycolysis as, again, only cellular ATP demand will be met. Once enough ATP is produced, cells will stop increasing glycolytic rates and therefore might not reach maximal glycolytic capacity. Therefore, it is well possible that subtle impairments of glycolytic activity might not be accounted for in these measurements. However, considering basal glycolytic activity, it becomes more intriguing when comparing to lactate levels: although lactate does not actively contribute to the acidification of the medium, but rather buffers it as the conversion of pyruvate to L-lactate is slightly alkalizing (Divakaruni et al., 2014), it has been established that lactate levels rather accurately correlate to glycolytic activity (Keuper et al., 2014). To this purpose, L-lactate levels from cells exposed to only glucose or pyruvate as substrate were assessed (Fig. 38)

and it became apparent that there were no significant alterations between iPD patients' and controls' iPSCs. Surprisingly, L-lactate levels, when given pyruvate as substrate, were significantly reduced to when giving glucose as substrate, independent of the health state. This might be explained by a reduced necessity to metabolize pyruvate to lactate, as rates of glycolysis will be reduced drastically upon the removal of glucose and regeneration of NAD^+ from $NADH/H^+$ for activity of glycerinaldehyde-3-phosphate dehydrogenase (GAPDH) in the glycolytic cascade is drastically reduced. Furthermore, as increased amounts of pyruvate will be fed into mitochondria to meet cellular ATP demands since glucose is not present as substrate, cytoplasmic NAD^+/NADH metabolism will drastically decrease while mitochondrial NAD^+/NADH metabolism will increase, reducing the necessity of the NAD^+ recycling activity of the lactate dehydrogenase.

In summary, following picture is obtained in iPSCs: with glucose as substrate (1) no differences in the capability of glucose uptake could be detected and (2) increased ECAR rates, likely corresponding to an increased glycolytic flux in iPD patients' iPSCs were observed. This is complemented by (3) reduced mitochondrial oxygen consumption at basal levels and reduced oxygen consumption attributed to ATP production as well as (4) reduced maximal respiratory capacity, yet (5) the mitochondria themselves seem not impaired in iPD patients' iPSCs. Furthermore, there are no indications that (6) transport of substrate into mitochondria is affected (as seen by no differences in maximal respiration with pyruvate as substrate) and no changes in (7) lactate production could be detected, indicating that an estimated equal regeneration of the cytoplasmic NAD^+ pool in iPD patients' and controls' iPSCs is sufficient for the present glycolytic flux. Regeneration of NAD^+ using mitochondrial shuttles can be assumed to be decreased due to diminished basal oxygen consumption as no changes in OXPHOS capability could be observed. Last but not least, also (8) no changes in the whole cell NAD^+/NADH ratio were found. Taken together, this data suggests again that in iPD patients' iPSCs substrate is drawn from the glycolytic flux. It has been published before that particularly in proliferating cells, glucose derived carbon is often diverted from the glycolytic flux to drive a multitude of e.g. biosynthetic pathways like lipid biosynthesis, amino acid biosynthesis, NADPH generation or nucleotide generation (Divakaruni et al., 2014; Lunt and Heiden, 2011). Even if ECAR values would not be elevated in iPD patients' cells, but at same levels compared to controls' iPSCs, this would suggest that a surplus of substrate is devoted to a non L-lactate or OXPHOS fate.

So far, it only has been published that neuronal or glial cells are affected in PD, therefore iPSCs were differentiated into neuronal-type cells. When taking neuronal precursor cells into consideration, on first sight, a similar picture is obtained like in iPSCs. NPCs originating from low passage iPSCs recapitulate the respiratory phenotypes (Fig. 20, 21, 23 and Fig. 24, 25, 27) observed in their corresponding low-passage iPSCs (Fig. 12, 13, 15 and Fig. 16, 17, 19), with the exception that no significant differences in basal

respiration were observed. Similarly to high-passage iPSCs, NPCs derived from those display a significant reduction in basal and maximal oxygen consumption with glucose as sole substrate (Fig. 24) and also a significant increase in the basal rate of glycolysis in iPD patients' NPCs was observed (Fig. 25). The hypothesis created on base of the iPSCs models also holds for their NPC counterparts, with two exceptions: (a) differential expression of engrailed may take an influence on cellular bioenergetics and will be discussed in section 3.4 and (b) a complex I deficiency was detected in NPCs derived from high-passage iPSCs, however most likely not in NPCs derived from low-passage iPSCs.

A complex I activity assay was only performed on NPCs from high-passage iPSCs, as those showed a significantly decreased maximal oxygen consumption when exposed to pyruvate only (Fig. 27C), which was not the case for NPCs derived from low-passage iPSCs (Fig. 23C). When analyzing complex I activity (Fig. 28), a significant decrease in iPD patients' NPCs complex I activity of about 34% could be detected, which would be, if comparing to iPSC phenotypes, an additional phenotype. The decrease in complex I activity can be due to two reasons only, thanks to the make-up and principle of the complex I activity assay kit (Abcam): complex I activity measured by this kit is solely dependent on NADH oxidation, which means that either the oxidative subunits (N-module of complex I) are impaired or complex I subunit assembly was defective in some way. A relation of iPD and complex I deficiency has been established long ago: post-mortem analysis of complex I activity was found to be around 30% decreased in iPD patients' substantia nigra and frontal cortex (Exner et al., 2012; Schapira et al., 1989). Other studies demonstrated that there is an increased amount of oxidative damage in nuclear and mitochondrial DNA, hypothesized to stem from miss-assembly of complex I subunits (Keeney et al., 2006). Last but not least, a study showed that upon exposure to the complex I inhibitor rotenone, fibroblasts from iPD patients showed a significantly enhanced rate of necrotic cell death, indicating higher sensitivity of iPD patients' cells towards complex I insults (Ambrosi et al., 2014). This is of particular interest, since the iPD patients' iPSCs used in this thesis were reprogrammed from biopsied skin fibroblasts. Reprogramming does not affect the sequence of mitochondrial DNA per se, however, it is very likely to affect the amount of mtDNA molecules. Studies have shown that undifferentiated cells possess high amounts of copies of mtDNA (up to 1500 copies per cell), more than their fibroblast counterpart, while the amount of mtDNA copies decreased significantly upon differentiation to NPCs, accompanied by a reduction in ATP demand of the cells (Birket et al., 2011). Albeit mtDNA copy number was not analyzed comparing iPSCs and their differentiated counterparts, a reduction in oxygen consumption between iPSCs and NPCs could also be observed in this thesis (e.g. when comparing low-passage iPSCs to their differentiation products, an approximately 25% decrease in basal respiration could be observed). Another study which recently received great attention, demonstrated that upon reprogramming, heteroplasmy patterns can vary greatly between iPSCs and their biological sources (Kang et al., 2016). Heteroplasmy describes the penetrance of one mutation in the mtDNA in relation to all

mtDNA copies in one cell. In the context of mutation rates, mutations of mtDNA are believed to be approximately 10-20fold more frequent than in nuclear DNA, likely due to increased oxidative stress and comparatively drastically reduced replication control mechanisms. It has been known for a while that even within one cell, mutated and wild-type mtDNA copies coexist, although the extent of mtDNA defects in proliferating peripheral tissues, from which iPSCs are typically derived, is far less compared to post-mitotic tissues like neurons (Kang et al., 2016). Generally speaking, accumulation of mtDNA variants in, for example skin, was insignificant with age (Nooteboom et al., 2010), as for heteroplasmy, a pathological threshold for levels of heteroplasmy of about 15% has been established (Chinnery and Hudson, 2013; Kang et al., 2016; Rossignol et al., 2003). In any case, it is possible that levels of heteroplasmy may greatly vary between fibroblasts, derived iPSCs and NPCs differentiated from them - Kang et al., 2016 showed that levels of heteroplasmy for a specific mutation increased from 19% in parental fibroblasts up to 93% in the corresponding iPSC clone, or from 2% in fibroblasts, which is well below pathological threshold, up to 50% in derived iPSCs. This is owed not only to the reprogramming process, with a likely increase in mtDNA copy number, but also to the clonal selection of iPSCs (Birket et al., 2011; Kang et al., 2016). To cut a long story short, it may well be possible that in course of the reprogramming and differentiation process the level and pattern of heteroplasmy changed dramatically in both, iPD patients' and control individuals' cells, resulting in a complex I deficiency due to mutational load or miss-assembly, which otherwise would not have been detected and was unapparent on iPSC and fibroblast level. In any case, it would definitely be worthwhile to sequence the mtDNA molecules of iPD patients' and controls' samples, at fibroblast, iPSC and NPC stage. Not only to compare levels and effects of heteroplasmy, but also to get a general impression of a possible complex I miss-assembly. Complex I consists of 45 subunits, of which 7 are encoded on mtDNA, while 38 are encoded nuclearly and imported into mitochondria. Even though none of the 7 subunits encoded on the mtDNA are in the core unit of complex I responsible for the oxidation of NADH and the electrons transfer, but rather are located in the Q-module of complex I, which is responsible for the electron transfer to ubiquinone, mutations in those 7 complexes may still very much affect assembly and structure of the whole complex I (Mimaki et al., 2012), thereby causing faulty assembly and enzymatic deficiency.

3.1.1. Proton leak – linked oxygen consumption in iPSCs and NPCs on the test-bed

As the proton leak-linked oxygen consumption was detected to be changed rather inconsistently, those variances will be discussed shortly in this chapter. The proton leak-linked respiration is the amount of oxygen consumption which is attributed to the dissipation of oxygen without the generation of ATP. Such plasticity of the coupling the nutrient oxidation is generally useful for a cell to regulate mitochondrial ROS

production and to disengage the carbon-flux from ATP demand and for specific cells plays a role in heat production (brown fat cells) and glucose stimulated insulin secretion (beta-cells) (Divakaruni and Brand, 2011). Usually, the fraction of proton loss by diffusion across the lipid bilayer is very small, the proton leak-linked oxygen consumption is rather dependent on the abundance of the adenine nucleotide translocase (Jastroch et al., 2010) and actively driven by the family of uncoupling proteins (UCP1-3) (Divakaruni et al., 2014; Jastroch et al., 2010). In fact, a study showed that UCP2 is a regulator of human pluripotent stem cell (hPSC) metabolism. Zhang et al., 2011 demonstrated that UCP2 is an important modifier of glucose metabolism in hPSCs, pushing glucose metabolism away from conversion to pyruvate and mitochondrial respiration towards oxidation of glucose in other pathways like the PPP. Furthermore, they were able to demonstrate that UCP2 repression is necessary to induce differentiation from hPSCs into other lineages since otherwise the necessary metabolic switch is not facilitated as easily. Also, UCP2 has been proposed to be linked to type 2 diabetes by negatively regulating insulin secretion and it may act as protector against oxidative stress (Souza et al., 2011), which may even provide a link to iPD. However, when measuring proton leak-linked oxygen consumption in a Seahorse setup, interpretation needs to be made very carefully. The proton leak depends on the membrane potential, and if changes in oligomycin and FCCP-dependent respiration are detected, changes in the proton leak may only be an artefact of the changes in mitochondrial membrane potential, as oligomycin tends to slightly hyperpolarize mitochondria, leading to an overestimation of the proton leak and FCCP breaks down membrane potential completely (Divakaruni and Brand, 2011; Divakaruni et al., 2014; Jastroch et al., 2010). In addition, a reduction of the proton leak does not per se indicate a dysfunction but can well be a physiological response to a trigger.

In this thesis, an iPD specific, significant decrease in proton leak-linked respiration was discovered in iPSCs, independent from substrate. However, Post-Hoc analysis of the proton leak in low- and high-passage iPSCs did not reveal any differences. Furthermore, NPCs derived from low-passage iPSCs showed significantly decreased proton leak-linked oxygen consumption, while NPCs derived from high-passage iPSCs did not. To get a further indication if the proton leak really is significantly altered, coupling efficiency was calculated. Coupling efficiency determines the amount of oxygen used to drive ATP synthesis, is therefore a function of basal respiration and the proton leak. In all cases, no significant change of coupling efficiency was observed, leading to the assumption that the significant changes detected in proton leak-linked respiration may be artificial. To ultimately verify this hypothesis, membrane potential of iPD patients' and controls' samples must be assessed. Unfortunately, Mitotracker staining, a mitochondrial stain depending on membrane polarization, did not work due to technical limitations in this thesis (supplementary Fig. 7).

3.2. Mitochondrial fusion and fission – cause or consequence?

In the light of the results obtained and the conclusions drawn from the same, the question arises if the phenotype observed in the fusion and fission machinery in iPD patients' iPSCs compared to corresponding controls may be cause or consequence of the phenotypes observed in respiratory analyses, or if it may even be another, complete unrelated phenotype of iPD. Unfortunately, this question is not addressed easily. The issue presents itself already at the very basic level: when mitochondria react to changes, it's not by changing either fusion or fission processes, but rather by fine-tuning both processes in a highly specific manner. Mitochondrial dynamics are controlled by a balance of fission and fusion events, with often drastic phenotypes if one becomes dysregulated. This means, however, that an increase in fusion may be mediated by an increased activity of the fusion machinery and a decrease in the activity of the fission machinery. Yet, an increase in fusion may also only be mediated by either one of these activity changes, which may arise from a multitude of complex regulatory processes. Naturally, the same also goes for regulation of mitochondrial fission. Furthermore, as mitochondria exercise not only one function, but are at the center of bioenergetics, cellular metabolism of carbohydrates and fatty acids, calcium handling, heme-biosynthesis and apoptotic signaling, it is only natural that mitochondrial metabolism, including mitochondrial dynamics, is regulated by the requirements of these processes (Mishra and Chan, 2016). Therefore, it is not surprising that cellular metabolism and nutrient sensing systems are coupled to the regulation of mitochondrial fusion and fission, e.g. by activity of PKA or AMPK, which both have been shown to be essential regulators of Drp1 or its adaptor proteins and thereby the mitochondrial fission machinery (Mishra and Chan, 2016). Other factors, like for example calcium (Ca^{2+})-homeostasis, are capable of regulating mitochondrial fission and fusion in similar manner, in this case by activity of the Ca^{2+}-sensing phosphatase calcineurin. It has been shown that mice which carry a knockout in calcineurin show increased levels of OXPHOS, elongated mitochondria and resistance to obesity, mediated by Drp1-dependent mitochondrial fission events (Pfluger et al., 2015) as calcineurin controls mitochondrial fission by promoting Drp1 activation by dephosphorylating the phospho-$Serin^{637}$ of Drp1 (Cereghetti et al., 2008).

As mentioned earlier, fusion and fission processes rely on different kinds of regulation control. While the mitofusins Mfn1 and Mfn2 are largely controlled by protein degradation via ubiquitination events, the fusion protein for the inner mitochondrial membrane, Opa1, is mainly controlled by cleavage processes by two ATP-dependent metalloproteases, YME1L1 and OMA1, which cleave Opa1 into eight different isoforms with different functions (reviewed in Mishra and Chan, 2016; Westermann, 2010, 2012). Drp1, and thereby fission activity, is largely controlled by (de-)phosphorylation of two to three important serines (Ser^{616}, Ser^{637} and Ser^{693}) by a variety of kinases and phosphatases, or phosphorylation and thereby activation of Drp1 adaptor proteins, like the mitochondrial fission factor (Mff). To add complexity, it has to be noted that Drp1

activity is also controlled by S-nitrosylation, SUMOylation and acetylation (reviewed in Mishra and Chan, 2016).

Within this thesis, expression on mRNA level of the mitofusins *Mfn1, Mfn2* and *Opa1* has been analyzed in iPSCs and corresponding NPCs (Fig. 35 and Fig. 40A-C respectively), alongside with mRNA levels of the *mitochondrial fission protein 1 (Fis1)* and *AMPK* (supplementary Fig. 8B and Fig. 8A respectively). It can be assumed that differences in regulation of the protein product from these genes results in differences in expression, albeit it has to be admitted that direct analysis of protein levels may have been more accurate. Expression of *Fis1* was analyzed, as *Fis1* mRNA levels have been found altered in neurodegenerative diseases and have been shown to accompany increased mitochondrial fragmentation events (Wang et al., 2012). Regulation of Drp1 was assessed by immunoblotting for total Drp1 levels as well as phospho-Ser^{616}- and phospho-Ser^{637}-Drp1 levels in iPSCs and NPCs (Fig. 36 and Fig. 40D-E respectively). Expression analysis of the mitofusins did not reveal significant differences in iPD patients' iPSCs, nor did the mRNA levels of *Fis1* and *AMPK*. This indicates that there are, most likely, no changes in the regulation of the fusion machinery between iPD patients' iPSCs and corresponding controls and that cells may not be subject to starvation, which could be assessed by e.g. elevated AMP levels. However, unfortunately mRNA levels do not reveal details about the activity of AMPK, therefore it cannot be excluded that there may be AMPK dependent effects.

While no changes could be detected in the fusion machinery of iPSCs, an iPD specific decline of total Drp1 levels was revealed. As this was assessed from cellular fractions, it cannot be accounted for an even more drastic reduction of Drp1 levels in the mitochondrial fraction, however, it can be assumed that a total decrease of Drp1 levels also leads to a decrease in mitochondrially recruited Drp1. Furthermore, levels of phospho-Ser^{616}-Drp1 were found to be significantly decreased in iPD patients' samples, when normalized to both, actin-beta expression or total Drp1 expression, while phospho-Ser^{637}-Drp1 levels remained unchanged. As phosphorylation at Serin^{616} of Drp1 promotes mitochondrial fission, it can be assumed that there may be a decrease in fission activity in iPD patients' iPSCs compared to corresponding controls' cells. This in turn allows the assumption that mitochondrial networks in iPD patients' samples possess a rather fused conformation compared to corresponding controls' cells' mitochondria. To ultimately confirm this hypothesis, confocal microscopy has to be done and mitochondrial elongation analyzed and quantified.

This result is rather surprising, as a multitude of studies points towards opposite effects in PD. A variety of studies demonstrated that in peripheral blood mononuclear cells (PMBCs, i.e. lymphocytes and monocytes) from iPD patients Drp1 levels are elevated and Opa1 levels decreased, accompanied by increased levels of mitochondrial fragmentation and respiratory deficits (Barroso et al., 1993; Cardoso et al., 2005; Santos et al., 2015; Yoshino et al., 1992). However, Santos et al., 2015 showed in cybrid models (where the mtDNA from platelets of idiopathic PD patients is transferred into mtDNA depleted cells) that cells with idiopathic

PD patients' mtDNA were affected in similar ways as we see it here: even though immunoblotting did not reveal an imbalance of protein levels of mitofusins or fission proteins between control and iPD samples, upon MPP^+ treatment significantly reduced phospho-Ser^{616}-Drp1 levels in iPD samples were observed, accompanied by increased cleavage of long Opa1 isoforms into short ones. They concluded that acute complex I inhibition may regulate levels of fission and fusion differently than chronic complex I deficiency. Similar observations were made in this thesis, albeit not with toxic insults but rather nutrient depending – with glucose or pyruvate only as energy source. In fact, a clear link between nutrients and mitochondrial fusion has been made not only on mechanistic level: it has been established long since that mitochondrial fusion is important for OXPHOS activity: on short term, it has been shown that elongated mitochondria are formed under conditions of increased ATP production (Mitra et al., 2009; Tondera et al., 2009). Moreover, it has been shown that in tumor cells, which likely are closest to an iPSC-like metabolism compared to other cells, mitochondria enlarge during growth in galactose media, which forces the cells to rely heavily on OXPHOS instead of glycolysis, comparable to pyruvate (Rossignol et al., 2004) and that elongated mitochondria are more efficient at energy generation (Skulachev, 2001). In the light of the respiratory results obtained in this thesis, decreased fission might be a mechanistic response in iPD patients' iPSCs to the assessed decreased basal and maximal respiration with glucose as substrate. As cellular ATP levels are determined by a demand and supply function, an increased ATP demand might trigger increased fusion of mitochondrial networks, without actually increasing rates of respiration as the substrate arriving in mitochondria is limited by the very same processes which consume ATP and intermediary carbon products. Therefore, the conclusion can be drawn that a negative regulation of mitochondrial fission may not be cause, but rather consequence of the observed respiratory phenotypes, even maybe a mechanism to cope with the bioenergetic challenges present in iPD patients' cells.

In contrast to the differences in the fission and fusion machinery in iPSCs from iPD patients' and controls' samples, no differences could be detected in NPCs derived from these iPSCs. Albeit detected respiratory phenotypes were similar, no changes in the protein level of Drp1 and phospho-Ser^{616}-Drp1 could be detected, nor were there iPD specific differences in the expression of the mitofusins. However, changes in mRNA levels of the mitofusins were detected depending on the substrate given – glucose or pyruvate. In all three cases (*Mfn1*, *Mfn2* and *Opa1*), an increase of expression was detected when cells were exposed to pyruvate, in accordance with an increase in OXPHOS as discussed before. As no substrate dependent changes could be detected in iPSCs, the assumption lies close that the fusion and fission machinery of iPSCs and NPCs cannot be compared directly and phenotypes as well as sensitivity to substrate have to rather be interpreted in a cell type specific manner.

3.3. A translational aspect - dysregulated glucose metabolism in PD

Generally speaking, oxidative stress and energy failure, often associated with mitochondrial dysfunction, are hallmarks of neuronal death in neurodegenerative diseases (Cobb and Cole, 2015). Not only in PD, but also in other neurodegenerative diseases like Alzheimer's (disruption of glucose uptake) or Huntington's (decreased glucose metabolism in basal ganglia), alterations in the general glucose metabolism have been observed. ^{18}F-deoxyglucose positron emission tomography (PET) studies have shown that in both, idiopathic and familiar variants of PD, glucose hypo-metabolism in the brain of patients could be detected (Borghammer, 2012; De Rosa et al., 2009). Furthermore, dysregulation of glucose metabolism has been found in post-mortem brains of iPD patients (Dunn et al., 2014a). This fact deserves particular consideration, as in the brain glucose is the primary energy substrate. This, in turn, means that coupling of bioenergetics and central carbon metabolism is especially tight in the brain (Anandhan et al., 2017). Particularly neurons are very high energy consumers in order to maintain their firing power – to which purpose they do high amounts of OXPHOS. However, as neurons are thought to metabolize glucose primarily through the PPP in order to provide a necessary pool of reducing equivalents (NADPH) to maintain antioxidant defenses, they are in turn believed to have low, steady state glycolytic activity due to lack of glycolytic activation by the 6-phosphofructose-2-kinase/fructose-2,6-bisphosphatase-3 (PFKFB3) (reviewed in Anandhan et al., 2017 and Magistretti and Allaman, 2015). In consequence, most of their substrate for OXPHOS is delivered by glial cells which maintain high levels of glycolysis and low rates of OXPHOS conversely, namely astrocytes and oligodendrocytes. They deliver substrate to neurons in form of L-lactate and ketone bodies (3-beta-hydroxybutyrate, acetoacetate and acetone), derived from glucose, lactate, fatty acid and ketone body metabolism (Iglesias et al., 2017; Schönfeld and Reiser, 2013). Indeed, increased levels of lactate (Henchcliffe and Beal, 2008) and pyruvate, accompanied by decreased levels of citrate, acetate, succinate and malate have been found in brains of PD patients (Ahmed et al., 2009), again indicating deranged glucose metabolism and possibly compensatory mechanisms. Molecularly, microarray studies provided a strong association of deranged glucose metabolism with the regulation of the transcriptional regulator PGC-1α, which has been proposed to be a key mediator of control of glucose usage (Zheng et al., 2010).

As previously mentioned, mitochondrial dysfunction has been heavily associated with PD, especially a decrease in ETC activity, largely due to complex I deficiency found in the pre-frontal cortex and SNpc of iPD patients. However, also an increase in mtDNA mutations (somatic, acquired), mutations in the polymerase-gamma linked to complex I and IV defects or mutations in the mitochondrial transcription factor TFAM have been associated to PD. In this regard, the results obtained in NPCs from high-passage iPSCs match the published data perfectly. NPCs displayed a decrease in complex I activity as well as maximal

respiratory activity with glucose as substrate. The result of a mitochondrial dysfunction in neurons has a major energy failure as consequence, linked to their inability to increase glycolytic rates for compensation purposes. While this might, however, not be the case in neuronal precursor cells, still a clear decrease in complex I activity was already detectable. Nevertheless, it has been suggested that an approximately 30% reduction of complex I activity might not be the only reason for neuronal cell death, as a reduction to about 50% activity of complex I would be needed to cause a significant ATP depletion (Anandhan et al., 2017). Furthermore, mitochondrial energy failure, especially in neurons, would be expected to withdraw ATP from other ATP-dependent processes in order to maintain neuronal excitability. Such processes would encompass protein quality control mechanisms, transport of mitochondria and mitochondrial biogenesis and dynamics. Indeed, a deficiency of all the named processes has been observed in PD, which in turn has been reported to affect (oxidative) stress levels in cells (reviewed in Anandhan et al., 2017). Another important factor to take into account is the role played by each cell type and thus their metabolic specifications. It has been reported that an artificial (chemically induced) increase in glycolytic activity can counteract energy failure in dopaminergic neurons (Chaudhuri et al., 2015). Therefore it may be reasoned that increased rates of glycolysis, not only in neurons, but also astrocytes, thereby increasing substrate supply to neurons, may play a protective role for neuronal survival. This again becomes particularly interesting as a decrease in glucose metabolism, accompanied by a decrease in pyruvate and lactate levels, has been observed in PD patients and disruption of glycolysis in glial cells is accompanied by neuronal axon damage and neurodegeneration (Ahmed et al., 2009; Anandhan et al., 2017; Henchcliffe and Beal, 2008; Volkenhoff et al., 2015). In addition, increased oxidation of glycolytic enzymes like GAPDH, enolase-1 and aldolase-A was found in the cortex of PD patients and fPD related genes, namely *SNCA, Parkin, Pink-1* and *DJ-1* were shown to regulate glycolytic activity by modulation of mediators of glycolysis like p53, HIF1-alpha and AMPK (Anandhan et al., 2017). The main effectors of such deficits will most likely be glial cells due to their high glycolytic rates – a phenomenon which is also found in iPSCs. Therefore, it should be considered that iPSCs may serve as valid model in terms of cellular metabolism with both, high glycolytic and OXPHOS activity, which both can be monitored well and may already at this cellular stage indicate metabolic deficiencies carried over into later, more terminally differentiated cell types. With this underlying assumption, the results obtained in this thesis again integrate well into published data. Glucose metabolism definitely has been shown to be impaired in some way, while mitochondrial dysfunction could be shown not to be the causative reason in the iPSCs in this thesis. Therefore, alterations in the central carbon metabolism in iPD patients' iPSCs seem to be at least one logic explanation. Where exactly this alteration lies remains to be elucidated – a variety of studies reached a multitude of results, in which also cell type specificity plays a vital role. For example, Meiser et al., 2016 published an impairment of the one-carbon metabolism in microglia with DJ-1 deficiency. Other studies found a more general dysregulation of the ADP-ribose polymerase-1 (PARP-1),

which is involved in DNA repair and uses NAD^+ as well as ADP-ribose, which is synthesized from ribose-5-phosphoate from the PPP (reviewed in Anandhan et al., 2017; Brighina et al., 2011) and thereby possibly strongly impacts cellular metabolism if stress levels already are increased, ultimately resulting in energy depletion (Kim et al., 2013). Another link between carbon metabolism and PD has been made via pharmacological inhibition of the PPP (Herken, 1990): inhibition of the PPP in rodents caused a global decrease in NADPH levels, resulting in a selective degenerative effect on dopaminergic neurons ultimately yielding motor deficits. Again, iPSCs also rely heavily on the PPP, as this pathway is necessary to deliver precursors for e.g. nucleotide synthesis and cell growth – therefore a dysregulation in the PPP might also derange glucose metabolism in iPSCs, albeit the final, major yield of the pathway will differ for post-mitotic neurons and highly proliferative stem cells. Ultimately, one needs to ask the question if mitochondrial dysfunction really may be the cause for the metabolic phenotypes observed, or if it presents another major hit of many and is a "*knock-on effect"* (Dunn et al., 2014b), since there already may be an upstream dysregulation of metabolic events.

3.4. Engrailed and its implications in disease and metabolism

It has been briefly mentioned before that the homeobox transcription factors Engrailed-1 and -2 are highly conserved transcription factors, possibly playing a role in the development for PD. However, the fact that they are highly conserved, to the point that they can replace each other functionally (Hanks et al., 1995), makes the discrimination in the investigation of faulty regulations of these genes very hard.

Traditionally, the Engrailed proteins were attributed to the isthmic organizer, which is responsible for the correct and specific development of the mid- and hindbrain (Kouwenhoven et al., 2016; Simon et al., 2001). Indeed, mDAN ontogenesis is largely controlled by the concerted action of the transcription factors En-1 and -2, Forkhead box protein A1 and A2 (FoxA-1 and -2), Lmx1-A and -B, Otx2, Pitx3 and several growth factors such as Shh, Fgf8, Tgf-beta and Wnt1 (Prakash, 2006; Rekaik et al., 2015a; Smidt and Burbach, 2007). However, expression of these transcription factors has been shown to be important not only for the development, but also for the maintenance of adult mDANs, not only linking PD to En-1 and -2 (e.g. Alvarez-Fischer et al., 2011; Fuchs et al., 2012; Genestine et al., 2015; Haubenberger et al., 2011; Nordströma et al., 2015; Rissling et al., 2009) but also to Nurr1 (Le et al., 2003), Lmx1b (Laguna et al., 2015) and Pitx3 (Fuchs et al., 2009; Kouwenhoven et al., 2017; Li et al., 2009b). A recent study specified Nurr1 expression as link to the maintenance of TH and DAT expression, while developmentally, expression is induced by En-1 and Pitx3. Loss of Nurr1 expression however does not affect Pitx3 or Engrailed expression. Loss of Pitx3 expression causes an increase in Engrailed expression while not affecting Nurr1 expression and loss of En-1 expression in mice has been shown to result in loss of the entire SNpc and the

majority of the VTA, as well as in a decrease of Pitx3 expression, again not affecting Nurr1 expression (Kouwenhoven et al., 2017). Most importantly however, this study was able to identify the Adh family, which is involved in the metabolism of retinoic acid and DOPAL, as marker for the subset of mDANs which is most vulnerable and lost first in PD. Again, Pitx3 is vital for the expression of Adh-2, linking these factors even tighter to PD (Kouwenhoven et al., 2017). In adulthood, En-1 and -2 expression confines to the mid- and hindbrain (Prochiantz and Di Nardo, 2015; Prochiantz et al., 2014) and is constricted to mDANs of the SNpc and VTA in the midbrain (Simon et al., 2003). Engrailed functions in the adult system not only by its transcriptional activity, but also has been shown to regulate and increase translation of specific targets by its ability to bind the translation initiation factor eIF4E (Topisirovic and Borden, 2005).

Insights into implications of En-1 but especially En-2 on the adult level can also be gained from other diseases and their models, for example autism spectrum disorders (ASDs). In ASDs, predominantly *En-2* seems to be affected: GWAS studies revealed that *En-2* links to ASDs (Benayed et al., 2009) and variations in the expression and methylation profile of *En-2* have been reported in the cerebellum of ASD patients (James et al., 2013, 2014). *En-2* knockout mouse models reveal neuropathological changes related to ASDs, which also are closely related to PD pathology: first, and probably most widely recognized, is the fact that *En-2*$^{-/-}$ mice show a reduction in the number of Purkinje neurons in the cerebellum (Joyner et al., 1991; Kuemerle et al., 1997; Millen et al., 1994, 1995), which may be interconnected to PD as the cerebellum also has been implicated in PD pathogenesis and is known to interconnect to the basal ganglia (Bostan and Strick, 2010; Starkstein et al., 2015; Wu and Hallett, 2013). Second, defective GABAergic (Provenzano et al., 2016; Sgadò et al., 2013) and reduced monoaminergic innervations (Brielmaier et al., 2014; Genestine et al., 2015) into the forebrain have been detected in *En-2* $^{-/-}$ mice, which directly links to PD as well as the fact that brain abnormalities have been detected in individuals with ASD in regions linked to the motor system, the striatum and the primary motor cortex (Hollander et al., 2005; Nebel et al., 2014; Starkstein et al., 2015). Furthermore, not only *En-2* links to ASDs and PD, but first studies might provide a link for *En-1* as well: *En1*$^{+/-}$ mice have been shown to also display a decrease of striatal dopamine, PD-like motor symptoms and non-motor symptoms, under which depressive-like behavior and poor social interaction fall, likely due to moderate loss of mDANs in the VTA, affecting the mesolimbic system also affected in ASD (Sonnier et al., 2007). In summary, a study conservatively estimated a prevalence of about 20% of ASD patients over 39 years to show Parkinsonism-related symptoms (Starkstein et al., 2015), which might likely be at least partially linked to Engrailed dysregulation.

The strongest link of Engrailed and PD, however, has been established through the involvement of Engrailed and its activities as translational modifier in bioenergetics. Studies have shown that Engrailed can stimulate the translation of the nuclearly encoded complex I subunits Ndufs-1 and -3, thereby protecting neurons from bioenergetic insults due to complex I deficiency (Alvarez-Fischer et al., 2011). As a reminder, Ndufs-1 and

-3 are two of seven core units of complex I and are involved in the oxidation of NADH and its electron transfer (Mimaki et al., 2012). Therefore it is not surprising that as consequence of Engrailed activity increased ATP production in retinal growth cones and elevated complex I activity in midbrain synaptosomes could be demonstrated (Stettler et al., 2012). Vice versa, the same studies were able to show that *En-1*$^{+/-}$ mice display decreased levels of Ndufs-1. Additionally, a decrease in the mitophagy marker Microtubule-associated protein 1A/1B light chain 3 (LC3) could be shown in mDANs of *En-1*$^{+/-}$ mice (Nordströma et al., 2015), suggesting an additional role of Engrailed in mitochondrial dynamics. On another level, it could be demonstrated that Engrailed has the capability to influence cellular bioenergetics not just by regulation of mitochondrial complex I, but also by translational regulation of *Lamin-B2*, a major constituent of the nuclear envelope – which in turn has the capability to regulate mitochondrial size and mitochondrial membrane potential, supporting e.g. axon survival (Rekaik et al., 2015a; Yoon et al., 2012). In addition to Engrailed, other transcription factors from the Nurr1-Pitx3-Lmx1a-Engrailed network (Arenas et al., 2015; Prakash, 2006) have been reported to exert regulatory functions in cellular bioenergetics. Nurr1 has been published to have several nuclearly encoded mitochondrial genes as potential transcription targets (Kadkhodaei et al., 2013) and Lmx1a was identified to have potential transcriptional targets in some mitochondrial subunits of the ETC (Doucet-Beaupré et al., 2016; Hoekstra et al., 2013).

In this thesis, varying changes in *Engrailed* gene expression have been determined depending on the cell types used. While *En-1* expression was unchanged in low-passage iPSCs, a significant reduction was found in iPD patients' high-passage iPSCs compared to corresponding controls. In contrast, *En-2* expression was significantly decreased in low- and high-passage iPSCs from iPD patients when compared to corresponding controls. Expression of *Lmx1a, Pitx3 and Nurr1* could not be detected at this stage of cellar development. Surprising was the fact that *Engrailed* expression was already detectable at the stage of pluripotency, as well as being reduced in iPD patients' iPSCs. This gives rise to the question, if *Engrailed* dysregulation can be detected in the primary material, the biopsied fibroblasts already. Furthermore, epigenetic patterning of the promotor region of *En-1* and *-2* would be worthwhile to analyze to get an idea why there are passage dependent regulations and if *Engrailed* methylation patterns did change during reprogramming, as would be expected. As to the passage related differences in *En-1* expression, one explanation might be some sort of co-regulation or an auto-regulatory effect exerted by En-2 on En-1, by which reduced *En-2* expression might also reduce *En-1* expression over time.

When considering NPCs derived from low- and high-passage iPSCs from iPD patients and corresponding controls, a similar picture is obtained. While, this time, in both cases *En-1* expression remains unchanged, *En-2* expression again is reduced in NPCs differentiated from high-passage iPSCs but unchanged in NPCs differentiated from low-passage NPCs. In addition, expression of *Lmx1a* is significantly reduced in iPD patients' NPCs (Fig. 43), while *Nurr1* and *Pitx3* expression are not affected. It is likely that differential

regulation of *En-1* in low- and high-passage iPSCs also effects regulation of *Engrailed* during differentiation. In turn, decrease of *Lmx1a* expression might be due a dose-dependent dysregulation in the Nurr1-Pitx3-Lmx1a-Engrailed network (Arenas et al., 2015; Rekaik et al., 2015b). Upon differentiation of NPCs derived from high-passage iPSCs to neurons, using a protocol adapted for dopaminergic neuron differentiation, the same pattern as in NPCs could be detected. Again, no changes in *En-1* expression were detected, while *En-2* and *Lmx1a* were significantly reduced in iPD patients' samples. *Nurr-1* and *Pitx3* expression remained unchanged, and no significant differences in the differentiation efficiency, i.e. the percentage of TH^+ neurons obtained, could be found.

The expression patterns of *En-1* and *-2* detected in this thesis fit well into what has been published and discussed. Generally speaking, this thesis shows that an impairment in *Engrailed* expression that correlates with bioenergetic phenotypes – albeit no differences in Ndufs-1 and -3 protein levels could be detected in neither NPCs nor neurons. However, as neither *Lamin-B2* expression nor translation was analyzed here, it may well be that changed levels of *Engrailed* expression exert a negative effect here. This might result in altered mitochondrial dynamics, as detected in high-passage iPSCs of iPD patients, or differences in the mitochondrial membrane potential as discussed before.

In the case of NPCs differentiated from low-passage iPSCs, no variations in *En-1* and *-2* expression were found – again correlating with no bioenergetic phenotype being detected. Further, it comes into notice that bioenergetic phenotypes observed in all of these cell types do not necessarily seem to be affected by or correlate with *En-1* expression, but rather expression of *En-2* seems to be the determining factor here. More analyses in this regard have to be made to make an educated correlation, however, this might shift the focus, just like in ASDs, more towards En-2 instead of En-1. Generally, more focus should be put on Engrailed research in connection with PD, as results obtained during this thesis might suggest yet another possible role of Engrailed, being in the control of glucose- and carbon metabolism rather than purely controlling mitochondrial function by direct (Ndufs-1 and -3) or indirect (Lamin-B2) translational modification of effectors.

3.5. Passage dependent differences in iPSCs and their derivatives and insights into the oxidative share of iPSC metabolism

Passage dependent differences detected in iPSCs and their derivates might arise from a multitude of factors, in which the oxidative share of iPSC metabolism and iPSC metabolism in general play a major role since there is strong connection between metabolism, epigenetics and pluripotency. First, metabolic activity of iPSCs will be discussed as this is needed for the subsequent link to epigenetic regulation.

It has been widely recognized that hESCs and generally all hPSCs strongly depend on glycolytic metabolism (Folmes et al., 2012; Lees et al., 2017; Prigione et al., 2014). It has been shown that a strong glycolytic metabolism is necessary to maintain high cellular levels of redox equivalents (NADPH, glutathione (GSH)) and allows rapid proliferation through sufficient amino acid and nucleotide synthesis (Lehninger et al., 2008; Newsholme et al., 1985). Glycolysis furthermore delivers intermediary products like pyruvate which can be oxidized in the TCA to fuel lipid and carbon donors necessary for membrane synthesis as well as the synthesis of some amino-acids and cofactors like acetyl-CoA, alpha-ketoglutarate and succinate. Downstream reactions like the reduction of pyruvate to lactate or electron transfer to the mitochondrial ETC regenerate other cofactors like NAD^+. Divergent pathways like the PPP are, depending on the cell type, responsible for the majority of NADPH generation which is abundant in cellular redox-reactions and stress defenses (Lehninger et al., 2008). As for hESCs, it has been shown that depending on the state of pluripotency and maintenance conditions up to 80% of glucose can be metabolized to lactate, while glucose-derived carbon metabolized trough the PPP contributes up to 70% to the cytosolic NADPH (Pfeiffer et al., 2001; Zhang et al., 2016). The strong lactate metabolism has two reasons: first, NAD^+ is needed as cofactor for GAPDH and is therefore a prerequisite for a fast and smoothly running glycolytic cascade in the cell – the faster glycolysis runs, the more glucose is taken up, the more ATP and intermediary products are produced. This is furthermore important as glycolysis presents the means of generating ATP without ROS production. Second, glycolytic activity has been linked to improved reprogramming and enhancement of pluripotency in hPSCs (reviewed in Lees et al., 2017). However, when considering the OCR/ECAR ratios obtained in iPSCs and NPCs in this thesis, it becomes clear that there is a very strong oxidative metabolism present in the iPSCs used in this thesis. OCR/ECAR ratios significantly changed in-between low- and high-passage iPSCs. It becomes obvious that low-passage iPSCs with ratios around 2.0-2.3 rely much more on oxidative metabolism compared to high-passage iPSCs with ratios around 1.1-1.5. In addition, controls' iPSCs display a significantly higher OCR/ECAR ratio than iPD patients' iPSCs. In contrast, a drop in OCR/ECAR ratio down to 0.8-1.0 can be observed in NPCs, with no health state specific changes observed. Generally speaking, the strong oxidative share in iPSCs may have a variety of reasons. First, it has been published that different stages of pluripotency, to name naïve and primed pluripotency as the two extremes, have varying proportions of oxygen consuming metabolism at their base with an increased aerobic share in naïve pluripotent states (Lees et al., 2017; Teslaa and Teitell, 2015). However, primed versus naïve pluripotency as explanation for obtained OCR/ECAR ratios is rather unlikely, as specific protocols and maintenance conditions are necessary to convert iPSCs from primed to ground state pluripotency – usually there is only a very small subset of iPSCs in culture (less than 1%) reverted to a ground state - first indications for this are that in ground state pluripotency the second X chromosome is active, while it remains silent upon reprogramming of somatic cells to iPSCs (Romito and Cobellis, 2016).

A more likely explanation for the high proportion of oxidative metabolism in iPSCs in this thesis and its reduction during passaging are epigenetic modifications caused by multiple factors. Pluripotency, (mitochondrial) metabolism and therefore by default epigenetics depend strongly on the amount of oxygen supplied to hESCs. Supply of physiological oxygen concentrations, i.e. concentrations below 5-7% oxygen to hESC has been reported to be beneficial for the maintenance of pluripotency (Forristal et al., 2010; Zachar et al., 2010), the preservation of methylation status (Petruzzelli et al., 2014), activity of the second X-chromosome (Lengner et al., 2010) and decrease of lineage specific markers in hESCs while increasing efficiency of embryoid body (EB) formation (Chen et al., 2010; reviewed in Lees et al., 2017). However, iPSCs in this thesis were maintained under atmospheric oxygen conditions, i.e. 20% oxygen. While physiological oxygen levels have been shown to promote glycolytic flux and increase glycolysis gene expression (Harvey et al., 2016a; Lees et al., 2015), an increasing body of evidence shows that atmospheric oxygen levels regulate and increase mitochondrial activity and biogenesis, increasing mtDNA copies, cellular ATP levels, mitochondrial mass and expression of metabolic genes associated with mitochondrial activity and replication in hESCs (Forristal et al., 2013; Lees et al., 2015). This would be a rather likely explanation for the strong oxidative phenotype observed in iPSCs in this thesis. However, even though there is a consensus in literature that an increase of mitochondrial function is necessary for directed differentiation and facilitates spontaneous differentiation (Folmes et al., 2012; Prigione and Adjaye, 2010; Prigione et al., 2010), there is also evidence that this is not necessarily the consequence of an increased mitochondrial metabolism. When considering OCR/ECAR ratios and the absolute numbers of respiratory activity, it becomes apparent that the iPSCs in this thesis not only have a strong respiratory proportion of oxidative metabolism, but also high levels of glycolytic activity. In fact, cells always need to maintain the proper balance of both. It has been postulated that despite having high respiratory values, the cells derive ATP still primarily from glycolysis. There have been several mechanisms published in iPSCs which actually may prevent high rates of glucose-derived pyruvate dependent OXPHOS: first, pyruvate flux is regulated by transporters in the inner mitochondrial membrane (mitochondrial pyruvate transporter) and by activity of UCP2. It has been mentioned before that UCP2 decreases mitochondrial metabolism in hESCs and pushes metabolism further towards the PPP and glycolysis (Zhang et al., 2011). Second, it has been published that hESCs contain low levels of aconitase 2 and isocitrate dehydrogenase 2/3 – complemented by high levels of ATP citrate lyase (Tohyama et al., 2016), limiting the ATP produced by OXPHOS. On the other hand, high respiratory levels need to be accounted for somehow – indeed, it has been shown that inhibition of pyruvate oxidation stimulates glutamine metabolism in hESCs, facilitating glutamine-derived acetyl-CoA production (Moussaieff et al., 2015; Tohyama et al., 2016; Yang et al., 2014). In fact, it has been demonstrated that glutamine, next to glucose, is the most facilitated substrate of hPSCs and mitochondria in hPSCs (Zhang et al., 2016) and that glutaminolysis is strongly used for ATP synthesis, synthesis of

antioxidants such as GSH and NADPH and for fueling anaplerotic pathways (Turner et al., 2014). It has to be noted here that standard Seahorse XF Assay medium contains 2 mM GlutaMax (Seahorse Bioscience / Agilent Technologies) and iPSC maintenance medium (mTesR1, StemCell Technologies) even close to 3 mM glutamine. Therefore, a vivid glutamine metabolism in iPSCs can be assumed. Another vital issue to consider, and this goes hand in hand with mitochondrial glutamine metabolism, is that mitochondrial functions have been shown to be essential for maintenance of pluripotency and cellular self-renewal (Mandal et al., 2011). Loss of mitochondrial function in hPSCs has been shown to result in increased mitochondrial fragmentation, accompanied by decreased pluripotency until it is lost as well as decreased EB formation capability and cell survival (Chandel, 2014; Hämäläinen et al., 2015; Todd et al., 2010), despite the fact that an increase in glycolysis has been shown beneficial for pluripotency (Lees et al., 2017). This is likely attributed to the fact that mitochondrial activity produces ROS. ROS have been implicated in many negative ways, like oxidative stress, but are increasingly recognized also for signaling properties. ROS can directly modulate various pathways by modification of kinases, transcription factors and other proteins involved in nutrient pathways – ultimately stimulating cellular proliferation (Diebold and Chandel, 2016; Lees et al., 2017). In NPCs derived from hPSCs, for example, self-renewal depends on high levels of endogenous ROS from cytoplasmic NOX activity (Anandhan et al., 2017; Le Belle et al., 2011; Yoneyama et al., 2010), supporting regulatory effects of ROS on stemness (Lees et al., 2017). Furthermore, it has been hypothesized that the perinuclear arrangement of mitochondria (Folmes et al., 2012; Prigione et al., 2015) with acute proximity of mitochondria and nucleus may be due to relevant ROS signaling activity (Al-Mehdi et al., 2012). This hypothesis is plausible as HIF is stabilized in the presence of specific concentrations of mitochondrial peroxide (H_2O_2), even under atmospherically oxygen conditions (Patten et al., 2010). HIF, in turn, has been shown to modulate Oct4 activity, promote self-renewal and a transcriptional network beneficial for pluripotency (Covello et al., 2006; Lees et al., 2017; Petruzzelli et al., 2014). Furthermore, an increase of glycolytic activity in hPSCs can be expected upon increase of mitochondrial activity in hPSCs, due to e.g. atmospheric oxygen levels. An increase in OXPHOS likely results in an increased production of ROS, to the extent that they increase cellular stress levels. Especially under atmospheric oxygen conditions which enhance mitochondrial activity ROS levels may increase. In order to compensate for those ROS levels, increased levels of GSH and NADPH will be necessary – which in turn will increase OXPHOS and glycolytic activity to generate sufficient ROS for H_2O_2 production to maintain HIF signaling as well as ATP and reduction equivalents (Lees et al., 2017). Other evidence pointing into this direction is the fact that hESCs have been published to maintain high levels of GSH and NADPH superoxide dismutase 2 (SOD2) (Cho et al., 2006; Dannenmann et al., 2015). SODs are responsible for reducing cytoplasmic O_2^- to H_2O_2, while ROS generated by mitochondrial complexes (e.g. complex I & III) have to be reduced to H_2O by the glutathione-peroxidase (GSH/GPX) system using NADPH (Berg et al., 2012).

While all of this may explain why the OXPHOS share is so high in the iPSCs in this thesis, it still does not account for passage dependent changes. However, also here nutrient usage plays a vital role, therefore possibly accounting not only for passage but also health state dependent changes. The vast amount of epigenetic regulation depends on a handful enzymes: DNA methylation is regulated by DNA methyltransferases (DNMTs) usually restricting gene expression. Vice versa, active de-methylation usually activating gene expression is catalyzed by ten-eleven translocation dioxygenases (TETs). Methylation of residues on histones H3 and H4 is mediated by histone methyltransferases (HMTs) which may act as either transcriptional activation or repression. Histone acetylation is mediated by histone acetyltransferases (HATs) which are associated with an euchromatic state, while histone deacetylation, mediated by histone deacetylases (HDACs) is associated with condensed heterochromatin, i.e. transcriptional repression (reviewed in Berg et al., 2012). For proper functioning, all of these systems need cofactors – mainly supplied by the central carbon metabolism (reviewed in Lees et al., 2017). The primary methyl donor for methylation events is S-adenosylmethionine (SAM) produced in the folate and methionine cycles of the one carbon metabolism (Donohoe and Bultman, 2012; Harvey et al., 2016b; Xiao et al., 2012) – therefore there is a direct link between glucose metabolism and epigenetic activity. This is further supported by the fact that cellular levels of alpha-ketoglutarate and succinate have been reported to regulate TET activity (Xiao et al., 2012). But not only methylation, also acetylation events are dependent on cellular metabolic activity – HAT activity needs acetyl-CoA produced in either glucose or lipid oxidation as acetyl-group donor and HDAC activity is regulated by NAD^+-dependent mechanisms (Seto and Yoshida, 2014). Consequently, a disturbed cellular glucose metabolism in iPD patients' samples, already apparent albeit at lower levels in low-passage iPSCs, may well gain in severity upon epigenetic regulation events in high-passage iPSCs which may lead to even stronger impairment in iPD patients' iPSCs compared to controls' iPSCs. Yet, not only the health state specific decrease but also the general decrease of OXPHOS share from low- to high passage iPSCs may be explained in such way. First, epigenetic regulation may change in the long run in such way that OXPHOS and glycolysis are balanced better by decreasing or increasing shares of either one. This could be reasoned with long-term adaptation to atmospheric oxygen conditions. Second, epigenetic regulation of mtDNA may play a role. In 2011, epigenetic regulation of the mitochondrial genome itself was hypothesized, after a group discovered the translocation of a nuclear DNMT1 with a mitochondrial target sequence into mitochondria (Shock et al., 2011). Other studies identified methylated cytosine-groups in the control region of mtDNA (Bellizzi et al., 2013) and the existence of histones within the mitochondrial membrane (Choi et al., 2011). While this area of research is still in its baby shoes, it may well be that passage dependent differences in metabolic activity may be mediated by epigenetic regulation of the mitochondria itself. Again, changes in levels of heteroplasmy upon reprogramming (Kang et al., 2016), as discussed before, may also make a major impact when considering this together with mitochondrial epigenetics.

Supporting this idea may also be the fact that even though the epigenetic clock is modified during the process of reprogramming, this does not affect somatic mitochondrial DNA mutations which should remain (Lorenz and Prigione, 2016).

3.6. Conclusions and future perspectives

In this thesis it could be shown that PD has an impact not only on neuronal or glial level, but also already on pluripotent level, in iPSCs reprogrammed from iPD patients and their derivatives. As it was not possible to detect a mitochondrial defect in iPSCs from iPD patients, a dysregulation of glucose and carbon metabolism presents itself as likely explanation of the respiratory phenotypes observed with glucose as substrate – a fact to which an increasing body of evidence in PD research points to. Upon differentiation of iPSCs to cells with neuronal identity, a "gain-of-phenotype", a complex I deficiency could be observed in iPD patients' NPCs, yet still accompanied by a dysregulated glucose metabolism. These bioenergetic phenotypes could be additionally linked to the impaired expression of an important transcriptional and translational regulator in dopaminergic neurons – Engrailed. With Engrailed being one of the most important transcription factors in dopaminergic neuron development and life-long maintenance, a clear link, not only via deranged glucose metabolism of complex I deficiency, can be made to the pathogenesis of iPD. In this thesis no clear results towards a mechanistic link of bioenergetics and PD could be found. To this purpose, both, glucose-derived carbon flux analysis and non-targeted metabolomics in high-passage iPSCs were done. Unfortunately, results of both will not be obtained in the time course of this thesis anymore. However, both approaches promise to gain an even more detailed insight into cellular metabolism and dysregulated carbon flux, from the one side by actually analyzing glycolytic carbon flux using ^{13}C-labeled glucose and therefore labeled intermediates and end-products, on the other side by getting a quantitative picture of stable intermediary and end products of processes like amino acid synthesis, lipid synthesis, redox equivalent synthesis and other pathways. To confirm the link of the Engrailed dysregulation and bioenergetic deficiencies in iPD, it will be worthwhile to attempt to rescue those bioenergetic impairments using Engrailed over-expression or application of Engrailed protein. Furthermore, an in-depth analysis of the epigenetic state of iPD patients' and controls' iPSCs and NPCs would be desirable to be able to compare epigenetic regulation and resulting Engrailed activity and bioenergetics in these models of iPD. Last but not least, sequencing of mtDNA and their epigenetic patterning has been tried in cooperation with Prof. M. Riemenschneider and Dr. M. Schulze (TP 3 of the ForiPS consortium), however, results also have not been obtained yet. This likely will give insights into levels of mitochondrial heteroplasmy, somatic mutations and epigenetic regulation.

Taken together, this thesis successfully was able to contribute to PD research in new, so-far not analyzed model systems. It was able to demonstrate that not only neuronal type cells, but also induced pluripotent stem cells are already affected by the disease, indicating a strong reminiscent genomic or epigenetic background in iPD patients' cells. Results obtained from all cell types are consistent within each other and integrate well into previously published data in PD research, fortifying the increasing body of research on metabolic dysregulation in Parkinson's disease.

4. Material and Methods

4.1. Material

4.1.1. Chemicals

Chemical	Catalogue Number	Supplier
2-Deoxy-D-Glucose, Grade II	D8375-25G	Sigma-Aldrich
2-Mercaptoethanol (cell culture suitable) 2-Mercaptoethanol	31350010 M7522	Thermo Fisher Scientific Sigma-Aldrich
Accutase Solution	A6964	Sigma-Aldrich
Acetic acid	W200603	Sigma-Aldrich
Agarose	870055	Biozym, Germany
Ampuwa	B230673	Fresenius Kabi
Antimycin A	A8674	Sigma-Aldrich
Ascorbic acid 2-phosphate	A8960-5G	Sigma-Aldrich
Bovine Serum Album (BSA)	A7906-500G	Sigma-Aldrich
Bovine Serum Albumin (BSA), essentially fatty acid free	A6003-25G	Sigma-Aldrich
Carbonyl cyanide 4-(trifluoromethoxy)phenylhydrazone (FCCP)	C2920	Sigma-Aldrich
CHIR99021	4423/10	Tocris Bioscience
Collagenase, Type IV, powder	17104019	Thermo Fisher Scientific
DAPI-Solution	62248	Thermo Fisher Scientific
Dimethyl sulfoxide, >=99.5% (DMSO)	D5879-100ML	Sigma-Aldrich
Dorsomorphin dihydrochloride	3093/10	Tocris Bioscience
EmbryoMax Ultra-Pure Water	TMS-006-B	Merck Millipore
Ethanol absol. P.A 2,5L M983	Merck 1009832500	Merck Millipore

Ethidium bromide	2218.2	Carl Roth GmbH
Ethylenediaminetetraacetic acid solution (EDTA 0.02% in DPBS)	E8008-100mL	Sigma-Aldrich
Ethylenediamintetraacetic acid (EDTA)	EDS-1KG	Sigma-Aldrich
Formalin, 10%	F5554	Sigma-Aldrich
Gentle Cell Dissociation Reagent	07174	STEMCELL Technologies
Glucose Solution	A2494001	Thermo Fisher Scientific
L-Glutamine (200mM), 100 mL	25030024	Thermo Fisher Scientific
L-Lysine monohydrochloride	L8662-25G	Sigma-Aldrich
Methanol	1.06009.2500	Merck Millipore
Methanol, LC-MS Ultra CHROMASOLV, tested for UHPLC-MS	14626-1L	Sigma-Aldrich
Milk powder	70166-500G	Sigma-Aldrich
N^6,2′-O-Dibutyryladenosine 3′,5′-cyclic monophosphate sodium salt (dbcAMP)	D0627-250MG D0627-1G	Sigma-Aldrich
Non-essential amino acids, 100mL	11140035	Thermo Fisher Scientific
NuPAGE LDS Sample Buffer (4X)	NP0007	Thermo Fisher Scientific
Oligomycin A	75351	Sigma-Aldrich
Phosphate buffered saline D´Beccos (DPBS) W/O CA	14190169	Thermo Fisher Scientific
Purmorphamin	4551	R&D Systems, Germany
ReLeSR™	05872	STEMCELL Technologies
Rotenone	R8875	Sigma-Aldrich
Sodium chloride	106404	Merck KGaA
Sodium deoxycholate	D6750	Sigma-Aldrich

Sodium dodecyl sulfate (SDS)	L3771	Sigma-Aldrich
Sodium pyruvate (100 mM)	11360039	Thermo Fisher Scientific
StemMACS SB431542	130-106-275	Miltenyi Biotec
StemPro Accutase Cell Dissociation Reagent	A1110501	Thermo Fisher Scientific
Tert-butylhydroperoxide (TBHP)	B2633	Sigma-Aldrich
Tris (Trizma-Base)	93352	Sigma-Aldrich
Triton X-100	T9284	Sigma-Aldrich
Trizma hydrochloride	T3253	Sigma-Aldrich
Tween 20	P1379	Sigma-Aldrich
UK5099	PZ0160	Sigma-Aldrich
Y-27632.dihydrochloride	ALX-270-333-M005	Enzo Life Sciences, Germany

Table 4: List of chemicals.

4.1.2. Cell Culture Media and Supplements

Media / Supplement	Catalogue Number	Supplier
B-27 Supplement (50X), minus vitamin A	12587010	Thermo Fisher Scientific
Cryostor cell cryopreservation media CS10	C2874-100ML	Sigma-Aldrich
DMEM	21969	Thermo Fisher Scientific
DMEM Medium 43,70 874,00 w/o L-Glutamine, w/o Glucose, w/o Pyruvate with 3.7g/L NaHCO3, with Phe, Leu, Ile, Val, Met, Thr, Trp, Tyr	custom made	Genaxxon, Germany
DMEM/F-12	11320074	Thermo Fisher Scientific
DMEM/F12 GlutaMAX	10565018	Thermo Fisher Scientific

Insulin-Transferrin-Selenium (ITS-G), 100x	41400045	Thermo Fisher Scientific
Knockout DMEM	10829018	Thermo Fisher Scientific
KnockOut Serum Replacement	10828028	Thermo Fisher Scientific
mFreSR	05885	STEMCELL Technologies
mTeSR1	05850	STEMCELL Technologies
N-2 Supplement (100X)	17502048	Thermo Fisher Scientific
Neurobasal Medium	21103049	Thermo Fisher Scientific
Seahorse XF Assay Medium	102365100	Agilent Technologies
Seahorse XF Base Medium	102353100	Agilent Technologies
Seahorse XF Calibrant Solution	100840000	Agilent Technologies

Table 5: List of cell culture media and supplements.

4.1.3. Coating and Growth Factors

Coating & Growth Factors	Catalogue Number	Supplier
Geltrex	A1413302	Life Technologies, Germany
Human BDNF, research grade	130-093-811	Miltenyi Biotec
Human FGF-2, premium grade	130-093-839	Miltenyi Biotec
Human FGF-8b, premium grade	130-095-740 130-095-741	Miltenyi Biotec
Human GDNF, research grade	130-096-291	Miltenyi Biotec
Human TGF-β3, research grade	130-094-008	Miltenyi Biotec
Laminin Mouse Protein, Natural	23017015	Life Technologies, Germany
Matrigel Mix, 10mL	354234	BD Biosciences, Germany

Matrigel-Matrix, 10 ml	354230	BD Biosciences, Germany
Poly-L-Ornithine hydrobromide Mol WT*300 00-70000	P3655	Sigma-Aldrich

Table 6: List of coatings and growth factors.

4.1.4. Antibodies

Primary Antibody	Dilution	Catalogue Number	Supplier
Alpha-Tubulin (GT114)	1:10.000 (WB)	GTX628802	GeneTex
Anti-Slc25A1	1:1000 (WB)	SAB2105540	Sigma Aldrich
ATP5A [15H4C4]	1:4000 (WB)	ab14748	Abcam
Beta-Actin	1:10.000 (WB)	GTX26276	GeneTex
Beta-Tubulin III	1:500 (ICC)	Ab18207	Abcam
Drp1 (D8H5)	1:1000 (WB)	5391S	Cell Signaling
Glycerol 3 Phosphate Dehydrogenase	1:2000 (WB)	ab87286	Abcam
Glycerol 3 Phosphate Dehydrogenase 2 [EPR14260]	1:2000 (WB)	ab182144	Abcam
Mtco2 [12C4F12]	1:1000 (WB)	ab110258	Abcam
Nanog	1:200 (ICC)	AF1997	R&D Systems
Ndufb8	1:1000 (WB)	459210	Thermo Fisher Scientific
Ndufs1 [EPR11522(B)]	1:10.000 (WB)	AB157221	Abcam
Ndufs3 [EPR12781]	1:10.000 (WB)	AB183733	Abcam
Nestin (10C2)	1:250 (ICC)	MA1110	Thermo Fisher Scientific
Oct4 [C30A3]	1:400 (ICC)	2840S	Cell Signaling
Pax6	1:200 (ICC)	Ab78545	Abcam

Phospho-DRP1 (Ser616) (D9A1)	1:1000 (WB)	4494S	Cell Signaling
Phospho-DRP1 (Ser637) (D3A4)	1:1000 (WB)	6319S	Cell Signaling
Sdhb [21A11AE7]	1:500 (WB)	459230	Thermo Fisher Scientific
Sox1	1:500 (ICC)	Ab87775	Abcam
Sox2	1:500 (ICC)	Sc17320	Santa Cruz
Tyrosin Hydroxylase	1:600 (ICC)	P40101	PelFreez
Uqcrc2 [13G12AF12BB11]	1:2500 (WB)	Ab14745	Abcam

Table 7: List of primary antibodies.

Secondary Antibody	**Dilution**	**Catalogue Number**	**Supplier**
Donkey-anti-goat IgG Alexa488	1:500 (ICC)	A11055	Thermo Fisher Scientific
Donkey-anti-mouse IgG Alexa488	1:500 (ICC)	A21202	Thermo Fisher Scientific
Donkey-anti-mouse IgG Alexa594	1:500 (ICC)	A21203	Thermo Fisher Scientific
Donkey-anti-goat IgG Alexa594	1:500 (ICC)	A11058	Thermo Fisher Scientific
Donkey-anti-rabbit IgG Alexa488	1:500 (ICC)	A21206	Thermo Fisher Scientific
Donkey-anti-rabbit IgG Alexa594	1:500 (ICC)	A21207	Thermo Fisher Scientific
Goat-anti-mouse IgG Peroxidase	1:10.000 (WB)	115-035-146	Dianova
Goat-anti-rabbit IgG Peroxidase	1:10.000 (WB)	111-035-003	Dianova

Table 8: List of secondary antibodies.

4.1.5. Consumables

Consumable	Catalogue Number	Supplier
10x Tris/Glycine Buffer	1610771	BioRad, Germany
Amersham ECL Western Blotting Detection Reagent	RPN2106OL/AF	GE Healthcare, Germany
Aqua-Poly/Mount	18606	Polysciences Inc, USA
BD Plastipak Syringe 30ML	WC0605153700	Th. Geyer, Germany
C-Chip Neubauer Improved	PK361	Carl Roth GmbH
Cell scraper 25CM	83.1830	Sarstedt, Germany
Criterion XT 4 - 12% Bis-Tris Gels	3450124	BioRad, Germany
GeneRuler 1kb DNA Ladder	SM0243	Thermo Fisher Scientific
Immobilon-P PVDF Membrane	IPVH00010	Merck Millipore
Microplate 96/F-PP wh/bl	30601700	Neolab, Germany
Multi-well plate, 24 well	353047	Corning, Germany
Multi-well plate, 6 well	353046	Corning, Germany
Multi-well plate, 96 well	9407473	Thermo Fisher Scientific
NuPage LDS Sample Buffer (4x)	NP0007	Thermo Fisher Scientific
Phosphatase Inhibitor Cocktail	04906837001	Roche, Germany
Protease Inhibitor Cocktail	04906837001	Roche, Germany
Protein Marker VI	A8889	AppliChem, Germany
SafeSeal SurPhob Filtertips, 1250 µl, sterile	VT0270	Biozym, Germany
Seahorse XFe96 FluxPak	102416100	Agilent Technologies, Germany

Sterile filter 0,2 µM	INTG156608	VWR, Germany
SuperFrost™ Plus Glass Slides	4951PLUS4	Thermo Fisher Scientific
Whatman Cellulose Chromatography Paper	WHA3030931	Sigma Aldrich, Germany
XF96 V3 PS Cell Culture Microplates	101085004	Agilent Technologies, Germany
XT MOPS Running Buffer	1610788	BioRad, Germany

Table 9: List of consumables.

4.1.6. Commercial Kits

Kit	Catalogue Number	Supplier
5 PRIME MasterMix	2200110	5 Prime
Complex I Enzyme Activity Microplate Assay Kit	AB109721	Abcam
EasySep™ Human ES/iPS Cell TRA-1-60 Positive Selection Kit	18166	STEMCELL Technologies
Glucose Uptake Assay Kit	AB136955	Abcam
L-Lactate Assay Kit	AB65330100TES	Abcam
NAD/NADH Assay Kit	ab176723	Abcam
Pierce BCA Protein Assay Kit	23225	Thermo Fisher Scientific
Quant-iT™ PicoGreen® dsDNA Assay Kit	P11496	Thermo Fisher Scientific
REDTaq ReadyMix PCR Reaction Mix	R2523	Sigma-Aldrich
RNeasy Plus Mini Kit	74134	Qiagen
SuperScript VILO cDNA Synthesis Kit	11754050	Thermo Fisher Scientific
TaqMan Assay 18S rRNA (Hs99999901_s1)	4331182	Thermo Fisher Scientific
TaqMan Assay ACTB (Hs99999903_m1)	4331182	Thermo Fisher Scientific

TaqMan Assay AMPKa1 (Hs01562315_m1)	4331182	Thermo Fisher Scientific
TaqMan Assay En1 (Hs00154977_m1)	4331182	Thermo Fisher Scientific
TaqMan Assay En2 (Hs00171321_m1)	4331182	Thermo Fisher Scientific
TaqMan Assay Fis1 (Hs00211420_m1)	4331182	Thermo Fisher Scientific
TaqMan Assay HPRT1 (Hs01003267_m1)	4331182	Thermo Fisher Scientific
TaqMan Assay Lmx1a (Hs00898455_m1)	4331182	Thermo Fisher Scientific
TaqMan Assay Mfn1 (Hs00966851_m1)	4331182	Thermo Fisher Scientific
TaqMan Assay Mfn2 (Hs00208382_m1)	4331182	Thermo Fisher Scientific
TaqMan Assay MT-RNRN1 (Hs02596859_g1)	4331182	Thermo Fisher Scientific
TaqMan Assay NR4A2 (Hs01117527_g1)	4331182	Thermo Fisher Scientific
TaqMan Assay OPA1 (Hs01047018_m1)	4331182	Thermo Fisher Scientific
TaqMan Assay Pitx3 (Hs01013935_g1)	4331182	Thermo Fisher Scientific
TaqMan Assay SLC2A1 (Hs00892681_m1)	4331182	Thermo Fisher Scientific
TaqMan Assay SLC2A2 (Hs01096908_m1)	4331182	Thermo Fisher Scientific
TaqMan Assay SLC2A3 (Hs00359840_m1)	4331182	Thermo Fisher Scientific
TaqMan Assay SLC2A4 (Hs00168966_m1)	4331182	Thermo Fisher Scientific
TaqMan Universal PCR Master Mix	4324018	Thermo Fisher Scientific

Table 10: List of commercially obtained kits.

4.1.7. Equipment

Instrument	Supplier
ABI Prism 7900 HT Real-Time PCR System	Applied Biosystems, USA
AxioCam HRc Camera	Zeiss, Germany
Axioplan 2 Microscope	Zeiss, Germany
Biological Safety Cabinet, Herasafe	Thermo Fisher Scientific
ChemiDoc MP Imaging System	BioRad, Germany
Criterion™ Blotter	BioRad, Germany
Criterion™ Cell System	BioRad, Germany
Gel-Documentation System E.A.S.Y. Win32	Herolab, Germany
Milli-Q® Integral Water Purification System	Merck Millipore
Mr. Frosty™ Freezing Container	Thermo Fisher Scientific
NanoDrop Spectrophotometer ND-1000	Peqlab, Germany
Orbital Shaker (7-0030)	Neolab
Seahorse XF96 Analyzer	Agilent Technologies, Germany
SpectraMax M5 Microplate Reader	Molecular Devices, Germany
Transilluminator	Herolab, Germany
Centro LB 960 Luminometer	Berthold Technologies, Germany

Table 11: List of equipment.

4.1.8. Solutions and Buffers

Solution	Composition
10x TBS, pH8	12.1g Tris (100mM) 80.23g NaCl (1.4M) 1L H_2O Adjust to pH 8
1x TBS-T	100ml 10x TBS 1ml Tween20 Adjust to 1L with H_2O
1x Tris/Glycine Buffer Transfer Buffer	200mL 10x Tris/Glycine Buffer (10x, BioRad) 400ml Methanol 1.4L H_2O
1x XT MOPS Running Buffer	50ml MOPS Buffer (20x, BioRad) 950ml H_2O
Blocking Buffer (Immunocytochemistry)	1% BSA 0.5% Triton X-100 PBS
Blocking Buffer (Western Blot)	5% skim milk powder (or 5% BSA) 1x TBS-T buffer
Mitochondrial Assay Solution (MAS, 1x)	70mM Sucrose 200mM Mannitol 10mM KH_2PO_4 5mM $MgCl_2$ 2mM HEPES 1mM EGTA
PBS (1x)	171 mM NaCl 3,4 mM KCl 10 mM Na_2HPO_4 1,8 mM KH_2PO_4 pH 7.4
RIPA Buffer	50mM Tris-HCL 150mM NaCl 1% Triton X-100 0.5% Sodium-Deoxycholate 0.1% SDS

	3mM EDTA Addition of phosphatase / protease inhibitors
TAE Buffer	40mM Tris 20mM acetic acid 1mM EDTA
TBE (10x)	0,89 M Tris-base 0,89 M boric acid 0,02 M EDTA

Table 12: List and composition of buffers.

4.2. Methods

4.2.1. Cell Culture

4.2.1.1. Coating of cell culture dishes

Human iPS cells were maintained in Matrigel coated 6-well plates. Matrigel stock solution was thawed overnight at 4°C and quickly aliquoted in 1mL aliquots using a pre-cooled (-20°C) pipette and metal rack for Eppendorf reaction tubes. Aliquots were frozen and stored at -20°C until further use. For coating of cell culture dishes, 1mL of Matrigel was thawed for approx. 1h at 4°C and diluted with cool (4°C) DMEM/F12-Glutamax in a 1:30 ratio. Subsequently, 1mL of the dilution was applied per 6-well and incubated for 45min – 1.5h at 37°C, 7% CO_2. Before using the coated plates, the DMEM/F12-Glutamax was removed and the plates washed with PBS once. It is important to note that the plates should be never allowed to dry.
Human NPCs were maintained in Geltrex coated 6-well plates. Handling of Geltrex and Matrigel was very similar only aliquot volume (Geltrex: 0.5mL) and dilution in DMEM/F12-Glutamax (1:100) differed. 1mL of the Geltrex dilution was added per 6-well and an additional 0.5mL of plain DMEM/F12-Glutamax was added to obtain a total volume of 1.5mL in order to get a more homogenous distribution of the coating. Geltrex coated plates were incubated at 37°C, 7% CO_2 at least for 1h, usually overnight.

4.2.1.2. Thawing of cells

In preparation for thawing cells, sufficient 6-well plates were coated (1-2 wells / vial of cells), washed once with PBS and subsequently allowed to warm to 37°C with 2mL of maintenance media for about 30min.

Human iPS cells were thawed quickly in a water bath at 37°C and the content of the vials transferred into a falcon containing 2mL of pre-warmed mTesR1 supplemented with 10µM Y-27632 dihydrochloride (inhibitor of Rho-associated coiled-coil containing protein kinase (ROCK), added to increase cellular survival by blocking apoptosis). The fragments of the iPS colonies were allowed to sediment (if no fragments were visible, cells were shortly spun down at 90xg for 2min), the supernatant was removed and cells were resuspended in 1mL of pre-warmed mTesR1 supplemented with 10µM Y-27632 dihydrochloride, pipetted 1-2 times to break down too large fragments and plated on the previously prepared, coated 6-well plates and incubated at 37°C, 5% CO_2. The next day, cells were washed once with PBS to remove debris and residual Y-27632 dihydrochloride from the medium and the medium was changed to normal growth medium.

Human NPCs were thawed quickly at 37°C and the content of the vials transferred into a falcon containing 2mL of pre-warmed growth medium. Cells were spun down for 5min at 200xg, the supernatant removed and the cell pellet resuspended in 1mL of growth medium. Subsequently the resuspended cells were plated on previously coated and prepared plates and incubated at 37°C, 7% CO_2 overnight. The next day cells were washed once with PBS to remove dead cells and debris and the medium was changed.

4.2.1.3. Determination of cell numbers

To determine the number of cells in suspension (e.g. during passaging), 10µl of the suspension were transferred onto a Neubauer cell-counting-chamber. Cell count in all four outer squares (top-left, top-right, bottom-left and bottom right) was determined and cell number was calculated as follows:

$$\frac{Total\ number\ of\ cells}{4} * 10.000 = \frac{Number\ of\ cells}{ml}$$

4.2.1.4. Immunocytochemistry

Cells were split and plated in adequate concentration on previously coated 96-well plates or glass slides in 24-well plates as described above. When reaching confluency, the maintenance medium was removed, the cells washed once with PBS and an appropriate amount (96-well: 50µL/well; 24-well 200µL/well) of 4% paraformaldehyde (PFA) or 10% formalin was added and cells were fixed for 10-15 min at RT. Subsequently, the PFA or formalin was removed and replaced with PBS (96-well: 100µL/well; 24-well: 400µL/well) and cells stored at 4°C until staining.

For immunofluorescent staining, the PBS was replaced by an appropriate amount of PBS supplemented with 1% bovine serum albumin (BSA) and 0.3% Triton X-100 (PBS/BSA/Triton-solution) and incubated for 15 min at RT. Subsequently, the solution was removed, replaced by a PBS/BSA/Triton-solution containing a dilution of the primary antibodies (ABs) (see Tab.7) and incubated for at least 1 hour at RT. Afterwards, cells were washed twice with PBS and incubated with a PBS/BSA/Triton-solution containing a dilution of the secondary ABs (see Tab.8) for 1 hour at RT, plates covered with tinfoil. Subsequently, cells were washed twice with PBS and an appropriate amount of DAPI solution (1:10.000 in PBS) was added for 2-3 min. Finally, cells on 96-well plates were washed again three times with PBS and stored in PBS in the dark at 4°C until analysis. Glass slides were transferred to microscope slides fixed with embedding medium (Aqua-Poly/Mount, Polysciences Inc.) and allowed to dry over night at 4°C.

4.2.2. Maintenance and differentiation of human iPS and neuronal precursor cells

4.2.2.1. Maintenance of iPSCs

iPSCs were maintained on growth-factor reduced Matrigel in 2mL growth medium (mTesR1, Stemcell Technologies) with daily medium changes. In course of maintenance, cells were observed daily on morphological level in terms of colony integrity and spontaneous differentiation. Differentiated cells or areas were removed by manual scraping or splitting with either ReLeSR (Stemcell Technologies) or collagenase type IV in extreme cases.

4.2.2.2. Splitting and picking of iPSCs

Standard splitting procedure of iPSCs was done with ReLeSR according to manufacturer's instructions. The growth medium was aspirated and the cells were washed once with PBS. Subsequently, 1mL of ReLeSR per well was applied and incubated for 40-60 seconds at RT. Following, ReLeSR was aspirated and the cells were incubated dry at 37°C, 5% CO_2 for 4 min. When taken out of the incubator, cells were detached by tapping against the plate until colonies were visibly broken down. Finally, 1mL of mTesR1 was added and the broken colonies were transferred into a 15mL falcon tube. Depending on desired split ratio, 50-200µL / 6-well of the suspension were seeded on a fresh, previously coated plate.

In case of increased spontaneous differentiation in large areas or intentional further downstream differentiation of the cells, iPSCs were split with collagenase type IV. Collagenase was prepared in DMEM/F12 at a concentration of 2mg/mL and stored at 4°C for up to two weeks. The growth medium was aspirated from the iPSCs and the cells were washed with PBS once. Following, 1mL of collagenase was applied and cells incubated for 40-60 min at 37°C, 5% CO_2. This results in complete detachment of whole, unbroken colonies yet no detachment of differentiated cells. The suspension was transferred into a 15mL falcon tube, 1mL of mTesR1 was added and colonies were allowed to sediment for about 3-5 min and excess medium was removed. If to be split, colonies were broken down using 1mL of growth medium and 1250µL pipette tips (Biozym). Depending on desired split ratio, 50-200µL / 6-well of the suspension were seeded on a fresh, previously coated plate. If cells were to go into differentiation, colonies were left intact and transferred into the proper differentiation medium.

In extreme cases of spontaneous differentiation in large areas, intact colonies were picked from the plate. Picking was done using an inverted microscope (Leica DMIL LED) and a 10x objective placed in a Herasafe Class II biological safety cabinet (2020 1.2, Thermo Fisher) with inserted microscopy pane. Colonies were picked without pretreatment and collected in a 15mL falcon tube. Subsequently, colonies were broken down

using 1mL of growth medium and 1250µL pipette tips (Biozym). Depending on desired split ratio, 50-200µL / 6-well of the suspension were seeded on a fresh, previously coated plate.

4.2.2.3. Differentiation of iPSCs

iPSCs were differentiated into smNPCs according to a protocol adapted from Reinhardt et al. (2013). Differentiation was achieved by dual Smad-inhibition using small molecules (1µM Dorsomorphin (DM) (Tocris Bioscience) and 10µM SB431542 (SB) (Miltenyi Biotec)) with additional stimulation of the Wnt-pathway (3 µM CHIR99021 (CHIR) (Tocris Bioscience) and 100 ng/mL (= 4.44 nM) FGF-8b (Miltenyi Biotec)) and stimulation of the Sonic Hedgehog (SHH) pathway (0.5 µM Purmorphamin (PA) (Tocris Bioscience)).

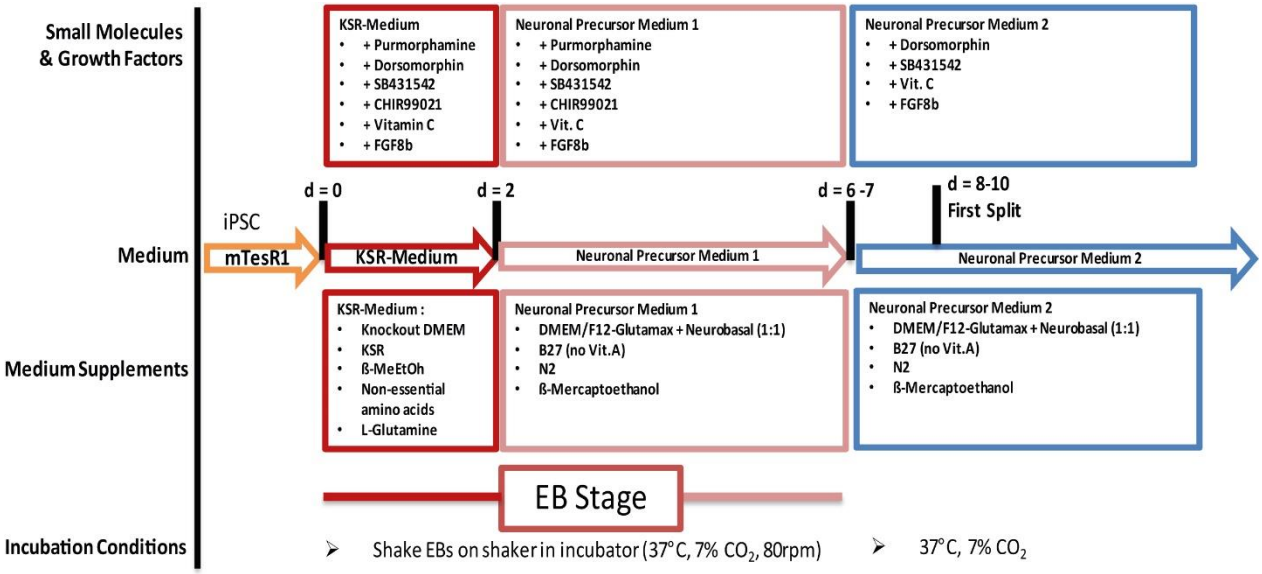

Fig. 47: Differentiation protocol of iPSCs to smNPCs. Protocol adapted from Reinhardt et al, 2013.

When reaching approx. 70% confluence, iPSC colonies were detached using collagenase type IV as described before (1.2.2.2). Detached colonies were transferred into KnockOut-Serum-Replacement Medium (KSR-Medium) consisting of 80% KnockOut-DMEM (Gibco / Life Technologies) supplemented with 20% KSR (Gibco / Life Technologies) and 10µM SB, 3µM CHIR, 0.5µM PA, 1µM DM, 4.44nM FGF-8b, 150µM Vitamin C (Ascorbic acid 2-phosphate, Sigma), 1% non-essential amino acids (Gibco / Life Technologies), 1% L-Glutamine (Gibco / Life Technologies) and 0.02% beta-mercaptoethanol (β-ME, Gibco / Life Technologies) in 6-well plates. The plates were incubated on a shaker in a 37°C, 5% CO_2 incubator at 80rpm with daily medium change for 2 days. At day 3, when colonies had already obtained an EB-like shape, the EB's were transferred into the Neuronal Precursor Medium 1 (NPM1), consisting of 50% DMEM/F12-GlutaMAX and 50% Neurobasal supplemented with 1% B27 supplement (without Vit. A,

Gibco / Life Technologies), 1% N2 supplement (Gibco / Life Technologies), 0.02% β-ME and consistent concentrations of the molecules SB, CHIR, PA, DM, Vitamin C and FGF-8b as in the KSR-medium. Cells were incubated at 70rpm, 37°C and 7% CO_2 with daily medium changes until day 6-8 when the EB's displayed intensive neuro-epithelial outgrowth (like described in Reinhardt et al, 2013). EB's were seeded unharmed on Geltrex coated plates and at the same time CHIR and PA were removed from NPM1 (i.e. NPM2 = maintenance medium). The adhered EB's were allowed to expand for another 1-2 days until split for the first time at day 8-10.

For the first split, growth medium was carefully removed from the adherent EB's, cells were carefully washed with PBS once and incubated approx. 10 min with Accutase until EB's were digested into small fragments and single cells. The cell suspension was transferred into 1mL of NPM2 and spun down at 200xg for 3 min and the supernatant removed. The pellet was resuspended in NPM2 and re-plated in an appropriate amount of 6-wells (1-3, depending on amount of EB's digested). Cells were allowed to attach and the medium changed the next day, with medium change every two days from this time-point on.

NPM2 on cells differentiated from high-passage iPSCs still contained 0.5µM PA as the protocol was further optimized afterwards.

4.2.2.4. Maintenance and splitting of smNPCs

Human smNPCs were maintained on previously coated 6-well plates with a medium change every two days. Maintenance medium (NPM2) was composed as described above (1.2.2.3). Cells were grown until reaching 85-95% confluence. Splitting was done using Accutase: the maintenance medium was removed, cells were washed with PBS once and incubated with Accutase at 37°C for approx. 10 min. Suspended cells were transferred into a 15mL Falcon tube with 1-2mL of maintenance medium and spun down for 3 min at 200xg. The supernatant was removed, the pellet resuspended in growth medium and cells seeded in a 1:5 - 1:10 ratio onto previously coated plates. Medium change was done the next day.

4.2.3. Cell based assays

4.2.3.1. Respiratory analysis ("Seahorse")

4.2.3.1.1. Preparation of plates and seeding of cells

In preparation for respiratory analysis of iPS cells, XF96 V3 PS cell culture microplates were coated with 50µL of Matrigel or Geltrex, depending on cell type, per well and incubated for at least 1-2 hours, like described previously. Subsequently, the Matrigel / Geltrex solution was removed, wells were washed once with PBS when coated with Matrigel and finally 100µL of mTesR1 supplemented with 10µM Rock-

inhibitor or 100µL of smNPC growth medium respectively were added per well and allowed to pre-warm to 37°C.

iPSCs were washed once with PBS and treated with 1mL Accutase per 6-well for approx. 10 minutes at 37°C until single cells were obtained. The cell solution was pipetted up and down 4-5 times with 1250µL pipette tips (Biozym) to facilitate the breakdown of residual colony fragments to single cells, and subsequently transferred into 3mL of mTesR1 supplemented with 10µM Rock-inhibitor. 10µL of this solution were used to assess the total number of cells for each line like described above. While counting, cells were spun down at 90xg for twelve minutes, the supernatant was removed and the pellet resuspended in mTesR1 with 10µL Rock-inhibitor at such concentration that a count of 100.000-200.000 cells/mL was obtained. Finally, 50µL to 100µL (10.000-15.000 cells/well) were transferred into each 96-well of the XF96 V3 PS cell culture microplates. Depending on the amount of lines, three to four technical replicas per line and condition (glucose or pyruvate) were done. The next day, medium was changed to mTesR1 without Rock-inhibitor and cells were allowed to grow with daily medium changes for 4-6 days until reaching confluency, at which point respiratory analysis was performed.

In equal manner, smNPCs were washed once with PBS and treated with Accutase, but incubated for 15 min at 37°C. After pipetting, cells were transferred into 3 mL of maintenance medium and the total amount of cells/vial was assessed like with iPS cells. After counting, cells were spun down at 200xg for 5 min and resuspended in growth medium at such concentration that 1.000.000 cells/mL were obtained. Following, 50µL (50.000 cells) were seeded into each 96 well of the XF96 V3 PS cell culture microplates and cells allowed to recover for 2-3 days with daily medium changes. As with iPSCs, three to four technical replicas per line and condition (glucose or pyruvate) were done.

One day before respiratory analysis was performed, an XF 96 FluxPak (cartridge) was hydrated with 200µL of Seahorse XF calibrant according to manufacturer's protocol.

4.2.3.1.2. Respiratory analysis of cells

In this thesis, respiratory analysis was always done with two different substrates, glucose and pyruvate. The maintenance media of the iPSCs used in this thesis is highly complex and contains, next to a variety of growth factors, vitamins and lipids, both, glucose (3.72 mM) and pyruvate (1.44 mM). Preliminary measurements of the basal oxygen consumption in the maintenance media or Seahorse XF Assay media with corresponding concentrations of both energy substrates did not show any differences (data not shown). Furthermore, as there were concerns about exposing cells to an osmotic shock when raising the glucose

concentrations from 3.7 mM to 25 mM, preliminary titration experiments from 1 mM to 25 mM glucose were done, yielding highest respiration at 25mM glucose (data not shown). Similarly, pyruvate was titrated from a 1 mM to 5 mM concentration with no differences observed (data not shown). Therefore, to ensure that there would be no issue with substrate limitation, the excess concentrations of 25 mM glucose and 5mM pyruvate were used and both substrates applied alone to obtain a divided measurement of whole-cell (glucose) and mitochondrial (pyruvate) respiration and gain further insight into metabolic pathways, which would not have been possible if both substrates were supplied at the same time.

Respiratory analysis requires a unique medium which had to be prepared freshly every time. In order to assess OCR and ECAR in parallel an unbuffered medium is required. Therefore, all measurements were done in Seahorse XF Assay Medium (Seahorse Bioscience / Agilent Technologies) freshly supplemented with one energy substrate / carbon source only, 25 mM glucose or 5 mM pyruvate respectively. Before cellular respiration could be measured, the medium had to be changed to the unbuffered assay medium and cells had to be allowed to equilibrate to the new medium. The maintenance medium was removed, cells were washed once with plain XF Assay Medium and then supplied with 180 µL XF Assay Medium either supplemented with 25 mM glucose or 5 mM pyruvate. Subsequently, the cell plate was transferred into a 37°C incubator with atmospheric concentrations of CO_2 and O_2 and allowed to equilibrate for 45 min to 1 hour. Meanwhile, desired concentrations of oligomycin, FCCP, rotenone, antimycin A and 2-DG were prepared (Tab. 13) and the previously hydrated cartridge was loaded. Each port of the cartridge was loaded as follows: port A was loaded with 20 µL of 12.64 µM oligomycin, port B with 22 µL of 5 µM FCCP, port C with 25 µL of 50 µM rotenone and 20 µM antimycin A and port D with 27 µL of 1 M 2-DG.

Port	Substance	Stock-concentration.	Port-concentration	Assay-concentration
A	Oligomycin	1 mg/mL (1.264 mM)	10 µg/mL (12.64 µM)	1 µg/mL (1.264 µM)
B	FCCP	2.5 mM	5 µM	0.5 µM
C	Rotenone Antimycin A	2.5 mM 2.5 mM	50 µM 20 µM	5 µM 2 µM
D	2-Deoxyglucose	1 M	1 M	100 mM

Table 13: Concentrations and dilutions, with final assay concentration on the plate, of each chemical used to assay respiratory characteristics of cells. Port stands for corresponding port on cartridge (A-D). *All chemicals were diluted at stated concentrations*

in DMSO to obtain stock concentrations. Dilution to port concentration was done in XF Assay Medium. Port concentrations were ten-fold to final assay concentrations on the ports on as the cartridge only allows small volumes (max. 40µL-50µl). All chemicals were always kept on ice.

After the cartridge was loaded, the Seahorse XF96 software was programmed including correct labeling of all wells and background wells and the correct assay protocol (Fig. 48 and Fig. 49) and the measurement was started.

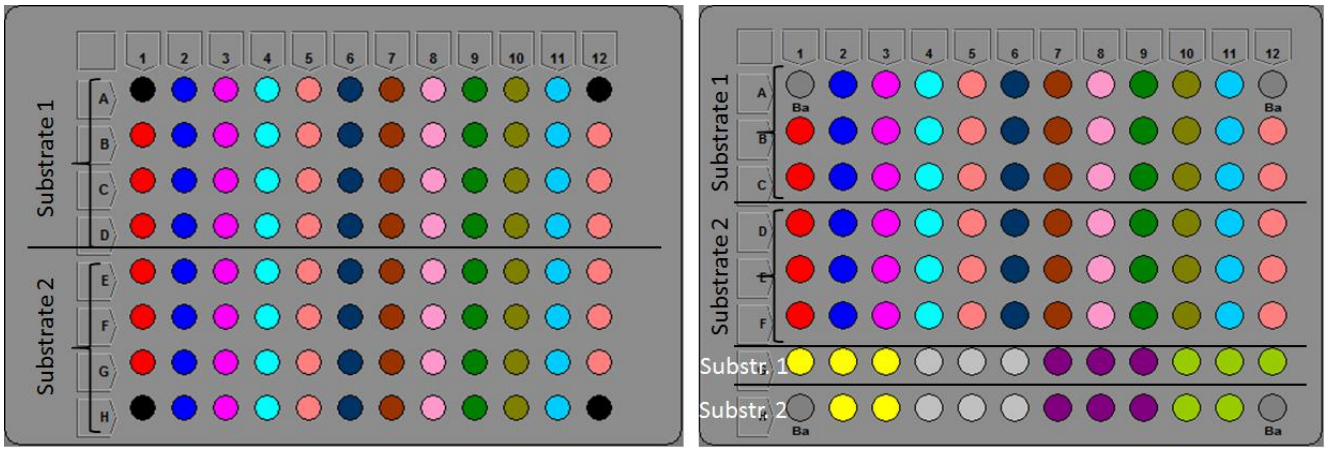

Fig. 48: Example layout of a XF 96 cell culture microplate with twelve or sixteen iPSC lines per plate*. Each color represents one line. Always two substrates (glucose and pyruvate) were measured in parallel. Wells A1, A12, H1 and H12 did not contain cells and were used for background correction. Substrate and line setups were always randomly rotated to avoid technical measurement errors.*

For iPS cells, after the measurement, medium was removed from the plates and the plate with the cells only frozen and stored at -20°C for quantification of DNA content (normalization). As smNPCs start to dissociate towards the end of a measurement, plates were thrown away and equally seeded and treated plates were used for quantification (see section 1.4.1).

In case of iPSCs, cells did not detach during the measurements and the same plates were used for determination of DNA concentration and thereby normalization of the respiratory data to DNA content. In case of NPCs, plates were discarded after a Seahorse run, as cells started to dissociate due to the stressful conditions. Instead, an equally seeded and treated plate was used for DNA quantification to allow normalization to DNA content.

Statistical analysis of Seahorse measurements was done as described in section 4.2.5. For analysis, the mean (± standard deviation) values for individuals (7 patients and 5 control individuals) was used and subjected to either two-way ANOVA if applicable or (non-) parametrical analysis. In all cases, raw data obtained was also subjected to statistical analysis, if both analyses were significant results were considered statistically significant.

Seahorse protocol iPS cells				Seahorse protocol smNPCs			
Action	**Time**	**Action**	**Time**	**Action**	**Time**	**Action**	**Time**
Calibrate Probes				***Calibrate Probes***			
(1)Mix	1 min	***Inject Port B***		(1)Mix	1 min	***Inject Port C***	
Time Delay	2 min	(12)Mix	1 min	Time Delay	2 min	(11)Mix	1 min
(1)Measure	3 min	Time Delay	2 min	(1)Measure	3 min	Time Delay	2 min
(2)Mix	1 min	(12)Measure	3 min	(2)Mix	1 min	(11)Measure	3 min
Time Delay	2 min	(13)Mix	1 min	Time Delay	2 min	(12)Mix	1 min
(2)Measure	3 min	Time Delay	2 min	(2)Measure	3 min	Time Delay	2 min
(3)Mix	1 min	(13)Measure	3 min	(3)Mix	1 min	(12)Measure	3 min
Time Delay	2 min	(14)Mix	1 min	Time Delay	2 min	(13)Mix	1 min
(3)Measure	3 min	Time Delay	2 min	(3)Measure	3 min	Time Delay	2 min
(4)Mix	1 min	(14)Measure	3 min	(4)Mix	1 min	(13)Measure	3 min
Time Delay	2 min	***Inject Port C***		Time Delay	2 min	***Inject Port D***	
(4)Measure	3 min	(15)Mix	1 min	(4)Measure	3 min	(14)Mix	1 min
(5)Mix	1 min	Time Delay	2 min	***Inject Port A***		Time Delay	2 min
Time Delay	2 min	(15)Measure	3 min	(5)Mix	1 min	(14)Measure	3 min
(5)Measure	3 min	(16)Mix	1 min	Time Delay	2 min	(15)Mix	1 min
(6)Mix	1 min	Time Delay	2 min	(5)Measure	3 min	Time Delay	2 min
Time Delay	2 min	(16)Measure	3 min	(6)Mix	1 min	(15)Measure	3 min
(6)Measure	3 min	(17)Mix	1 min	Time Delay	2 min	(16)Mix	1 min
(7)Mix	1 min	Time Delay	2 min	(6)Measure	3 min	Time Delay	2 min
Time Delay	2 min	(17)Measure	3 min	(7)Mix	1 min	(16)Measure	3 min
(7)Measure	3 min	***Inject Port D***		Time Delay	2 min	***Program End***	
(8)Mix	1 min	(18)Mix	1 min	(7)Measure	3 min		
Time Delay	2 min	Time Delay	2 min	***Inject Port B***			
(8)Measure	3 min	(18)Measure	3 min	(8)Mix	1 min		
Inject Port A		(19)Mix	1 min	Time Delay	2 min		
(9)Mix	1 min	Time Delay	2 min	(8)Measure	3 min		
Time Delay	2 min	(19Measure	3 min	(9)Mix	1 min		
(9)Measure	3 min	(20)Mix	1 min	Time Delay	2 min		
(10)Mix	1 min	Time Delay	2 min	(9)Measure	3 min		
Time Delay	2 min	(20)Measure	3 min	(10)Mix	1 min		
(10)Measure	3 min	***Program End***		Time Delay	2 min		
(11)Mix	1 min			(10)Measure	3 min		
Time Delay	2 min						
(11)Measure	3 min						

Fig. 49: Protocol layout of the assay protocol for iPS cells and smNPCs.

4.2.3.2. Seahorse analysis of permeabilized cells (electron flow and coupling efficiency)

There are two possibilities to assess electron flow across the ETC on the mitochondrial membrane and coupling efficiency of the OXPHOS with the ETC: (1) by isolation of mitochondria and measurement of isolated mitochondria or (2) by permeabilization of cells, thereby opening cellular membranes and allowing free metabolite diffusion in and out of the cells yet not into mitochondria, effectively resulting in measurements of mitochondrial function on specifically delivered substrates only.

Both, measurements of the electron flow across the mitochondrial complexes and of the coupling efficiency of OXPHOS and ETC were assessed indirectly as function of oxygen consumption. Cells were prepared and grown like for normal Seahorse assays (see section 4.2.3.1.1). Before the assay, the Seahorse XF96 software was programmed (Fig. 50), the cartridge loaded (see Tab.14) and cartridge calibration started. Meanwhile cells were washed once with mitochondrial assay solution (1x MAS) and given the correct assay buffer.

Assay buffer electron flow assay					**Assay buffer coupling efficiency assay**				
1x MAS supplemented with ▪ ADP [4mM] ▪ BSA, fatty acid free [0.2%] ▪ Digitonin [0.003%, 24.4µM] ▪ FCCP [4µM] ▪ Malonate [2mM] ▪ Pyruvate [10mM]					1x MAS supplemented with ▪ BSA, fatty acid free [0.2%] ▪ Digitonin [0.003%, 24.4µM] ▪ Rotenone [2µM] ▪ Succinate [10mM] ➢ adjusted to pH 7 – 7.2 with KOH				
Port	**Substance**	**Stock-conc.**	**Port-conc.**	**Assay-conc.**	**Port**	**Substance**	**Stock-conc.**	**Port-conc.**	**Assay-conc.**
A	Rotenone	2.5mM	25µM	2.5µM	A	ADP	500mM	40mM	4mM
B	Succinate	1M	100mM	10mM	B	Oligomycin	2mg/mL	25µg/mL	2.5µg/mL
C	Antimycin-A	2mM	25µM	2.5µM	C	FCCP	2.5mM	50µM	5µM
D	TMPD Ascorbic acid (pH 6)	100mM 1M	1mM 100mM	100µM 10mM	D	Antimycin-A	2mM	40µM	4µM

Table 14: Composition of assay buffers for electron flow assays and coupling efficiency assays and loading scheme of the corresponding cartridge.

When calibration was completed, without any further incubation time, the cell plate was loaded to the Seahorse XF96 analyzer and mitochondrial function was measured. Upon completion, the cell plate was thrown away and normalization was done with a second, equally seeded and grown XF assay plate (see section 4.2.4.1). Statistical analysis was done as for normal Seahorse analysis.

Start Protocol	
Command	***Time***
Calibrate	
Mix	1 min
Wait	3 min
Mix	1 min
Wait	3 min
Mix	0.5 min
Measure	2 min
Mix	1 min
Measure	2 min
Mix	1 min
Inject Port A	
Mix	1 min
Measure	3 min
Mix	1 min
Inject Port B	
Mix	0.5 min
Measure	3 min
Mix	1 min
Inject Port C	
Mix	0.5 min
Measure	3 min
Mix	1 min
Inject Port D	
Mix	0.5 min
Measure	3 min
End Protocol	

Fig. 50: Protocol layout of the assay protocol for electron flow and coupling efficiency assays.

4.2.3.3. L-Lactate determination

L-lactate levels were determined in order to measure glycolytic activity and output. For determination of L-lactate levels a commercial kit (L-Lactate Assay Kit (Fluorometric), ab65330, Abcam) was used.
Six to seven days before the experiment was performed, a 96-well plate was coated with Matrigel and cells were plated as described before (see sections 4.2.1.1 and 4.2.2.1) and cells were allowed to reach 80-90% confluency. At the day of the experiment, cells were washed once with Seahorse XF assay minimal medium (Seahorse Bioscience / Agilent Technologies) and subsequently supplied with Seahorse XF assay minimal medium, with either 25 mM glucose or 5 mM pyruvate. Following, cells were incubated at 37°C, 0% CO_2 for 2.5 to 3 hours. The medium was taken from the cells, diluted 1:1000 and the assay was performed as described by the manufacturer. Finally, the remaining cells on the plate were used for DNA-normalization (see section 4.2.4.1). Every line was analyzed with 3-4 technical and 3 biological replicas per condition.

4.2.3.4. NAD^+ / NADH ratio determination

NAD^+/NADH ratios were determined using a commercially available kit (NAD+/NADH Assay Kit (Fluorometric), ab176723, Abcam). As described before, a 96-well microplate was coated and cells transferred and allowed to reach 80-90% confluency. Subsequently the assay was performed as stated in manufacturer's protocol, a second plate seeded in parallel and maintained equally was used for DNA quantification and normalization.

4.2.3.5. Cell Viability Assay

Cell viability was tested using the CellTiter-Glo™ Luminescent Cell Viability Assay (Promega). To this purpose, cells were seeded in a coated 96-well plate and allowed to grow to 80-90% confluency. Just before the assay was performed, medium was changed to an amount appropriate (100 µL) for the assay and the assay performed according to manufacturer's instructions.

4.2.4. Molecular Methods

4.2.4.1. Quantification of cellular DNA content

As most of the cell based assays performed depend on the amount of cells used, a way to normalize the obtained results had to be applied. In this thesis, assays were usually normalized to cellular DNA content, as determination of DNA concentrations proofed itself to be a highly replicative and reliable system. DNA quantification was done using Quant-iT™ PicoGreen® dsDNA Assay Kit (Thermo Fisher).

For quantification of DNA, either the cell plate measured was cleaned of medium or supernatant, frozen and stored at -20°C directly, or a second, equally in parallel seeded cell plate was used. Usually, 6-8 replicas of one line were done.

Frozen cell plates were thawed for 20 min on ice and subsequently cells were lysed for 20 min on ice using 60 µL RIPA buffer per well. Accordingly, standards with concentrations ranging from 0 µg/mL to 6-8 µg/mL, depending on the format of the plate, were also prepared in RIPA buffer. Enough standards were prepared to allow at least three replicas per standard concentration. Afterwards, cells lysates were mixed thoroughly by pipetting up and down and 30 µL of lysate or standard were transferred to a microplate for fluorescence-based assays (Eppendorf, black bottom).

During incubation, the supplied 20x TE buffer was diluted to 1x TE buffer with water and the Quant-iT PicoGreen reagent was diluted 1:200 in 1x TE buffer. 100 µL of diluted reagent were added per well of sample or standard and incubated in the dark at RT for 5 min. Finally, relative fluorescence units (RFU) were measured at Ex*480*nm and Em*520*nm. DNA concentrations were calculated using linear quantitation.

4.2.4.2. Preparation and quantification of whole cell RNA

RNA was prepared either directly from 6-well microplate or from cell pellets using the commercially available RNAeasy (Plus) Mini Kit (Qiagen). For this purpose, cells were seeded as previously described on coated 6-well microplates. When prepared from pellets, cells were first treated 8-12min with Accutase, transferred into a 15 mL Falcon tube and spun down at 200xg for 3 min. The supernatant was removed and an appropriate amount of lysis buffer (RLT buffer supplemented with beta-mercaptoethanol) applied as stated in manufacturer's protocol. Cells obtained directly from a 6-well microplate were rinsed twice with PBS and an appropriate amount of lysis buffer was directly applied as stated in manufacturer's protocol. Subsequent RNA preparation was done following to manufacturer's instructions until RNA was finally eluted in 30µL of ultra-pure RNase-free water. Concentration and purity of RNA were determined using the NanoDrop-2000 system (Thermo Fisher) and samples stored at -80°C until further use.

4.2.4.3. Preparation of complimentary DNA (cDNA)

Complementary DNA (cDNA) was prepared from previously isolated whole cell RNA using the SuperScript® VILO cDNA Synthesis Kit (Thermo Fisher). For the purpose of standardization, always 1 µg of RNA per sample were transcribed according to manufacturer's instructions. The obtained yield of 20 µL of cDNA with a concentration of 50 ng/µL was diluted 10-fold using ultra-pure water (Thermo Fisher Scientific) to a final concentration of 5 ng/µL and stored at -20°C or -80°C until further usage.

4.2.4.4. Quantitative Real-Time Polymerase Chain Reaction (qRT-PCR)

qRT-PCR was performed in a 384-well format using an ABI PRISM 7900HT analyzer (Applied Biosystems). First, a master mix of *TaqMan Universal PCR Master Mix* and desired probe was prepared (10 µL *TaqMan Master Mix* + 1 µL probe per well). Subsequently, 9 µl of the diluted cDNA (5 ng/µL) were applied per well and 11 µL of *TaqMan PCR Mix* and probe master mix were added. All work was done on ice. The plate was covered with a *PCR Foil Seal* and shortly centrifuged to mix components. Following, the plate was loaded and the qRT-PCR program (Tab.15) started. Subsequent analysis of data was done using the program SDS2.4 (Applied Biosystems) and Microsoft Excel, statistical analysis was done using Graphpad Prism 6 (Graphpad).

Step	Temperature [°C]	Duration [sec]	Cycles
Initial denaturation	95	600	1
Denaturation	95	15	40
Annealing and amplification	60	60	40

Table 15: Sequence of qRT-PCR program.

4.2.4.5. Preparation and quantification of whole cell protein

Prior to protein isolation, cells were grown to appropriate confluency as described before (section 4.2.2.1) and fresh RIPA buffer was prepared and supplemented with proteinase inhibitors (cOmplete, Mini Protease Inhibitor cocktail, Sigma) and phosphatase inhibitors (PhosStop, Sigma) if necessary. In order to remove excess protein from medium, growth medium was removed and cells were washed once with ice-cold PBS. From here on, all steps were performed on ice. PBS was removed and an appropriate amount (150-200 µL per 6-well) of RIPA buffer was applied and the plates were allowed to incubate 10 min on ice. Subsequently, the lysate was transferred to an Eppendorf reaction tube and centrifuged at maximal speed (13.000xg) for 10 min at 4°C. The supernatant was transferred into a fresh Eppendorf reaction tube, immediately used or stored at -80°C.

Concentration of protein in collected samples was determined using Pierce BCA Protein assay kit (Thermo Fisher Scientific). According to the manufacturer's instructions, a standard series from bovine serum albumin was created and measured together with the samples. Concentration of samples was obtained by linear regression analysis in Microsoft Excel.

4.2.4.6. Immunoblotting (Western Blot)

Western Blot analysis (WB) of whole cell protein lysate was done using a Criterion™ Cell System (BioRad). Protein, either used freshly or thawed on ice, was diluted in such way that 20 µL of RIPA-buffer and protein solution contained the desired amount of protein (5-15 µg per pocket) and an appropriate amount of 4x Loading Dye (NuPAGE, Invitrogen) freshly supplemented with 4% beta-mercaptoethanol (Sigma) was added. Subsequently, samples were heated to 65°C (mitochondrial proteins) or 95°C (all other proteins) for 5 min and allowed to cool to RT afterwards. For electrophoresis, Criterion XT 4-12 % Bis-Tris (BioRad) gels were used. After removal of the comb, pockets were washed with running buffer before loading 25µL of sample or 5 µL of protein ladder (protein marker VI, AppliChem) per pocket. Empty pockets were filled with RIPA and Loading Dye solution prepared like the samples to ensure linear running of the gel. Subsequent to loading, the whole chamber was filled with 1x running buffer (XT MOPS Running Buffer, BioRad) and the electrophoresis done at a voltage of 180 V for approximately 70 min.

Prior to blotting, 1x transfer buffer (10x Tris/Glycine Buffer, BioRad) was prepared according to manufacturer's instructions. Following electrophoresis, the precast gel set was cracked open and the gel transferred onto a filter paper (Whatman cellulose chromatography paper, Sigma) soaked in transfer buffer. The PVDF membrane (Immobilon-P PVDF membrane, Merck Millipore) was shortly activated in 100 % methanol (Merck Millipore), slewed in transfer buffer and subsequently put on the gel and covered by another soaked filter paper. Following, soaked sponges were placed on both sides and the stack placed in the blotting chamber (Criterion™ Blotter, BioRad) as described in manufacturer's manual. Blotting was done at 4°C and a voltage of 20 V overnight.

After blotting, the membrane was blocked in 5 % milk (Sigma) in 1x TBST for 75 min at RT. Subsequently, membranes were transferred into a 50 mL Falcon tube with 5 mL 0.5 % milk in 1x TBST, primary antibody was applied in desired concentration and incubated at 4°C overnight on a tube roller with 30 rpm. The next morning, the membrane was washed three times for 10 min with 20 mL 1x TBST. Following, 10 mL of 5 % milk in 1x TBST was added per Falcon tube, the secondary antibody was added in desired concentration and incubated at RT for 60 min. After incubation, membrane was washed three times with 1x TBST for 10 min. Detection of bands was done using ECL detection substrate (Amersham ECL Western Blotting Detection Reagent, GE Healthcare) and a transilluminator (Herolab).

4.2.4.7. Mycoplasma Testing

To ensure contamination free cell culture of iPSCs and NPCs, frequent mycoplasma testing using polymerase chain reaction (PCR) was done. Medium samples from cells with at least 70 % confluency were taken after two days incubation, diluted in a 1:1 ratio with ultra-pure water (Thermo Fisher Scientific) and heated to 95°C for 15 min to inactivate and destroy potential mycoplasma. 5 µL of the inactivated samples were added to the PCR reaction and PCR was performed as described in Tab. 16. Results of the PCR were evaluated using gel electrophoresis with a 1 % agarose-TAE gel containing ethidium bromide. Gels were visualized using Gel-Documentation system E.A.S.Y Win32 (Herolab). The primers used (5-prime: Myco-5' CACCATCTGTCACTCTGTTAACC and 3-prime: Myco-3' GGAGCAAACAGGATTAGATACCC) yield an approximately 300bp fragment if test is positive for mycoplasma, positive controls were included in every testing round.

PCR Mix	Volume [µL]	PCR Program	Time & Temperature	Cycles
5-prime Mastermix	10	Denaturation	3 min, 94°C	1
Primer 5'	1 [10 pmol]			
Primer 3'	1 [10 pmol]	{Denaturation	15 sec, 94°C	
Inactivated Medium	5	{Annealing	30 sec, 65°C	} 35
ddH2O:	8	{Replication	30 sec, 72°C	
		Replication	3 min, 72°c	1

Table 16: Standard procedure of mycoplasma testing using PCR.

4.2.5. Statistical analysis

Statistical analysis was performed using Graphpad Prism 6 software. All experiments were analyzed with at least three replicates. If applicable (for comparison of more than two groups) two-way ANOVA with Tukey's Post-hoc test was performed. F-tests are displayed in supplementary Tab. 2. If only two groups could be compared, samples were tested for out-layers and Gaussian distribution was assessed by D'Agostino and Pearson omnibus normality tests. In case of normal distribution, t-test was applied, in case of non-Gaussian distribution data was analyzed using Mann-Whitney test. P-values below 0.05 are considered significant. Data displaying a measurement progression are shown with mean ± standard error of the mean (SEM), bar-graphs are displayed with mean ± 95 % confidence interval (95 % CI).

5. Appendix

Project in ForiPS	Group	Title of Project	Location
1 (central project)	Beate Winner Zacharias Kohl Jürgen Winkler	Central project of ForiPS: human induced pluripotent stem cells	IZFK Erlangen UKFZ Erlangen UKFZ Erlangen
2	Andrè Reis	Genetics of PD and genetic stability of human iPSCs and their cellular derivates.	UKFZ Erlangen
3	Markus Riemenschneider	Epigenetic stability of IPSCs and their derivates.	University of Regensburg
4	Peter Dabrock	Bioethics at the interface of research, therapy and commercialization.	FAU Erlangen
5	Helmut Brandstätter Jürgen Winkler	Analysis of neurites and chemical synapses from iPSCs and their neuronal derivates.	FAU Erlangen UKFZ Erlangen
6	Wolfgang Wurst Daniela Vogt Weisenhorn	Mitochondrial function in iPSCs and their dopaminergic derivates from PD patients.	TUM München
7	Jochen Klucken Dieter Chichung Lie	Dysfunction of autophagy in iPSC based neuronal precursors and differentiated neurons of PD patients.	FAU Erlangen
8	Sigrid Schwarz Günter Höglinger	Mirkotubuli associated protein Tau as pathogenic factors of iPD.	TUM München
9	Michael Sendtner	Generation and validation of iPSCs for the research of pathomechanisms of motorneuron diseases.	JMU Würzburg
10	Michael Wegner	Investigation of disease-relevant disturbances of the bowl nervous system from iPD patients in in vivo and in vitro models.	FAU, Erlangen
11	Iryna Prots Beate Winner	Human in vitro model of neuroinflammation in iPD.	IZKF Erlangen
12	Magdalena Götz	Astropathy in PD – functional analysis of PD patients' astrocytes from iPSCs.	LMU, München
13	Marisa Karow Benedict Berninger	Programming and reprogramming of striatal interneurons from human iPSCs and pericytes.	LMU, München
14	Jens Volkmann	Influence of deep brain stimulation of the nucleus subthalamicus on neurodegeneration and –regeneration in a rat model of PD.	JMU Würzburg

15A	Arne Manzeschke	ForiPS – individual- and social-ethical perspectives on a translational research project.	LMU, München
15B	Rosa-Maria Lederer Jasmin Burcyk	Coordination / administration	FAU, Erlangen
16	Frank Edenhofer	Analysis of aging-dependent cellular processes in Parkinson syndrome using novel reprogramming strategies.	JMU Würzburg

Supplementary Table 1: List of projects in the ForiPS consortium (Erlangen, Bavaria).

Figure	ANOVA table	F (DFn, DFd)	P value
Fig. 8C	Interaction	F (1, 188) = 1.077	P = 0.3007
	Health State	F (1, 188) = 35.77	P < 0.0001
	Passage	F (1, 188) = 7.960	P = 0.0053
Fig. 8D	Interaction	F (1, 68) = 22.58	P < 0.0001
	Health State	F (1, 68) = 36.74	P < 0.0001
	Passage	F (1, 68) = 33.83	P < 0.0001
Fig. 8E	Interaction	F (1, 68) = 0.7774	P = 0.3810
	Health State	F (1, 68) = 5.668	P = 0.0201
	Passage	F (1, 68) = 5.589	P = 0.0209
Fig. 8F	Interaction	F (1, 20) = 0.1720	P = 0.6828
	Health State	F (1, 20) = 7.955	P = 0.0106
	Passage	F (1, 20) = 1.283	P = 0.2707
Fig. 8G	Interaction	F (1, 20) = 3.999	P = 0.0593
	Health State	F (1, 20) = 0.6820	P = 0.4186
	Passage	F (1, 20) = 19.80	P = 0.0002
Fig. 9C	Interaction	F (1, 157) = 39.27	P < 0.0001
	Health State	F (1, 157) = 27.80	P < 0.0001
	Passage	F (1, 157) = 344.7	P < 0.0001
Fig. 9D	Interaction	F (1, 20) = 0.9347	P = 0.3452
	Health State	F (1, 20) = 0.4112	P = 0.5287
	Passage	F (1, 20) = 33.78	P < 0.0001
Fig. 9E	Interaction	F (1, 20) = 0.3805	P = 0.5443
	Health State	F (1, 20) = 0.01825	P = 0.8939
	Passage	F (1, 20) = 35.88	P < 0.0001
Fig. 10C	Interaction	F (1, 188) = 1.978	P = 0.1612
	Health State	F (1, 188) = 16.01	P < 0.0001
	Passage	F (1, 188) = 2.658	P = 0.1047
Fig. 10D	Interaction	F (1, 68) = 0.3780	P = 0.5407
	Health State	F (1, 68) = 2.281	P = 0.1356
	Passage	F (1, 68) = 0.2991	P = 0.5863
Fig. 10E	Interaction	F (1, 68) = 0.2002	P = 0.6560
	Health State	F (1, 68) = 9.584	P = 0.0029
	Passage	F (1, 68) = 2.289	P = 0.1350
Fig. 10F	Interaction	F (1, 20) = 0.08841	P = 0.7693
	Health State	F (1, 20) = 3.555	P = 0.0740
	Passage	F (1, 20) = 0.03834	P = 0.8467
Fig. 10G	Interaction	F (1, 20) = 0.1404	P = 0.7118

	Health State	F (1, 20) = 0.1134	P = 0.7399
	Passage	F (1, 20) = 5.502	P = 0.0294
	Interaction	F (1, 78) = 0.1122	P = 0.7385
Fig. 11	Health State	F (1, 78) = 3.942	P = 0.0506
	Passage	F (1, 78) = 1.224	P = 0.2719
	Interaction	F (1, 75) = 0.05566	P = 0.8141
Fig. 29	Health State	F (1, 75) = 4.318	P = 0.0411
	Passage	F (1, 75) = 27.00	P < 0.0001
	Interaction	F (1, 68) = 4.092	P = 0.0470
Fig. 30	Health State	F (1, 68) = 1.603	P = 0.2097
	Passage	F (1, 68) = 1.026	P = 0.3147
	Interaction	F (1, 67) = 0.1101	P = 0.7411
Fig. 35A	Health State	F (1, 67) = 2.319	P = 0.1325
	Substrate	F (1, 67) = 0.2080	P = 0.6498
	Interaction	F (1, 68) = 0.8798	P = 0.3516
Fig. 35B	Health State	F (1, 68) = 1.307	P = 0.2570
	Substrate	F (1, 68) = 10.20	P = 0.0021
	Interaction	F (1, 67) = 0.01750	P = 0.8952
Fig. 35C	Health State	F (1, 67) = 1.549	P = 0.2176
	Substrate	F (1, 67) = 0.5142	P = 0.4758
	Interaction	F (1, 66) = 0.1116	P = 0.7393
Fig. 36A	Health State	F (1, 66) = 5.347	P = 0.0235
	Substrate	F (1, 66) = 0.02713	P = 0.8697
	Interaction	F (1, 66) = 0.1047	P = 0.7473
Fig. 36B	Health State	F (1, 66) = 6.126	P = 0.0159
	Substrate	F (1, 66) = 3.884	P = 0.0529
	Interaction	F (1, 66) = 0.5566	P = 0.4583
Fig. 36C	Health State	F (1, 66) = 1.573	P = 0.2142
	Substrate	F (1, 66) = 0.03325	P = 0.8559
	Interaction	F (1, 60) = 8.298	P = 0.0055
Fig. 41A	Health State	F (1, 60) = 9.318	P = 0.0034
	Passage	F (1, 60) = 8.199	P = 0.0058
	Interaction	F (1, 58) = 0.1281	P = 0.7218
Fig. 41B	Health State	F (1, 58) = 24.26	P < 0.0001
	Passage	F (1, 58) = 0.1202	P = 0.7301
	Interaction	F (1, 70) = 1.041	P = 0.3111
Fig. 42A	Health State	F (1, 70) = 0.5125	P = 0.4764
	Passage	F (1, 70) = 45.76	P < 0.0001
	Interaction	F (1, 65) = 12.83	P = 0.0007
Fig. 42B	Health State	F (1, 65) = 5.507	P = 0.0220
	Passage	F (1, 65) = 15.02	P = 0.0002
	Interaction	F (1, 70) = 3.922	P = 0.0516
Fig. 43A	Health State	F (1, 70) = 8.807	P = 0.0041
	Passage	F (1, 70) = 2.336	P = 0.1309
	Interaction	F (1, 63) = 0.02631	P = 0.8717
Fig. 43B	Health State	F (1, 63) = 3.219	P = 0.0776
	Passage	F (1, 63) = 39.13	P < 0.0001
	Interaction	F (1, 66) = 0.02384	P = 0.8778
Fig. 43C	Health State	F (1, 66) = 0.01996	P = 0.8881
	Passage	F (1, 66) = 4.336	P = 0.0405

Supplementary Table 2: List of ANOVA analysis with corresponding figures.

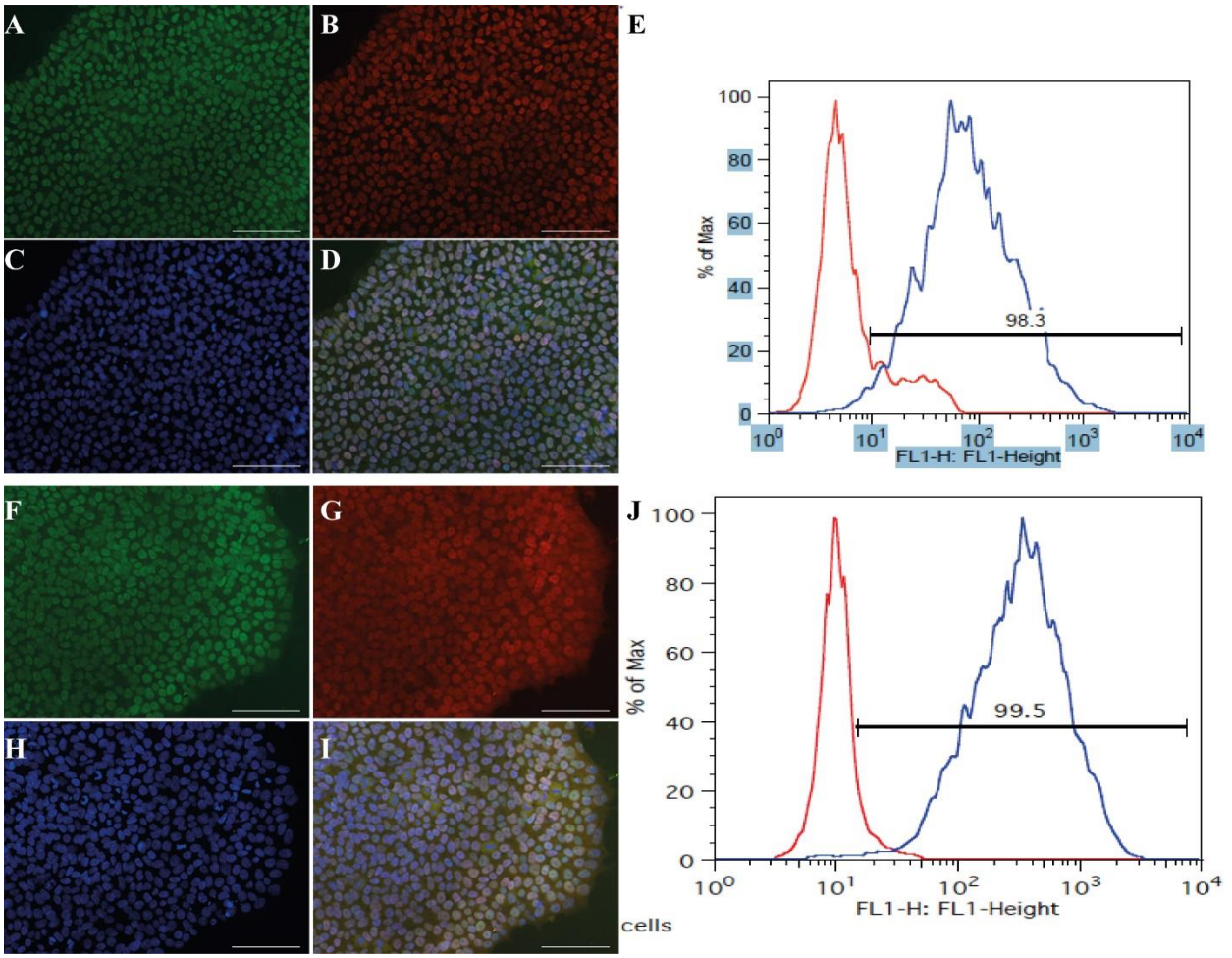

Supplementary Fig. 1: Characterization of pluripotency of freshly reprogrammed iPSCs exemplary for 2 different clones as obtained from TP1 of the ForiPS consortium. *Images 1A-E are from iPD patient UKERiM89 (A Oct4; B Nanog; C DAPI; D Merge; E Tra-1-60 fluorescence in FACS compared to reference). Fig. 1F-J are from control UKERiJF (F Oct4; G Nanog; H DAPI; I Merge; J Tra-1-60 fluorescence in FACS compared to reference). All figures were obtained from Dr. Zacharias Kohl from TP 1. Scale bar is for 200µM.*

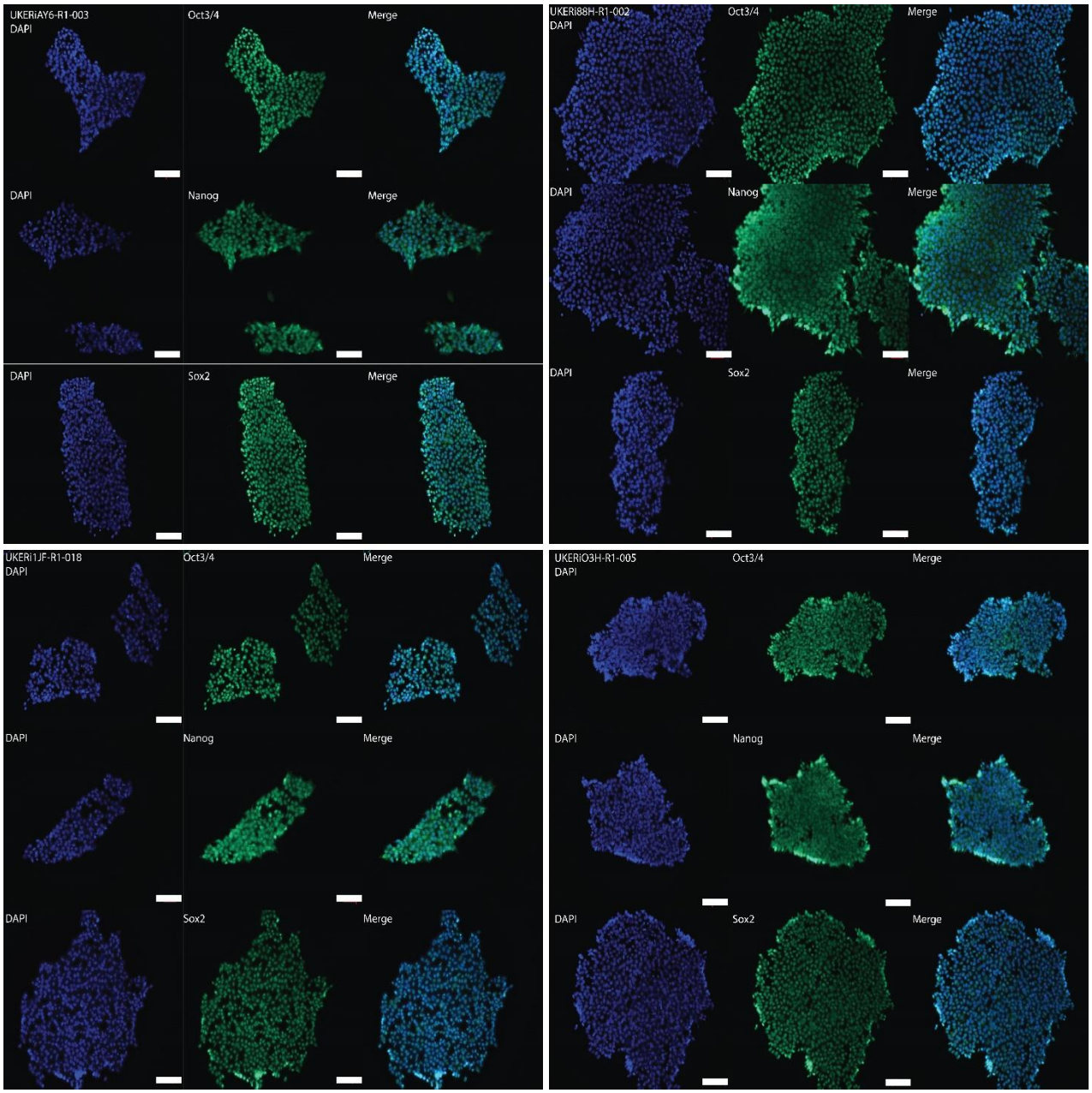

Supplementary Fig. 2: The positive staining for the three major pluripotency factors Oct3/4, Nanog and Sox2 in two iPD lines (UKERiAY6-R1-003 and UKERi88H-R1-002) and two control lines (UKERi1JF-R1-018 and UKERiO3H-R1-005) confirm that cells clearly still are pluripotent albeit the passaging. *Scale bar (white) is for 100µM.*

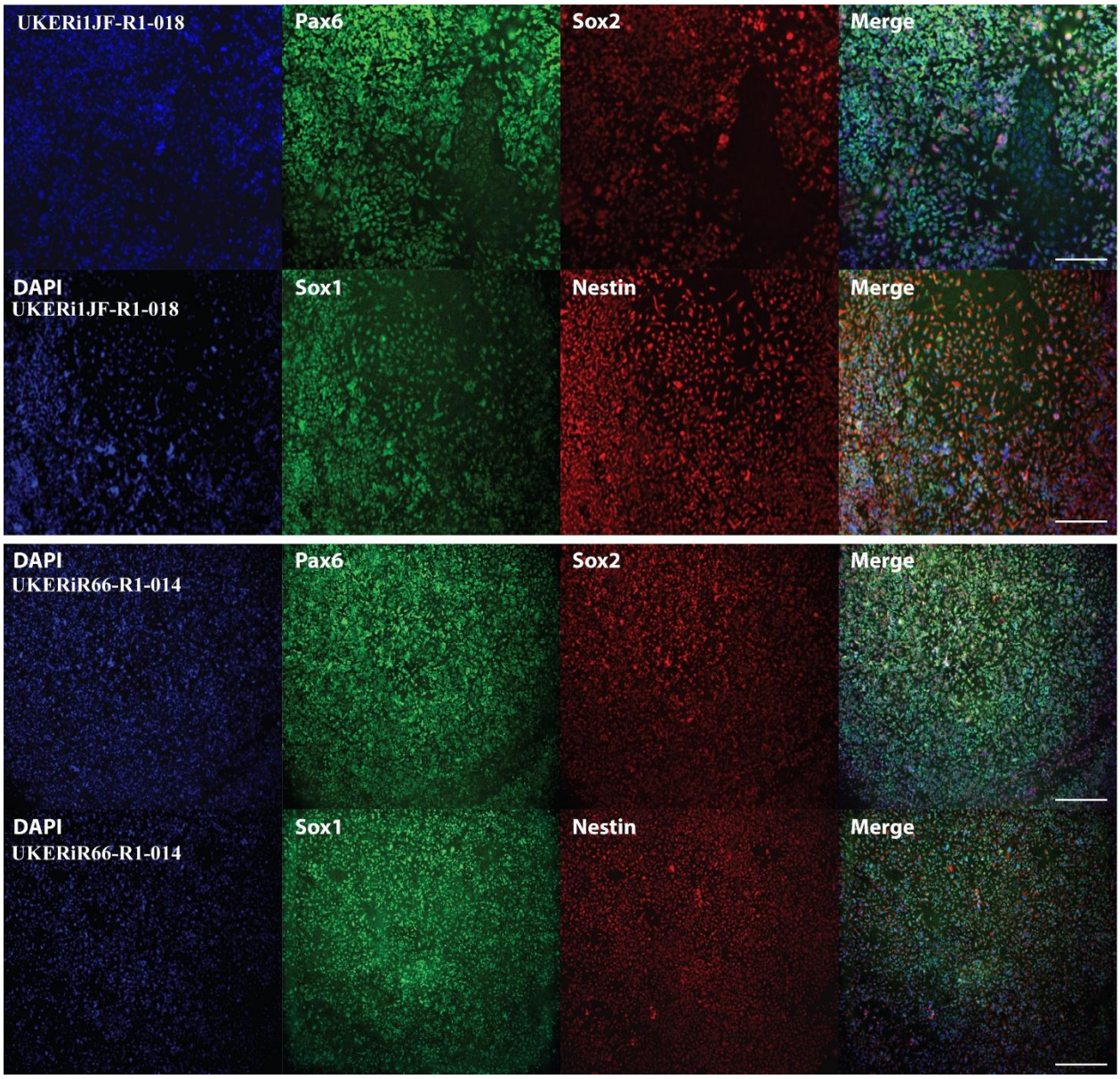

Supplementary Fig. 3: Staining of NPCs derived from low-passage iPSCs from iPD patients and control individuals. *NPCs were stained for the markers Pax6, Sox1, Sox2 and Nestin to confirm neuronal precursor identity. Scale bar is for 200µM.*

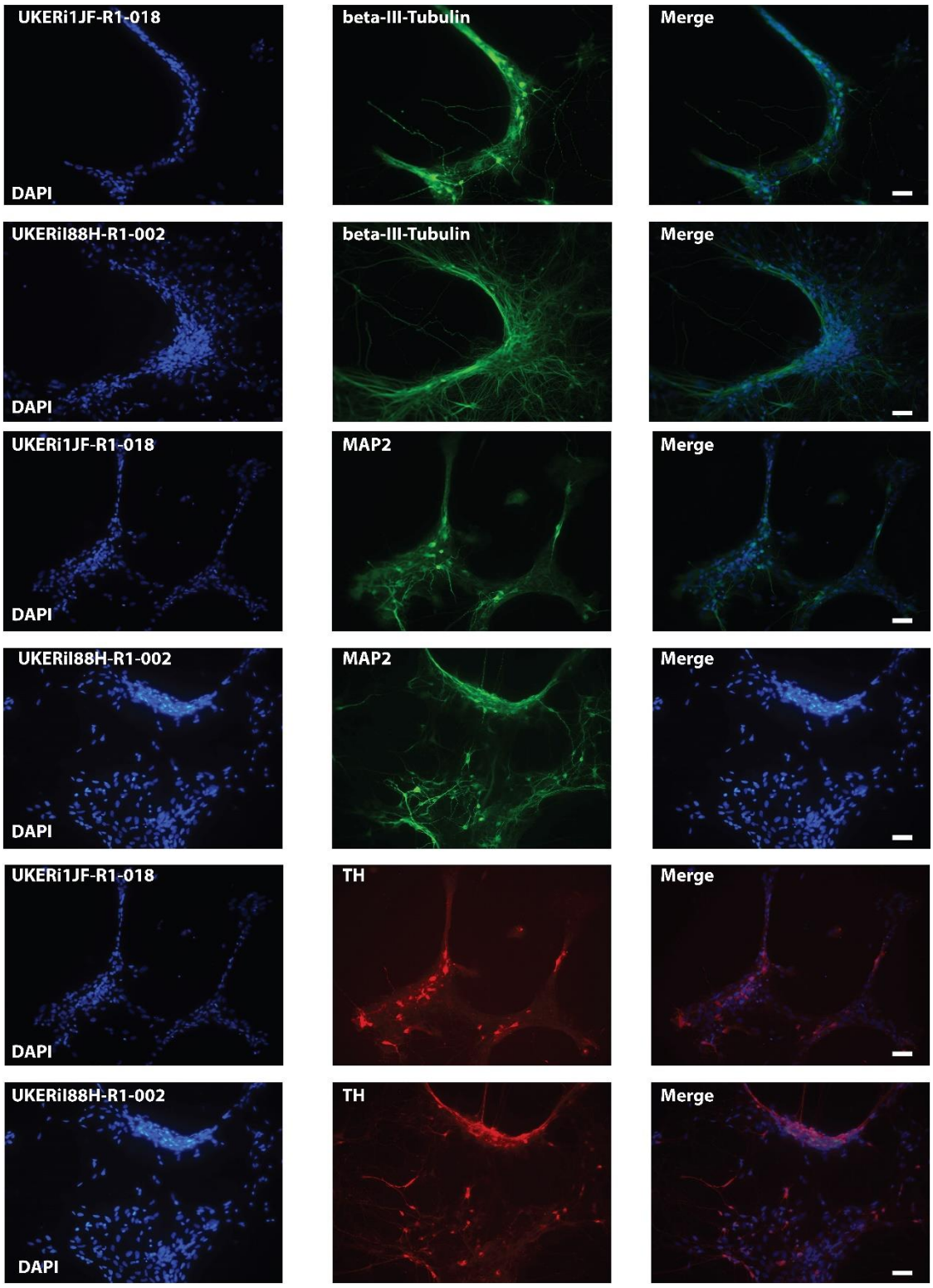

Supplementary Fig. 4: Confirmation of neuronal identity of neurons retrieved from differentiation of NPCs to mDANs. *Positive immunocytochemistry staining for beta-III-tubulin and MAP2 confirm neuronal identity, while staining for TH confirms dopaminergic identity. Approximately 40% of all neurons stained positive for TH. Scale bar is for 100µM. All graphs provided by S. Schmidt.*

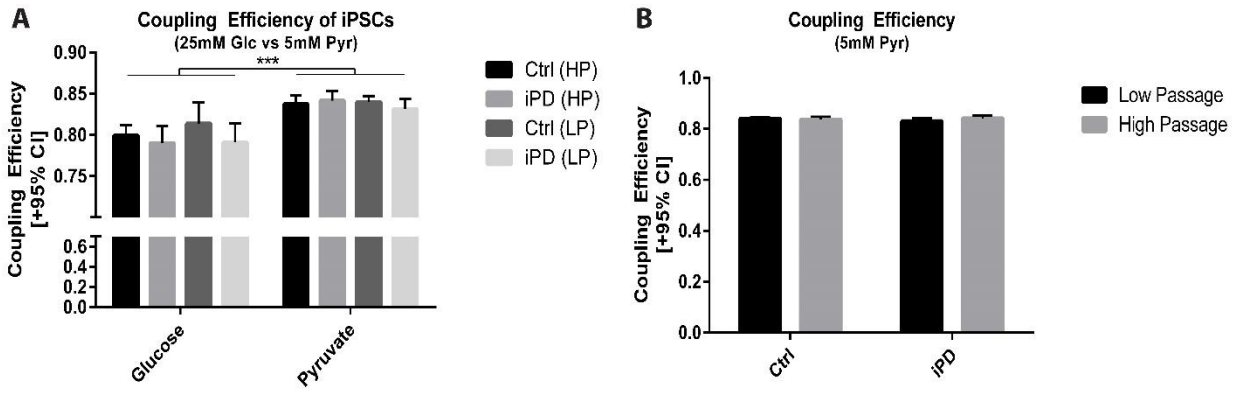

Supplementary Fig. 5: Coupling Efficiency of iPSCs with glucose and pyruvate as substrate in comparison. *(A) Displays the coupling efficiency of low- and high-passage iPSCs with glucose and pyruvate as substrate in comparison (substrate dependent effect, $p < 0.0001$), (B) depicts coupling efficiency with only pyruvate as substrate. All samples were analyzed with n = 3, statistical analysis was done with Graphpad prism 6 using two-way ANOVA and Tukey's Post-hoc testing.*

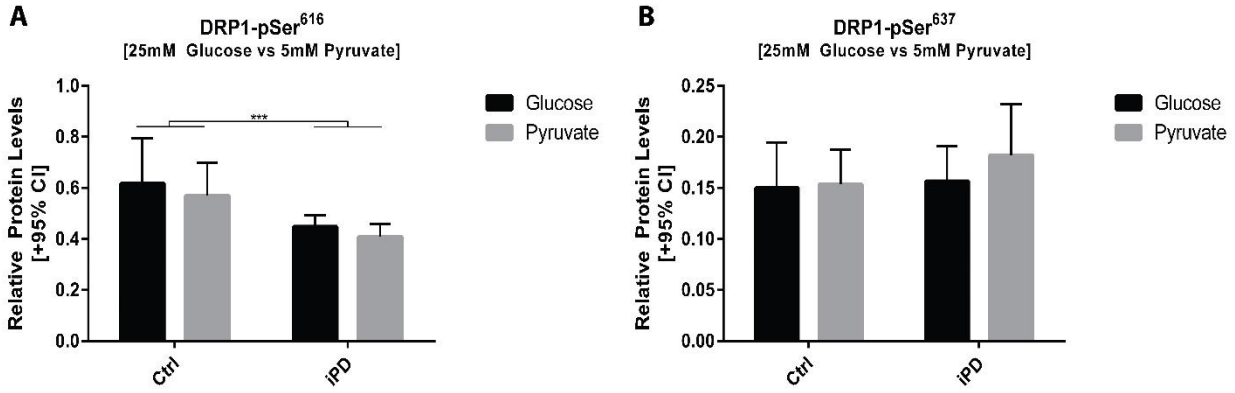

Supplementary Fig. 6: Analysis of protein level and phosphorylation state of mitochondrial fission machinery by looking at Drp1 and its phosphorylation sites. *Drp1 expression and expression of phospho-Serin^{616}-Drp1 and phospho-Serin^{637}-Drp1 was assessed by immunoblotting. (A) Depicts the expression of phospho-Serin^{616} -Drp1 normalized to Actin-beta expression ($p = 0.0008$), (B) shows the expression of phospho-Serin^{637} -Drp1 normalized to Actin-beta expression. All samples were analyzed with n = 3, statistical analysis was done with Graphpad prism 6 using two-way Anova and Tukey's Post-hoc test, a value of $p < 0.05$ is considered significant. No significant p-values of interaction or substrate dependency were observed.*

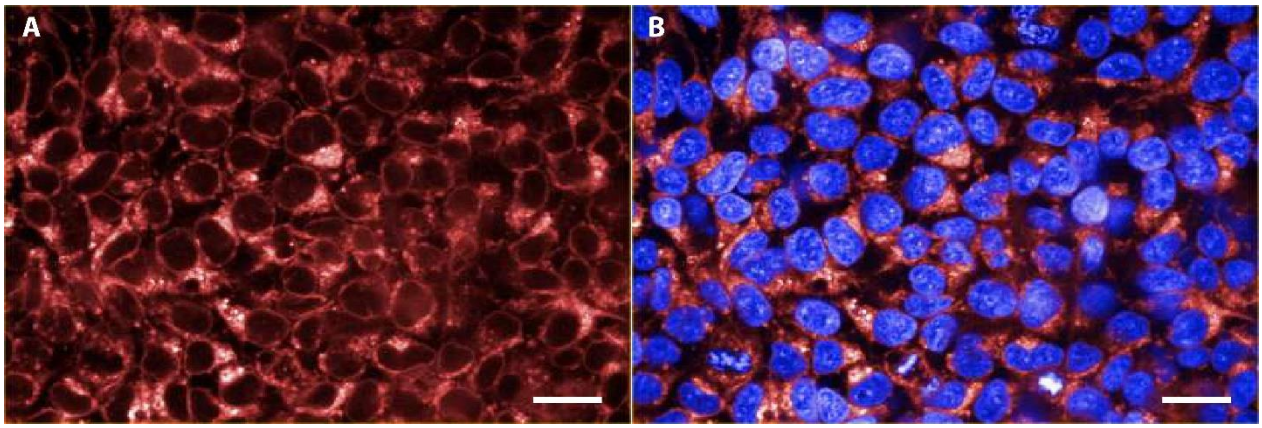

Supplementary Fig. 7: MitoTracker Red staining of mitochondria. *(A) Depicts a trial staining of mitochondria in iPSCs with MitoTracker Red, (B) merged with DAPI staining. As visible, sufficient resolution to count mitochondria and assess differences in membrane potential could not be achieved. Staining done and data provided by T. Orschmann / S. Desbordes, SCADEV platform. Scale bar is for 100µM.*

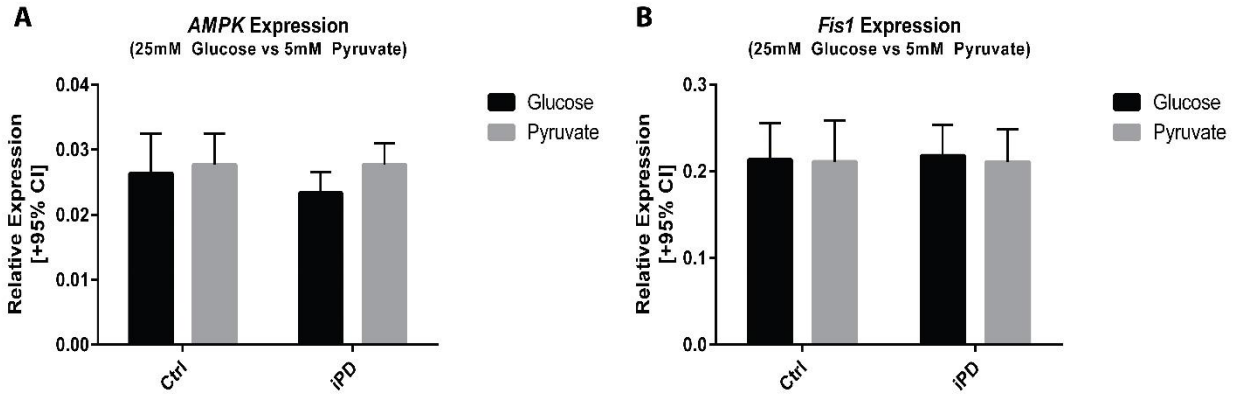

Supplementary Fig. 8: Expression of AMPK and Fis1 in high-passage iPSCs depending on substrate supplied. *(A) Depicts AMPK expression changes depending on glucose or pyruvate as substrate, (B) shows Fis1 expression depending on the two substrates. In both cases, no changes in expression could be observed in response to the corresponding substrate or the health state. All samples were analyzed with n = 3, statistical analysis was performed using Graphpad prism 6 and two-way ANOVA with Tukey's Post-hoc analyses.*

6. List of figures

7. List of tables

8. List of abbreviations

(Acetyl) CoA	(Acetyl) coenzyme-A
2-DG	2-Deoxyglucose
5-HT	Serotonin
6-OHDA	6-hydroxydopamine
AB	Antibody
AD	Alzheimer's disease
Adh2	Aldehyde dehydrogenase 2
ADP	Adenosine diphosphate
Ald1	Alkaline phosphatase
ALP	Autophagy lysosomal pathway
AMP	Adenosine monophosphate
AMPK	AMP-activated protein kinase
ASD	Autism spectrum disorder
ATP	Adenosine triphosphate
BER	Base excision repair
BSA	Bovine serum albumin
Ca^{2+}	Calcium
CAMK-Ia	Calcium/calmodulin-dependent protein kinase 1 alpha
Ccnd1	Cyclin-D1
Cdh1	Cadherin-1
CDK1/CyclinB	Cyclin dependent kinase 1
cDNA	Complementary DNA
CHIR	CHIRR99021
CI	Confidence interval
Ctrl	control
DAPI	4',6-Diamidin-2-phenylindol
DAT	Dopamine transporter
DM	Dorsomorphin
DMEM	Dulbecco's modified eagle medium
DNA	Deoxyribonucleic acid
DNMT	DNA methyltransferase
DOPAC	3,4-dihydroxyphenylacetic acid

DOPAL	3,4-dihydroxyphenyl-acetaldehyde
Drp1	Dynamin-related protein 1
EB	Embryoid body
ECAR	Extracellular acidification rate
eIF4E	Eukaryotic translation initiation factor 4E
En-1 /-2	Enrgailed-1 and Engrailed-2
ER	Endoplasmic reticulum
Erk-1/2 MAPK	Extracellular-signal-regulated kinases-1/2 mitogen activated protein kinase
Essrb	Estrogen-related receptor beta
ETC	Electron transport chain
FAD/ FADH/ $FADH_2$	Flavin adenine dinucleotide
FBOX7	F-box only protein 7
FCCP	Carbonyl-cyanide-4-(trifluoromethoxy)-phenylhydrazone
Fgf8	Fibroblast growth factor 8
Fis1	Mitochondrial fission protein 1
FoxA-1 /-2	Forkhead box protein A1 / A2
fPD	Familial Parkinson's disease
GABA	Gamma-aminobutyric acid
GAPDH	Glycerinaldehyde-3-phosphate dehydrogenase
Gba	Glucocerebrosidase
GED	GTPase effector domain
Glc	Glucose
GLUT	Glucose transporter
GPe	Globus pallidus pars externa
GPi	Globus pallidus pars interna
GSH	Glutathione
GSH/GPX	Glutathione-peroxidase system
GTP	Guanine triphosphate
GWAS	Genome-wide association studies
HAT	Histone acetyltransferase
HDAC	Histone deacetylase
hESC	Human embryonic stem cell

HIF	Hypoxia inducible factor
HMT	Histone methyltransferase
HP	High-passage
hPSCs	Human pluripotent stem cells
HR	Homologous recombination
IO	Isthmic organizer
iPD	Idiopathic Parkinson's disease
iPSC	Induced pluripotent stem cell
JNK	C-Jun-N-terminal kinase
Klf4	Kruppel-like factor 4
KSR	Knockout serum replacement
LB	Lewy body
LC3	Microtubule-associates protein 1A/1B light chain 3
Lmx1-A / -B	LIM homeobox transcription factor-1-A / -B
lncRNA	Long non coding RNA
LOF	Loss-of-function
LP	Low-passage
Lrrk2	Leucine-rich repeat kinase 2
MAO-A / -B	Monoamine oxidase –A and –B
Mapt	Microtubule-associated protein tau
MAS	Mitochondrial assay solution
mDAN	mesodiencephalic dopaminergic neurons
Mff	Mitochondrial fission factor 1
Mfn-1 / -2	Mitofusin-1 and -2
miRNA	Micro RNA
mmRNA	Modified messenger RNA
MPP^+	1-methyl-4-phenyl-pyridin
MPTP	1-methyl-4-phenyl-1,2,3,6-tretrahydropyridin
mRNA	Messenger ribonucleic acid
mtDNA	Mitochondrial DNA
NAD or NADH	Nicotinamide adenine dinucleotide
NADPH	Nicotinamide adenine dinucleotide phosphate
Ndufs1	NADH-ubiquinone oxidoreductase 75kDa subunit, mitochondrial

Ndufs3	NADH dehydrogenase [ubiquinone] iron-sulfur protein 3, mitochondrial
NF-κB	Nuclear factor kappa-light-chain-enhancer of activated B-cells
NHEJ	Non-homologous end joining
NOX	NADPH-oxidase
NPC	Neuronal precursor cell
NPM	Neuronal precursor medium
NSC	Neural stem cell
Nurr1	Nuclear receptor related protein 1
OCR	Oxygen consumption rate
Oct3/4	Octamer binding transcription factor ¾
Opa1	Optic atrophy 1
OSKM	Oct4-Sox2-Klf4-c-Myc
Otx2	Orthodenticle homeobox 2
OXPHOS	Oxidative phosphorylation
$P75^{NTR}$	Neurotrophin receptor p75
PA	Purmorphamin
PARIS	Parkin-interacting substrate
Pax6	Paired box protein Pax6
PBMC	Peripheral blood mononuclear cells
PBS	Phosphate-buffered saline
PCR	Polymerase chain reaction
PD	Parkinson's disease
PET	Positron emission tomography
PFA	Paraformaldehyde
PFKFB3	6-phosphofructose-2-kinase/fructose-2,6-bisphosphatase-3
PGC-1α	Peroxisome-proliferator-activated receptor gamma-co-activator-1-alpha
P_i	Inorganic phosphate
Pink1	PTEN-induced putative kinase-1
Pitx3	Pituitary homeobox 3
PKA	Protein kinase A
PKC	Protein kinase C delta
PL	Proton leak
POLG	DNA polymerase subunit gamma

Poli	DNA polymerase iota
PPP	Pentose phosphate pathway
PSP	Progressive supranuclear palsy
Pyr	Pyruvate
qRT-PCR	Quantitative real-time polymerase chain reaction
R5P	Ribose-5-phosphate
RFU	Relative fluorescence units
RIPA	Radioimmunoprecipitation assay buffer
RNA	Ribonucleic acid
ROCK	Rho-associated coiled-coil containing protein kinase
ROS	Reactive oxygen species
rRNA	Ribosomal RNA
RT	Room temperature
Sall4	Sal-like protein 4
SAM	S-adenosylmethionine
SB	Sleeping beauty
SB	SB431542
SEM	Standard error of mean
Shh	Sonic hedgehog
smRNA	Synthetic messenger RNA
SNARE	Soluble NSF attachment protein receptor
SNCA	Alpha-synuclein (gene)
SNEL	Sall4-Nanog-Esrrb-Lin28
SNpc	Substantia nigra pars compacta
SNpr	Substantia nigra pars reticulate
SOD2	Superoxide dismutase 2
Sox2	(sex determining region Y)-box 2
SSEA-1/-3/-4	Stage-specific embryonic antigen -1 / -3 / -4
STN	Subthalamic nucleus
TBST	Tris-buffered saline with Tween-20
TCA	Tri-carbonic cycle (Krebs cycle)
TET	Ten-eleven translocation dioxygenase
TFAM	Mitochondrial transcription factor A

Tgf-β	Transforming growth factor beta
TH	Tyrosine hydroxylase
TMPD	Tetramethylphenylendiamin
tRNA	Transfer ribonucleic acid
UCP 1-3	Uncoupling protein-1 / -2 / -3
UPS	Ubiquitin proteasome system
UTR	Untranslated region
VL	Ventrolateral
Vsp35	Vacuolar protein-sorting associated protein 35
VTA	Ventral tegmental area
WB	Western Blot
α-Syn	Alpha-synuclein (protein)
β-ME	Beta-mercaptoethanol

9. Bibliography

Ahmed, S.S., Santosh, W., Kumar, S., and Christlet, H.T.T. (2009). Metabolic profiling of Parkinson's disease: evidence of biomarker from gene expression analysis and rapid neural network detection. J. Biomed. Sci. *16*, 63.

Alavian, K.N., Sgadò, P., Alberi, L., Subramaniam, S., and Simon, H.H. (2009). Elevated P75NTR expression causes death of engrailed-deficient midbrain dopaminergic neurons by Erk1/2 suppression. Neural Develop. *4*, 11.

Alavian, K.N., Jeddi, S., Naghipour, S.I., Nabili, P., Licznerski, P., and Tierney, T.S. (2014). The lifelong maintenance of mesencephalic dopaminergic neurons by Nurr1 and engrailed. J. Biomed. Sci. *21*, 27.

Alexeyev, M., Shokolenko, I., Wilson, G., and LeDoux, S. (2013). The Maintenance of Mitochondrial DNA Integrity—Critical Analysis and Update. Cold Spring Harb. Perspect. Biol. *5*.

Alkhuja, S. (2013). Parkinson disease: research update and clinical management. South. Med. J. *106*, 334.

Al-Mehdi, A.-B., Pastukh, V.M., Swiger, B.M., Reed, D.J., Patel, M.R., Bardwell, G.C., Pastukh, V.V., Alexeyev, M.F., and Gillespie, M.N. (2012). Perinuclear Mitochondrial Clustering Creates an Oxidant-Rich Nuclear Domain Required for Hypoxia-Induced Transcription. Sci. Signal. *5*, ra47.

Alvarez-Fischer, D., Fuchs, J., Castagner, F., Stettler, O., Massiani-Beaudoin, O., Moya, K.L., Bouillot, C., Oertel, W.H., Lombès, A., Faigle, W., et al. (2011). Engrailed protects mouse midbrain dopaminergic neurons against mitochondrial complex I insults. Nat. Neurosci. *14*, 1260–1266.

Ambrosi, G., Ghezzi, C., Sepe, S., Milanese, C., Payan-Gomez, C., Bombardieri, C.R., Armentero, M.-T., Zangaglia, R., Pacchetti, C., Mastroberardino, P.G., et al. (2014). Bioenergetic and proteolytic defects in fibroblasts from patients with sporadic Parkinson's disease. Biochim. Biophys. Acta BBA - Mol. Basis Dis. *1842*, 1385–1394.

Anandhan, A., Jacome, M.S., Lei, S., Hernandez-Franco, P., Pappa, A., Panayiotidis, M.I., Powers, R., and Franco, R. (2017). Metabolic Dysfunction in Parkinson's Disease: Bioenergetics, Redox Homeostasis and Central Carbon Metabolism. Brain Res. Bull. *133*, 12–30.

Anderson, M.F., and Sims, N.R. (2000). Improved recovery of highly enriched mitochondrial fractions from small brain tissue samples. Brain Res. Brain Res. Protoc. *5*, 95–101.

Arenas, E., Denham, M., and Villaescusa, J.C. (2015). How to make a midbrain dopaminergic neuron. Dev. Camb. Engl. *142*, 1918–1936.

Baldereschi, M., Di Carlo, A., Rocca, W.A., Vanni, P., Maggi, S., Perissinotto, E., Grigoletto, F., Amaducci, L., and Inzitari, D. (2000). Parkinson's disease and parkinsonism in a longitudinal study: two-fold higher incidence in men. ILSA Working Group. Italian Longitudinal Study on Aging. Neurology *55*, 1358–1363.

Barroso, N., Campos, Y., Huertas, R., Esteban, J., Molina, J.A., Alonso, A., Gutierrez-Rivas, E., and Arenas, J. (1993). Respiratory chain enzyme activities in lymphocytes from untreated patients with Parkinson disease. Clin. Chem. *39*, 667–669.

Beckervordersandforth, R. (2017). Mitochondrial Metabolism-Mediated Regulation of Adult Neurogenesis. Brain Plast. *3*, 73–87.

Bellizzi, D., D'Aquila, P., Scafone, T., Giordano, M., Riso, V., Riccio, A., and Passarino, G. (2013). The Control Region of Mitochondrial DNA Shows an Unusual CpG and Non-CpG Methylation Pattern. DNA Res. Int. J. Rapid Publ. Rep. Genes Genomes *20*, 537–547.

Benayed, R., Choi, J., Matteson, P.G., Gharani, N., Kamdar, S., Brzustowicz, L.M., and Millonig, J.H. (2009). Autism Associated Haplotype Affects the Regulation of the Homeobox Gene, ENGRAILED 2. Biol. Psychiatry *66*, 911–917.

Benz, R., and McLaughlin, S. (1983). The molecular mechanism of action of the proton ionophore FCCP (carbonylcyanide p-trifluoromethoxyphenylhydrazone). Biophys. J. *41*, 381–398.

Berg, J.M., Tymoczko, J.L., and Stryer, L. (2012). Biochemistry (Basingstoke: W.H. Freeman).

Betarbet, R., Sherer, T.B., MacKenzie, G., Garcia-Osuna, M., Panov, A.V., and Greenamyre, J.T. (2000). Chronic systemic pesticide exposure reproduces features of Parkinson's disease. Nat. Neurosci. *3*, 1301–1306.

Birch-Machin, M. a., and Bowman, A. (2016). Oxidative stress and ageing. Br. J. Dermatol. *175*, 26–29.

Birket, M.J., Orr, A.L., Gerencser, A.A., Madden, D.T., Vitelli, C., Swistowski, A., Brand, M.D., and Zeng, X. (2011). A reduction in ATP demand and mitochondrial activity with neural differentiation of human embryonic stem cells. J. Cell Sci. *124*, 348–358.

Biswas, D., and Jiang, P. (2016). Chemically Induced Reprogramming of Somatic Cells to Pluripotent Stem Cells and Neural Cells. Int. J. Mol. Sci. *17*.

van der Bliek, A.M., Shen, Q., and Kawajiri, S. (2013). Mechanisms of Mitochondrial Fission and Fusion. Cold Spring Harb. Perspect. Biol. *5*, a011072–a011072.

Bonifati, V., Rizzu, P., van Baren, M.J., Schaap, O., Breedveld, G.J., Krieger, E., Dekker, M.C.J., Squitieri, F., Ibanez, P., Joosse, M., et al. (2003). Mutations in the DJ-1 gene associated with autosomal recessive early-onset parkinsonism. Science *299*, 256–259.

Borghammer, P. (2012). Perfusion and metabolism imaging studies in Parkinson's disease. Dan. Med. J. *59*, B4466.

Bostan, A.C., and Strick, P.L. (2010). The Cerebellum and Basal Ganglia are Interconnected. Neuropsychol. Rev. *20*, 261–270.

Braak, H., Del Tredici, K., Rüb, U., de Vos, R.A.I., Jansen Steur, E.N.H., and Braak, E. (2003). Staging of brain pathology related to sporadic Parkinson's disease. Neurobiol. Aging *24*, 197–211.

Brand, M.D., Orr, A.L., Perevoshchikova, I.V., and Quinlan, C.L. (2013). The role of mitochondrial function and cellular bioenergetics in ageing and disease. Br. J. Dermatol. *169*, 1–8.

Brielmaier, J., Senerth, J.M., Silverman, J.L., Matteson, P.G., Millonig, J.H., DiCicco-Bloom, E., and Crawley, J.N. (2014). Chronic Desipramine Treatment Rescues Depression-Related, Social and Cognitive Deficits in Engrailed-2 Knockout Mice. Genes Brain Behav. *13*, 286–298.

Brighina, L., Riva, C., Bertola, F., Fermi, S., Saracchi, E., Piolti, R., Goldwurm, S., Pezzoli, G., and Ferrarese, C. (2011). Association analysis of PARP1 polymorphisms with Parkinson's disease. Parkinsonism Relat. Disord. *17*, 701–704.

Brooks, A.I., Chadwick, C.A., Gelbard, H.A., Cory-Slechta, D.A., and Federoff, H.J. (1999). Paraquat elicited neurobehavioral syndrome caused by dopaminergic neuron loss. Brain Res. *823*, 1–10.

Brunet, I., Weinl, C., Piper, M., Trembleau, A., Volovitch, M., Harris, W., Prochiantz, A., and Holt, C. (2005). The transcription factor Engrailed-2 guides retinal axons. Nature *438*, 94–98.

Brunk, U.T., and Terman, A. (2002). The mitochondrial-lysosomal axis theory of aging: accumulation of damaged mitochondria as a result of imperfect autophagocytosis. Eur. J. Biochem. *269*, 1996–2002.

Buganim, Y., Markoulaki, S., van Wietmarschen, N., Hoke, H., Wu, T., Ganz, K., Akhtar-Zaidi, B., He, Y., Abraham, B.J., Porubsky, D., et al. (2014). The Developmental Potential of iPSCs Is Greatly Influenced by Reprogramming Factor Selection. Cell Stem Cell *15*, 295–309.

Cairns, R.A., Harris, I.S., and Mak, T.W. (2011). Regulation of cancer cell metabolism. Nat. Rev. Cancer *11*, 85–95.

Cardoso, S.M., Moreira, P.I., Agostinho, P., Pereira, C., and Oliveira, C.R. (2005). Neurodegenerative pathways in Parkinson's disease: therapeutic strategies. Curr. Drug Targets CNS Neurol. Disord. *4*, 405–419.

Carey, B.W., Markoulaki, S., Hanna, J.H., Faddah, D.A., Buganim, Y., Kim, J., Ganz, K., Steine, E.J., Cassady, J.P., Creyghton, M.P., et al. (2011). Reprogramming Factor Stoichiometry Influences the Epigenetic State and Biological Properties of Induced Pluripotent Stem Cells. Cell Stem Cell *9*, 588–598.

Castillo-Quan, J.I. (2011). Parkin' control: regulation of PGC-1α through PARIS in Parkinson's disease. Dis. Model. Mech. *4*, 427–429.

Cereghetti, G.M., Stangherlin, A., De Brito, O.M., Chang, C.R., Blackstone, C., Bernardi, P., and Scorrano, L. (2008). Dephosphorylation by calcineurin regulates translocation of Drp1 to mitochondria. Proc. Natl. Acad. Sci. *105*, 15803–15808.

Chandel, N.S. (2014). Mitochondria as signaling organelles. BMC Biol. *12*, 34.

Chang, C.-R., and Blackstone, C. (2010). Dynamic regulation of mitochondrial fission through modification of the dynamin-related protein Drp1. Ann. N. Y. Acad. Sci. *1201*, 34–39.

Chartier-Harlin, M.-C., Kachergus, J., Roumier, C., Mouroux, V., Douay, X., Lincoln, S., Levecque, C., Larvor, L., Andrieux, J., Hulihan, M., et al. (2004). Alpha-synuclein locus duplication as a cause of familial Parkinson's disease. Lancet Lond. Engl. *364*, 1167–1169.

Chaudhuri, A.D., Kabaria, S., Choi, D.C., Mouradian, M.M., and Junn, E. (2015). MicroRNA-7 Promotes Glycolysis to Protect against 1-Methyl-4-phenylpyridinium-induced Cell Death. J. Biol. Chem. *290*, 12425–12434.

Chen, H., Detmer, S.A., Ewald, A.J., Griffin, E.E., Fraser, S.E., and Chan, D.C. (2003). Mitofusins Mfn1 and Mfn2 coordinately regulate mitochondrial fusion and are essential for embryonic development. J. Cell Biol. *160*, 189–200.

Chen, H.-F., Kuo, H.-C., Lin, S.-P., Chien, C.-L., Chiang, M.-S., and Ho, H.-N. (2010). Hypoxic Culture Maintains Self-Renewal and Enhances Embryoid Body Formation of Human Embryonic Stem Cells. Tissue Eng. Part A *16*, 2901–2913.

Cheong, H., Lu, C., Lindsten, T., and Thompson, C.B. (2012). Therapeutic targets in cancer cell metabolism and autophagy. Nat. Biotechnol. *30*, 671–678.

Chillag-Talmor, O., Giladi, N., Linn, S., Gurevich, T., El-Ad, B., Silverman, B., Friedman, N., and Peretz, C. (2011). Use of a refined drug tracer algorithm to estimate prevalence and incidence of Parkinson's disease in a large israeli population. J. Park. Dis. *1*, 35–47.

Chinnery, P.F., and Hudson, G. (2013). Mitochondrial genetics. Br. Med. Bull. *106*, 135–159.

Cho, Y.M., Kwon, S., Pak, Y.K., Seol, H.W., Choi, Y.M., Park, D.J., Park, K.S., and Lee, H.K. (2006). Dynamic changes in mitochondrial biogenesis and antioxidant enzymes during the spontaneous differentiation of human embryonic stem cells. Biochem. Biophys. Res. Commun. *348*, 1472–1478.

Choi, H.W., Kim, J.H., Chung, M.K., Hong, Y.J., Jang, H.S., Seo, B.J., Jung, T.H., Kim, J.S., Chung, H.M., Byun, S.J., et al. (2015). Mitochondrial and metabolic remodeling during reprogramming and differentiation of the reprogrammed cells. Stem Cells Dev. *24*, 1366–1373.

Choi, Y.-S., Hoon Jeong, J., Min, H.-K., Jung, H.-J., Hwang, D., Lee, S.-W., and Kim Pak, Y. (2011). Shot-gun proteomic analysis of mitochondrial D-loop DNA binding proteins: identification of mitochondrial histones. Mol. Biosyst. *7*, 1523–1536.

Clarke, D.D., and Sokoloff, L. (1999). Substrates of Cerebral Metabolism.

Cobb, C.A., and Cole, M.P. (2015). Oxidative and nitrative stress in neurodegeneration. Neurobiol. Dis. *84*, 4–21.

Covello, K.L., Kehler, J., Yu, H., Gordan, J.D., Arsham, A.M., Hu, C.-J., Labosky, P.A., Simon, M.C., and Keith, B. (2006). HIF-2α regulates Oct-4: effects of hypoxiaon stem cell function, embryonic development, and tumor growth. Genes Dev. *20*, 557–570.

Dannenmann, B., Lehle, S., Hildebrand, D.G., Kübler, A., Grondona, P., Schmid, V., Holzer, K., Fröschl, M., Essmann, F., Rothfuss, O., et al. (2015). High Glutathione and Glutathione Peroxidase-2 Levels Mediate Cell-Type-Specific DNA Damage Protection in Human Induced Pluripotent Stem Cells. Stem Cell Rep. *4*, 886–898.

De Rosa, A., Criscuolo, C., Mancini, P., De Martino, M., Giordano, I.A., Pappatà, S., Filla, A., and De Michele, G. (2009). Genetic screening for LRRK2 gene G2019S mutation in Parkinson's disease patients from Southern Italy. Parkinsonism Relat. Disord. *15*, 242–244.

Dias, V., Junn, E., and Mouradian, M.M. (2013). The Role of Oxidative Stress in Parkinson's Disease. J. Park. Dis. *3*, 461–491.

Dickson, D.W. (2012). Parkinson's Disease and Parkinsonism: Neuropathology. Cold Spring Harb. Perspect. Med. *2*, a009258–a009258.

Dickson, D.W., Rademakers, R., and Hutton, M.L. (2007). Progressive supranuclear palsy: pathology and genetics. Brain Pathol. Zurich Switz. *17*, 74–82.

Dickson, D.W., Braak, H., Duda, J.E., Duyckaerts, C., Gasser, T., Halliday, G.M., Hardy, J., Leverenz, J.B., Del Tredici, K., Wszolek, Z.K., et al. (2009). Neuropathological assessment of Parkinson's disease: refining the diagnostic criteria. Lancet Neurol. *8*, 1150–1157.

Diebold, L., and Chandel, N.S. (2016). Mitochondrial ROS regulation of proliferating cells. Free Radic. Biol. Med. *100*, 86–93.

Dikiy, I., and Eliezer, D. (2012). Folding and misfolding of alpha-synuclein on membranes. Biochim. Biophys. Acta *1818*, 1013–1018.

Divakaruni, A.S., and Brand, M.D. (2011). The Regulation and Physiology of Mitochondrial Proton Leak. Physiology *26*, 192–205.

Divakaruni, A.S., Paradyse, A., Ferrick, D.A., Murphy, A.N., and Jastroch, M. (2014). Analysis and Interpretation of Microplate-Based Oxygen Consumption and pH Data. In Methods in Enzymology, (Elsevier), pp. 309–354.

Donohoe, D.R., and Bultman, S.J. (2012). Metaboloepigenetics: Interrelationships between energy metabolism and epigenetic control of gene expression. J. Cell. Physiol. *227*, 3169–3177.

Dorsey, E.R., Constantinescu, R., Thompson, J.P., Biglan, K.M., Holloway, R.G., Kieburtz, K., Marshall, F.J., Ravina, B.M., Schifitto, G., Siderowf, A., et al. (2007). Projected number of people with Parkinson disease in the most populous nations, 2005 through 2030. Neurology *68*, 384–386.

Doucet-Beaupré, H., Gilbert, C., Profes, M.S., Chabrat, A., Pacelli, C., Giguère, N., Rioux, V., Charest, J., Deng, Q., Laguna, A., et al. (2016). Lmx1a and Lmx1b regulate mitochondrial functions and survival of adult midbrain dopaminergic neurons. Proc. Natl. Acad. Sci. *113*, E4387–E4396.

Dunn, L., Allen, G.F., Mamais, A., Ling, H., Li, A., Duberley, K.E., Hargreaves, I.P., Pope, S., Holton, J.L., Lees, A., et al. (2014a). Dysregulation of glucose metabolism is an early event in sporadic Parkinson's disease. Neurobiol. Aging *35*, 1111–1115.

Dunn, L., Fairfield, V., Daham, S., Bolaños, J., and Heales, S. (2014b). Pentose-phosphate pathway disruption in the pathogenesis of Parkinson's disease. Transl. Neurosci. *5*, 179–184.

Ekstrand, M.I., Terzioglu, M., Galter, D., Zhu, S., Hofstetter, C., Lindqvist, E., Thams, S., Bergstrand, A., Hansson, F.S., Trifunovic, A., et al. (2007). Progressive parkinsonism in mice with respiratory-chain-deficient dopamine neurons. Proc. Natl. Acad. Sci. U. S. A. *104*, 1325–1330.

Elobeid, A., Libard, S., Leino, M., Popova, S.N., and Alafuzoff, I. (2016). Altered Proteins in the Aging Brain. J. Neuropathol. Exp. Neurol. *75*, 316–325.

Erikson, G.A., Bodian, D.L., Rueda, M., Molparia, B., Scott, E.R., Scott-Van Zeeland, A.A., Topol, S.E., Wineinger, N.E., Niederhuber, J.E., Topol, E.J., et al. (2016). Whole Genome Sequencing of a Healthy Aging Cohort. Cell *165*, 1002–1011.

Esteban, M.A., and Pei, D. (2012). Vitamin C improves the quality of somatic cell reprogramming. Nat. Genet. *44*, 366–367.

Exner, N., Lutz, A.K., Haass, C., and Winklhofer, K.F. (2012). Mitochondrial dysfunction in Parkinson's disease: molecular mechanisms and pathophysiological consequences. EMBO J. *31*, 3038–3062.

Farrer, M.J. (2006). Genetics of Parkinson disease: paradigm shifts and future prospects. Nat. Rev. Genet. *7*, 306–318.

Folmes, C.D., Nelson, T.J., and Terzic, A. (2011). Energy metabolism in nuclear reprogramming. Biomark. Med. *5*, 715–729.

Folmes, C.D.L., Dzeja, P.P., Nelson, T.J., and Terzic, A. (2012). Metabolic Plasticity in Stem Cell Homeostasis and Differentiation. Cell Stem Cell *11*, 596–606.

Forristal, C.E., Wright, K.L., Hanley, N.A., Oreffo, R.O.C., and Houghton, F.D. (2010). Hypoxia inducible factors regulate pluripotency and proliferation in human embryonic stem cells cultured at reduced oxygen tensions. Reprod. Camb. Engl. *139*, 85–97.

Forristal, C.E., Christensen, D.R., Chinnery, F.E., Petruzzelli, R., Parry, K.L., Sanchez-Elsner, T., and Houghton, F.D. (2013). Environmental Oxygen Tension Regulates the Energy Metabolism and Self-Renewal of Human Embryonic Stem Cells. PLOS ONE *8*, e62507.

Fuchs, J., Mueller, J.C., Lichtner, P., Schulte, C., Munz, M., Berg, D., Wüllner, U., Illig, T., Sharma, M., and Gasser, T. (2009). The transcription factor PITX3 is associated with sporadic Parkinson's disease. Neurobiol. Aging *30*, 731–738.

Fuchs, J., Stettler, O., Alvarez-Fischer, D., Prochiantz, A., Moya, K.L., and Joshi, R.L. (2012). Engrailed signaling in axon guidance and neuron survival: Engrailed signaling mechanisms. Eur. J. Neurosci. *35*, 1837–1845.

Fusaki, N., Ban, H., Nishiyama, A., Saeki, K., and Hasegawa, M. (2009). Efficient induction of transgene-free human pluripotent stem cells using a vector based on Sendai virus, an RNA virus that does not integrate into the host genome. Proc. Jpn. Acad. Ser. B Phys. Biol. Sci. *85*, 348–362.

Ganguly, G., Chakrabarti, S., Chatterjee, U., and Saso, L. (2017). Proteinopathy, oxidative stress and mitochondrial dysfunction: cross talk in Alzheimer's disease and Parkinson's disease. Drug Des. Devel. Ther. *11*, 797–810.

Gao, H.-M., and Hong, J. (2011). Gene–environment interactions: key to unraveling the mystery of Parkinson's disease. Prog. Neurobiol. *94*, 1–19.

Gasser, T., Hardy, J., and Mizuno, Y. (2011). Milestones in PD genetics. Mov. Disord. *26*, 1042–1048.

Gautier, C.A., Kitada, T., and Shen, J. (2008). Loss of PINK1 causes mitochondrial functional defects and increased sensitivity to oxidative stress. Proc. Natl. Acad. Sci. U. S. A. *105*, 11364–11369.

Genestine, M., Lin, L., Durens, M., Yan, Y., Jiang, Y., Prem, S., Bailoor, K., Kelly, B., Sonsalla, P.K., Matteson, P.G., et al. (2015). Engrailed-2 (En2) deletion produces multiple neurodevelopmental defects in monoamine systems, forebrain structures and neurogenesis and behavior. Hum. Mol. Genet. *24*, 5805–5827.

Gispert, S., Ricciardi, F., Kurz, A., Azizov, M., Hoepken, H.-H., Becker, D., Voos, W., Leuner, K., Müller, W.E., Kudin, A.P., et al. (2009). Parkinson Phenotype in Aged PINK1-Deficient Mice Is Accompanied by Progressive Mitochondrial Dysfunction in Absence of Neurodegeneration. PLOS ONE *4*, e5777.

Goetz, C.G. (2011). The History of Parkinson's Disease: Early Clinical Descriptions and Neurological Therapies. Cold Spring Harb. Perspect. Med. *1*.

González, F., and Huangfu, D. (2016). Mechanisms underlying the formation of induced pluripotent stem cells. Wiley Interdiscip. Rev. Dev. Biol. *5*, 39–65.

Gordan, J.D., Thompson, C.B., and Simon, M.C. (2007). HIF and c-Myc: sibling rivals for control of cancer cell metabolism and proliferation. Cancer Cell *12*, 108–113.

Gordon, P.H., Mehal, J.M., Holman, R.C., Rowland, A.S., and Cheek, J.E. (2012). Parkinson's disease among American Indians and Alaska natives: a nationwide prevalence study. Mov. Disord. Off. J. Mov. Disord. Soc. *27*, 1456–1459.

Hämäläinen, R.H., Ahlqvist, K.J., Ellonen, P., Lepistö, M., Logan, A., Otonkoski, T., Murphy, M.P., and Suomalainen, A. (2015). mtDNA Mutagenesis Disrupts Pluripotent Stem Cell Function by Altering Redox Signaling. Cell Rep. *11*, 1614–1624.

Hamanaka, R.B., and Chandel, N.S. (2012). Targeting glucose metabolism for cancer therapy. J. Exp. Med. *209*, 211–215.

Hanks, M., Wurst, W., Anson-Cartwright, L., Auerbach, A.B., and Joyner, A.L. (1995). Rescue of the En-1 Mutant Phenotype by Replacement of En-1 with En-2. Sci. Rep. 679–682.

Hanks, M.C., Loomis, C.A., Harris, E., Tong, C.X., Anson-Cartwright, L., Auerbach, A., and Joyner, A. (1998). Drosophila engrailed can substitute for mouse Engrailed1 function in mid-hindbrain, but not limb development. Dev. Camb. Engl. *125*, 4521–4530.

Harvey, A.J., Rathjen, J., Yu, L.J., and Gardner, D.K. (2016a). Oxygen modulates human embryonic stem cell metabolism in the absence of changes in self-renewal. Reprod. Fertil. Dev. *28*, 446–458.

Harvey, A.J., Rathjen, J., and Gardner, D.K. (2016b). Metaboloepigenetic Regulation of Pluripotent Stem Cells. Stem Cells Int. *2016*.

Hastings, T.G. (2009). The role of dopamine oxidation in mitochondrial dysfunction: implications for Parkinson's disease. J. Bioenerg. Biomembr. *41*, 469–472.

Haubenberger, D., Reinthaler, E., Mueller, J.C., Pirker, W., Katzenschlager, R., Froehlich, R., Bruecke, T., Daniel, G., Auff, E., and Zimprich, A. (2011). Association of transcription factor polymorphisms PITX3 and EN1 with Parkinson's disease. Neurobiol. Aging *32*, 302–307.

Hawkes, C.H. (2008). The prodromal phase of sporadic Parkinson's disease: does it exist and if so how long is it? Mov. Disord. Off. J. Mov. Disord. Soc. *23*, 1799–1807.

Henchcliffe, C., and Beal, M.F. (2008). Mitochondrial biology and oxidative stress in Parkinson disease pathogenesis. Nat. Rev. Neurol. *4*, 600–609.

Herken, H. (1990). Neurotoxin-induced impairment of biopterin synthesis and function: Initial stage of a Parkinson-like dopamine deficiency syndrome. Neurochem. Int. *17*, 223–238.

Hoekstra, E.J., Oerthel, L. von, Heide, L.P. van der, Kouwenhoven, W.M., Veenvliet, J.V., Wever, I., Jin, Y.-R., Yoon, J.K., Linden, A.J.A. van der, Holstege, F.C.P., et al. (2013). Lmx1a Encodes a Rostral Set of Mesodiencephalic Dopaminergic Neurons Marked by the Wnt/B-Catenin Signaling Activator R-spondin 2. PLOS ONE *8*, e74049.

Hoitzing, H., Johnston, I.G., and Jones, N.S. (2015). What is the function of mitochondrial networks? A theoretical assessment of hypotheses and proposal for future research. Bioessays *37*, 687–700.

Hollander, E., Anagnostou, E., Chaplin, W., Esposito, K., Haznedar, M.M., Licalzi, E., Wasserman, S., Soorya, L., and Buchsbaum, M. (2005). Striatal volume on magnetic resonance imaging and repetitive behaviors in autism. Biol. Psychiatry *58*, 226–232.

Hou, P., Li, Y., Zhang, X., Liu, C., Guan, J., Li, H., Zhao, T., Ye, J., Yang, W., Liu, K., et al. (2013). Pluripotent Stem Cells Induced from Mouse Somatic Cells by Small-Molecule Compounds. Science *341*, 651–654.

Iglesias, J., Morales, L., and Barreto, G.E. (2017). Metabolic and Inflammatory Adaptation of Reactive Astrocytes: Role of PPARs. Mol. Neurobiol. *54*, 2518–2538.

Jacobs, F.M.J., Smits, S.M., Noorlander, C.W., von Oerthel, L., Linden, V.D., A, A.J., Burbach, J.P.H., and Smidt, M.P. (2007). Retinoic acid counteracts developmental defects in the substantia nigra caused by Pitx3 deficiency. DEVELOPMENT *134*, 2673–2684.

Jain, S. (2011). Multi-organ autonomic dysfunction in Parkinson disease. Parkinsonism Relat. Disord. *17*, 77–83.

James, S.J., Shpyleva, S., Melnyk, S., Pavliv, O., and Pogribny, I.P. (2013). Complex epigenetic regulation of Engrailed-2 (EN-2) homeobox gene in the autism cerebellum. Transl. Psychiatry *3*, e232.

James, S.J., Shpyleva, S., Melnyk, S., Pavliv, O., and Pogribny, I.P. (2014). Elevated 5-hydroxymethylcytosine in the Engrailed-2 (EN-2) promoter is associated with increased gene expression and decreased MeCP2 binding in autism cerebellum. Transl. Psychiatry *4*, e460.

Jastroch, M., Divakaruni, A.S., Mookerjee, S., Treberg, J.R., and Brand, M.D. (2010). Mitochondrial proton and electron leaks. Essays Biochem. *47*, 53–67.

Jin, K. (2010). Modern Biological Theories of Aging. Aging Dis. *1*, 72–74.

Johri, A., and Beal, M.F. (2012). Mitochondrial Dysfunction in Neurodegenerative Diseases. J. Pharmacol. Exp. Ther. *342*, 619–630.

Joyner, A.L., Herrup, K., Auerbach, B.A., Davis, C.A., and Rossant, J. (1991). Subtle cerebellar phenotype in mice homozygous for a targeted deletion of the En-2 homeobox. Science *251*, 1239–1243.

Kadkhodaei, B., Alvarsson, A., Schintu, N., Ramsköld, D., Volakakis, N., Joodmardi, E., Yoshitake, T., Kehr, J., Decressac, M., Björklund, A., et al. (2013). Transcription factor Nurr1 maintains fiber integrity and nuclear-encoded mitochondrial gene expression in dopamine neurons. Proc. Natl. Acad. Sci. U. S. A. *110*, 2360–2365.

Kang, E., Wang, X., Tippner-Hedges, R., Ma, H., Folmes, C.D.L., Gutierrez, N.M., Lee, Y., Van Dyken, C., Ahmed, R., Li, Y., et al. (2016). Age-Related Accumulation of Somatic Mitochondrial DNA Mutations in Adult-Derived Human iPSCs. Cell Stem Cell *18*, 625–636.

Keeney, P.M., Xie, J., Capaldi, R.A., and Bennett, J.P. (2006). Parkinson9s Disease Brain Mitochondrial Complex I Has Oxidatively Damaged Subunits and Is Functionally Impaired and Misassembled. J. Neurosci. *26*, 5256–5264.

Keuper, M., Jastroch, M., Yi, C.-X., Fischer-Posovszky, P., Wabitsch, M., Tschöp, M.H., and Hofmann, S.M. (2014). Spare mitochondrial respiratory capacity permits human adipocytes to maintain ATP homeostasis under hypoglycemic conditions. FASEB J. *28*, 761–770.

Kim, T.W., Cho, H.M., Choi, S.Y., Suguira, Y., Hayasaka, T., Setou, M., Koh, H.C., Mi Hwang, E., Park, J.Y., Kang, S.J., et al. (2013). (ADP-ribose) polymerase 1 and AMP-activated protein kinase mediate progressive dopaminergic neuronal degeneration in a mouse model of Parkinson's disease. Cell Death Dis. *4*, e919.

Knott, A.B., Perkins, G., Schwarzenbacher, R., and Bossy-Wetzel, E. (2008). Mitochondrial fragmentation in neurodegeneration. Nat. Rev. Neurosci. *9*, 505–518.

Kordower, J.H., Olanow, C.W., Dodiya, H.B., Chu, Y., Beach, T.G., Adler, C.H., Halliday, G.M., and Bartus, R.T. (2013). Disease duration and the integrity of the nigrostriatal system in Parkinson's disease. Brain *136*, 2419–2431.

Kouwenhoven, W.M., Veenvliet, J.V., van Hooft, J.A., van der Heide, L.P., and Smidt, M.P. (2016). Engrailed 1 shapes the dopaminergic and serotonergic landscape through proper isthmic organizer maintenance and function. Biol. Open *5*, 279–288.

Kouwenhoven, W.M., von Oerthel, L., and Smidt, M.P. (2017). Pitx3 and En1 determine the size and molecular programming of the dopaminergic neuronal pool. PLoS ONE *12*.

Kuemerle, B., Zanjani, H., Joyner, A., and Herrup, K. (1997). Pattern deformities and cell loss in Engrailed-2 mutant mice suggest two separate patterning events during cerebellar development. J. Neurosci. Off. J. Soc. Neurosci. *17*, 7881–7889.

Laguna, A., Schintu, N., Nobre, A., Alvarsson, A., Volakakis, N., Jacobsen, J.K., Gómez-Galán, M., Sopova, E., Joodmardi, E., Yoshitake, T., et al. (2015). Dopaminergic control of autophagic-lysosomal function implicates Lmx1b in Parkinson's disease. Nat. Neurosci. *18*, 826–835.

LaManna, J.C., Salem, N., Puchowicz, M., Erokwu, B., Koppaka, S., Flask, C., and Lee, Z. (2009). KETONES SUPPRESS BRAIN GLUCOSE CONSUMPTION. Adv. Exp. Med. Biol. *645*, 301–306.

Langston, J.W., Langston, E.B., and Irwin, I. (1984). MPTP-induced parkinsonism in human and non-human primates--clinical and experimental aspects. Acta Neurol. Scand. Suppl. *100*, 49–54.

Le, W.-D., Xu, P., Jankovic, J., Jiang, H., Appel, S.H., Smith, R.G., and Vassilatis, D.K. (2003). Mutations in NR4A2 associated with familial Parkinson disease. Nat. Genet. *33*, 85–89.

Le Belle, J.E., Orozco, N.M., Paucar, A.A., Saxe, J.P., Mottahedeh, J., Pyle, A.D., Wu, H., and Kornblum, H.I. (2011). Proliferative Neural Stem Cells Have High Endogenous ROS Levels that Regulate Self-Renewal and Neurogenesis in a PI3K/Akt-Dependant Manner. Cell Stem Cell *8*, 59–71.

Lees, J.G., Rathjen, J., Sheedy, J.R., Gardner, D.K., and Harvey, A.J. (2015). Distinct profiles of human embryonic stem cell metabolism and mitochondria identified by oxygen. Reproduction *150*, 367–382.

Lees, J.G., Gardner, D.K., and Harvey, A.J. (2017). Pluripotent Stem Cell Metabolism and Mitochondria: Beyond ATP.

Lehninger, A.L., Nelson, D.L., and Cox, M.M. (2008). Lehninger principles of biochemistry (New York: W.H. Freeman).

Lengner, C.J., Gimelbrant, A.A., Erwin, J.A., Cheng, A.W., Guenther, M.G., Welstead, G.G., Alagappan, R., Frampton, G.M., Xu, P., Muffat, J., et al. (2010). Derivation of pre-X inactivation human embryonic stem cells under physiological oxygen concentrations. Cell *141*, 872–883.

Lesage, S., and Brice, A. (2012). Role of mendelian genes in "sporadic" Parkinson's disease. Parkinsonism Relat. Disord. *18 Suppl 1*, S66-70.

Leverve, X., Batandier, C., and Fontaine, E. (2007). Choosing the right substrate. Novartis Found. Symp. *280*, 108-121; discussion 121-127, 160–164.

Li, H., Liu, H., Corrales, C.E., Risner, J.R., Forrester, J., Holt, J.R., Heller, S., and Edge, A.S. (2009a). Differentiation of neurons from neural precursors generated in floating spheres from embryonic stem cells. BMC Neurosci. *10*, 122.

Li, J., Dani, J.A., and Le, W. (2009b). The Role of Transcription Factor Pitx3 in Dopamine Neuron Development and Parkinson's Disease. Curr. Top. Med. Chem. *9*, 855–859.

Lodish, H.F., Berk, A., Kaiser, C.A., Krieger, M., Scott, M.P., Bretscher, A., Ploegh, H., and Matsudaira, P. (2013). Molecular cell biology (New York: W.H. Freeman and Company).

Löhle, M., Storch, A., and Reichmann, H. (2009). Beyond tremor and rigidity: non-motor features of Parkinson's disease. J. Neural Transm. Vienna Austria 1996 *116*, 1483–1492.

Lorenz, C., and Prigione, A. (2016). Aging vs. rejuvenation: reprogramming to iPSCs does not turn back the clock for somatic mitochondrial DNA mutations. Stem Cell Investig. *3*, 43–43.

Lunt, S.Y., and Heiden, M.G.V. (2011). Aerobic Glycolysis: Meeting the Metabolic Requirements of Cell Proliferation. Annu. Rev. Cell Dev. Biol. *27*, 441–464.

Magistretti, P.J., and Allaman, I. (2015). A Cellular Perspective on Brain Energy Metabolism and Functional Imaging. Neuron *86*, 883–901.

Mandal, S., Lindgren, A.G., Srivastava, A.S., Clark, A.T., and Banerjee, U. (2011). Mitochondrial function controls proliferation and early differentiation potential of embryonic stem cells. Stem Cells Dayt. Ohio *29*, 486–495.

Marchitti, S.A., Deitrich, R.A., and Vasiliou, V. (2007). Neurotoxicity and metabolism of the catecholamine-derived 3,4-dihydroxyphenylacetaldehyde and 3,4-dihydroxyphenylglycolaldehyde: the role of aldehyde dehydrogenase. Pharmacol. Rev. *59*, 125–150.

Martin, I., Dawson, V.L., and Dawson, T.M. (2011). Recent Advances in the Genetics of Parkinson's Disease. Annu. Rev. Genomics Hum. Genet. *12*, 301–325.

Martin, I., Kim, J.W., Dawson, V.L., and Dawson, T.M. (2014). LRRK2 Pathobiology in Parkinson's Disease. J. Neurochem. *131*, 554–565.

Mathieu, J., Zhou, W., Xing, Y., Sperber, H., Ferreccio, A., Agoston, Z., Kuppusamy, K.T., Moon, R.T., and Ruohola-Baker, H. (2014). Hypoxia Inducible Factors have distinct and stage-specific roles during reprogramming of human cells to pluripotency. Cell Stem Cell *14*, 592–605.

Meiser, J., Delcambre, S., Wegner, A., Jäger, C., Ghelfi, J., d'Herouel, A.F., Dong, X., Weindl, D., Stautner, C., Nonnenmacher, Y., et al. (2016). Loss of DJ-1 impairs antioxidant response by altered glutamine and serine metabolism. Neurobiol. Dis. *89*, 112–125.

Menges, S., Minakaki, G., Schaefer, P.M., Meixner, H., Prots, I., Schlötzer-Schrehardt, U., Friedland, K., Winner, B., Outeiro, T.F., Winklhofer, K.F., et al. (2017). Alpha-synuclein prevents the formation of spherical mitochondria and apoptosis under oxidative stress. Sci. Rep. *7*.

Millen, K.J., Wurst, W., Herrup, K., and Joyner, A.L. (1994). Abnormal embryonic cerebellar development and patterning of postnatal foliation in two mouse Engrailed-2 mutants. Dev. Camb. Engl. *120*, 695–706.

Millen, K.J., Hui, C.C., and Joyner, A.L. (1995). A role for En-2 and other murine homologues of Drosophila segment polarity genes in regulating positional information in the developing cerebellum. Development *121*, 3935–3945.

Miller, J., and Studer, L. (2014). Aging in iPS cells. Aging *6*, 246–247.

Miller, J.D., Ganat, Y.M., Kishinevsky, S., Bowman, R.L., Liu, B., Tu, E.Y., Mandal, P.K., Vera, E., Shim, J., Kriks, S., et al. (2013). Human iPSC-Based Modeling of Late-Onset Disease via Progerin-Induced Aging. Cell Stem Cell *13*, 691–705.

Mimaki, M., Wang, X., McKenzie, M., Thorburn, D.R., and Ryan, M.T. (2012). Understanding mitochondrial complex I assembly in health and disease. Biochim. Biophys. Acta BBA - Bioenerg. *1817*, 851–862.

Mishra, P., and Chan, D.C. (2016). Metabolic regulation of mitochondrial dynamics. J Cell Biol *212*, 379–387.

Mitra, K., Wunder, C., Roysam, B., Lin, G., and Lippincott-Schwartz, J. (2009). A hyperfused mitochondrial state achieved at G1–S regulates cyclin E buildup and entry into S phase. Proc. Natl. Acad. Sci. U. S. A. *106*, 11960–11965.

Mohyeldin, A., Garzón-Muvdi, T., and Quiñones-Hinojosa, A. (2010). Oxygen in stem cell biology: a critical component of the stem cell niche. Cell Stem Cell *7*, 150–161.

Moon, H.E., and Paek, S.H. (2015). Mitochondrial Dysfunction in Parkinson's Disease. Exp. Neurobiol. *24*, 103.

Moussaieff, A., Rouleau, M., Kitsberg, D., Cohen, M., Levy, G., Barasch, D., Nemirovski, A., Shen-Orr, S., Laevsky, I., Amit, M., et al. (2015). Glycolysis-Mediated Changes in Acetyl-CoA and Histone Acetylation Control the Early Differentiation of Embryonic Stem Cells. Cell Metab. *21*, 392–402.

Muñoz, P., Huenchuguala, S., Paris, I., and Segura-Aguilar, J. (2012). Dopamine Oxidation and Autophagy. Park. Dis. *2012*.

Nebel, M.B., Joel, S.E., Muschelli, J., Barber, A.D., Caffo, B.S., Pekar, J.J., and Mostofsky, S.H. (2014). Disruption of functional organization within the primary motor cortex in children with autism. Hum. Brain Mapp. *35*, 567–580.

Newman, A.B., and Murabito, J.M. (2013). The epidemiology of longevity and exceptional survival. Epidemiol. Rev. *35*, 181–197.

Newsholme, E.A., Crabtree, B., and Ardawi, M.S. (1985). The role of high rates of glycolysis and glutamine utilization in rapidly dividing cells. Biosci. Rep. *5*, 393–400.

Nicklas, W.J., Vyas, I., and Heikkila, R.E. (1985). Inhibition of NADH-linked oxidation in brain mitochondria by 1-methyl-4-phenyl-pyridine, a metabolite of the neurotoxin, 1-methyl-4-phenyl-1,2,5,6-tetrahydropyridine. Life Sci. *36*, 2503–2508.

Nooteboom, M., Johnson, R., Taylor, R.W., Wright, N.A., Lightowlers, R.N., Kirkwood, T.B.L., Mathers, J.C., Turnbull, D.M., and Greaves, L.C. (2010). Age-associated mitochondrial DNA mutations lead to small but significant changes in cell proliferation and apoptosis in human colonic crypts. Aging Cell *9*, 96–99.

Nordströma, U., Beauvais, G., Ghosh, A., Pulikkaparambil Sasidharan, B.C., Lundblad, M., Fuchs, J., Joshi, R.L., Lipton, J.W., Roholt, A., Medicetty, S., et al. (2015). Progressive nigrostriatal terminal dysfunction and degeneration in the engrailed1 heterozygous mouse model of Parkinson's disease. Neurobiol. Dis. *73*, 70–82.

Obeso, J.A., Rodríguez-Oroz, M.C., Benitez-Temino, B., Blesa, F.J., Guridi, J., Marin, C., and Rodriguez, M. (2008). Functional organization of the basal ganglia: therapeutic implications for Parkinson's disease. Mov. Disord. Off. J. Mov. Disord. Soc. *23 Suppl 3*, S548-559.

Olichon, A., Baricault, L., Gas, N., Guillou, E., Valette, A., Belenguer, P., and Lenaers, G. (2003). Loss of OPA1 Perturbates the Mitochondrial Inner Membrane Structure and Integrity, Leading to Cytochrome c Release and Apoptosis. J. Biol. Chem. *278*, 7743–7746.

Orsucci, D., Ienco, E.C., Mancuso, M., and Siciliano, G. (2011). POLG1-Related and other "Mitochondrial Parkinsonisms": an Overview. J. Mol. Neurosci. *44*, 17–24.

Ottolini, D., Calí, T., Szabò, I., and Brini, M. (2017). Alpha-synuclein at the intracellular and the extracellular side: functional and dysfunctional implications. Biol. Chem. *398*, 77–100.

Park, H.-S., Hwang, I., Choi, K.-A., Jeong, H., Lee, J.-Y., and Hong, S. (2015). Generation of induced pluripotent stem cells without genetic defects by small molecules. Biomaterials *39*, 47–58.

Parkinson, J. (2002). An essay on the shaking palsy. 1817. J. Neuropsychiatry Clin. Neurosci. *14*, 223–236; discussion 222.

Patten, D.A., Lafleur, V.N., Robitaille, G.A., Chan, D.A., Giaccia, A.J., and Richard, D.E. (2010). Hypoxia-inducible Factor-1 Activation in Nonhypoxic Conditions: The Essential Role of Mitochondrial-derived Reactive Oxygen Species. Mol. Biol. Cell *21*, 3247–3257.

Petrini, S., Borghi, R., D'Oria, V., Restaldi, F., Moreno, S., Novelli, A., Bertini, E., and Compagnucci, C. (2017). Aged induced pluripotent stem cell (iPSCs) as a new cellular model for studying premature aging. Aging *9*, 1453–1466.

Petruzzelli, R., Christensen, D.R., Parry, K.L., Sanchez-Elsner, T., and Houghton, F.D. (2014). HIF-2α Regulates NANOG Expression in Human Embryonic Stem Cells following Hypoxia and Reoxygenation through the Interaction with an Oct-Sox Cis Regulatory Element. PLOS ONE *9*, e108309.

Pfeiffer, T., Schuster, S., and Bonhoeffer, S. (2001). Cooperation and Competition in the Evolution of ATP-Producing Pathways. Science *292*, 504–507.

Pfluger, P.T., Kabra, D.G., Aichler, M., Schriever, S.C., Pfuhlmann, K., García, V.C., Lehti, M., Weber, J., Kutschke, M., Rozman, J., et al. (2015). Calcineurin Links Mitochondrial Elongation with Energy Metabolism. Cell Metab. *22*, 838–850.

Pinter, B., Diem-Zangerl, A., Wenning, G.K., Scherfler, C., Oberaigner, W., Seppi, K., and Poewe, W. (2015). Mortality in Parkinson's disease: a 38-year follow-up study. Mov. Disord. Off. J. Mov. Disord. Soc. *30*, 266–269.

Poewe, W., Seppi, K., Tanner, C.M., Halliday, G.M., Brundin, P., Volkmann, J., Schrag, A.-E., and Lang, A.E. (2017). Parkinson disease. Nat. Rev. Dis. Primer *3*, nrdp201713.

Prakash, N. (2006). A Wnt1-regulated genetic network controls the identity and fate of midbrain-dopaminergic progenitors in vivo. Development *133*, 89–98.

Prigione, A., and Adjaye, J. (2010). Modulation of mitochondrial biogenesis and bioenergetic metabolism upon in vitro and in vivo differentiation of human ES and iPS cells. Int. J. Dev. Biol. *54*, 1729–1741.

Prigione, A., Fauler, B., Lurz, R., Lehrach, H., and Adjaye, J. (2010). The Senescence-Related Mitochondrial/Oxidative Stress Pathway is Repressed in Human Induced Pluripotent Stem Cells. STEM CELLS *28*, 721–733.

Prigione, A., Rohwer, N., Hoffmann, S., Mlody, B., Drews, K., Bukowiecki, R., Blümlein, K., Wanker, E.E., Ralser, M., Cramer, T., et al. (2014). HIF1α Modulates Cell Fate Reprogramming Through Early Glycolytic Shift and Upregulation of PDK1-3 and PKM2: HIF1α Associated Metabolic Switch in iPSCs. STEM CELLS *32*, 364–376.

Prigione, A., Ruiz-Pérez, M.V., Bukowiecki, R., and Adjaye, J. (2015). Metabolic restructuring and cell fate conversion. Cell. Mol. Life Sci. *72*, 1759–1777.

Prince, A., Zhang, Y., Croniger, C., and Puchowicz, M. (2013). Oxidative metabolism: glucose versus ketones. Adv. Exp. Med. Biol. *789*, 323–328.

Pringsheim, T., Jette, N., Frolkis, A., and Steeves, T.D.L. (2014). The prevalence of Parkinson's disease: a systematic review and meta-analysis. Mov. Disord. Off. J. Mov. Disord. Soc. *29*, 1583–1590.

Prochiantz, A., and Di Nardo, A.A. (2015). Homeoprotein signaling in the developing and adult nervous system. Neuron *85*, 911–925.

Prochiantz, A., Fuchs, J., and Di Nardo, A.A. (2014). Postnatal signalling with homeoprotein transcription factors. Philos. Trans. R. Soc. B Biol. Sci. *369*.

Provenzano, G., Corradi, Z., Monsorno, K., Fedrizzi, T., Ricceri, L., Scattoni, M.L., and Bozzi, Y. (2016). Comparative Gene Expression Analysis of Two Mouse Models of Autism: Transcriptome Profiling of the BTBR and En2−/− Hippocampus. Front. Neurosci. *10*.

Pryde, K.R., Smith, H.L., Chau, K.-Y., and Schapira, A.H.V. (2016). PINK1 disables the anti-fission machinery to segregate damaged mitochondria for mitophagy. J. Cell Biol. *213*, 163–171.

Rao, M.S., and Malik, N. (2012). Assessing iPSC reprogramming methods for their suitability in translational medicine. J. Cell. Biochem. *113*, 3061–3068.

Reinhardt, P., Glatza, M., Hemmer, K., Tsytsyura, Y., Thiel, C.S., Höing, S., Moritz, S., Parga, J.A., Wagner, L., Bruder, J.M., et al. (2013). Derivation and Expansion Using Only Small Molecules of Human Neural Progenitors for Neurodegenerative Disease Modeling. PLoS ONE *8*, e59252.

Rekaik, H., Blaudin de Thé, F.-X., Prochiantz, A., Fuchs, J., and Joshi, R.L. (2015a). Dissecting the role of Engrailed in adult dopaminergic neurons - Insights into Parkinson disease pathogenesis. FEBS Lett. *589*, 3786–3794.

Rekaik, H., Blaudin de Thé, F.-X., Fuchs, J., Massiani-Beaudoin, O., Prochiantz, A., and Joshi, R.L. (2015b). Engrailed Homeoprotein Protects Mesencephalic Dopaminergic Neurons from Oxidative Stress. Cell Rep. *13*, 242–250.

Rideout, H.J., and Stefanis, L. (2014). The Neurobiology of LRRK2 and its Role in the Pathogenesis of Parkinson's Disease. Neurochem. Res. *39*, 576–592.

Riederer, P., Konradi, C., Schay, V., Kienzl, E., Birkmayer, G., Danielczyk, W., Sofic, E., and Youdim, M.B. (1987). Localization of MAO-A and MAO-B in human brain: a step in understanding the therapeutic action of L-deprenyl. Adv. Neurol. *45*, 111–118.

Rissling, I., Strauch, K., Höft, C., Oertel, W.H., and Möller, J.C. (2009). Haplotype Analysis of the Engrailed-2 Gene in Young-Onset Parkinson's Disease. Neurodegener. Dis. *6*, 102–105.

Rodriguez-Oroz, M.C., Jahanshahi, M., Krack, P., Litvan, I., Macias, R., Bezard, E., and Obeso, J.A. (2009). Initial clinical manifestations of Parkinson's disease: features and pathophysiological mechanisms. Lancet Neurol. *8*, 1128–1139.

Romito, A., and Cobellis, G. (2016). Pluripotent Stem Cells: Current Understanding and Future Directions. Stem Cells Int. *2016*.

Rossignol, R., Faustin, B., Rocher, C., Malgat, M., Mazat, J.-P., and Letellier, T. (2003). Mitochondrial threshold effects. Biochem. J. *370*, 751–762.

Rossignol, R., Gilkerson, R., Aggeler, R., Yamagata, K., Remington, S.J., and Capaldi, R.A. (2004). Energy Substrate Modulates Mitochondrial Structure and Oxidative Capacity in Cancer Cells. Cancer Res. *64*, 985–993.

Safiulina, D., and Kaasik, A. (2013). Energetic and Dynamic: How Mitochondria Meet Neuronal Energy Demands. PLoS Biol. *11*.

Santos, D., Esteves, A.R., Silva, D.F., Januário, C., and Cardoso, S.M. (2015). The Impact of Mitochondrial Fusion and Fission Modulation in Sporadic Parkinson's Disease. Mol. Neurobiol. *52*, 573–586.

Scarffe, L.A., Stevens, D.A., Dawson, V.L., and Dawson, T.M. (2014). Parkin and PINK1: Much More than Mitophagy. Trends Neurosci. *37*, 315–324.

Schapira, A.H., Cooper, J.M., Dexter, D., Jenner, P., Clark, J.B., and Marsden, C.D. (1989). Mitochondrial complex I deficiency in Parkinson's disease. Lancet Lond. Engl. *1*, 1269.

Schmidt, S. (2017). Engrailed in Parkinson's disease and its link to mitochondrial complex I deficiency. Technische Universität München.

Schönfeld, P., and Reiser, G. (2013). Why does Brain Metabolism not Favor Burning of Fatty Acids to Provide Energy? - Reflections on Disadvantages of the Use of Free Fatty Acids as Fuel for Brain. J. Cereb. Blood Flow Metab. *33*, 1493–1499.

Scott, L., Dawson, V.L., and Dawson, T.M. (2017). Trumping neurodegeneration: Targeting common pathways regulated by autosomal recessive Parkinson's disease genes. Exp. Neurol.

Sebe, A., and Ivics, Z. (2016). Reprogramming of Human Fibroblasts to Induced Pluripotent Stem Cells with Sleeping Beauty Transposon-Based Stable Gene Delivery. In Transposons and Retrotransposons, (Humana Press, New York, NY), pp. 419–427.

Segev, H., Fishman, B., Schulman, R., and Itskovitz-Eldor, J. (2012). The Expression of the Class 1 Glucose Transporter Isoforms in Human Embryonic Stem Cells, and the Potential Use of GLUT2 as a Marker for Pancreatic Progenitor Enrichment. Stem Cells Dev. *21*, 1653–1661.

Seto, E., and Yoshida, M. (2014). Erasers of histone acetylation: the histone deacetylase enzymes. Cold Spring Harb. Perspect. Biol. *6*, a018713.

Sgadò, P., Provenzano, G., Dassi, E., Adami, V., Zunino, G., Genovesi, S., Casarosa, S., and Bozzi, Y. (2013). Transcriptome profiling in engrailed-2 mutant mice reveals common molecular pathways associated with autism spectrum disorders. Mol. Autism *4*, 51.

Shadyab, A.H., and LaCroix, A.Z. (2015). Genetic factors associated with longevity: a review of recent findings. Ageing Res. Rev. *19*, 1–7.

Shen, Y., Tang, Y., Zhang, X., Huang, K., and Le, W. (2013). Adaptive changes in autophagy after UPS impairment in Parkinson's disease. Acta Pharmacol. Sin. *34*, 667–673.

Shi, Y., Inoue, H., Wu, J.C., and Yamanaka, S. (2017). Induced pluripotent stem cell technology: a decade of progress. Nat. Rev. Drug Discov. *16*, 115–130.

Shimura, H., Hattori, N., Kubo, S., Mizuno, Y., Asakawa, S., Minoshima, S., Shimizu, N., Iwai, K., Chiba, T., Tanaka, K., et al. (2000). Familial Parkinson disease gene product, parkin, is a ubiquitin-protein ligase. Nat. Genet. *25*, 302–305.

Shin, J.-H., Ko, H.S., Kang, H., Lee, Y., Lee, Y.-I., Pletinkova, O., Troconso, J.C., Dawson, V.L., and Dawson, T.M. (2011). PARIS (ZNF746) Repression of PGC-1α Contributes to Neurodegeneration in Parkinson's Disease. Cell *144*, 689–702.

Shock, L.S., Thakkar, P.V., Peterson, E.J., Moran, R.G., and Taylor, S.M. (2011). DNA methyltransferase 1, cytosine methylation, and cytosine hydroxymethylation in mammalian mitochondria. Proc. Natl. Acad. Sci. U. S. A. *108*, 3630–3635.

Shokolenko, I., Venediktova, N., Bochkareva, A., Wilson, G.L., and Alexeyev, M.F. (2009). Oxidative stress induces degradation of mitochondrial DNA. Nucleic Acids Res. *37*, 2539–2548.

Simon, H.H., Saueressig, H., Wurst, W., Goulding, M.D., and O'Leary, D.D.M. (2001). Fate of Midbrain Dopaminergic Neurons Controlled by the Engrailed Genes. J. Neurosci. *21*, 3126–3134.

Simon, H.H., Bhatt, L., Gherbassi, D., Sgadó, P., and Alberí, L. (2003). Midbrain dopaminergic neurons: determination of their developmental fate by transcription factors. Ann. N. Y. Acad. Sci. *991*, 36–47.

Simon, H.H., Scholz, C., and O'Leary, D.D.M. (2005). Engrailed genes control developmental fate of serotonergic and noradrenergic neurons in mid- and hindbrain in a gene dose-dependent manner. Mol. Cell. Neurosci. *28*, 96–105.

Skulachev, V.P. (2001). Mitochondrial filaments and clusters as intracellular power-transmitting cables. Trends Biochem. Sci. *26*, 23–29.

Smidt, M.P. (2009). Specific vulnerability of substantia nigra compacta neurons. J. Neural Transm. Suppl. 39–47.

Smidt, M.P., and Burbach, J.P.H. (2007). How to make a mesodiencephalic dopaminergic neuron. Nat. Rev. Neurosci. *8*, 21–32.

Soldner, F., Hockemeyer, D., Beard, C., Gao, Q., Bell, G.W., Cook, E.G., Hargus, G., Blak, A., Cooper, O., Mitalipova, M., et al. (2009). Parkinson's Disease Patient-Derived Induced Pluripotent Stem Cells Free of Viral Reprogramming Factors. Cell *136*, 964–977.

Sonnier, L., Le Pen, G., Hartmann, A., Bizot, J.-C., Trovero, F., Krebs, M.-O., and Prochiantz, A. (2007). Progressive loss of dopaminergic neurons in the ventral midbrain of adult mice heterozygote for Engrailed1. J. Neurosci. Off. J. Soc. Neurosci. *27*, 1063–1071.

Souza, B.M. de, Assmann, T.S., Kliemann, L.M., Gross, J.L., Canani, L.H., and Crispim, D. (2011). The role of uncoupling protein 2 (UCP2) on the development of type 2 diabetes mellitus and its chronic complications. Arq. Bras. Endocrinol. Metabol. *55*, 239–248.

Starkstein, S., Gellar, S., Parlier, M., Payne, L., and Piven, J. (2015). High rates of parkinsonism in adults with autism. J. Neurodev. Disord. *7*, 29.

Stettler, O., Joshi, R.L., Wizenmann, A., Reingruber, J., Holcman, D., Bouillot, C., Castagner, F., Prochiantz, A., and Moya, K.L. (2012). Engrailed homeoprotein recruits the adenosine A1 receptor to potentiate ephrin A5 function in retinal growth cones. Dev. Camb. Engl. *139*, 215–224.

Symersky, J., Osowski, D., Walters, D.E., and Mueller, D.M. (2012). Oligomycin frames a common drug-binding site in the ATP synthase. Proc. Natl. Acad. Sci. U. S. A. *109*, 13961–13965.

Takahashi, K., Tanabe, K., Ohnuki, M., Narita, M., Ichisaka, T., Tomoda, K., and Yamanaka, S. (2007). Induction of Pluripotent Stem Cells from Adult Human Fibroblasts by Defined Factors. Cell *131*, 861–872.

Tan, A.S., Baty, J.W., Dong, L.-F., Bezawork-Geleta, A., Endaya, B., Goodwin, J., Bajzikova, M., Kovarova, J., Peterka, M., Yan, B., et al. (2015). Mitochondrial Genome Acquisition Restores Respiratory Function and Tumorigenic Potential of Cancer Cells without Mitochondrial DNA. Cell Metab. *21*, 81–94.

Tan, J.M.M., Wong, E.S.P., and Lim, K.-L. (2009). Protein Misfolding and Aggregation in Parkinson's Disease. Antioxid. Redox Signal. *11*, 2119–2134.

Teslaa, T., and Teitell, M.A. (2015). Pluripotent stem cell energy metabolism: an update. EMBO J. *34*, 138–153.

Todd, L.R., Damin, M.N., Gomathinayagam, R., Horn, S.R., Means, A.R., and Sankar, U. (2010). Growth factor erv1-like modulates Drp1 to preserve mitochondrial dynamics and function in mouse embryonic stem cells. Mol. Biol. Cell *21*, 1225–1236.

Tohyama, S., Fujita, J., Hishiki, T., Matsuura, T., Hattori, F., Ohno, R., Kanazawa, H., Seki, T., Nakajima, K., Kishino, Y., et al. (2016). Glutamine Oxidation Is Indispensable for Survival of Human Pluripotent Stem Cells. Cell Metab. *23*, 663–674.

Tondera, D., Grandemange, S., Jourdain, A., Karbowski, M., Mattenberger, Y., Herzig, S., Da Cruz, S., Clerc, P., Raschke, I., Merkwirth, C., et al. (2009). SLP-2 is required for stress-induced mitochondrial hyperfusion. EMBO J. *28*, 1589–1600.

Topisirovic, I., and Borden, K.L. (2005). Homeodomain proteins and eukaryotic translation initiation factor 4E (eIF4E): an unexpected relationship. Histol. Histopathol. *20*, 1275–1284.

Turner, J., Quek, L.-E., Titmarsh, D., Krömer, J.O., Kao, L.-P., Nielsen, L., Wolvetang, E., and Cooper-White, J. (2014). Metabolic Profiling and Flux Analysis of MEL-2 Human Embryonic Stem Cells during Exponential Growth at Physiological and Atmospheric Oxygen Concentrations. PLOS ONE *9*, e112757.

United Nations World Population Prospects (2015). World Population Prospects - Population Division - United Nations.

Van Den Eeden, S.K., Tanner, C.M., Bernstein, A.L., Fross, R.D., Leimpeter, A., Bloch, D.A., and Nelson, L.M. (2003). Incidence of Parkinson's disease: variation by age, gender, and race/ethnicity. Am. J. Epidemiol. *157*, 1015–1022.

Van Raamsdonk, J.M., and Hekimi, S. (2009). Deletion of the Mitochondrial Superoxide Dismutase sod-2 Extends Lifespan in Caenorhabditis elegans. PLoS Genet. *5*.

Van Raamsdonk, J.M., and Hekimi, S. (2012). Superoxide dismutase is dispensable for normal animal lifespan. Proc. Natl. Acad. Sci. U. S. A. *109*, 5785–5790.

Vercesi, A.E., Bernardes, C.F., Hoffmann, M.E., Gadelha, F.R., and Docampo, R. (1991). Digitonin permeabilization does not affect mitochondrial function and allows the determination of the mitochondrial membrane potential of Trypanosoma cruzi in situ. J. Biol. Chem. *266*, 14431–14434.

Vogt Weisenhorn, D.M., Giesert, F., and Wurst, W. (2016). Diversity matters – heterogeneity of dopaminergic neurons in the ventral mesencephalon and its relation to Parkinson's Disease. J. Neurochem. *139*, 8–26.

Volkenhoff, A., Weiler, A., Letzel, M., Stehling, M., Klämbt, C., and Schirmeier, S. (2015). Glial Glycolysis Is Essential for Neuronal Survival in Drosophila. Cell Metab. *22*, 437–447.

Wang, S., Song, J., Tan, M., Albers, K.M., and Jia, J. (2012). Mitochondrial fission proteins in peripheral blood lymphocytes are potential biomarkers for Alzheimer's disease. Eur. J. Neurol. *19*, 1015–1022.

Webb, J.L., Ravikumar, B., Atkins, J., Skepper, J.N., and Rubinsztein, D.C. (2003). α-Synuclein Is Degraded by Both Autophagy and the Proteasome. J. Biol. Chem. *278*, 25009–25013.

Westermann, B. (2010). Mitochondrial fusion and fission in cell life and death. Nat. Rev. Mol. Cell Biol. *11*, 872–884.

Westermann, B. (2012). Bioenergetic role of mitochondrial fusion and fission. Biochim. Biophys. Acta BBA - Bioenerg. *1817*, 1833–1838.

Winklhofer, K.F., and Haass, C. (2010). Mitochondrial dysfunction in Parkinson's disease. Biochim. Biophys. Acta BBA - Mol. Basis Dis. *1802*, 29–44.

Winner, B., Jappelli, R., Maji, S.K., Desplats, P.A., Boyer, L., Aigner, S., Hetzer, C., Loher, T., Vilar, M., Campioni, S., et al. (2011). In vivo demonstration that α-synuclein oligomers are toxic. Proc. Natl. Acad. Sci. U. S. A. *108*, 4194–4199.

Wu, T., and Hallett, M. (2013). The cerebellum in Parkinson's disease. Brain J. Neurol. *136*, 696–709.

Wyss-Coray, T. (2016). Ageing, neurodegeneration and brain rejuvenation. Nature *539*, 180–186.

Xiao, M., Yang, H., Xu, W., Ma, S., Lin, H., Zhu, H., Liu, L., Liu, Y., Yang, C., Xu, Y., et al. (2012). Inhibition of α-KG-dependent histone and DNA demethylases by fumarate and succinate that are accumulated in mutations of FH and SDH tumor suppressors. Genes Dev. *26*, 1326–1338.

Yang, C., Ko, B., Hensley, C.T., Jiang, L., Wasti, A.T., Kim, J., Sudderth, J., Calvaruso, M.A., Lumata, L., Mitsche, M., et al. (2014). Glutamine Oxidation Maintains the TCA Cycle and Cell Survival during Impaired Mitochondrial Pyruvate Transport. Mol. Cell *56*, 414–424.

Yoneyama, M., Kawada, K., Gotoh, Y., Shiba, T., and Ogita, K. (2010). Endogenous reactive oxygen species are essential for proliferation of neural stem/progenitor cells. Neurochem. Int. *56*, 740–746.

Yoon, B.C., Jung, H., Dwivedy, A., O'Hare, C.M., Zivraj, K.H., and Holt, C.E. (2012). Local Translation of Extranuclear Lamin B Promotes Axon Maintenance. Cell *148*, 752–764.

Yoshida, Y., Takahashi, K., Okita, K., Ichisaka, T., and Yamanaka, S. (2009). Hypoxia enhances the generation of induced pluripotent stem cells. Cell Stem Cell *5*, 237–241.

Yoshino, H., Nakagawa-Hattori, Y., Kondo, T., and Mizuno, Y. (1992). Mitochondrial complex I and II activities of lymphocytes and platelets in Parkinson's disease. J. Neural Transm. Park. Dis. Dement. Sect. *4*, 27–34.

Youle, R.J., and van der Bliek, A.M. (2012). Mitochondrial Fission, Fusion, and Stress. Science *337*, 1062–1065.

Zachar, V., Prasad, S.M., Weli, S.C., Gabrielsen, A., Petersen, K., Petersen, M.B., and Fink, T. (2010). The effect of human embryonic stem cells (hESCs) long-term normoxic and hypoxic cultures on the maintenance of pluripotency. Vitro Cell. Dev. Biol. - Anim. *46*, 276–283.

Zhang, H., Badur, M.G., Divakaruni, A.S., Parker, S.J., Jäger, C., Hiller, K., Murphy, A.N., and Metallo, C.M. (2016). Distinct Metabolic States Can Support Self-Renewal and Lipogenesis in Human Pluripotent Stem Cells under Different Culture Conditions. Cell Rep. *16*, 1536–1547.

Zhang, J., Khvorostov, I., Hong, J.S., Oktay, Y., Vergnes, L., Nuebel, E., Wahjudi, P.N., Setoguchi, K., Wang, G., Do, A., et al. (2011). UCP2 regulates energy metabolism and differentiation potential of human pluripotent stem cells. EMBO J. *30*, 4860–4873.

Zhang, J., Götz, S., Vogt Weisenhorn, D.M., Simeone, A., Wurst, W., and Prakash, N. (2015). A WNT1-regulated developmental gene cascade prevents dopaminergic neurodegeneration in adult En1(+/-) mice. Neurobiol. Dis. *82*, 32–45.

Zhang, L., Shimoji, M., Thomas, B., Moore, D.J., Yu, S.-W., Marupudi, N.I., Torp, R., Torgner, I.A., Ottersen, O.P., Dawson, T.M., et al. (2005). Mitochondrial localization of the Parkinson's disease related protein DJ-1: implications for pathogenesis. Hum. Mol. Genet. *14*, 2063–2073.

Zheng, B., Liao, Z., Locascio, J.J., Lesniak, K.A., Roderick, S.S., Watt, M.L., Eklund, A.C., Zhang-James, Y., Kim, P.D., Hauser, M.A., et al. (2010). PGC-1 , A Potential Therapeutic Target for Early Intervention in Parkinson's Disease. Sci. Transl. Med. *2*, 52ra73-52ra73.

Zhu, S., Li, W., Zhou, H., Wei, W., Ambasudhan, R., Lin, T., Kim, J., Zhang, K., and Ding, S. (2010). Reprogramming of human primary somatic cells by OCT4 and chemical compounds. Cell Stem Cell *7*, 651–655.

Ziegler, D.V., Wiley, C.D., and Velarde, M.C. (2015). Mitochondrial effectors of cellular senescence: beyond the free radical theory of aging. Aging Cell *14*, 1–7.

10. Versicherung an Eides statt

Eidesstattliche Erklärung

Ich erkläre an Eides statt, dass ich die bei der Fakultät Wissenschaftszentrum Weihenstephan für Ernährung, Landnutzung und Umwelt (promotionsführende Einrichtung) der Technischen Universität München zur Promotionsprüfung vorgelegte Arbeit mit dem Titel: „*Mitochondrial Function in Cellular Models of Idiopathic Parkinson's Disease*“ / „*Mitochondrial Funktion in zellulären Modellen der idiopathischen Parkinson'schen Erkrankung“* unter der Anleitung und Betreuung durch Professor Dr. Wolfgang Wurst ohne sonstige Hilfe erstellt und bei der Abfassung nur die gemäß § 6 Abs. 6 und 7 Satz 2 angegebenen Hilfsmittel benutzt habe.

Ich habe keine Organisation eingeschaltet, die gegen Entgelt Betreuerinnen und Betreuer für die Anfertigung von Dissertationen sucht, oder die mir obliegenden Pflichten hinsichtlich der Prüfungsleistungen für mich ganz oder teilweise erledigt. Weder ich noch andere haben diese Dissertation in dieser oder ähnlicher Form in einem anderen Prüfungsverfahren als Prüfungsleistung vorgelegt. Ich habe den angestrebten Doktorgrad noch nicht erworben und bin nicht in einem früheren Promotionsverfahren für den angestrebten Doktorgrad endgültig gescheitert. Die öffentlich zugängliche Promotionsordnung der TUM ist mir bekannt, insbesondere habe ich die Bedeutung von § 28 (Nichtigkeit der Promotion) und § 29 (Entzug des Doktorgrades) zur Kenntnis genommen. Ich bin mir der Konsequenzen einer falschen Eidesstattlichen Erklärung bewusst.

_____ _____

Ort / Datum Constantin Stautner

11. Acknowledgements

Despite being a very challenging time in my life, I am very thankful for my time as doctoral student which taught me a lot about science, life and myself. Therefore, first I would like to first thank Prof. Wolfgang Wurst and Dr. Daniela Vogt Weisenhorn for the opportunity they gave me. I would like to thank Wolfgang, but particularly Daniela, for the support I always have received from you. Even in difficult times, you were always there to turn to and had an open ear for all troubles, may they be professional or personal. I highly appreciate the scientific input and guidance I got from you.

Along this line I would like to thank Dr. Florian Giesert who always had an open ear for all my professional issues but also bad jokes, for his great help and guidance during my work.

I would also like to thank Dr. Martin Jastroch and his team, especially Daniel Lamp, for great collaboration, a very productive work environment and guidance through the complex field of Seahorse analysis and bioenergetics whenever needed. I wish all of them all the best in their future endeavors.

I am very thankful to the members of my Thesis Committee, Prof. Wolfgang Wurst, Dr. Daniela Vogt Weisenhorn, Dr. Martin Jastroch, Dr. Florian Giesert, Prof. Rejko Krüger and Dr. Oskar Ortiz. All the discussions still make my brain ring but you have been highly helpful and appreciated.

I would like to thank our excellent lab team, Annerose Kurz-Drexler, Susanne Badeke, Irina Rodionova, Susanne Bourier and Denise Herold. You were always supportive, helpful and brilliant conversational partners.

Furthermore, I would like to mention the ForiPS consortium under the lead of Prof. Jürgen Winkler. I would like to thank Jürgen for the positive environment he created in this consortium and the great opportunities he gave me. Further, I would like to thank Prof. Zacharias Kohl, Prof. Beate Winner, Dr. Sigrid Schwarz and Dr. Markus Schulze as well as Sonja Plötz and Holger Wend for excellent collaboration at all times.

Along this line, I thank Marina Spona-Friedl, Dr. Alexander Braun and Prof. Martin Elsner for great collaboration, it was a pleasure. All the best to you all.

Special thanks also to Sebastian Schmidt, who's Master's Thesis was embedded in and contributed to this thesis. It was a pleasure to work with you.

I would also like to take the opportunity and thank the members of my examination committee, Prof. Aphrodite Kapurniotu, Prof. Wolfgang Wurst and Prof. Martin Klingenspor.

Next I would like to thank my outstanding colleagues, Petra Dirscherl, Benedikt Rauser, Ejona Rusha, Alexander Agapov, Artem Romanov and Jessica Schwab for the great time that I experienced the last years of my thesis. Equally, I thank Michaela Bosch, Clara Zoe Wende, Oskar Ortiz, Luise Ernst and Anke Wittmann for making my first two years such a memorable experience. I am very proud and thankful to have had you as my colleagues and now as my friends.

I am exceptionally thankful for the great support and awesome company I am always getting from my friends Anna-Sophie Geiersberger, Tim Bartel, Benjamin Jentsch and Anja Kluge, of whom most have accompanied me for almost my whole life.

Most importantly I would like to thank you, Petra. You have accompanied me through good, great, funny, bad and difficult times and always stood at my side. I can always count on you and I am more than just thankful for that. I hope for many more years of your companionship.

Last but definitely not least, I thank my family. I thank my father Ken who has tried everything he can to be with me and to be there for me. I thank my aunt Yala and my uncle Alex and his family, Helga, Bastienne and Larissa, as well as my grandparents Friedl and Hans. You have always supported and promoted me, you believed and continue to believe in me. Most importantly, I thank my mother Barbara, whom I owe everything to. Without you I would not be the person I am and I would never have achieved so much in life. Thank you all for all your love and support!